The Possibility of an Impact-Related Origin of Quasi-Conglomerate Pseudotachylytes on Barra, Outer Hebrides, Scotland. An Integrated Study.

Brigitte Vogt

Thesis submitted to the
Department of Civil and Environmental Engineering
University of Strathclyde
Glasgow, UK

in fulfilment of the requirements for the
degree of

Doctor of Philosophy

February 2021

Declaration

This thesis is the result of the author's original research. It has been composed by the author and has not been previously submitted for examination which has led to the award of a degree.

Signed:

Date:

Dazzled
followed by
an avalanche
of questions
Fundamental
some shaking
More than once
I hit solid ground
Trying
Tackling those
Why
How
Here
there is a result.

There are experiences of landscape that will always resist articulation, and of which words offer only a remote echo – or to which silence is by far the best response. Nature does not name itself. Granite does not self-identify as igneous. Light has no grammar. Language is always late for its subject. Sometimes on the top of a mountain I just say, 'Wow.'

Robert Macfarlane in Landmarks, 2015

Broken

It's broken
Seven years
And today I wake up and
It is broken

No
Bash
Bang
Cling
No

Barely noticeable

It's broken
Now
Finally
The spell
Is broken

Silently
Like a bud breaking open
To reveal
Its petals
Its colours
Its blossom
Broken
Like a seal
To reveal
The beauty of a sectretly brewing
Treasure

Vulnerable I feel
Tender
and a bit
Broken
too

Acknowledgements

Like any major project, a PhD cannot be done alone. On my journey I had a lot of help from friends and colleagues. I would like to express my gratitude to them, listed in no specific order.

Dr. Matej Pec and Prof. David Kohlstedt at the University Minneapolis for hosting my visit. Dr. Rüdiger Kilian at the University of Basel for help with thin section scanning. Dr. Kathryn Goodenough at the BGS for her supervision and last minute help with reference letters. Dr. Anne Kelly and Vincent Gallagher at SUERC East Kilbride, for their generous help with the geochemical analyses, and Prof. Rob Ellam for helping me interpret the data. Prof. W. Uwe Reimold and Dr. Lutz Hecht from the Museum für Naturkunde for making analyses possible. Dr. Tanja Mohr-Westheide for organising my stay in Berlin, her patient help with Raman analyses, and useful discussions. Peter at the Museum für Naturkunde, Berlin, for his friendly help with EMPA analyses. Felix Kaufmann at the Museum für Naturkunde, Berlin, for his help with the SEM. The colleagues at the Museum für Naturkunde, Berlin, for their warm welcome, their support and the lunch break entertainment, especially Astrid and Marie. Dr. Nick Hayman from the University of Texas at Austin for discussions and banter. The FAFF research group and my colleagues at the Department for support and ideas, feedback and lunches, and the odd day in the hills, afternoon in the park, evening in the pub.

Financially a lot of the research and especially trips would not have been possible without some generous grants. I would like to thank the Carnegie Trust for the research grant, the Knowledge Transfer Partnership at the University of Strathclyde for funding my trip to Minneapolis, the MacRobertson Scholarship for a grant to go to Berlin, the Geological Society of London for a grant towards fieldwork, and the Barringer Company for travel support to the Bridging the Gap conference and field trip.

During my fieldwork on Barra I had the pleasure to meet and stay with Dan and Maggie Currie and I am eternally grateful to them for looking after me, the

tatties, stories and moral support. Tapadh leibh. Thank you Zoë for everything – especially for believing in me when I needed it most, your patience, and letting me follow my own interests. My flat mates were responsible for keeping me sane, and I am sooo grateful for our friendships, eating together, your appreciation of my procrastinative meal production, and countless hours of discussions and laughter and music and space travels. Thank you Isla for your good advice and your positivity. Thanks to Ali especially in my early days in Glasgow for being a never ending source of information and help, and sharing our love of the mountains, field trips and wilderness. Thanks to the Italian community at the department, for sharing olive oil and chocolate, and to the Bright Night Circus school for sharing their skills and keeping my brain and body balanced. Thank you to my parents who made this all possible in the first place.

Abstract

This study investigates the origin of the quasi-conglomerate pseudotachylytes in the Lewisian Gneiss on Barra, Outer Hebrides, Scotland. These exceptionally large pseudotachylytes have either been ascribed to the Outer Hebrides Fault Zone (OHFZ) or considered to be at a distance from the OHFZ. The Barra quasi-conglomerates visually resemble the Sudbury Breccia and the Vredefort pseudotachylytes, both of which are situated in and related to two of the largest impact structures known on Earth. This thesis examines the evidence for an impact related origin of these enigmatic rocks.

A nested multi-scale mapping method was developed to capture the extent and structures of the pseudotachylytes. On the macro scale, outcrops in one square kilometre were mapped using a colour code for the pseudotachylyte mode of occurrence. Pseudotachylyte veins, networks and quasi-conglomerates were distinguished. Meso scale maps covered 10 x 10 cm, 30 x 30 cm or 1 x 1 m and were used to calculate the amount of pseudotachylyte (sensu stricto) versus clasts and host rock, with a resolution of up to a millimetre, and to document and illustrate structures and clast rotation. Thin sections were used for microstructural analyses by optical and electron beam microscopy. Stereographical data was collected to document a potential relationship between pseudotachylyte veining and pre-existing anisotropies. Geochemical analyses of the Sm / Nd and Rb / Sr isotopes were performed to exclude a fluid assisted process of quasi-conglomerate formation or a remobilisation during the later intrusion of the abundant dykes.

In the mapped area, all outcrops show some degree of pseudotachylyte occurrence. The quasi-conglomerates are found in two thirds of all outcrops and seem to occur in three quasi-continuous, foliation parallel zones. However, due to the outcrop situation, the preferential exposure of quasi-conglomerates on vertical outcrops, and their complicated three-dimensional nature and lack of a clear boundaries, it was not possible to map these zones with the methods available. Between 1 and 14% of the mapped square kilometre consists of pseudotachylyte sensu stricto. The meso and micro structures point to a formation of pseudotachylyte in situ rather than intrusion from an external generation locus. There

is a markable lack of finite shear displacement, apart from clast rotation. Pseudotachylyte formation appears to have been initiated by two separate processes: mafic minerals melted (though seemingly not by contact melting), producing a dark, opaque fluid characteristic for pseudotachylyte, and felsic minerals deformed cataclastically, forming a granular fluid. The two visually and geochemically different fluids mingled, creating schlieren or flow structures, and eventually mixed. The initial processes of mafic melting and felsic cataclasis continued to be initiated during progressive deformation. The results of the isotopic analyses confirm the formation of the quasi-conglomerates in a closed and dry system without later remobilisation.

The observations suggest that the quasi-conglomerates formed by seismic shaking rather than frictional (heat induced) melting along a (super) fault. Visually, in terms of size, and in terms of amount of pseudotachylyte sensu stricto, the quasi-conglomerates are more similar to the pseudotachylytes from two of the largest impact structures on Earth than to any documented fault related ('tectonic') pseudotachylytes. There is a strong likelihood that the quasi-conglomerates formed during an impact cratering event.

Contents

Chapter 1

Introduction

1.1 The Research Context

Pseudotachylytes are dark, aphanitic rocks with a flinty appearance. They occur in structural discontinuities and generally contain fragments of the host rock. Pseudotachylytes have been described from a variety of settings, and with a variety of definitions, for over a century. Shand coined the term pseudotachylyte in 1916, where he compared rocks from Vredefort (South Africa) to fault-related 'trap-shotten gneiss' from India and 'flinty crush rock' from Scotland (Shand, 1916). The Vredefort rocks examined by Shand are now recognised to have formed during an impact event (Daly, 1947; Dietz, 1961). However the examples Shand examined from Scotland are now thought to have formed on faults during the collapse of a caldera (Kokelaar, 2007; Muir, 2017), but others debate if they are actually pseudotachylytes (Burt and Brown, 1997).

Some of the Vredefort pseudotachylytes described by Shand (1916) fall in Sibson (1975)'s geometric pseudotachylyte classification category of 'quasi-conglomerates'. *Quasi-conglomerates* are breccias in which the fragments are commonly well rounded, similar to a conglomerate, embedded in a pseudotachylyte matrix – in the descriptive sense as above. The pseudotachylytes are very large. Shand (1916) measured the size of the pseudotachylytes in inches and feet. In contrast, the common geometry of *fault pseudotachylytes* consists of a fault vein (sometimes called generation plane) – its thickness in the size range of millimetres to a few centimetres (Sibson and Toy, 2006) – and injection veins which come off at high angles to the fault vein.

In the past few decades, pseudotachylytes in 'tectonic' settings have gained lots of attention. Pseudotachylytes that record an offset along a fault are thought to have formed as frictional melts (McKenzie and Brune, 1972; Sibson, 1975; Spray,

1987), with the injection veins acting as sinks for the fluid produced on the fault vein. It has become common in some parts of the literature to use the term pseudotachylyte as if it has a genetic definition (e.g. Gillespie et al., 2011; Campbell, 2016). Such fault pseudotachylytes are interpreted as evidence for paleoseismicity (Cowan, 1999) and are used to constrain earthquake source parameters (e.g. Di Toro et al., 2009). Frictional melts can also form during landslides (Masch et al., 1985). The process of formation is essentially the same as for fault pseudotachylytes, that of heating during frictional sliding. The theoretical limitation of frictional melt production is a fault vein in the order of 2 cm thickness (McKenzie and Brune, 1972). Thus, pseudotachylytes which are thicker than a few centimetres, that is, quasi-conglomerates, cannot be formed as frictional melts on a unidirectional shear fault, unless they represent multiple overprinting events.

In giant impact structures, such as in the pseudotachylyte type locality of Vredefort (Reimold et al., 2017), and the Sudbury impact structure in Canada (Thompson and Spray, 1996), massive volumes of pseudotachylytes have been found of quasi-conglomerate geometry. It is recognised that these quasi-conglomerates formed during the impact event, but it is still debated during which stage of the crater formation they have formed (e.g. Garde and Klausen, 2016; Reimold et al., 2017; Garde and Klausen, 2018; Reimold et al., 2018), and which process is responsible for their formation (Reimold et al., 2016). The pseudotachylytes that have clearly formed during an impact event are sometimes referred to as 'impact pseudotachylytes'. Because they are not associated with faults, in this study they are referred to as *off-fault pseudotachylytes*. The genetic definition of fault pseudotachylytes as friction melts has led some authors to state that there are tectonic pseudotachylytes with a known process of formation (frictional melting). Whereas publications on impact pseudotachylytes often state that while there are tectonic pseudotachylytes which can form by frictional melting during faulting, impact pseudotachylytes need treated separately because they do not fit this definition, and origin. This double use of the therm pseudotachylyte has led Reimold (1998) to the invention of a non-genetic term: 'pseudotachylitic breccias' or PTB, for all pseudotachylytes that are not definitely frictional melts, i.e. fall out of the genetic definition. The term however failed to find acceptance outwith his research group.

Several processes have been invoked to explain field observations of pseudotachylytes. High velocity rock friction experiments have produced frictional melts at 'seismic slip velocities' (Spray, 1987). Amorphous materials resembling pseudotachylytes on the micron scale have been formed in slow creep experiments (Pec et al., 2012). For the quasi-conglomerate geometry of pseudotachylytes, Garde et al. (2015), and Garde and Klausen (2016) propose seismic shaking as the formation process, based on a theoretical paper by (Melosh, 1979) and a

process called 'acoustic fluidization'. However, Reimold et al. (2017) argue for decompression melting, which is unique to the impact cratering process.

Sibson (1975)'s work on the Outer Hebridean Fault Zone is widely cited in the literature on (tectonic, fault) pseudotachylytes. This leads to the underlying assumption that all pseudotachylytes on the Outer Hebrides are 'tectonic friction melts', and the Outer Hebrides have been proclaimed the type locality for tectonic pseudotachylytes (O'Callaghan and Osinski, 2019). This is so, even though it has been stated (Francis and Sibson, 1973; Sibson, 1977b) that there are pseudotachylytes on the Outer Hebrides which are *not* related to the main fault zone, which implies that it is unknown how they have formed. In a circular argument, French (1998) argue that vast volumes of quasi-conglomerates may not be used as proof for impact because of the occurrence of quasi-conglomerates in tectonic settings, such as the Outer Hebrides.

To examine this issue further this thesis focusses on the quasi-conglomerate geometry of pseudotachylytes on the Outer Hebridean island of Barra, specifically in an area which is at a distance of several kilometres from the trace of the Outer Hebrides Fault Zone. The work aims to document characteristics of the Barra quasi-conglomerates which have previously not been documented in detail, and to map their occurrences on three different scales. The results from Barra are compared to other pseudotachylyte and quasi-conglomerate occurrences around the world in terms of volume (outcrop area) and structures, in an attempt to shed light on their origins.

1.2 The Research Question

If pseudotachylytes larger than a few centimetres – that is quasi-conglomerates – cannot be formed as frictional melts unless they represent multiple overprinting events, then what is the origin of the pseudotachylytes on Barra? This question is approached by visiting outcrops of quasi-conglomerates on Barra to conduct, for the first time, a detailed examination of their structures, extent and characteristics. According to Shipton et al. (2019) and Chamberlin (1965), a multi-hypotheses approach is good practice, the following hypotheses can be tested for the origin of the Barra pseudotachylytes.

Hypotheses:

The pseudotachylytes of quasi-conglomerate geometry on Barra, to the West and at a distance to the trace of the Outer Hebrides Fault Zone may have formed

- *origin:*
  - during an impact event,
  - during a single earthquake,
  - during multiple earthquakes,
- *location:*
  - as part of the Outer Hebrides Fault Zone (OHFZ),
  - independent of the OHFZ: older or younger than the OHFZ
- *process:*
  - through frictional (heat induced) melting,
  - through seismic shaking,
  - through an unknown process.

1.3 Thesis Structure

The thesis is organised as follows. Chapter 1 introduces the research question. Chapter 2 gives an introduction to pseudotachylytes, their geological setting and the terminology used in this thesis. In Chapter 3 the field area is described. The four chapters that follow present the data from the field site. Chapter 4 covers the macro scale, a headland on Barra encompassing an area of approximately one square kilometre, Chapter 5 is concerned with the meso scale (outcrop scale, what is visible by eye), and Chapter 6 looks at the micro scale (observations from thin sections, optical microscope and electron microscope). To rule out the association of the pseudotachylytes with the abundant igneous dykes, geochemical isotope analyses were performd which are presented in Chapter 7. In Chapter 8, the volume of pseudotachylyte in the field area is compared to pseudotachylyte occurrences around the world, and the evidence for processes and settings of formation are discussed in the context of the literature.

Chapter 2

Pseudotachylytes

2.1 Characterisation

Pseudotachylytes mark a structural discontinuity. The pseudotachylyte has a sharp contact with its host, which is characteristic for cataclastic fault rocks and is in contrast to more viscous fault rocks like mylonites. Following the 'British Geological Survey scheme for classifying discontinuities and fillings', pseudotachylytes are classified as fault rock fillings (Gillespie et al., 2011). In the field, pseudotachylytes might be difficult to distinguish from ultramylonite and ultracataclasite (Mohr-Westheide et al., 2009; Kirkpatrick and Rowe, 2013). The nature of the fault rock filling is generally dark in colour and has a vitreous flinty appearance in the outcrop. Pseudotachylytes are aphanitic. Fresh pseudotachylyte is often black, or dark grey with potentially a greenish hint. Pseudotachylyte weathers to reddish-rusty, grey or greenish to turquoise, and may look very similar to weathered gneiss or igneous dykes. Host rock fragments are often suspended in the matrix, with a broad range of shape and size, the latter obviously limited by the extent of the fault. These host rock fragments may contain cracks filled with pseudotachylyte. Flow structures may occur, but no lamination. In the outcrop, and similarly on the micro-scale, pseudotachylytes occur in a variety of geometries. In two dimensions, i.e. on a surface, the geometries can be roughly put into two categories:

- linear features such as veins, faults, lenses, cracks
- features that are non-linear, such as blebs, breccias or quasi-conglomerates

In his seminal publication, Sibson (1975) published a variety of geometries which are commonly referred to in the literature and are shown in Figure 2.1.

The term pseudotachylyte can be an ambiguous term because of it is often used with a genetic implication. "Injection veins" is another example of genetic

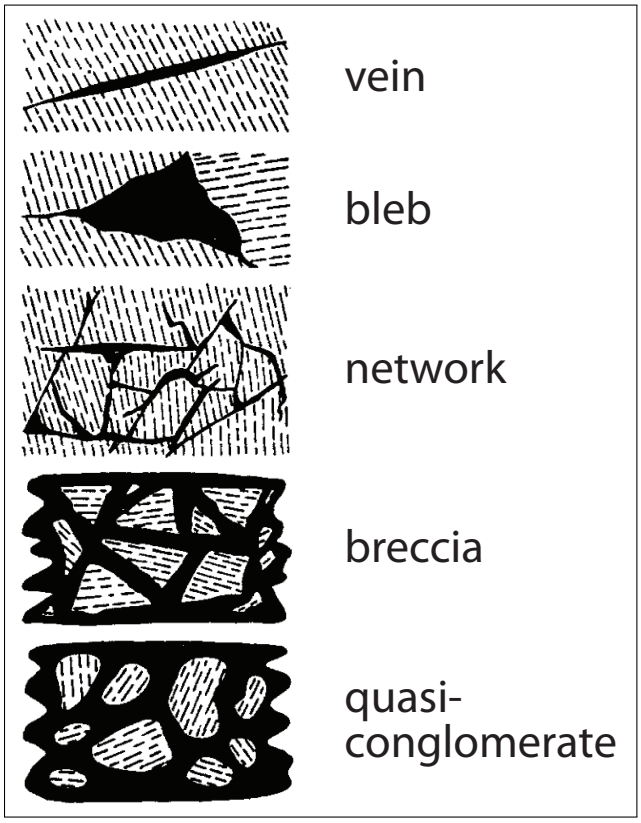

Figure 2.1 – A range of pseudotachylyte geometries after Sibson (1975), part of his Fig. 2. Veins ("lenses") occur both discordant and concordant.

terminology. "Injection vein" has a genetic association - that the filling has been injected into these veins. This genetic interpretation has been used to estimate shear strain on a fault (Rowe et al., 2012). However, injection vein also refers to a specific geometry shown in Figure 2.2. A long vein, the fault vein, has shorter injection veins coming off at high angles. Sometimes these injection veins occur only on one side, sometimes on both sides. They may have regular spacing or not.

2.2 Tectonic Pseudotachylytes

"Tectonic" pseudotachylyte it is a term commonly used in the literature, to make a distinction from "impact" related pseudotachylytes, which are described in the following Section 2.4. The geometry generally associated with tectonic pseudotachyytes is the fault vein - injection vein geometry (Figure 2.2). The fault vein is sometimes called the generation surface or fault plane. In this thesis, these

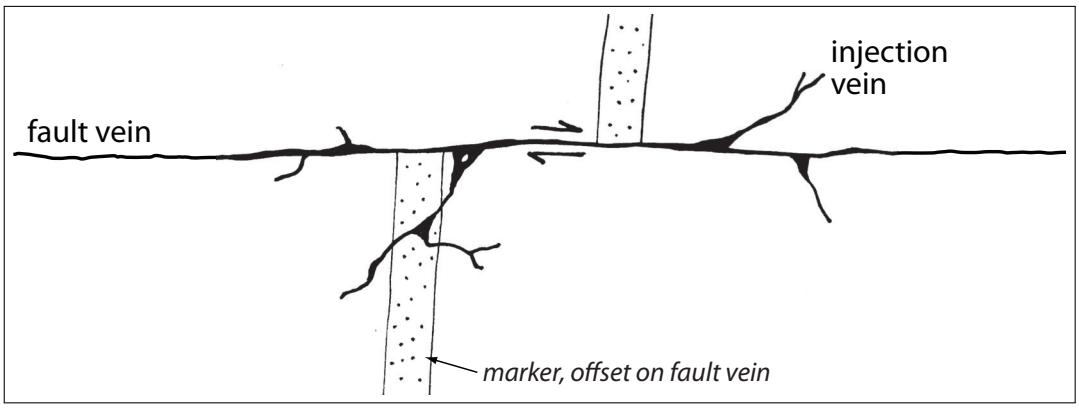

Figure 2.2 – Schematic drawing of the relationship between pseudotachylyte fault vein (horizontal) and injection veins. After Sibson (1975), from his Fig. 2.

pseudotachylytes are called *fault pseudotachylytes*[1]. Pseudotachylytes often occur inside or at the boundary of cataclastic shear zones (e.g. Niemeijer et al., 2012), or mylonitic shear zones (e.g. Bestmann et al., 2011). Many fault-related pseudotachylyte geometries are described as thin, planar to lensoid fault planes with irregular injection veins offshooting at high angles (e.g. Sibson, 1975). Although this geometry is also found in (ultra-) cataclasites (Rowe et al., 2012), it is one of the characteristic features of pseudotachylytes (Kirkpatrick and Rowe, 2013). Numerous studies of fault zones document pseudotachylyte occurrence in a variety of host rocks (see e.g. compilation in Sibson and Toy, 2006). It has been proposed that pseudotachylyte occurrence might be more common than reported upon (Kirkpatrick et al., 2009). The freshly glacier-polished outcrops of the Gole Larghe Fault in the Italian Southern Alps are laced with pseudotachylytes and cataclasites, as has been documented in detail for an area of 200 m^2 by Di Toro and Pennacchioni, 2005, (see their Figure 4). Allen (2005) investigated the pseudotachylyte bearing fault zones of the Homestake shear zone in the southern Rocky Mountains, USA, where the pseudotachylytes occur in conjunction with a variety of fault rocks, including mylonite, ultramylonite, and subordinate cataclasite and breccia. His detailed and multi-scale mapping revealed that the pseudotachylyte fault zones add up to a cumulative length of 21 kilometres in a 170 m x 7.3 km outcrop belt. The maximum thickness of one pseudotachylyte was reported to be 39 cm (Allen, 2005). However Sibson and Toy (2006) review literature on the thickness of pseudotachylytes and find that the vast majority of pseudotachylytes are between 1mm and 50mm thick. (Rowe et al., 2005) describe a “massive” and “large scale” pseudotachylyte of 4 cm thickness.

[1]Terms that are newly defined for a certain usage in the context of this thesis are printed in *italics*.

2.2.1 Formation of Fault Pseudotachylytes

In his seminal paper 'Generation of Pseudotachylyte by Ancient Seismic Faulting', Sibson (1975) uses field observations, thin section analyses and theoretical studies to show that pseudotachylytes are "the products of earthquake faulting". Sibson (1975) finds an empirical relationship between the thickness of a pseudotachylyte (i.e. its fault vein) and the slip along this vein. The proposed concept is that friction at the rock interfaces produces heat during rapid (1 m/s) slip which in turn melts the rock. Frictional melting is widely accepted as the formation process of pseudotachylytes (Magloughlin and Spray, 1992), during rapid – in the order of 1 m/s – shear displacement along a fault. Fault-related pseudotachylytes have been described as the unly unequivocal evidence in the rock record that represents the traces of paleo seismic events (Cowan, 1999). In many publications, pseudotachylytes are used synonymously with "friction melt rocks" or "frictional heat induced melt" (e.g. Gillespie et al., 2011; Kirkpatrick and Rowe, 2013). Theoretical considerations estimate that the thickness of the melt layer could be between 2mm and 10mm (McKenzie and Brune, 1972; Melosh, 2005). Melt transport (for example for injection into veins or pooling (see next paragraph) over distances of the order of a metre would require a melt viscosity of fresh motor oil (Melosh, 2005). It has been pointed out by many (e.g. Maddock, 1992; Spray, 1995; Reimold, 1995; Thompson and Spray, 1996) that comminution (cataclasis) and frictional melting (heat) both play a role in the formation of shear fracture pseudotachylytes.

More complex geometries such as pseudotachylyte networks are thought to form by bridging of (sub-)parallel fault planes and their interconnection with fractures and injection veins. Where displacement continues, Sibson (1975), following Francis and Sibson (1973), suggested that the melt which is formed on the fault plane is discharged into dilational jugs when the network is losing cohesion, forming quasi-conglomerate geometries (Figure 2.3). Techmer et al. (1992) propose that quasi-conglomerates (their "vein breccias") develop as a result of the formation of pull-apart structures between two major fault planes Figure 2.4. If pseudotachylytes form solely by frictional melting, both of these sequences require continuous displacement, maintaining friction in the fault plane, and a mobility (i.e. viscosity) of the frictional melt that allows for transport to the dilational site.

Because pseudotachylytes are regarded as evidence for fossilised earthquakes (Cowan, 1999) they have gained a lot of interest in the recent decades. Data collected from pseudotachylytes has been used to establish earthquake source parameters, including the magnitude of earthquakes (e.g. Kanamori and Brodsky, 2004; Kirkpatrick et al., 2009; Heaton, 1990; Campbell, 2016) and O'Hara (2001) proposed the use of pseudotachylytes as a geothermometer.

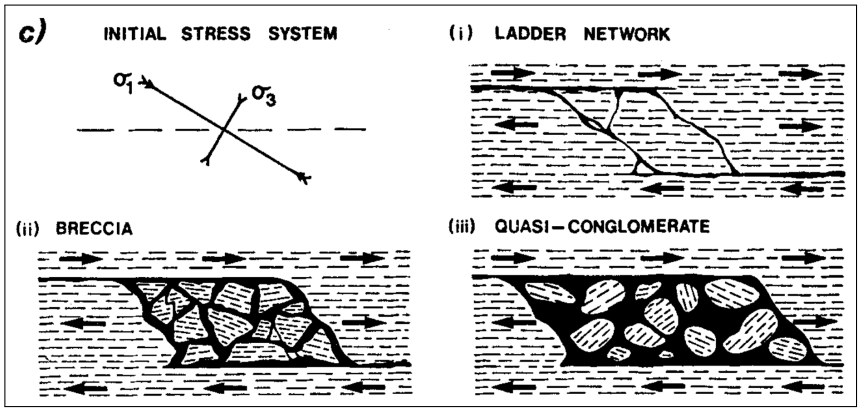

Figure 2.3 – Formation sequence of quasi-conglomerates (Sibson, 1975, his Figure 2). Quasi-conglomerate forms in dilational jugs during continuous unidirectional displacement along a paired fault system.

2.3 Artificially Produced Pseudotachylytes

In 1987, Spray published the first article on artificially produced pseudotachylytes by means of friction welding. The method had previously been used to join metals and plastics. Spalling, cataclasis and pulverisation were commonly observed as (initial) by-products of artificial pseudotachylyte formation (Spray, 1987, 1992, 1995). Spray (1995) established that pseudotachylyte forms in a strain rate window between pure comminution and "shock" veins which consist of 100% melt (Figure 2.5). Pseudotachylytes are thus formed by a combination of "fracture *and* fusion" (Spray, 1995). The result is a polyphase suspension, a fluid made up of rock and mineral fragments and a liquid phase. Spray argues that phyllosilicates and inosilicates have lower melting temperatures and lower fracture toughness (Figure 2.6), a combination which makes them less likely to survive as minerals to form clasts. There have been many experiments using high-velocity rock friction apparatus to examine processes along fault surfaces during frictional slip (e.g. Hirose and Shimamoto, 2003; Beeler, 2006; Niemeijer et al., 2008; Di Toro et al., 2012). However it is extremely challenging to set up these experiments at the ambient stress, temperature and fluid pressures that will occur at the depths relevant to earthquake rupture. At a conference in 2016, Spray presented first results on oscillatory friction welding experiments, where apparently pseudotachylyte was formed in a setting without finite displacement. While these experiments do not seem to have subsequently been published, it is evident that rocks resembling pseudotachylytes can be formed by processes other than unidirectional fault slip. These experiments also suffer from the limitation of all rock mechanics experiments in that they cannot explore processes related to rock mass heterogeneity at scales great than a few mm-cm.

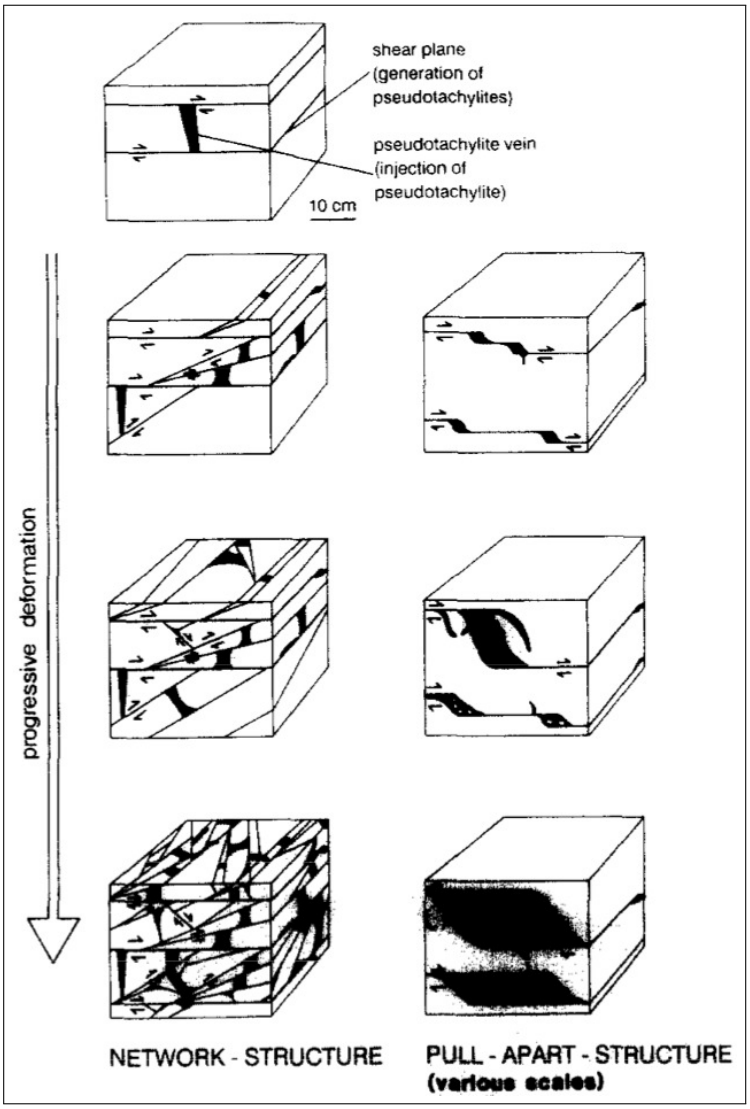

Figure 2.4 – Formation sequence of pseudotachylyte networks and larger bodies of pseudotachylyte (Techmer et al., 1992, their Figure 5).

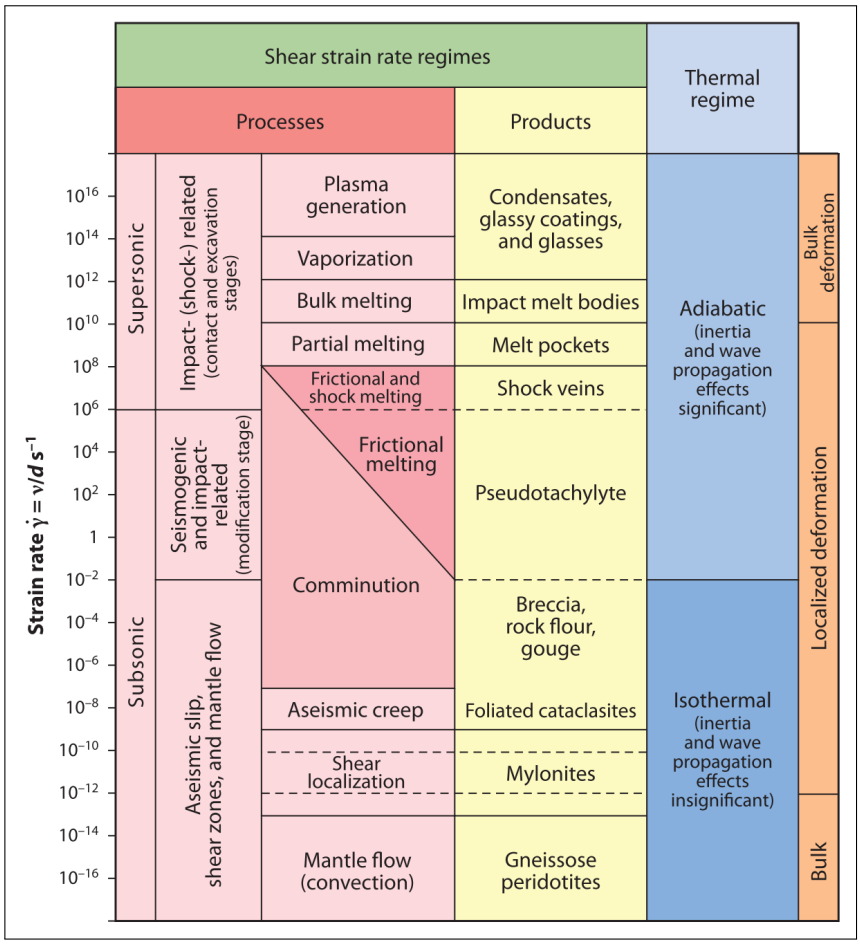

Figure 2.5 – Strain rate versus processes and products and their thermal regimes. Figure 3 in Spray (2010).

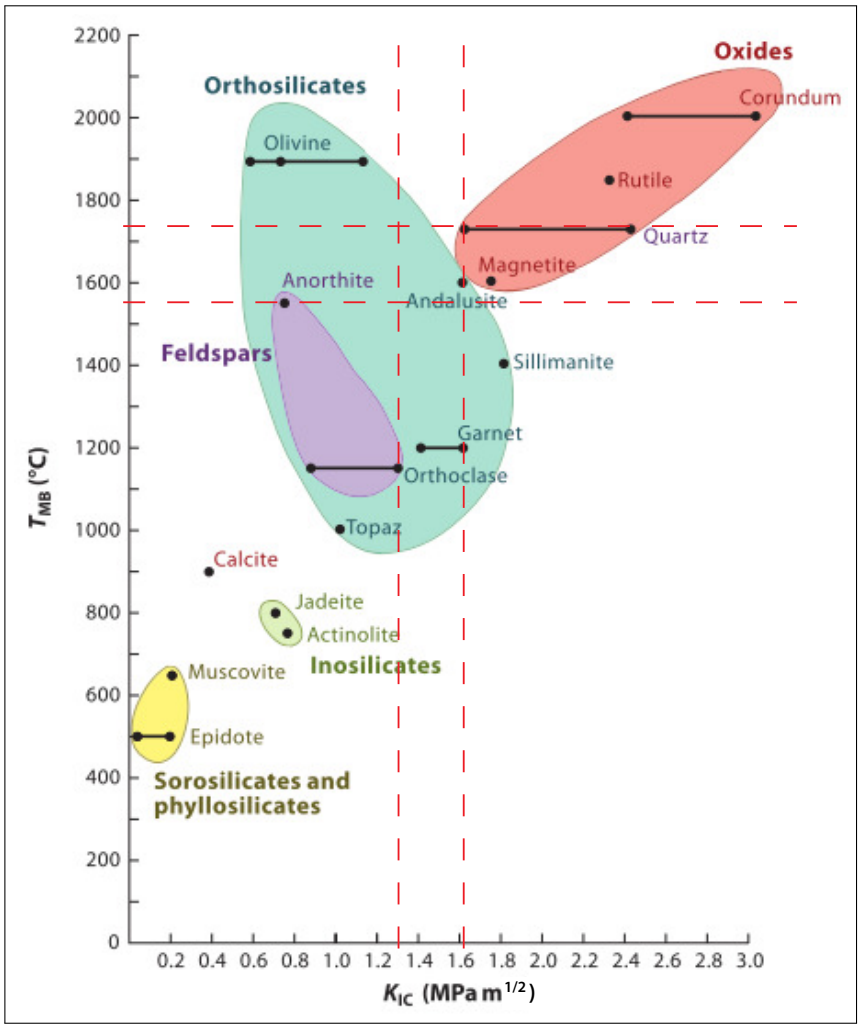

Figure 2.6 – Breakdown or melting temperature versus fracture toughness for a selection of mineral groups. Figure 6 in Spray (2010).

2.4 Pseudotachylytes in Impact Structures

Impact geology is a rather young field of research. Up to the 1960's, the collision of extraterrestrial bodies with the Earth were not considered significant (French, 1998). In the time when Shand coined the term *pseudotachylyte* (Shand, 1916), the Vredefort structure was discussed as a "crypto-explosion structure" (Reimold and Gibson, 1996). The main differences between impact cratering and other geological processes are:

There is an external source of energy, the kinetic energy of the bolide.

The strain rates and wave and material velocities are very high; the maximum impact speed in our solar system is 73 km/s (Collins et al., 2005).

The magnitude of energy released in a very short moment (an impact crater forms within seconds to minutes (Melosh, 1989)).

As long as no *diagnostic feature* for impact (list below) has been found, it is not considered an impact – in dubio pro reo!

2.4.1 Impact Crater Formation

The collision of a solid extraterrestrial body (hereafter called *meteorite*, irrespective of its size) with the Earth creates a *transient crater*, which subsequently collapses to form the *final crater*. Figure 2.7 is a simplified cartoon of the moments "before" and "after" the collisional contact.

The impact cratering event is commonly divided into three stages: the contact and compression stage, the excavation stage, and the modification stage. The final crater is subsequently modified by other geological processes such as erosion or isostatic uplift to form an *impact structure* of past events. The impact structure might or might not have the topography of a crater, or a circular structure of lithologies on the surface. Also geophysical signatures are possible, such as gravity or magnetic anomalies. None of these signatures however represent diagnostic impact features. Small craters (up to approximately 2 km diameter on Earth) are bowl shaped and called *simple craters*. Craters that are larger exhibit more complex geometries and are thus named *complex craters*. Complex craters have a *central uplift*, and may form *multi-ring basins* with terraces formed by normal faulting. Crater formation is a dynamic, non-equilibrium and highly complicated process (Melosh, 1989). The diameter of the final impact crater is approximately 20 times the meteorite's diameter (French, 1998). The web-based computer program *Impact: Earth!* developed by Collins et al. (2005), allows to quickly estimate regional environmental effects of impact events on Earth.

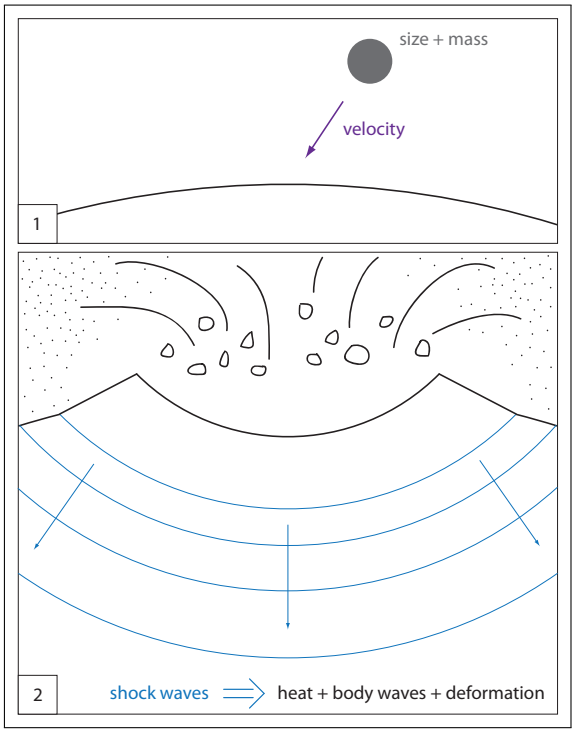

Figure 2.7 – Simplified cartoon capturing the moments "before" and "after" a meteorite impact. Not to scale.
1 – A meteorite with a certain diameter and mass approaches the Earth at a certain velocity.
2 – At the time of contact, the kinetic energy carried by the meteorite is translated into shock waves, body waves, heat, deformation and kinetic energy.

2.4.2 Shock Deformation

One of the aspects that discriminates extraterrestrial impacts from other natural geological processes is the magnitude of the velocities and strain rates. The combination of the short contact time, and the high impact velocity (around 20 km s^{-1}) results in strain rates in the range of 10^6 to 10^9 s^{-1} (Langenhorst, 2002). For comparison: plate tectonic strain rates are in the order of 10^{-9} s^{-1} (Holt et al., 2005; Serpelloni et al., 2005), which is up to 18 orders of magnitude slower. Seismogenic slip velocities on faults are thought to be 1 m s^{-1} (Sibson, 1975). Average fault rupture velocities for large earthquakes are in the order of 3 km s^{-1} (compilation in Heaton, 1990), which is slower than, but in the order of, the speed of sound in rocks (in granite around 6 km s^{-1}). These impact related high strain rates are capable of producing shock waves which are characteristic for impact events. During the collision, the meteorite's kinetic energy is nearly instantaneously and completely translated into other forms of energy. This instantaneous translation of energy creates a shock front which affects both the meteorite and its target, the Earth. The formation of shock waves is characteristic for impact events. Even small meteorites carry a high kinetic energy due to

their high travel velocity.

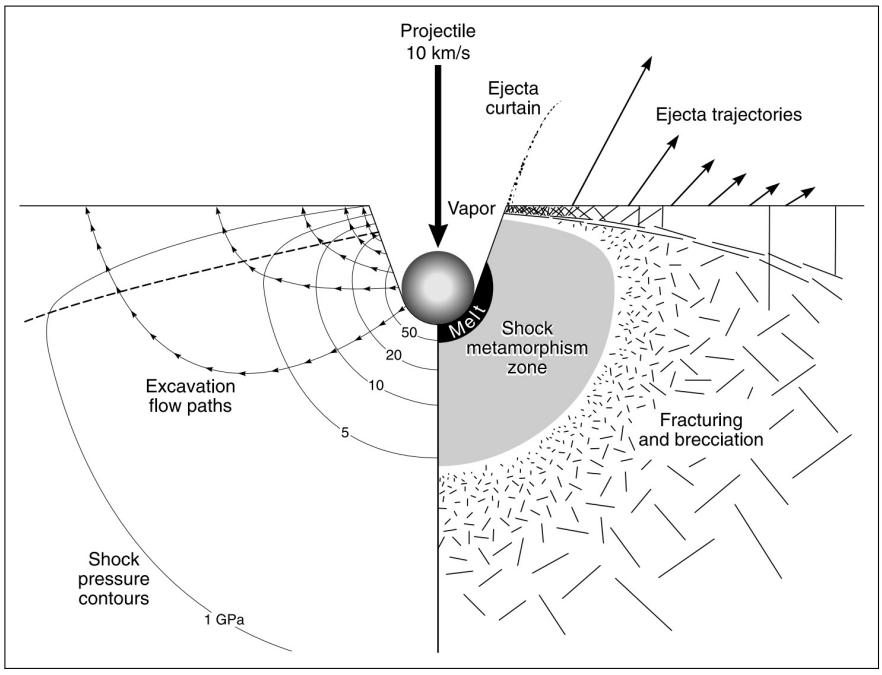

Figure 2.8 – Figure 3.2 in French (1998) – Schematic cross-section showing the contact and compression stage. Shock waves radiate from the projectile-target interface and decline rapidly outward, peak pressure isobars shown on the left side and create zones of distinctive shock effects (right side). From the original interface outward, these zones involve: (1) melting at ¿50 GPa (2) shock-deformation effects (5–50 GPa) and (3) fracturing and brecciation (1–5 GPa).

Shock waves are different to elastic waves in that they travel supersonically, that means faster than the speed of sound for the given medium, i.e. faster than elastic shear waves (e.g. Krehl, 2011). Shock waves are body waves which, unlike elastic waves, are strongly irreversible. A shock front represents an infinite discontinuity, that means, a sudden change, of all state parameters (Melosh, 1989), such as pressure, temperature, specific volume (density), and energy. In contrast to elastic waves, such as seismic waves, shock waves decay rapidly. At approximately the outer rim of an impact crater, shock waves decay to a low enough pressure to transform into low-pressure elastic stress waves, that is seismic waves (French, 1998). It follows that impact cratering events are accompanied by earthquakes. Figure 2.8 shows a schematic cross section of the contact and compression stage of an impact from French (1998). Closest to the projectile, the material melts. Shock metamorphic features (described in the following paragraphs) occur down to approximately 5 GPa, whereas at lower shock pressures the initial shock energy is mainly translated into fracturing. Figure 2.9 represents the second stage in the crater forming process (French, 1998). The dashed lines are the material

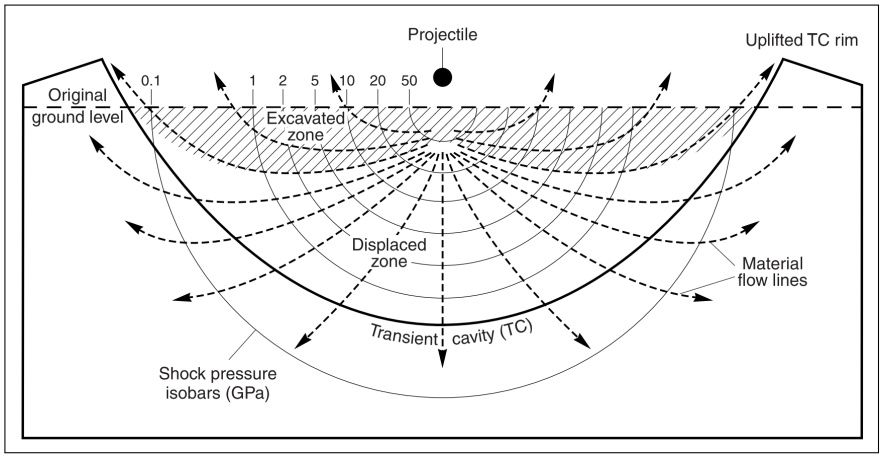

Figure 2.9 – Figure 3.4 in French (1998) – Schematic cross-section showing the excavation stage during which complex interactions of the shock wave, the ground surface, and the subsequent rarefaction wave produce an outward excavation flow (dashed arrows) that opens up the transient crater. In the upper part of this region (excavated zone; ruled area), target material is fractured, excavated, and ejected beyond the transient crater rim. In the lower region (displaced zone), target material is driven downward and outward, and does not reach the surface.

flow lines for the excavation stage. Outside the transient cavity, the material flow lines are mainly directed downwards (in the central part) and outwards, and they terminate before they reach the Earth's surface.

The shock pressures which the target rocks experience are much higher than "normal" static geological pressures. In what is to become the impact crater, large rock volumes experience pressures of 10 to 60 GPa (e.g. French and Koeberl, 2010). These high pressures that are applied nearly instantaneously may evoke shock metamorphic features in the target rocks. A shock metamorphic feature, i.e. a feature which is only formed during a shock event, is considered definite proof (i.e. a diagnostic feature) for impact. Shock deformation is a very heterogeneous phenomenon (e.g. French, 1998). Most shock metamorphic features that are diagnostic impact criteria occur on the micro scale , only shatter cones are mesoscopic features and visible by the naked eye. Shock metamorphic features on the micro scale reflect the interaction of the shock wave with mineral grains.

High Pressure Phases and Diaplectic Glass

In the very high pressure regime close to the point of impact, *bulk melting* occurs, or even closer, the rock volume *vaporizes*. At intermediate (in the context of impacts) pressures, i.e. below around 50 GPa, melting occurs only incipiently (e.g. Reimold and Koeberl, 2014). Some minerals can respond to high pressures

by rearranging their lattice into *high pressure phases*, such as graphite which transforms to diamond, or quartz to coesite or stishovite. The high pressure induced by the shock front can locally cause a plastic behaviour of deformation of mineral grains. This happens where the Hugoniot elastic limit of a mineral is exceeded, and it cannot respond by elastic or brittle deformation. The material loses its shear strength and behaves like a fluid. In the shock pressure regime between 35 and 60 GPa, *diaplectic silicate glass* can be formed (Stöffler and Grieve, 2007). Diaplectic glass is a phase that still has the long-range order of the precursor mineral but is isotropic due to disorder at the atomic scale (Reimold and Koeberl, 2014). Both quartz and feldspars may transform into diaplectic glasses.

Planar Deformation Features and Planar Fractures

At lower peak pressures, between 5 and 35 GPa, quartz and feldspar may exhibit *planar deformation features (PDFs)*. These PDFs, also called *shock lamellae*, are crystallographically controlled micron to submicron planar features, which are glassy and represent former shock induced melt (e.g. Gratz et al., 1988).

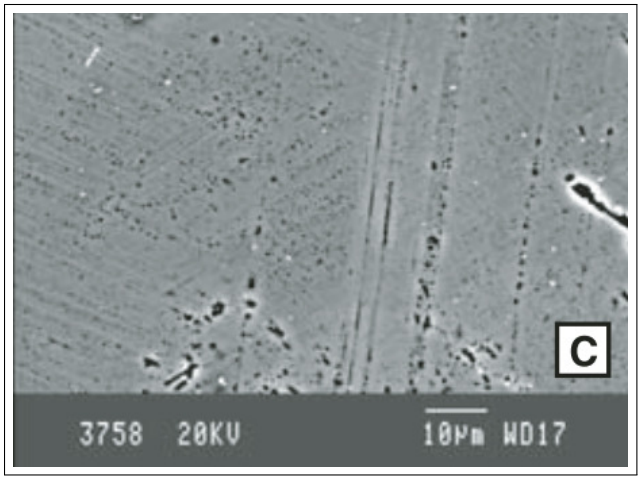

Figure 2.10 – Planar deformation features (PDFs) in quartz, (Amor et al., 2008, their Figure 2).

Planar fractures (PFs) occur at the lower end of this pressure regime in silicate minerals such as quartz and olivine (e.g. Langenhorst, 2002). If shock induced, they are oriented parallel to low index crystallographic planes.

Diagnostic impact criteria – In order to be diagnostic for impact, both PDFs and PFs need to occur in multiple sets in single grains and not cross cut grain boundaries. Planar fractures are more difficult to identify as being shock induced, and their recognition as diagnostic impact criteria is mineral and orientation dependent (French and Koeberl, 2010; Langenhorst, 2002). High pressure

mineral phases (in consideration of the geological context), high temperature melts (>1500°C), diaplectic glasses, and PDFs are recognised diagnostic impact criteria.

Shatter Cones

Only one characteristic shock feature is known from the meso scale. Shatter cones are commonly small, such as displayed in Figure 2.11. The figure shows shatter cones in limestone from the Ries impact crater in Germany. Shatter cones can reach decimetres in length, and form in all rock types, however they preferrably form in homogeneous, small grained and isotropic rocks such as cabonates and quartzites (French and Koeberl, 2010). Shatter cones are penetrating fracture surfaces and form at pressures between 2 and 30 GPa.

Figure 2.11 – Shatter cones in limestone from the Ries impact crater in Germany. Arrow points to apex. Coin for scale is 1.6 cm in diameter.

Extraterrestrial Material

Meterorites carry extraterrestrial chemical or isotopic signals. These elements or isotopes may be detected in impact melt rocks, impact produced breccias, and ejecta, even if they generally occur only in traces (French and Koeberl, 2010). Distinct chemical or isotopic signatures are regarded as conclusive diagnostic impact features.

Ejecta

Some of the target (Earth) material that is excavated during crater formation gets ejected from the site of the crater and is deposited outside the crater rim. The extent of the ejecta naturally depends on the size of the impact and thus the material excavated. For very large impact events, the smallest fraction (dust) of ejecta may be deposited globally as fallout (Glass and Simonson, 2013). This dust gets subsequently deposited as a sediment, which may show increased concentrations of, for example, platinum group elements. This chemical signature led Alvarez et al. (1980) to raise the hypothesis that the Cretaceous-Paleogene (K-Pg) boundary extinction was caused by an impact of a meteorite. It is now generally accepted that the Chicxulub impact structure in the Gulf of Mexico is correlated with the K-Pg boundary extinction (Schulte et al., 2010).

2.4.3 Pseudotachylyte Occurrence in Impact Structures

The impact structure is characterized by its shape and by the occurrence of rocks which have been differently affected by shock. Figure 2.12 shows a schematic cross section through an impact structure and illustrates the localities of pseudotachylyte development (in grey, "zone of pseudotachylytic breccia development"). This diagram is based on the occurrence of large pseudotachylyte bodies in the Vredefort impact structure, which formed as a complex crater.

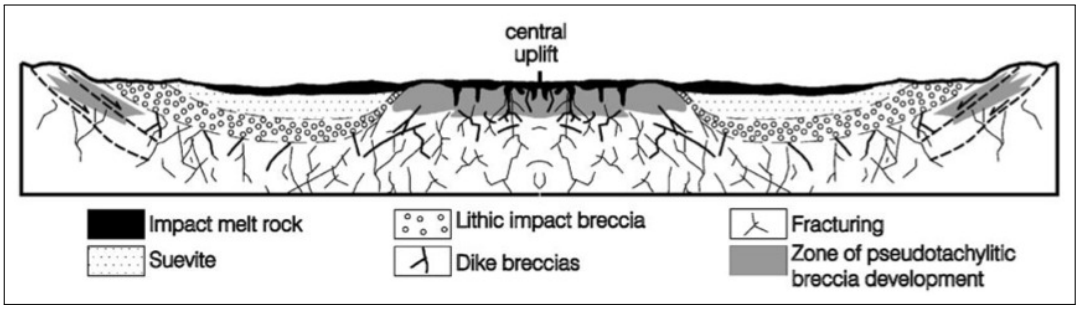

Figure 2.12 – *Cross section through a complex impact crater with central uplift: Figure 1 in Reimold and Gibson 2006.* Note the occurrence of pseudotachylyte ("zone of pseudotachylytic breccia development") indicated by the grey signature.

Figure 2.13 shows only half of the section with the crater rim on the left hand side, and the centre of the crater on the right hand side of the figure. This crater is a simple crater (i.e. smaller diameter). Peak shock pressures are indicated by the labelled circle segments. The distinguishing factors between the dykes (dikes) in the crater floor (intrusive melt dyke, dyke with fragmental impact breccia, and pseudotachylyte) are still a subject of controversy. The shock peak pressures are indicative for the shock metamorphic features to be found. However, the impact is also accompanied by raised temperatures. From bulk melt in the centre, which is deposited as *impact melt*, the rocks range from granulite facies to amphibolite and greenschist facies towards the outer rim. Pseudotachylytes occur both inside the centre of impact structures and at the rim, like for example in the Vredefort Dome (central uplift) and the Witwatersrand Basin (crater rim), see Figure 2.12 (e.g. Reimold and Koeberl, 2014). The pseudotachylytes occur in the upper crater floor of the central uplift, and along fault zones in the outer parts of the structure. The authors of the figures explicitly state that it cannot be excluded that pseudotachylytes also occur below the crater moat (Reimold and Gibson, 2006). Both the Vredefort and the Sudbury impact structures are deeply eroded, however not to a level to reach the crater floor below the moat.

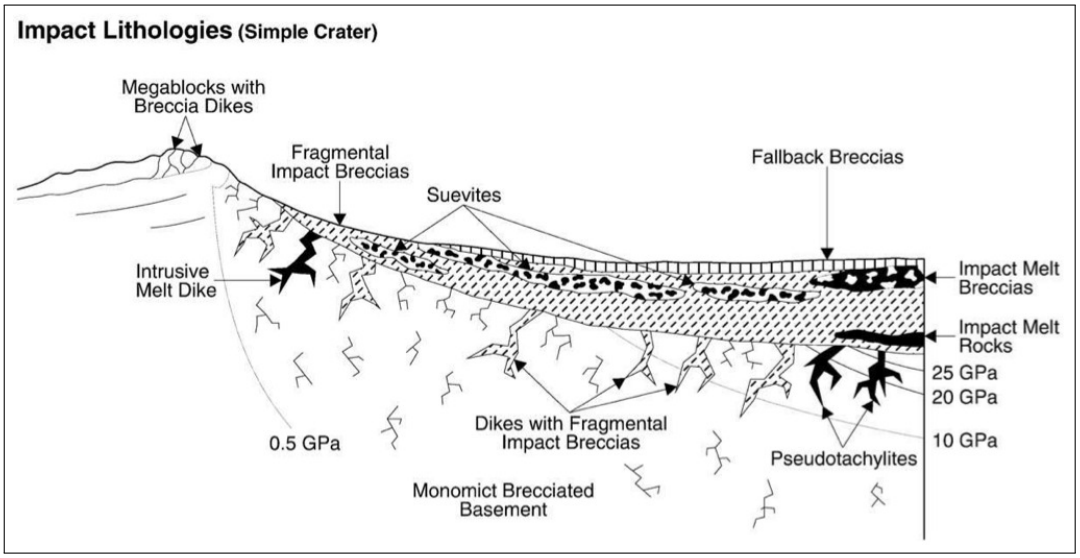

Figure 2.13 – *Half of a cross section through a simple impact crater. Figure 1 in French and Koeberl 2010.* Note the occurrence of a variety of dyke-like rock types in the crater floor.

2.4.4 Pseudotachylyte Geometry, Size and Extent

Some impact-related pseudotachylytes are related to faults that have been triggered by the impact and show typical fault-related characteristics such as a narrow zone of a localized shear displacement , very much alike the aforementioned geometry of tectonic pseudotachylytes. Martini (1991) found the high pressure silica

polymorphs coesite and stishovite in the vicinity of some of these thin pseudotachylyte veins. Other impact-related pseudotachylties are much larger in extent, occur in dyke-like structures, similar to Sibson (1975)'s quasi-conglomerates (Killick and Reimold, 1990; Garde and Klausen, 2016), or exhibit complex, chaotic appearing geometries. These are much less common and only occur in large volumes in the Vredefort and Sudbury impact structure (Reimold, 2012). Figure 2.14 and Figure 2.16 show a couple of examples of the Vredefort pseudotachylytes from the literature, and one from Sudbury in Figure 2.15.

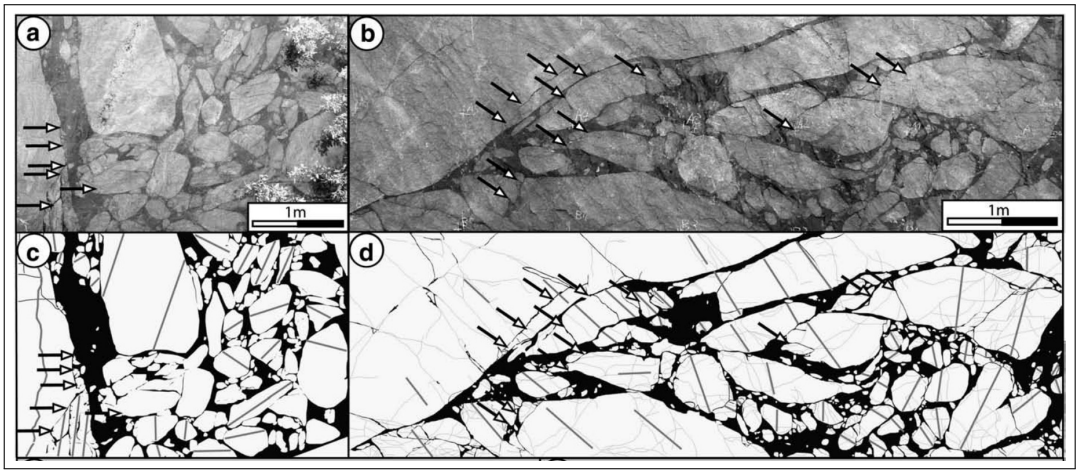

Figure 2.14 – Figure 8 in Lieger et al. (2009) – (a) and (b): pseudotachylyte in quasi-conglomerate geometry from the central uplift in the Vredefort impact structure and (c) and (d) respective digitised maps. Grey lines indicate traces of pre-impact planar mineral fabrics used to indicate rotation of fragments.

In both Vredefort and Sudbury impact structures, the pseudotachylytes with quasi-conglomerate geometry (henceforth: quasi-conglomerates) occur in a central part, and in one or several zones at a distance of tens of kilometers from the geometrical centre of the impact structure. Figure 2.17 shows a map of the distribution of pseudotachylytes in the Vredefort impact structure by Killick and Reimold (1990). The authors note that the pseudotachylytes in the Witwatersrand Basin (the SW-NE trending zone SW of Johannesburg) are more commonly associated with faults and other deformation such as mylonites and cataclasites. The Southern continuation of this pseudotachylyte zone is characterised by an abundance of mylonites and a marked absence of pseudotachlytes. It should be noted that the vast majority of published photographs of quasi-conglomerates with reasonable quality stems from the central uplift of the Vredefort structure, which coincides with the abundance of pseudotachylytes around Vredefort in Figure 2.17. Figure 2.18 illustrates the quality of some of the photographs from the literature of quasi-conglomerates from Sudbury and from the Vredefort occurrences outwith the central uplift. There is a noted absence of field photographs

Figure 2.15 – Figure 9c in Rousell et al. (2003) – Sudbury Breccia with pseudotachylyte matrix. Hammer for scale.

in particular of quasi-conglomerates in Fletcher and Reimold (1989); Reimold et al. (1999).

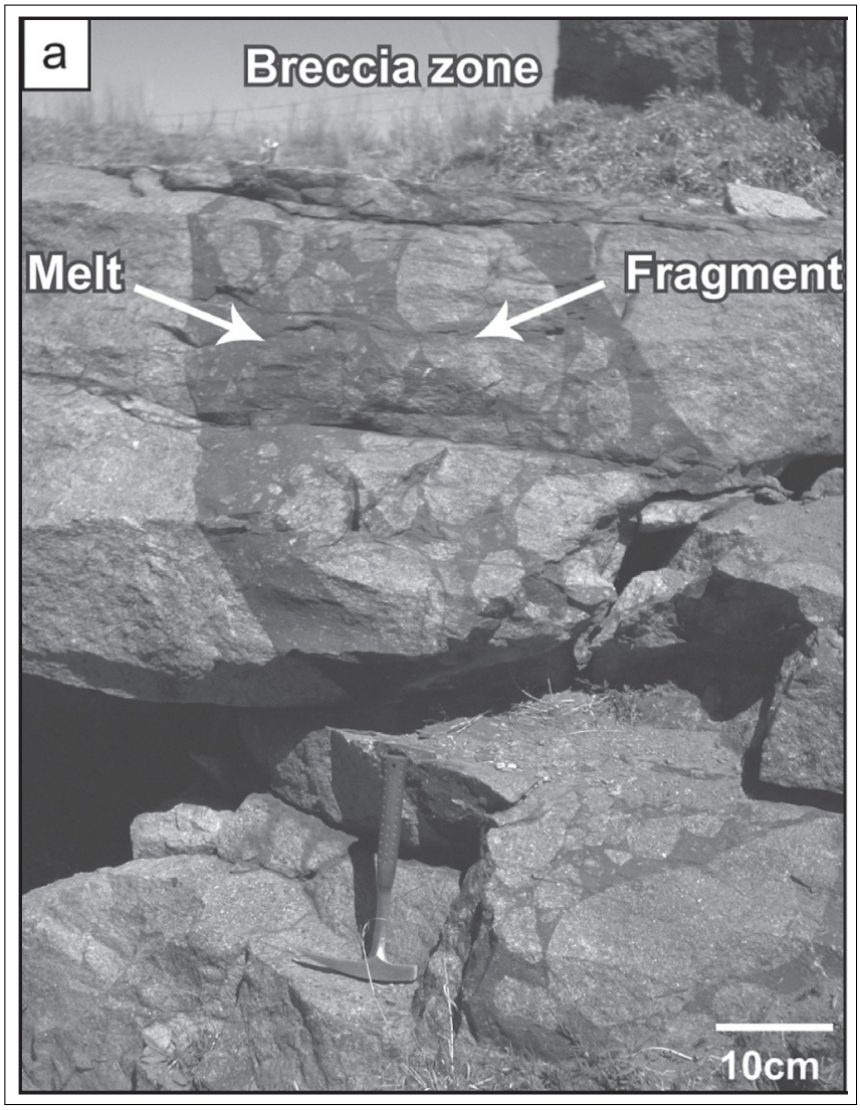

Figure 2.16 – Figure 2a in Mohr-Westheide et al. (2009) – Pseudotachylyte in quasi-conglomerate geometry from the central uplift in the Vredefort impact structure. Melt refers to matrix.

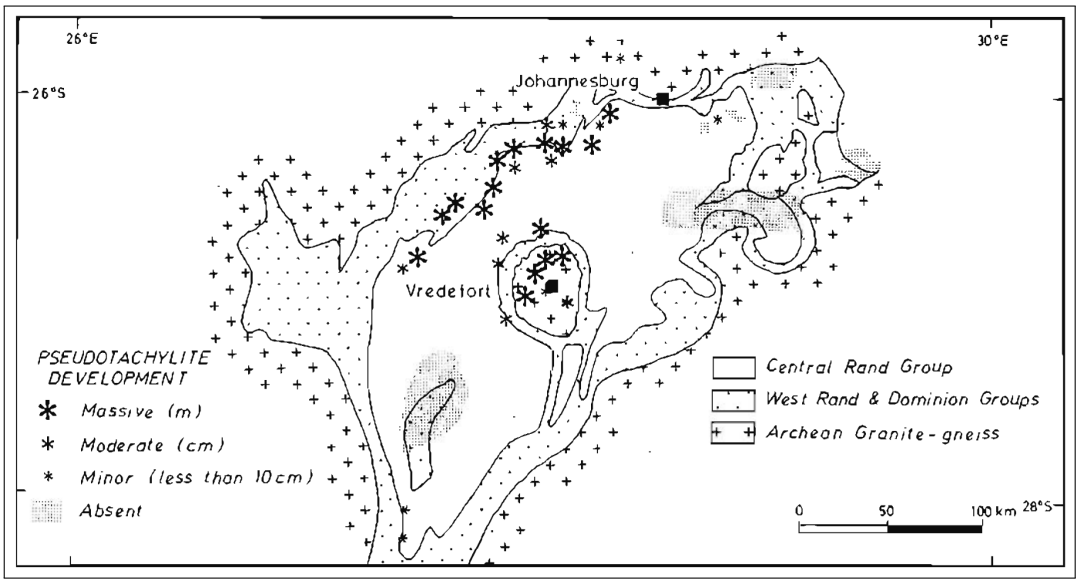

Figure 2.17 – Figure 5 in Killick and Reimold (1990) – Map of the area of the Vredefort impact structure indicating the occurrence of pseudotachylyte. Note an abundance of pseudotachylyte in the central uplift – the central circular structure around Vredefort itself – and a second abundance in a SW-NE trending zone NW of Vredefort. This zone is sometimes referred to as the Witwatersrand Basin pseudotachylyte zone.

Figure 2.18 – Figure 3b in Killick and Reimold (1990) – Photograph of a quasi-conglomerate from the Witwatersrand Basin to illustrate the poor image quality in many publications.

2.4.5 Formation of Pseudotachylytes in Impact Structures

It has been suggested that these large pseudotachylyte bodies form in a similar manner to the thinner, fault pseudotachylytes, for example by bridging of parallel faults (Sibson, 1975) and forming pull apart structures (Techmer et al., 1992). Based on the comparison with extraterrestrial impact structures, Spray (1997) proposed the 'super fault' hypothesis, where metres to tens of metres thick pseudotachylyte zones are thought to accommodate displacement of several kilometres. Theoretical considerations have shown that the frictional melt production is limited by (1) the amount of melt that can be produced on a frictional interface (McKenzie and Brune, 1972) and (2) the viscosity of the melt if it was discharged from the fault (Melosh, 2005) (see also Section 2.2.1). A number of processes have been proposed for the formation of pseudotachylytes which do not exhibit a relationship with a fault (in the following: "off-fault pseudotachylytes"). Some of the processes are unique to the impact cratering setting, such as decompression melting (e.g. Reimold et al., 2017) or flash replacement melting (Dressler and Reimold, 2004); whereas seismic shaking and acoustic fluidisation have been proposed for the formation of both cataclasites (pulverised rocks, e.g. Mitchell et al., 2011), fault pseudotachylytes (Garde et al., 2015) and off-fault pseudotachylytes (Garde and Klausen, 2016). These processes are discussed in more detail in Chapter 8.

2.5 Pseudotachylyte Terminology

In the literature the definition of pseudotachylyte commonly entails the genetic aspect of friction melt, despite the above mentioned limitations of the classic idea of unidirectional friction melting on an interface. Gillespie et al. (2011), for example, in the *British Geological Survey scheme for classifying discontinuities and fillings* state "Pseudotachylyte is a cataclasite produced by frictional heating and melting (through extreme cataclasis) followed by quenching; the result is a highly strained but non-foliated rock consisting typically of fine clasts enclosed in glass; in hand specimen, the glass is generally cryptocrystalline, vitreous-looking material, with a black, flinty appearance." A genetic definition is useful in the sense of Schmid and Handy (1991) in that it alone provides the tools to distinguish and categorise the entirety of fault rocks. It may also prove a hinderance in both communication and the advance of science (e.g. Reimold, 1998), if the definition is treated as a end product and not seen as a dynamic construct which requires continuous review. In the case of pseudotachylytes, ongoing debate concerns formation of the quasi-conglomerates and other off-fault occurrences of pseudotachylytes. This has led Reimold (1998) to introduce the term "pseudotachylytic breccia", abbreviated to PTB, which encompasses all off-fault pseudotachylytes. However, the term has not found much use in the scientific community outwith his research group.

One of the difficulties of genetic definitions of fault rocks is that they may be based on analytical tools which are not available in the field, such as microscopy. In certain circumstances it is necessary to have a terminology available for the field, which might differ from a terminology based on laboratory analyses. In the Sudbury impact structure this was solved by the term "Sudbury Breccia", which covers all brecciated rock related to the impact structure and does not as such differentiate between cataclasite and pseudotachylyte. In Vredefort the case seems more complex not least because of the presense of so-called Granophyre dykes which are dykes of impact melt (i.e. melt from the contact of the bolide with the Earth) which have brecciated and intruded the country rock and look very much like quasi-conglomerates. The rocks in the Outer Hebrides have been described as flinty crush rock (e.g. Jehu and Craig, 1924) or crush zones, which have both the genetic implication of an aspect of brittle deformation, however these terms do not specify the nature of the matrix. In this thesis, the term pseudotachylyte is used as a descriptive umbrella term for an aphanitic fault rock with flinty appearance which may occur in different geometries. Potentially, some of the rocks here classified as pseudotachylytes are actually ultracataclasites, because the distinction in the field cannot always be made.

Chapter 3

Field Area

3.1 Geography

3.1.1 Outer Hebrides

The Outer Hebrides form an island chain off the North West coast of Scotland (Figure 3.1). Barra is the southern most inhabited island of the Outer Hebrides with a diameter of about five to ten kilometres.

3.1.2 Barra

Figure 3.2 shows the Isle of Barra. Castlebay is situated in the South of the island and is the main town, which is served by a ferry from Oban on the main land. The archipelago is separated from the Scottish mainland by the Minch trough. The North Atlantic Ocean lies on the West, dominating the maritime climate of the islands. The highest point on Barra is Heabhal at 384 metres above sea level, located approximately one mile NE of Castlebay. Most of the data presented in this thesis was collected on Greian Head / Àird Ghrèin, a headland on the NW corner of Barra.

3.1.3 Barra's Landscape

The land surface on Barra is boggy and rocky, with sandy and pebbly beaches and cliffs mainly along the shore. Heather and moorland cover the land. Figure 3.3 shows some photographs of Barra to illustrate the landscape. Figure 3.4 on page 31 shows photographs of the headland Àird Ghrèin where most of the data in this study was collected.

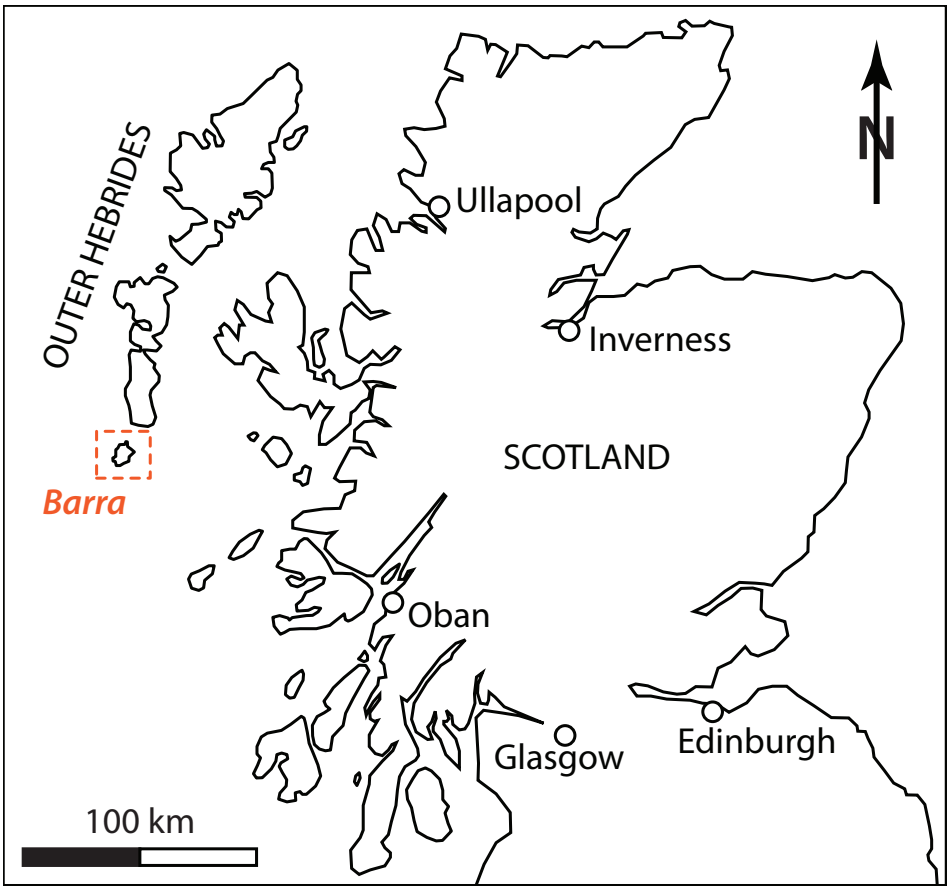

Figure 3.1 – Map of Scotland showing the Outer Hebrides including the locality of this study, Barra.

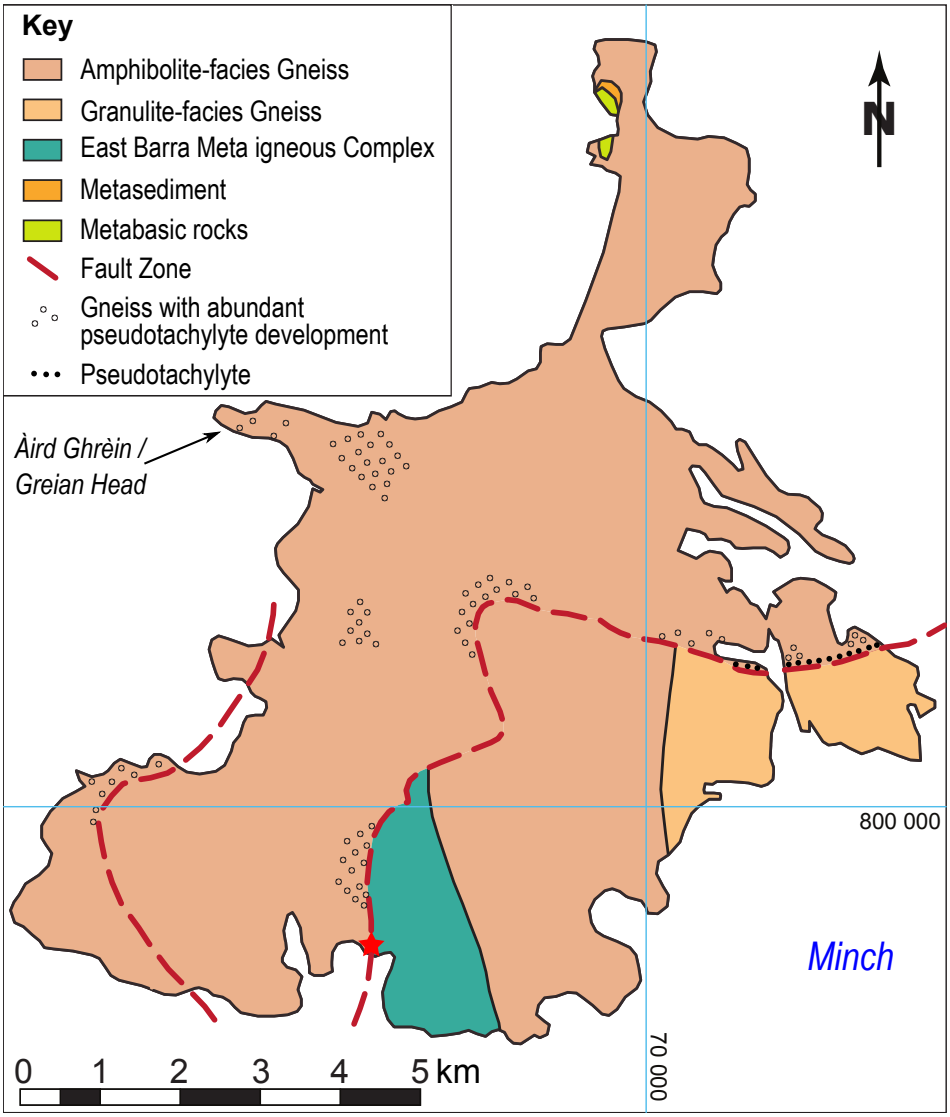

Figure 3.2 – Geological map of Barra after the British Geological Survey (BGS, 1981). The red star indicates the location of the main town Castlebay. Greian Head / Àird Ghrèin is the headland where most of the data in this study stems from.

Figure 3.3 – Photographs of Barra to illustrate the landscape.
A: Ben Martin / Beinn Mhartainn viewed from the Golf Course (photo SSE) (Photo locality: NF 657 041). **B**: View ENE from the shore at Cleat / Cleit, just East of Greian Head (NF 665 049). **C**: Bagh a' Chaisteil / Castlebay (photo W) (NL 665 982). **D**: Bagh a' Chaisteil / Castlebay (photo W) (NL 665 982). **E**: Barra's airport is the only one in the world where scheduled flights use a beach as the runway (NF 694 059). **F**: View from behind Castlebay ENE towards the highest point of the island, Heabhal / Heaval at 383 m (Heabhal: NL 678 994).

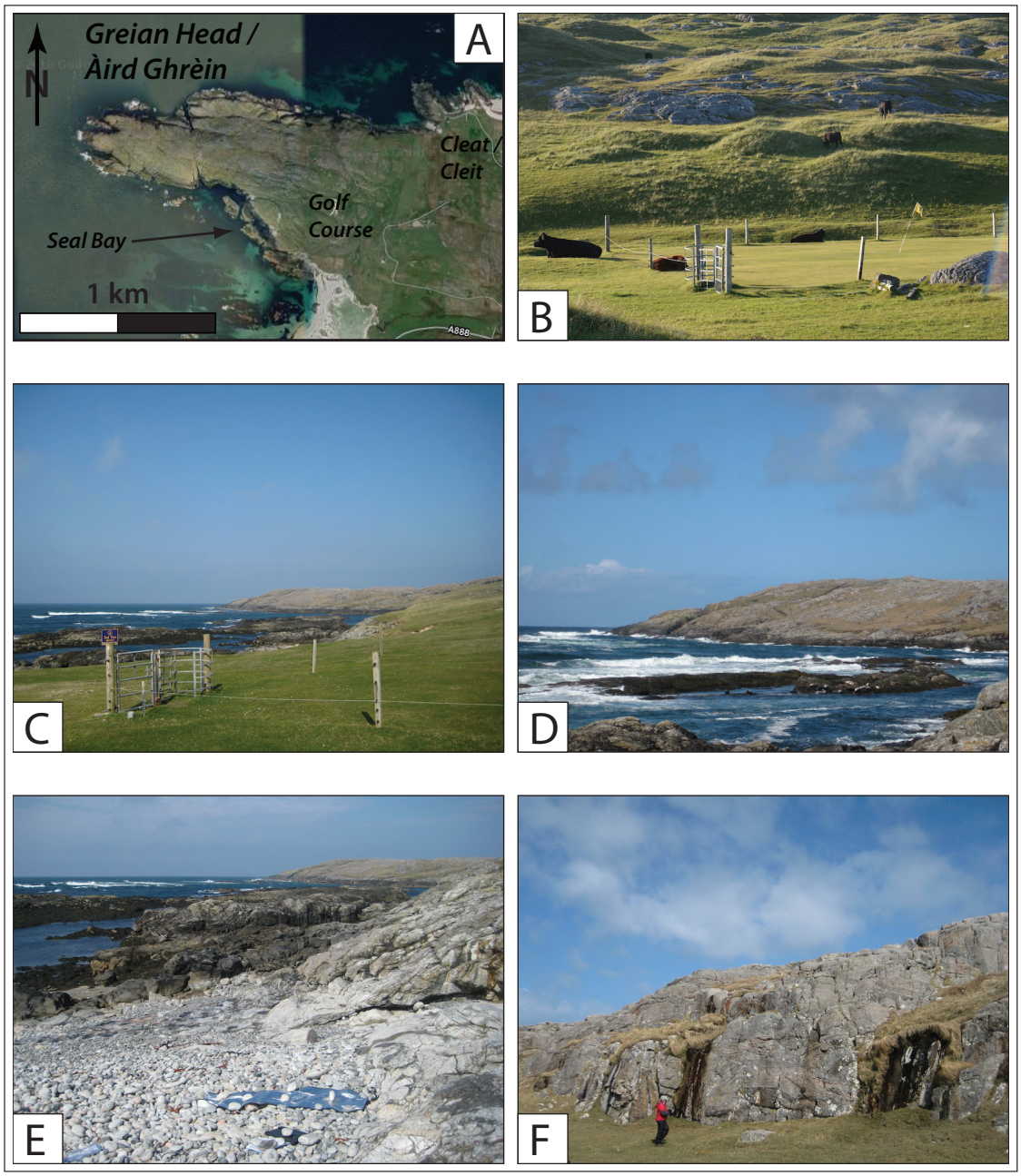

Figure 3.4 – Photographs of Greian Head / Àird Ghrèin to illustrate the landscape.
A: Google Satellite map of Greian Head / Àird Ghrèin (Google Maps). The Golf Course and Seal Bay are indicated. **B**: Outcrop situation on the Golf Course (NF 660 042). **C**: Looking WNW from the Golf Course, with Seal Bay and the tip of the headland in the background (NF 656 042). **D**: Seal Bay (looking NW) with seals (NF 656 042). **E**: Seal Bay (looking NW) at low tide (NF 656 042). **F**: NW of the Golf Course is the highest point of the head land. The landscape forms terraces with small cliffs. Photo taken W of the highest point looking NNE (NF 657 046).

3.2 Geology

3.2.1 Summary

Lewisian Gneiss is the oldest basement rock of Scotland and is the lithology which makes up the majority of the Outer Hebridean island chain. Lewisian Gneiss also crops out along the shore on the North West coast of Scotland. The pseudotachylytes have developed in Lewisian Gneiss. The Outer Hebrides Fault Zone is the structure to which most of the Outer Hebridean pseudotachylytes are asigned to, however, not the ones on Àird Ghrèin.

3.2.2 Lewisian Gneiss

The Lewisian Gneiss Complex is of Archean-Palaeoproterozoic age and represents some of the oldest rocks on Earth. Ages range from 2.9 Ga to 1.6 Ga. These crystalline basement rocks constitute most of the Outer Hebrides, two islands of the Inner Hebrides, Coll and Tiree, and also crop out on the North West coast of Scotland, in Greenland and in North America, surrounding the North Atlantic. Figure 3.5 shows the distribution of Lewisian Gneiss outcrops in Scotland after Imber et al. (2002).

In the field, the gneisses generally show a clear foliation and several generations of folding have been distinguished (Fettes et al., 1992). A series of both mafic (e.g. the Scourie Dykes) and pegmatitic bodies are incorporated in the Lewisian structures, forming bands and boudins, which in places give the Lewisian Gneiss a heterogenous appearance. The tectonothermal event which formed the predominant structures and reworked the gneiss is generally correlated with the Inverian and Laxfordian (references in MacDonald and Goodenough, 2013).

The Lewisian Gneiss Complex is thought to have formed as an aggregation of several terranes (Friend and Kinny, 2001; Kinny et al., 2005; Goodenough et al., 2010; Wheeler et al., 2010). The terranes are distinguished in terms of geochemical and isotopic differences, and metamorphic history and age (Friend and Kinny, 2001).

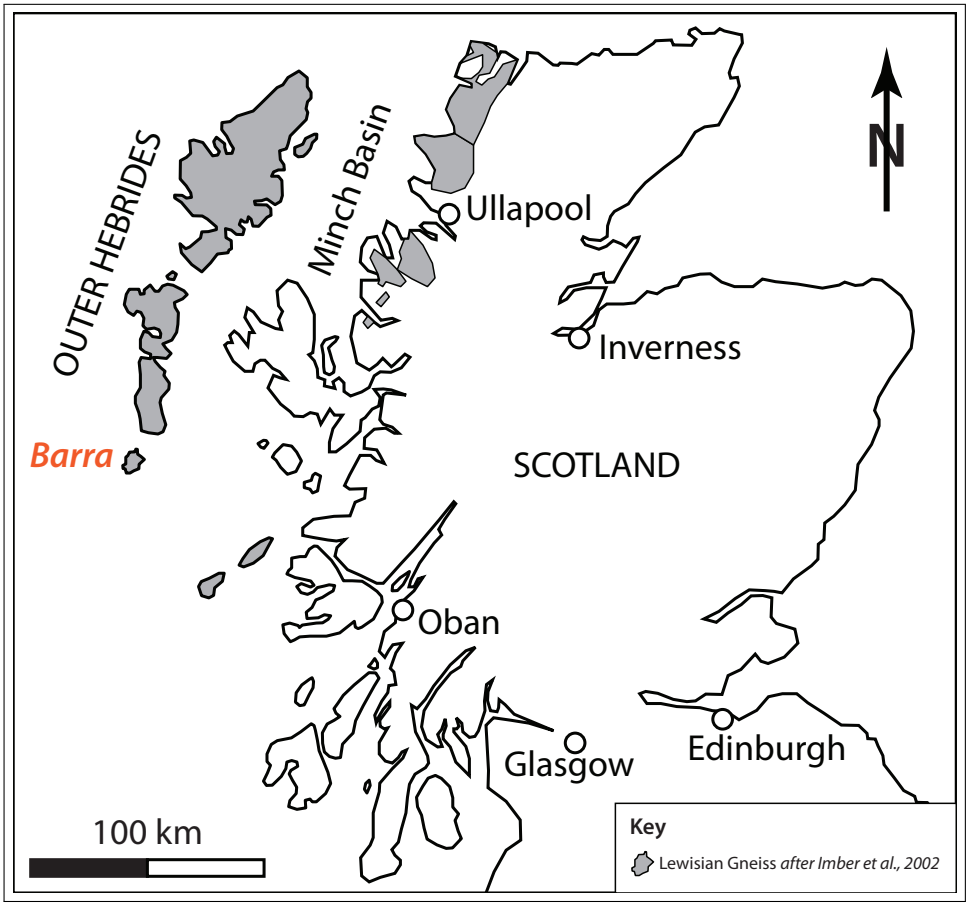

Figure 3.5 – Map of Scotland showing the distribution of Lewisian Gneiss outcrops. Lewisian Gneiss outcrops are confined to the NW of Scotland: the lithology crops out on the Outer Hebrides, the two islands of the Inner Hebrides, Coll and Tiree, and along the NW coast of Scotland as the oldest and lowest lying basement rock in Scotland.

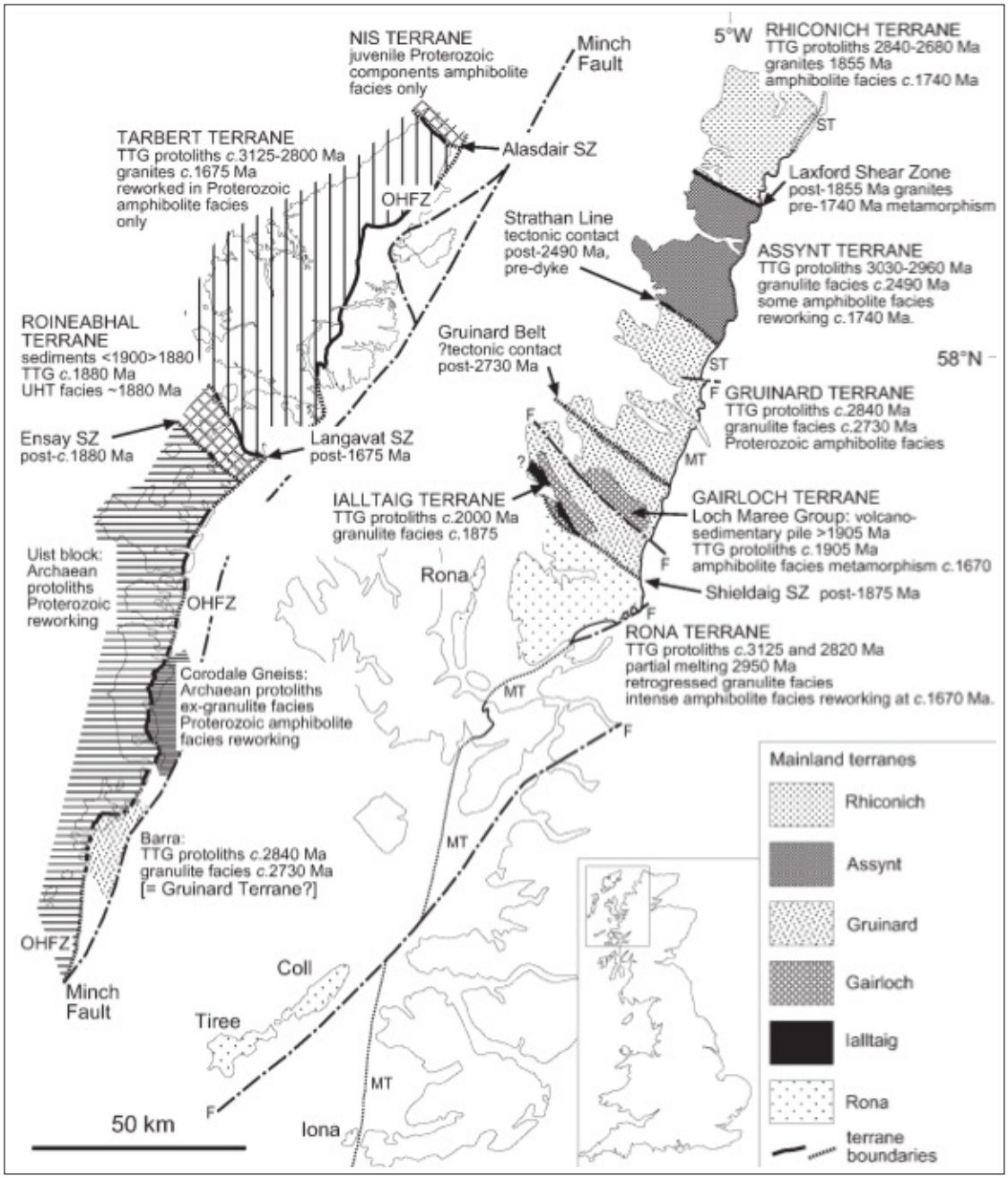

Figure 3.6 – Figure from Kinny et al. (2005), their Figure 1. Lewisian Gneiss Complex showing the positions of the proposed terranes. Inset shows the location of the Complex in NW Scotland. ST, Sole Thrust of the Moine Thrust Zone; MT, Moine Thrust; OHFZ, Outer Hebrides Fault Zone; SZ, shear zone. Note that in this context the Outer Hebrides Fault Zone represents a terrane boundary.

3.2.3 Outer Hebrides Fault Zone

Onshore

The Outer Hebrides Fault Zone (OHFZ), also Outer Hebrides Thrust or Outer Isles Thrust (offshore), is one of the major fault zones in the British Isles (Imber et al., 2002). It is shown on geological maps as a more or less distinct feature cropping out over nearly 200 km predominantly along the East coast of the Outer Hebridean islands (Figure 3.8). The structure dips with local variations at 20–30 degrees to the East–South East. In the field, the zone reaches a width of 25 km or more (Francis and Sibson, 1973): this variability is poorly represented on the BGS geological map (BGS, 1981).

Offshore

Offshore, the Outer Isles Thrust (OIT) is a distinct reflector visible on seismic profiles in the Minch and North of the Minch (e.g. Smythe et al., 1982). A several kilometre thick feature extends from the Outer Hebrides towards the East into the Minch basin where it meets the Moho at about 25 km depth. The Outer Isles Thrust dips to the E(SE) at about 20–30 degrees (Smythe et al., 1982; Brewer and Smythe, 1984; Lailey et al., 1989; Stein and Blundell, 1990). Figure 3.7 shows an interpreted line drawing (Smythe et al., 1982, their Figure 3) of the MOIST seismic profile. The MOIST profile trends East–West just North of the Outer Hebrides, along the Northern margin of Figure 3.5 on page 33.

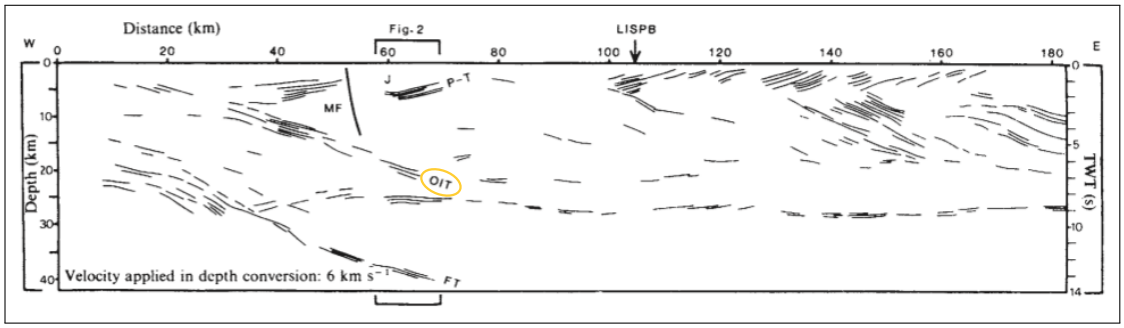

Figure 3.7 – Line drawing of the MOIST seismic profile, North of Scotland. OIT denotes the reflectors of the Outer Isles Thrust. Note the extent and thickness of the OIT feature. TWT is two way travel time. Figure from Smythe et al. (1982), their Figure 3.

The OHFZ is characterised by a diversity of rocks that record the deformation: mylonites, ultramylonites, 'crushed rock', cataclasite, pseudotachylyte and phyllonites (Sibson, 1977a; Fettes et al., 1992).

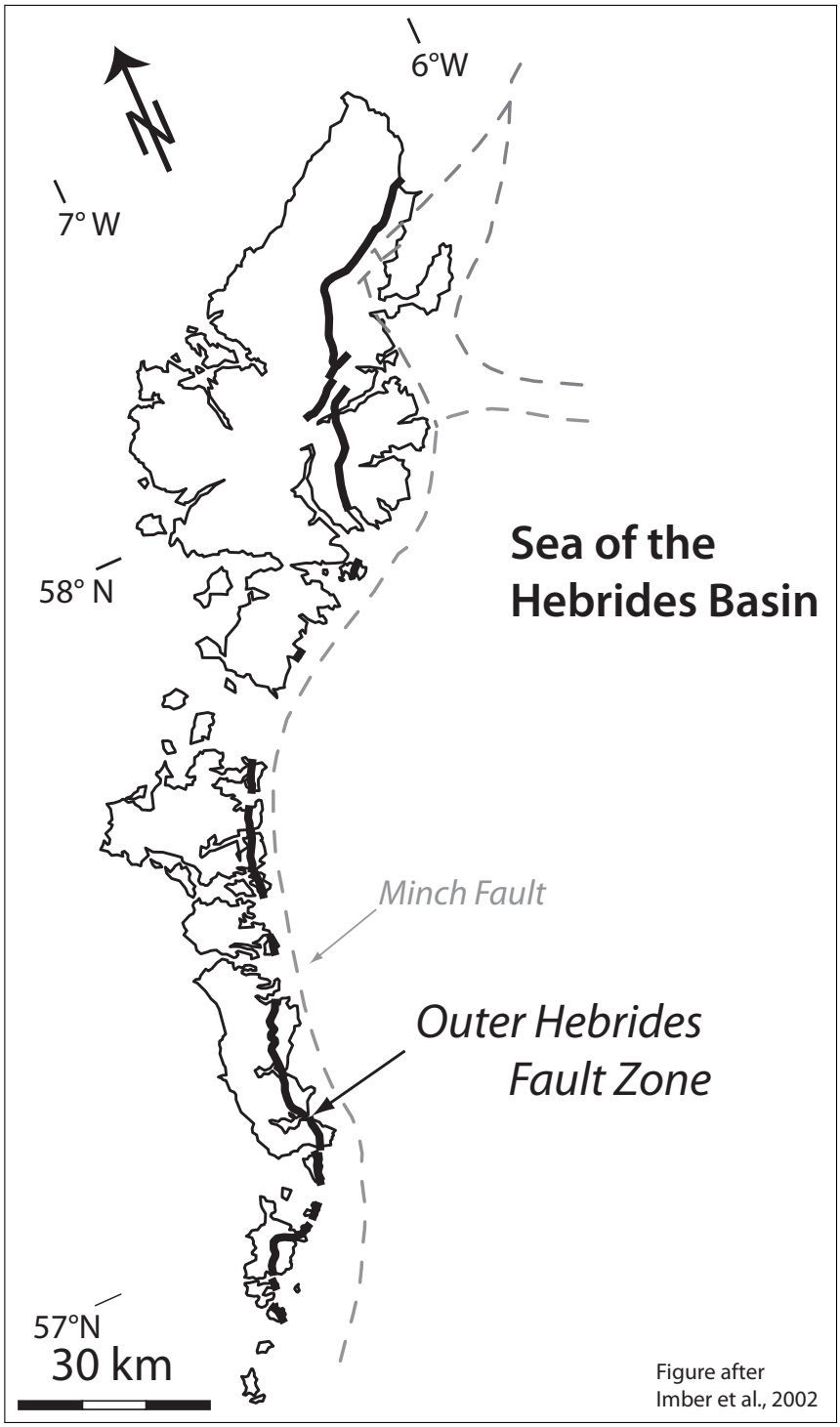

Figure 3.8 – The Outer Hebrides Fault Zone is commonly published as a through-going fault affecting most of the Outer Isles on their Eastern side. The Minch Fault is a normal fault and related to the opening of the Minch Through in the Mesozoic. Figure after (Imber et al., 2002).

3.2.4 Episodes of Deformation attributed to the OHFZ

Several episodes of deformation have been identified (Fettes et al., 1992; Butler, 1995; Macinnes et al., 2000; Imber et al., 2001; Osinski et al., 2001), but not all of them are present on all of the islands. Figure 3.9 gives an overview of the kinetics and structures and their chronology. The following description starts with the oldest deformation episode which affects Laxfordian fabrics.

1) Mylonite Episode

The oldest fault rocks preserve viscous deformation. The mylonites predominantly record movements top NW (thrusting), with varying lateral components. These mylonites are predominantly found in the Northern part of the Fault zone (mainly on Lewis), and not on Barra. However, Macinnes et al. (2000) found evidence for early ductile shears and NW-verging folds on the small islands North of Barra.

2) Pseudotachylyte Forming Episode

Both Imber et al. (2001) and Macinnes et al. (2000) refer to the formation of the pseudotachylytes, cataclasites and 'crush zones' as top to NW brittle thrusting, which is supported by the findings of Francis and Sibson (1973). Macinnes et al. (2000) also find pseudotachylytes recording sinistral and dextral shear. Osinski et al. (2001) stress that, similar to Macinnes et al. (2000), they find no unequivocal evidence for thrusting during the pseudotachylyte forming episode. They record that pseudotachylytes seem to form mainly under extension. This episode is often referred to as a "brittle" episode, and alongside pseudotachylytes, there are also cataclasites, ultracataclasites and 'crush zones' (Sibson, 1977a; Fettes et al., 1992).

3) Phyllonitisation Episode

The first event related to phyllonite formation is a sinistral, top NE strike-slip event producing narrow, lower greenschist facies shear zones (Imber et al., 2001) in the Uists. Phyllonites are shear zones rich in phyllosilicates. However, Osinski et al. (2001) mention that these sinistral fabrics were not found in their field area in South Uist, and Macinnes et al. (2000) found no evidence for this episode north of Barra.

4) Low Angle Extension Episode

The second event associated with phyllonitisation comprised a top to the East, SE or South dipslip. This event reworked the phyllonitic fabric. The younger dipslip fabric is more predominant according to Macinnes et al. (2000); Osinski

et al. (2001). Localized brittle deformation on foliation parallel faults is also recorded for this low angle extensional episode (e.g. Butler, 1995).

5) Brittle Extension Episode

This extensional episode is characterised by brittle, high angle normal faults.

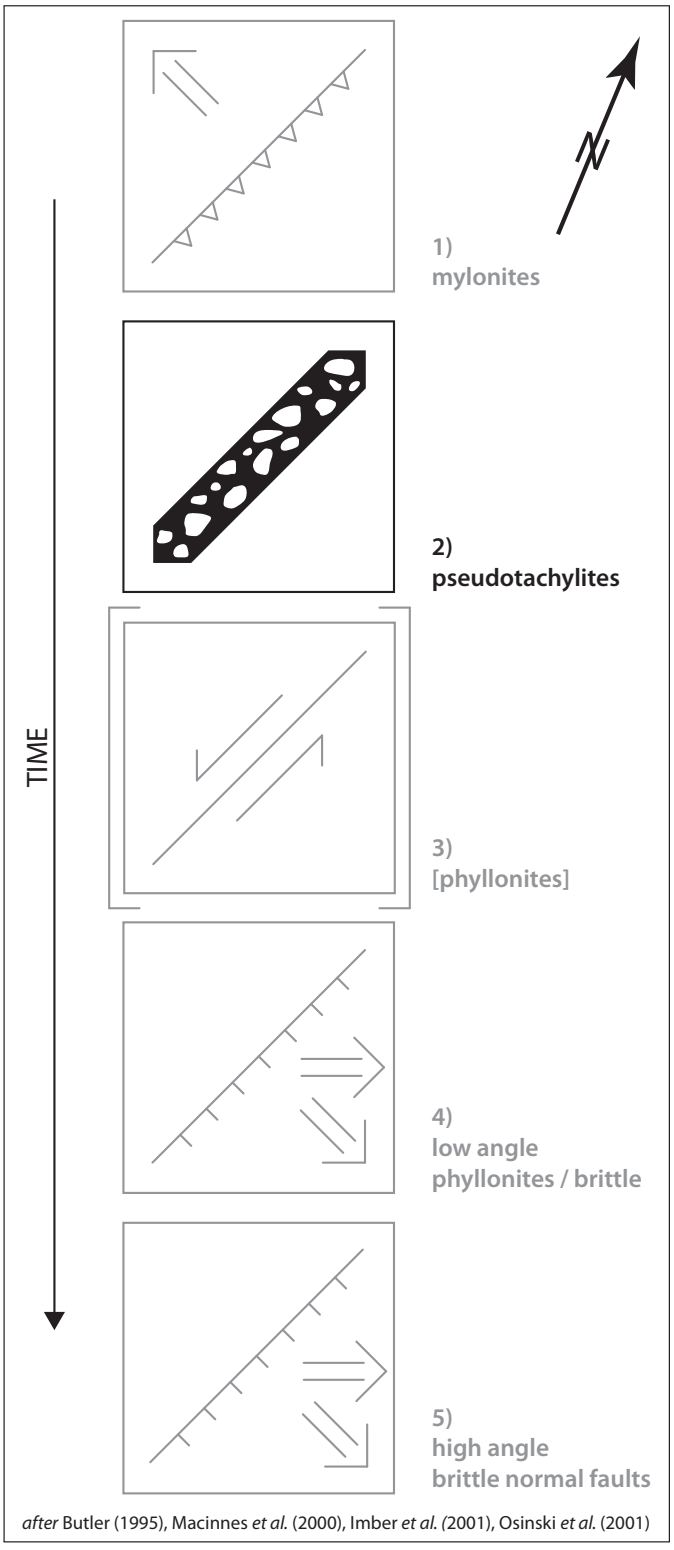

Figure 3.9 – Chronology of the five distinct episodes of deformation, kinetics and structures attributed to the Outer Hebrides Fault Zone.

3.2.5 Occurrence of Abundant Pseudotachylyte on Barra

Several authors have mapped the occurrence of "abundant pseudotachylyte" on Barra. Figure 3.10 shows in black the data published on the BGS map (1981), which represents a compilation of data from various sources. The grey dots represent where Jehu and Craig (1924) have mapped abundant pseudotachylyte.

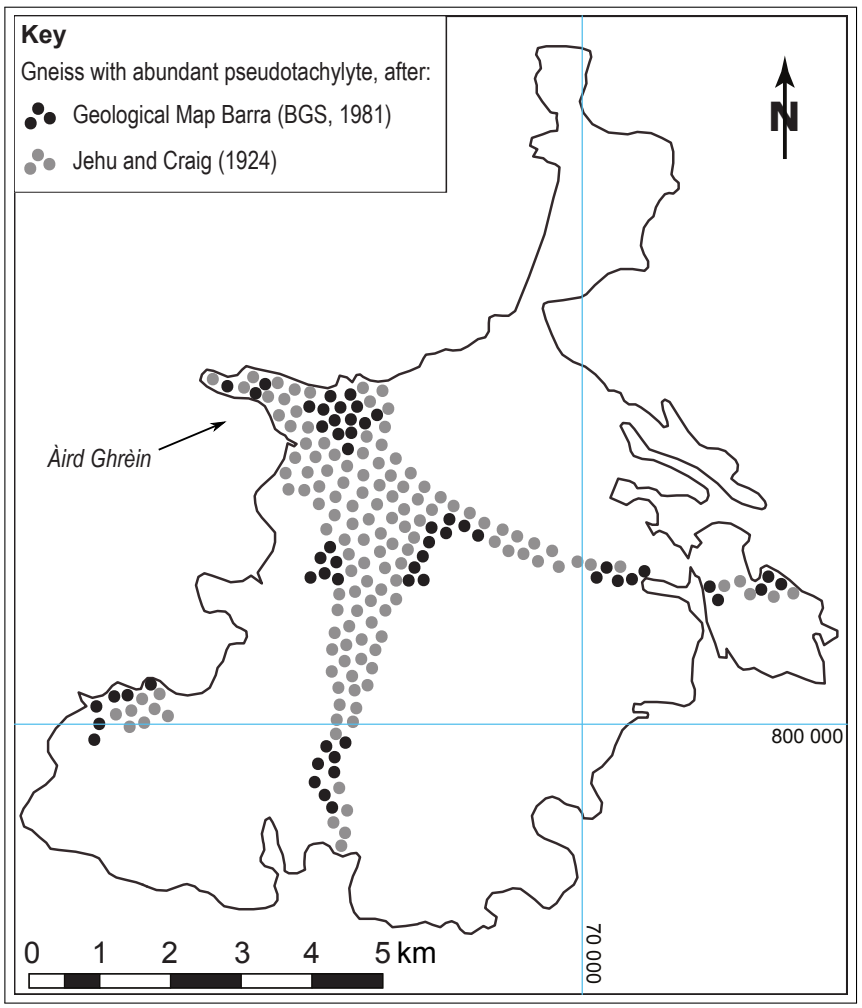

Figure 3.10 – Map of Barra showing the occurrence of abundant pseudotachylytes. Black dots after the Geological Map of Barra (BGS, 1981), grey dots mapped by Jehu and Craig (1924).

3.2.6 Pseudotachylytes in Lewisian Gneiss Elsewhere

Pseudotachylytes have been found and described for all regions where the Lewisian Archean basement gneisses crop out:

Maine, USA: Swanson (1989)

Greenland: Maddock et al. (1987); Karson et al. (1998)

Scotland:

Gairloch and Loch Maree region: Park et al. (1987),
Coll and Tiree: Westbrook (1972)
Outer Hebrides: Jehu and Craig (1924); Maddock et al. (1987); Maddock (1983); Sibson (1975)

3.2.7 Age of the Pseudotachylytes in the Lewisian in Scotland

Maximum Age

The maximum age of a fault zone is given by the youngest rocks it affects. These are the Laxfordian granites and pegmatites in the Lewisian Gneiss Complex which have been dated at 1.685 Ga. This is also the maximum age for the mylonites present in the Northern segment, on Harris and Lewis (Imber et al., 2002).

Minimum Age

On the Outer Hebrides, the minimum age for the pseudotachylytes is given by the sediments of the Stornoway Formation, which contain rock fragments with pseudotachylytes. The Stornoway Formation is the only sedimentary deposit on the Lewisian Gneiss preserved on the Outer Hebrides. Its age has been referred to as Permo-Triassic (e.g. Steel and Wilson, 1975).

On the Scottish mainland and Harris, the Lewisian Gneisses are overlain by the sediments of the Torridonian Supergroup. These rocks are not affected by pseudotachlites and therefore give a minimum age for the mainland pseudotachylytes. Their oldest member is the Stoer Group which has been dated by Turnbull et al. (1996) with an age of 1199 ± 70 Ma, which was confirmed by Parnell et al. (2011) at 1177 ± 5 Ma.

Dating of Pseudotachylytes

There is sparce and somewhat contradictory data for the age of the pseudotachylytes themselves. The most recent data stems from Argon-Argon analyses (Kelley et al., 1994; Sherlock et al., 2008, 2009) with an age range even wider than the structural age limits of crosscutting relationships mentioned above. This is a similar result to the study of Thompson et al. (1998) who find an inconclusive range

of Argon-Argon ages in pseudotachylytes from the Sudbury impact structure. Reimold et al. (1990) conclude that inconclusive Argon-Argon dates for pseudotachylytes is a common problem and questions the applicability of the method on pseudotachylytes. The interpretation of the available dating datain the Barra region is discussed in Chapter 8.

3.2.8 Torridonian Sediments

In the Minch basin, the Proterozoic Torridonian Sediments are up to 8 kilometers thick (Stein, 1992). They were deposited in a half-graben setting, thickening towards the west. Figure 3.11 shows a simplified cross-section of the Minch between Stornoway (Lewis) and Ullapool on the mainland, based on offshore seismic data. Stein (1992) note that there is evidence for extension, but not for reverse faulting or thrusting.

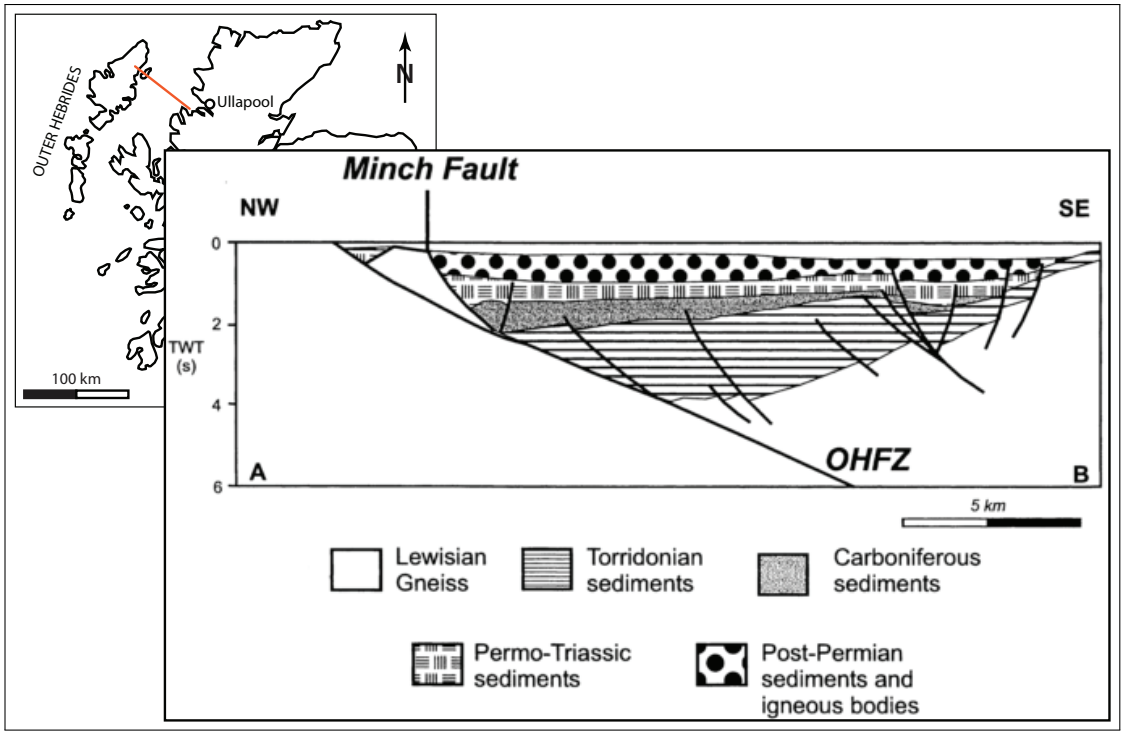

Figure 3.11 – The cross-section shows a half-graben bounded in the NW by the Outer Hebrides Fault Zone (OHFZ). The oldest sediments are the Torridonian sediments which are of Proterozoic age. The structures show evidence for normal faulting and extension, but not for reverse faulting or thrusting. Cross-section from Imber et al. (2001), after Stein (1992). Trace of cross-section in red on the map.

The Proterozoic sediments of the Torridonian succession are divided into three groups: The Stoer Group and the Sleat Group, and on top the Torridon Group.

Stoer Group

In the NW coastal area of Scotland, the sediments of the Stoer Group lie unconformably on the Lewisian Gneiss complex (e.g. Krabbendam et al., 2008). The succession of the Stoer Group is discontinuously exposed as far South as Loch Maree and reaches up to 2 kilometres thickness (Stewart and Allen, 2002). Its oldest rocks are dated at *c.* 1200 Ma and their source is likely to be the Lewisian Gneiss (Kinnaird et al., 2007, and references therein).

The Stac Fada Member which is part of the Stoer Group has recently been identified as an impact ejecta deposit (Amor et al., 2008). The impact structure is preserved as a gravity low at Lairg, with an approximate diameter of 40 km (Simms, 2015). The origin of the Stac Fada member is still controversial, and the impact structure is not officially acknowledged (*EarthImpact Database*, *Earth Impact Database*, last accessed 23/06/2020). Originally, the Stac Fada Member was interpreted to be of volcanoclastic origin (e.g. Young, 2002).

Sleat Group

Further South, the Sleat Group takes the place of the Stoer Group. The Sleat group consists of a short succession of sediments originating from the Lewisian Gneiss, which is deposited on top of the Lewisian Gneiss.

Torridon Group

With an angular unconformity, the Torridon Group lies on top of both the Stoer Group and the Sleat Group (Kinnaird et al., 2007).

3.2.9 Late Intrusions

On the Outer Hebrides, the majority of dykes have been eroded and are now present as gullies. No attempt has been made as part of this study to distinguish the different generations of dykes in the field (see Chapter 4). The dykes are referred to as Post-Lewisian Minor Intrusions. Figure 3.12 shows their distribution as published in the Geological Map of Uist and Barra (BGS, 1981).

Permo-Carboniferous Dykes

A few quartz-dioritic dykes of Permo-Carboniferous age are found on Barra, cutting the Lewisian Gneiss. These dykes have been related to the Variscan orogeny (Kirstein et al., 2006).

The North Atlantic Igneous Province

The North Atlantic Igneous Province (NAIP) comprises the igneous lithologies and structures which are related to the opening of the North Atlantic. The magmatism started about 62 Ma ago (Saunders et al., 1997). The British part of the NAIP is also known as the British Paleogene Igneous Province (BPIP). Lithologies in Britain which are associated with the NAIP are found in Western Scotland and Northern Ireland. They consist of igneous complexes and numerous dykes. The rocks of several of the Inner Hebridean islands such as Skye and Mull were formed as part of the NAIP.

The magmatism has been related to a mantle plume which was situated under the Scottish West coast, and subsequently formed the Faroe Islands, an apparent movement North. Numerous dykes which are related to the NAIP are present on Barra and will be discussed in Chapters 4 (structural) and 7 (isotope geochemistry).

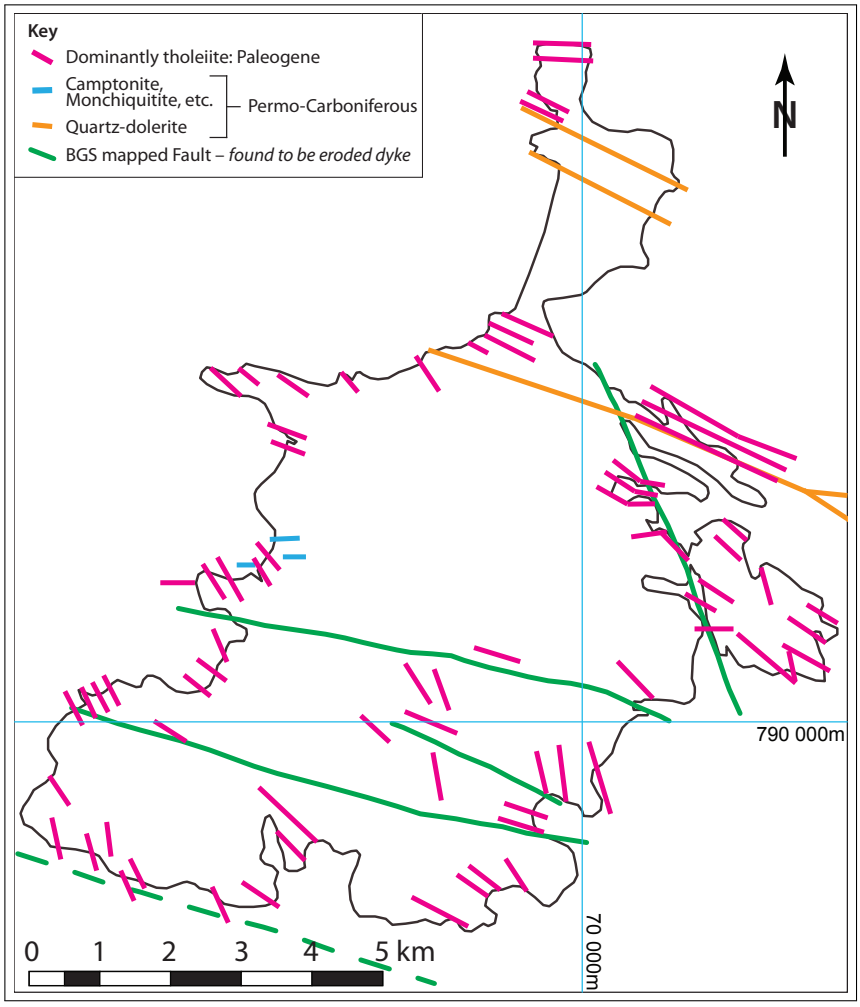

Figure 3.12 – Post-Lewisian Minor Intrusives (BGS, 1981). The "faults" mapped in green were found to be eroded dykes. Offshore data suggests that the island is disected by a vast amount of – now eroded – dykes.

3.3 Timeline of Geological Events

The following figure gives an overview of the main geological events outlined above. The minimum and maximum ages of pseudotachylyte formation is show for the Outer Hebrides (red dots) and the Scottish mainland (pink dots).

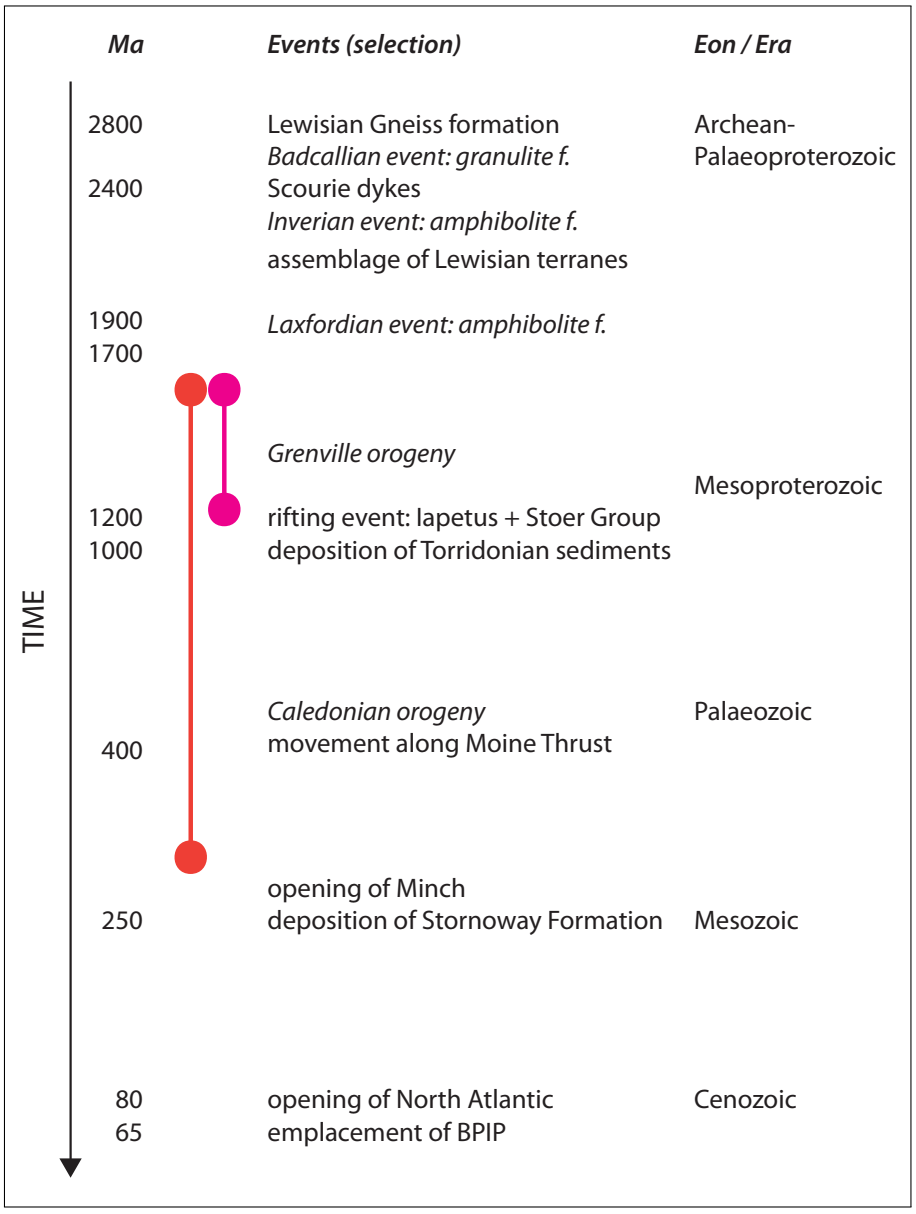

Figure 3.13 – Timeline of the events outlined in the text. The red dots represent the pseudotachylytes on the Outer Hebrides, the pink dots the pseudotachylytes on the Scottish mainland, i.e. their maximum and minimum ages. Not to scale. Time in Million years is approximate. BPIP is British Paleogene Igneous Province which forms part of the North Atlantic Igneous Province (NAIP).

Chapter 4

Macro Scale: Map and Structural Data

4.1 Introduction

In a paper analysing published data from about fifty world wide fault related pseudotachylyte occurrences, Sibson and Toy (2006) find that the average thickness of fault related pseudotachylytes is in the order of a few millimetres. Exceptionally large pseudotachylytes have only been reported from a handful of places on Earth (see Chapter 2). It has been suggested that exceptionally large occurrences of pseudotachylyte could be used as an indicator for an impact origin (French, 1998), this will be discussed in Chapter 8.

In order to quantify the pseudotachylyte occurrence a new method was developed which allows for comparison of different sites. In the literature, the pseudotachylyte (*sensu lato* or *sensu stricto*?) quantity is either estimated on the macro scale (Camacho et al., 1995), measured on the meso scale (pseudotachylyte *sensu stricto*) (Mohr-Westheide and Reimold, 2011), or measured on the meso scale and represented as an adapted dot-density map on the macro scale (Lieger et al., 2009; Fletcher and Reimold, 1989). The method presented combines the macro, meso and micro scales, and distinguishes between pseudotachylyte *sensu lato* and *sensu stricto* quantity.

An area of approximately one square kilometre was mapped, and stereographic data collected, to answer the research question posed in Chapter 1:

> What is the extent of the different pseudotachylyte geometries?
>
> Do the different pseudotachylyte geometries occur in distinct zones, and are they geometrically arranged?

What are the pseudotachylytes' relationship to other structures, such as host rock anisotropies?

4.2 Field Area

In terms of outcrop quality and exposure of pristine pseudotachylyte, the chosen field area is unrivalled amongst other localities in the Outer Hebrides. Àird Ghrèin (Grean Head), a headland on the NW coast of Barra (Figure 3.2 in Chapter 3), was chosen for a detailed map of pseudotachylyte occurrence. The headland is marked by a hill, whose highest point (90 masl) gives foundation to a mast. The area to the South and South East of the mast constitutes Barra's golf course. The mapped area is bordered in the South by the river, and to the East by the pasture land towards Cleit. In comparison to the exposure in other places on Barra, the field area contains relatively many well-connected outcrops, a few of which are superbly polished. The best outcrops are along the coast, between the River Mouth and the headland. In the upper intertidal and the stormtidal zone, rock surfaces are fresh and well polished by the beach pebbles. In the lower intertidal zone, algae and barnacles commonly cover the rock. The inland outcrop situation is very dispersed, with bare rock set between grassland and bog. Outcrops are prevalently covered in lichen that camouflages the rock textures exceptionally well. One feature of quasi-conglomerates is the rotation of clasts, which the trained eye learns to see as sudden changes in foliation orientation, marked by a micro topography due to preferential erosion of some gneiss layers. These features can sometimes be distinguished even where the rock is covered in lichen. These meso scale observations will be discussed in Chapter 5.

4.3 Mapping Method

To quantify the extent of pseudotachylyte development, a new mapping method was developed. Because pseudotachylytes do not represent a map-scale lithological unit, the resulting map is not a classic geological map. The map records a simplified, categorized pseudotachylyte geometry (the pseudotachylyte mode of occurrence, see Section 4.4.1), and the occurrence of dykes (as a lithology). The newly developed method takes into account the scale dependency of the pseudotachylyte features. This Chapter shows the data at the macro scale (covering one square kilometre), which will be complemented by the meso scale data (centimetre to metre, outcrop scale, Chapter 5) to calculate the total pseudotachylyte volume (thin section analyses, Chapter 8).

4.3.1 Scale and Resolution

The mapped area covers approximately one square kilometre. Every outcrop visited is coloured, that is, what is not coloured on the map is either not an outcrop, or was not visited. A 1 : 25 000 Colour Raster Map (Ordnance Survey, 2014) was used as topographic base map, enlarged to 1 : 5 000. On a 1 : 5 000 map, 1 mm represents 5 m in the field. This means a dot on the map represents an area of approximately 5 x 5 to 10 x 10 metres, which marks the resolution limit in terms of mapping. In the field, a 5 x 5 to 10 x 10 metres outcrop area was searched for pseudotachylyte occurrence and its geometry, which would define the colour given on the map. In practice, areas covered and coloured could be larger than that (i.e. up to 20 x 20 metres). However, also outcrops smaller than the resolution limit were mapped, if they were isolated. The mappable area in the order of 5 x 5 to 10 x 10 metres is, in the context of a mapped area, referred to as an outcrop.

4.3.2 Features on Vertical Walls

On Àird Ghrèin there is an abundance of vertical topographic features such as cliffs and gullies ('slocs' in Jehu and Craig, 1924). The area of these walls are not represented on a topographic map, due to the two dimensional projection. However, they constitute both a large amount of outcrop, generally of good quality. Figure 4.1 shows such an outcrop. To represent these outcrops, their area was mapped as if the surfaces were horizontal. The implications of this method are discussed below in Section 4.6.2.

Figure 4.1 – *Photograph of a vertical side wall of a dyke, exposing quasi-conglomerate.* – The quasi-conglomerate (not well visible from this distance) makes up a majority of this vertical outcrop, whereas on top of the vertical outcrop, the rock is masked by vegetation. Due to its steep slope, the here visible outcrop area is not represented on a topographic map. Grey box on right hand side is approximately 1 m high. North coast of Àird Ghrèin towards Cleit (NF 665 048).

4.4 The Map

4.4.1 Mapped Units

The mapped units encompass two lithologies, the Lewisian Gneiss, i.e. the pseudotachylyte host rock, and the post-Lewisian intrusives (paleogene dykes). Both the lithologies, and the pseudotachylyte geometries, are described in detail in Chapter 3. A short description below is followed by a colour coded key with a representative photograph of each unit. Figure 4.2 shows the mapping key with photographs of examples of the respective categories that are used to produce the map shown in Figure 4.3.

The categories are descriptive and based on field observations only. Thus if analysed with different methods, or indeed visited by another geologist, some of the outcrops which were mapped as pseudotachylyte might be interpreted differently. *Mode of occurrence* is added in the description of the pseudotachylyte bearing units, to distinguish them from the pseudotachylyte *geometry*. An example to illustrate the difference: A 10 x 10 cm area could have quasi-conglomerate *geometry*, however, its area is too small to be mapped as the quasi-conglomerate *mode of occurrence*.

Lewisian Gneiss *without* Pseudotachylyte – blue

The Lewisian Gneiss is the host rock to the pseudotachylytes, in this mapping unit *no* pseudotachylyte is observed on the outcrop scale. This unit was not found in the mapped area on Àird Ghrèin - there were no outcrops on the headland that did not contain pseudotachylytes.

Pseudotachylyte Veins – yellow

The pseudotachylyte vein mode of occurrence is represented in yellow on the map. Outcrops with a single pseudotachylyte vein, or a few veins that are widely spaced, or not interconnected, would be mapped with this signature.

Pseudotachylyte Networks – orange

In comparison to the pseudotachylyte vein mode of occurrence, the unit mapped in orange represents an outcrop where pseudotachylyte veins are abundant and / or interconnected.

Quasi-Conglomerate – red

The quasi-conglomerate mode of occurrence is mapped in red. Their minimum thickness for being classified as quasi-conglomerate mode of occurrence is 10 cm, with a minimum length of 40 cm. The quasi-conglomerate geometry sometimes

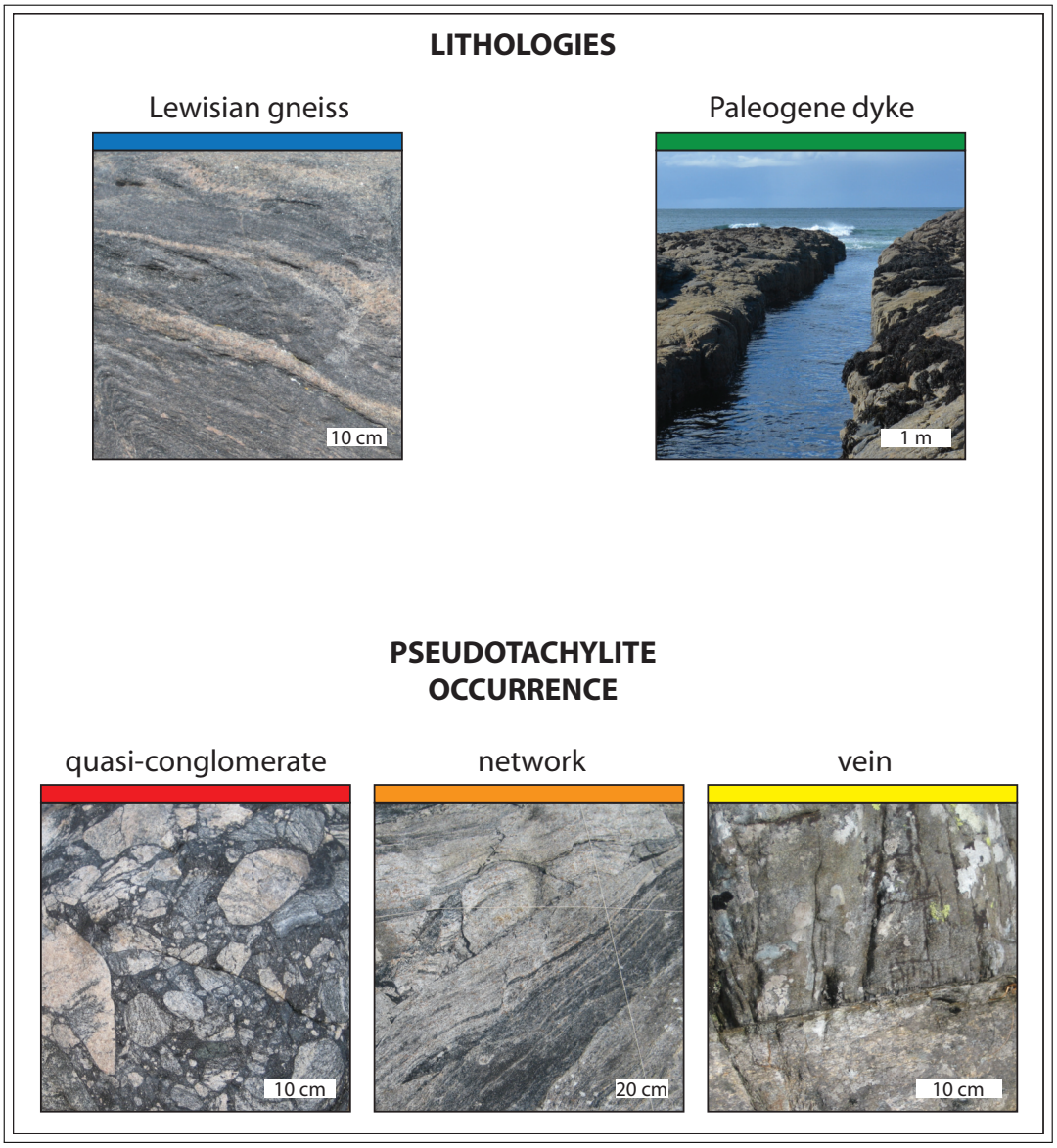

Figure 4.2 – Photographic mapping key of the map in Figure 4.3. The dykes (green) are the only lithological unit that has been mapped as such. The Lewisian Gneiss is subdivided into pseudotachlite occurrence: no pseudotachlite (blue), pseudotachylyte veins (yellow), pseudotachylyte veins that form networks, or small occurrences of quasi-conglomerates (orange), and quasi-conglomerate that exceeds 10 centimetres in thickness (red).

occurs in blebs, which were, if smaller than approximately 10 x 40 cm, mapped as pseudotachylyte network mode of occurrence.

Post-Lewisian Dykes – green

The fine-grained to aphanitic dykes, that crosscut the Lewisian gneiss and the pseudotachylytes, are notably absent in terms of material, and manifest mainly as gullies and cliffs. They were mapped along strike as dykes if somewhere along the respective wall, some outcrop of dyke material was found.

4.4.2 Pseudotachylyte Occurrence on Barra

Detailed mapping of pseudotachylyte occurrence was performed on Àird Ghrèin, whereas other parts of the island were visited for reconnaissance. Pseudotachylyte was found also in places where it has not been recorded on the geological map (BGS, 1981). Figure 4.4 shows an outline of Barra with pseudotachylyte occurrence published by different authors. The meaning of 'abundant' is not defined by the respective authors.

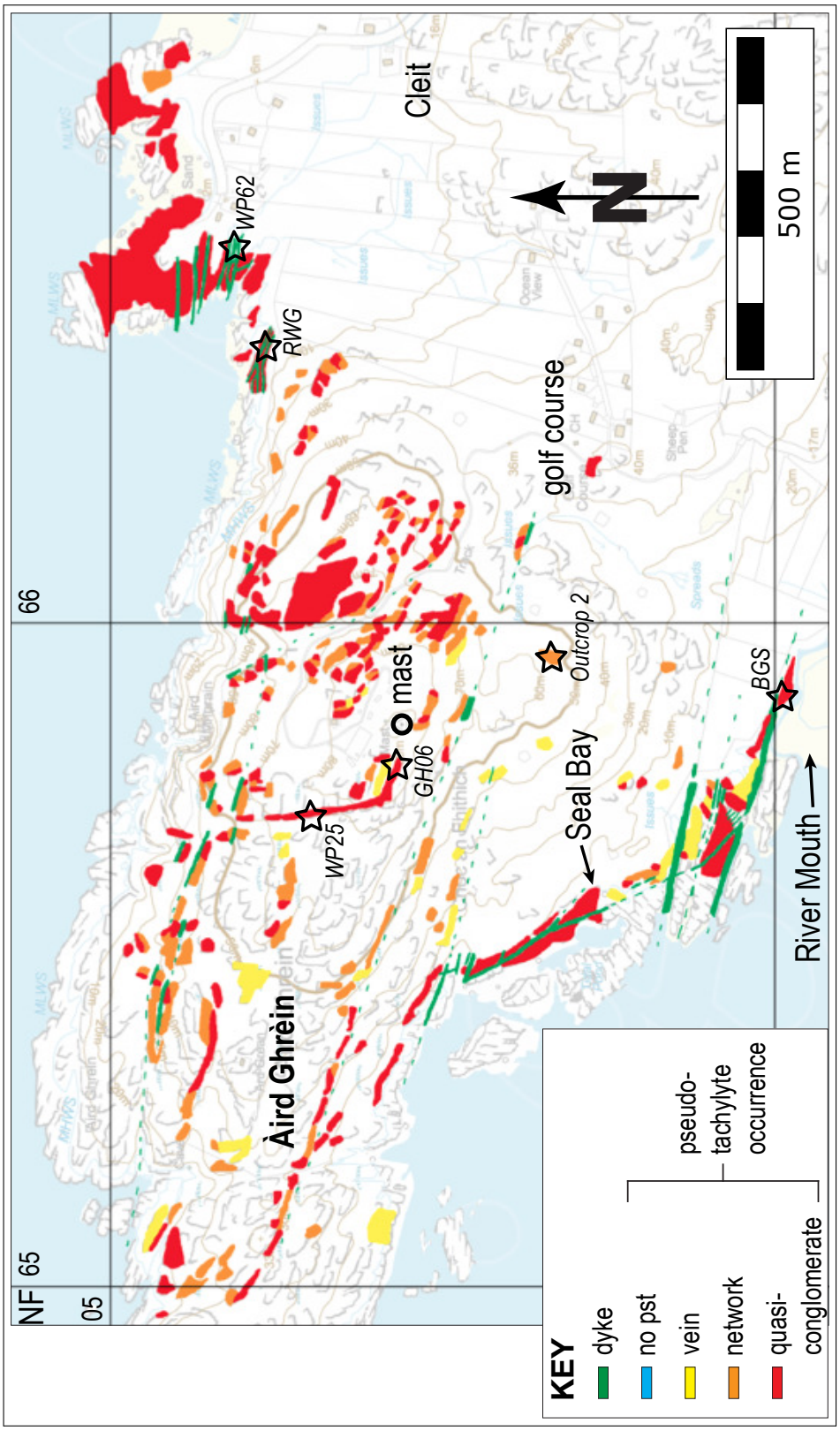

Figure 4.3 – Map showing the distribution of the mapped units as described above and shown in Figure 4.2. The pseudotachylyte occurrence is limited to the Lewisian Gneiss host rock, the dykes crosscut both the gneiss and the pseudotachlites. Areas coloured are visited outcrops. What is not coloured is either not visited, not an outcrop, or an outcrop of too poor quality.

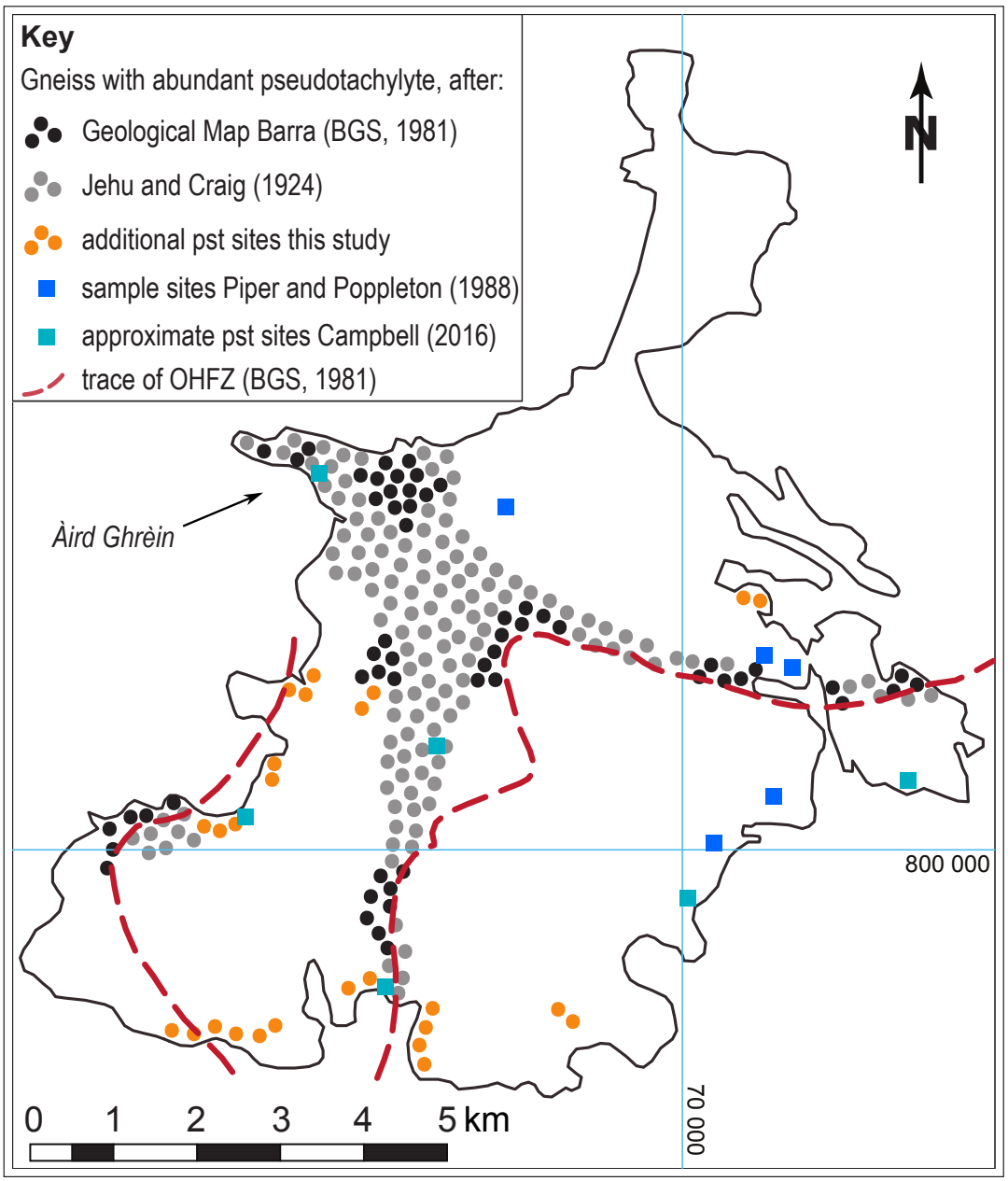

Figure 4.4 – Pseudotachylyte occurrence as published by different authors. The orange dots represent areas visited for this study where pseudotachylyte was found in addition to other published pseudotachylyte occurrences. The map also shows the trace of the OHFZ as published on the geological map (BGS, 1981). Many publications omit the western branch of the trace (see discussion in Chapter 8).

4.5 Stereographic Data

Stereographic data were collected to find structural relationships between the measured entities and compare them to regional trends. A number of structural features were measured in the field: gneissic foliation, pseudotachylyte veins, quasi-congolmerate zones, dykes, and cliff walls. pseudotachylyte veins were not differentiated, that means the data set comprises single veins and veins that are part of networks.

4.5.1 Representation of Stereographic Data

The Software *Stereonet, version 8.8.4* and *version 11.0.9*, was used for stereo plots (Allmendinger et al., 2013; Cardozo and Allmendinger, 2013). The projections are onto the lower hemisphere in equal area spherical projection. Statistics were executed through the program. Representative orientations (in dip direction / dip) are extracted as Bingham best fit vectors (cylindrical best fit), the number of data points (n) and R-values (R) of the Bingham best fit are given to indicate reliability of the statistical value. Some of the stereo plots contain representative orientations from other data sets in the form of the respective symbol for reference, which is indicated in the figure's lower right corner.

4.5.2 Lewisian Foliation

The Lewisian foliation shows a general dip of about 40 degrees towards ENE with a variability in orientation (R = 0.80). The locations of foliation measurements on Barra are shown in Figure 4.5. The variability is typical for Lewisian Gneiss (MacDonald and Goodenough, 2013). Figure 4.6 shows the poles of the foliation measurements. The foliation measurements were collected in different places on Barra (empty circles) and in the mapped area on Àird Ghrèin (full circles). The best fit poles are shown in respective star symbols. The general orientation of the foliation on Àird Ghrèin (063 / 39; R=0.83) is at about 30 degrees towards the North from the average orientation of the smaller data set from different localities on Barra (093 / 42; R=0.80).

4.5.3 Pseudotachylytes

Figure 4.7 shows that the orientations of pseudotachylyte depend on the pseudotachylyte geometry. Quasi-conglomerates (Figure 4.7 **A**), were plotted separately from pseudotachylyte veins (Figure 4.7 **B**).

Quasi-conglomerates

Figure 4.7 **A** shows the orientations of quasi-conglomerates where a boundary could be identified. The statistical orientation of the quasi-conglomerates (red

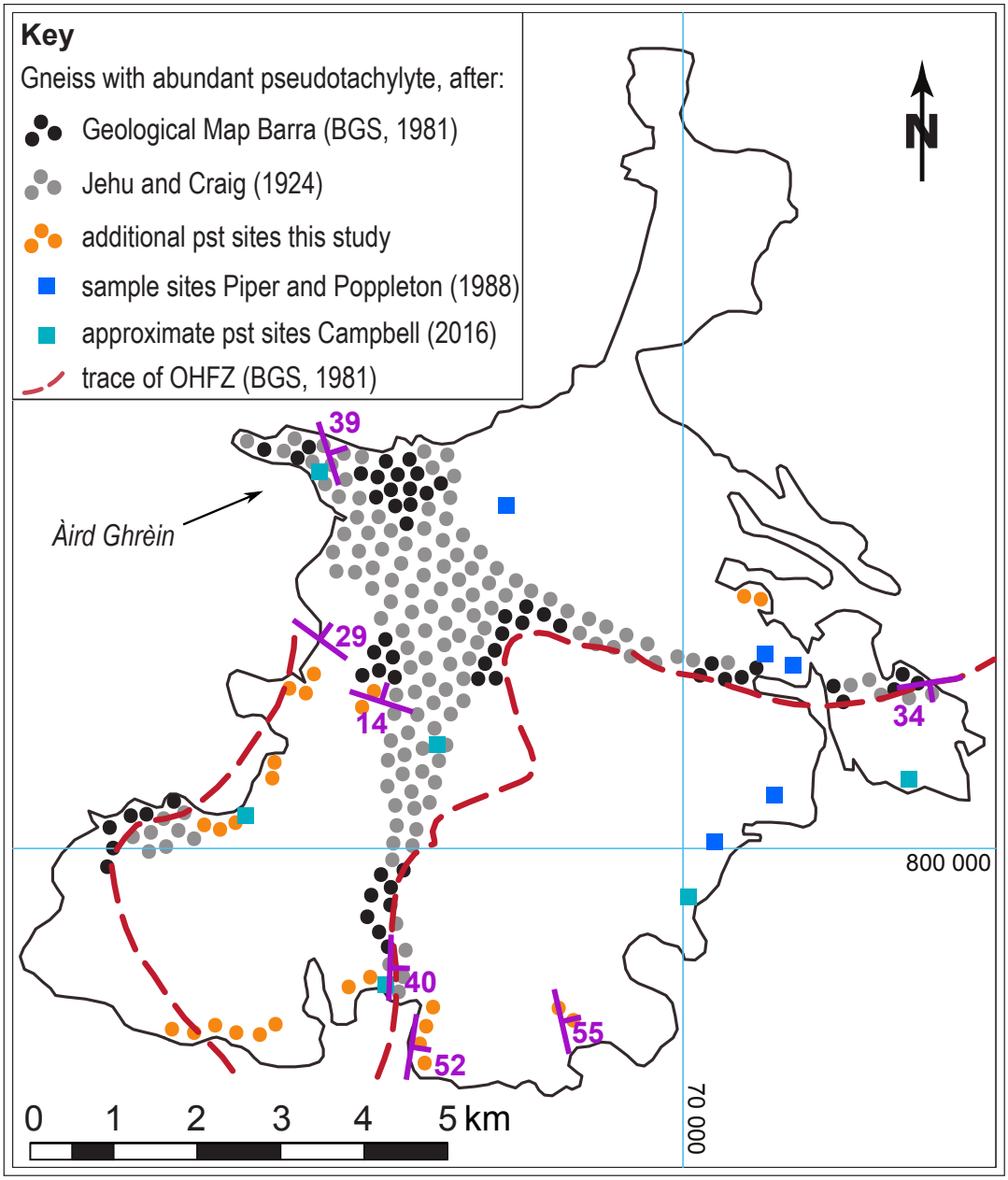

Figure 4.5 – Outline map of Barra showing foliation measurements. Where several measurements were taken in close proximity, the Bingham best fit was applied to represent the measurements.

circle and red great circle) is within measurement error (smaller than 5°) to the statistical orientation of the foliation (blue star and blue dashed great circle). Over two thirds of the quasi-conglomerate measurements (22 out of 29 data points) lay within the contour lines of the scatter of the foliation data.

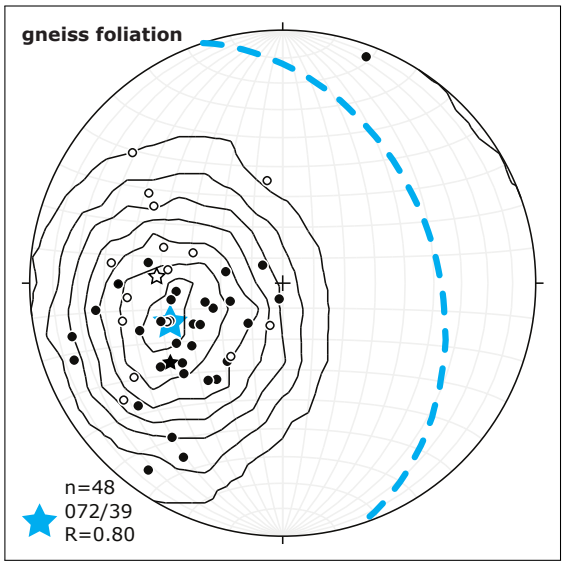

Figure 4.6 – Poles to foliation dip measurements. The statistical dip of the foliation is 072 / 39, indicated by the blue star and the dashed great circle. Full circles are from the mapped area (n=33), empty circles (n=15) from other locations on the island, with their statistical dip represented in the respectively colour-coded star.

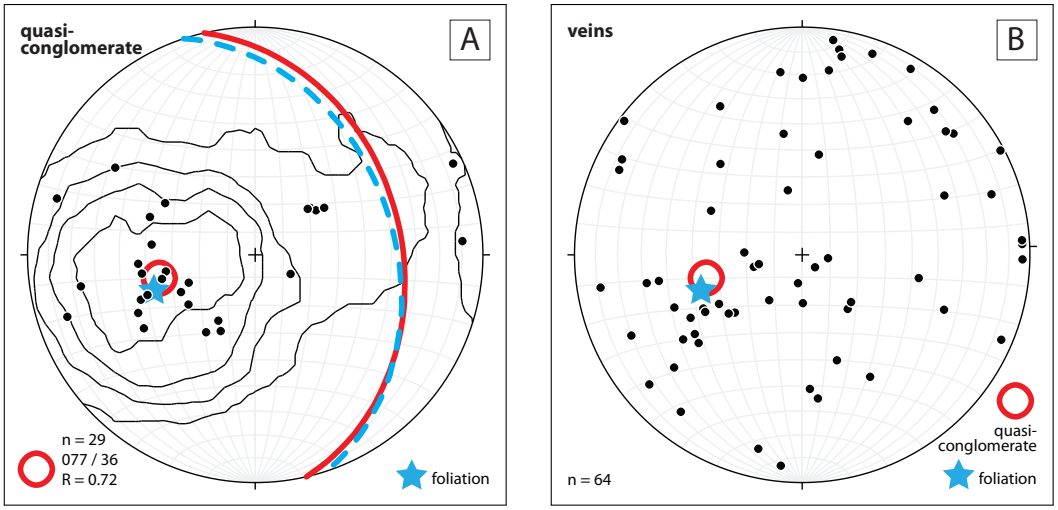

Figure 4.7 – (**A**) Poles to quasi-conglomerate layers, the Bingham best fit is indicated by the red open circle and the red great circle. – (**B**) Poles to pseudotachylyte veins. Data points show a higher density around the orientation of foliation and quasi-conglomerates. They are, however, found in a wide belt comprising all but steep ENE-WSW trending directions. The preferred orientation of the gneissic foliation is indicated by the blue star.

Pseudotachylyte veins

Figure 4.7 **B** shows orientations of pseudotachylyte veins. They exhibit no preferred orientation in this data set. However, the number of measurements is not very high compared to the variability in orientation. Possibly a larger number would yield a statistically preferred orientation.

Pseudotachylyte network: In one outcrop displaying a pseudotachylyte network (*Outcrop 2* in Figure 4.3), the orientations of pseudotachylyte veins and foliation were measured. The pseudotachylyte veins at a network boundary are foliation parallel, whereas the interconnecting veins are discordant (Figure 4.8).

4.5.4 Dykes

The orientations of all dykes are shown in Figure 4.9, represented by great circles. The subvertical dykes occur in two orientations, which have been separated by eye and are shown in Figure 4.10. The majority of dykes trends WNW–ESE (46 out of 70 measurements). The two dyke populations are at 45.5° to each other, based on Bingham best fit vectors.

4.5.5 Gullies and Cliffs

Vertical cliffs and gullies were measured for two reasons: Dykes could often only be identified after exhaustive searches for remnant dyke material along a prominent cliff or gully. And, cliffs are a prominent and predominant landscape feature. Nearly half of the gully wall and cliff measurements are in the same orientation as the WNW dyke orientation. The orientations of the dominant topographic features, gullies and cliffs, are shown in Figure 4.11 **A**. The rose diagram representation of orientations indicates a prominent population which is presented in Figure 4.11 **B**. The statistical orientation of the cliff population trending WNW–ESE is within measurement error equivalent to the WNW–ESE trending dyke population (Figure 4.10 **A**).

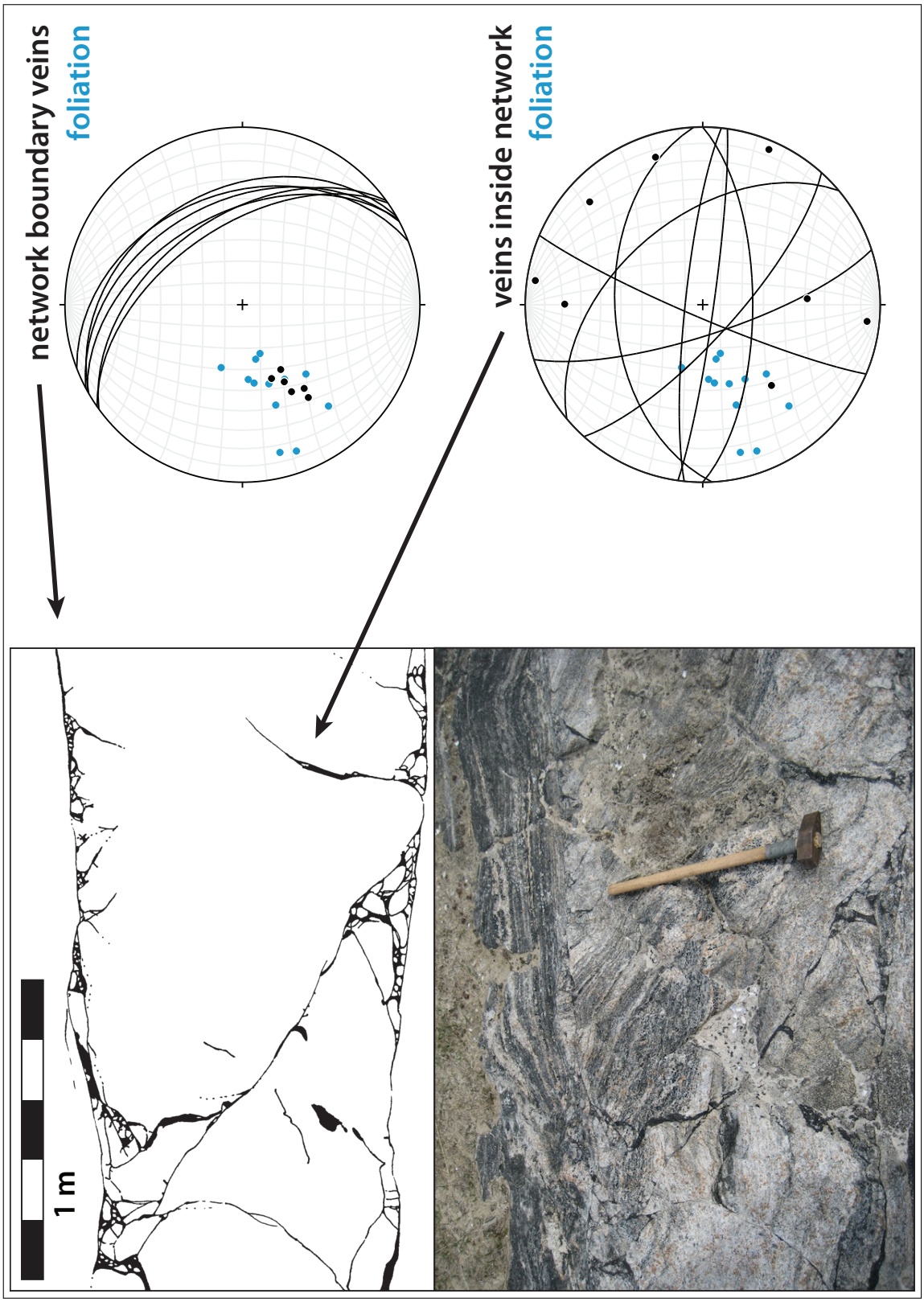

Figure 4.8 – *Outcrop 2*: Vein orientation data in stereoplots, poles and circles. The network boundary veins are foliation (blue poles) parallel, whereas the veins inside the network are discordant. Outcrop 2, NF 659 043.

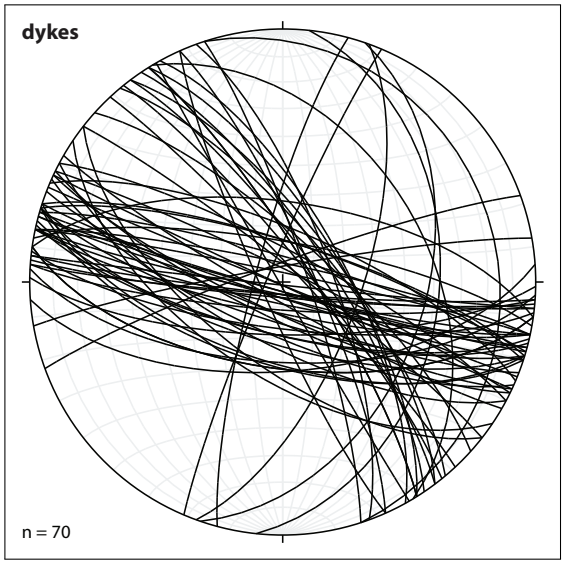

Figure 4.9 – Orientations of dykes represented in great circles. The majority of dykes trends WNW–ESE.

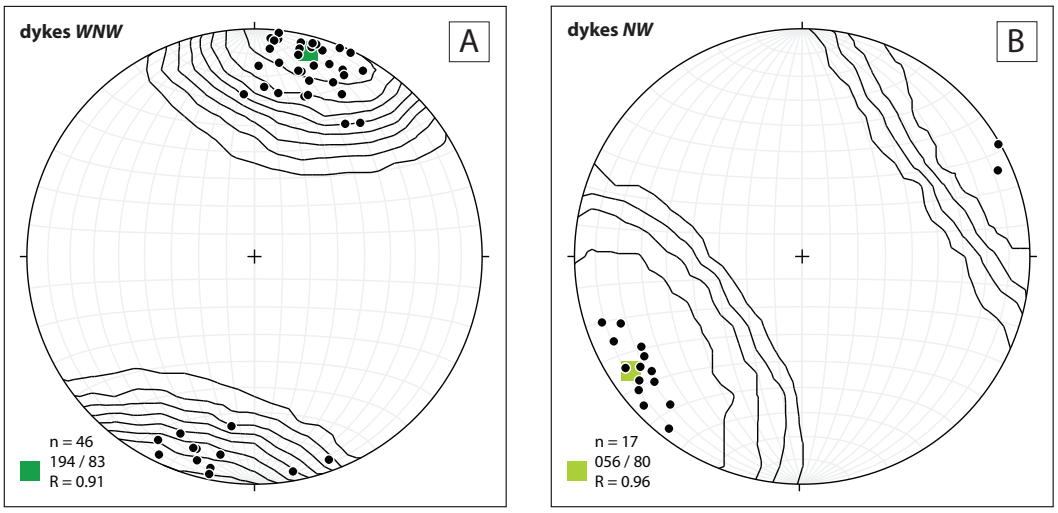

Figure 4.10 – The two main dyke populations, separated by eye. – (**A**) Dyke population with a WNW–ESE trend. This population makes up the majority of the orientation measurements (46 out of 70). – (**B**) Dyke population with a NW–SE trend.

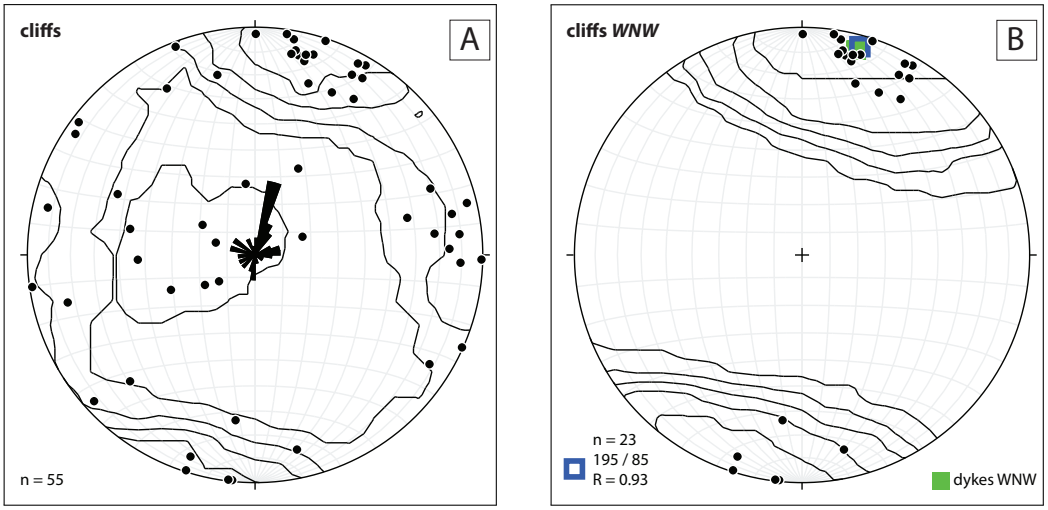

Figure 4.11 – (**A**) Poles of cliff orientations. The rose diagram indicates a population of cliffs trending WNW–ESE. – (**B**) Separated population of cliffs orientated in a WNW–ESE trend (rose diagram in **A**). The Bingham best fit highlights that this cliff population (blue empty square) has the same orientation as the WNW–ESE trending dyke population (green full square).

4.6 Discussion

4.6.1 Summary of Observations

An area of approximately one square kilometre was mapped in detail for pseudotachylyte occurrence. The outcrop areas of 5 x 5 metres to 10 x 10 metres were asigned one of four categories depending on the mode of occurrence of pseudotachylyte. Of the outcrops visited in that area, no outcrop was found without any pseudotachylyte occurrence. All outcrops visited show some degree of deformation which seems to be related to the formation of pseudotachylyte. There is a high abundance of quasi-conglomerate. The boundaries of the thickest quasi-conglomerate bodies could not be established due to smaller outcrop size, but is estimated (from clast and rotated foliation textures visible through lichen covered outcrops) to be around 15 metres or more. One quasi planar outcrop of approximately 10 x 20 metres showed continuous exposure of quasi-conglomerate. Due to the ubiquity of pseudotachylyte related deformation and the size of the outcrops it is difficult to identify boundaries with the host rock, which might itself be deformed (see Chapter 6).

The quasi-conglomerates seem to occur in quasi continuous zones which can be followed over tens to hundreds of meters. However, the thickness of these zones varies considerably. In places they are a few decimetres or over metres thick. In other places they step in thin, millimetres to centimetres thick veins, which connect quasi-conglomerate bodies in complex three dimensional geometries. These thin veins are not defined and thus mapped as quasi-conglomerates. The mapping strategy used here was therefore not able to capture these quasi continuous zones, but they can be followed in the field. Three main zones of quasi-conglomerate development were found (from sea level upwards):

1) *At sea level* from the River Mouth towards Seal Bay and north of it, and on the two small headlands north of Cleit.

2) *At around 70m (N) to 80m (S) asl*, in a well exposed zone at least 50cm thick on the cliff W and NW of the mast.

3) *On the mound NE of the mast* at 60-70m asl.

The stereographic data and field observations suggest that the quasi-conglomerates that occur in zones are mostly parallel to the gneissic foliation. This suggests the preexisting anisotropy at least partly controls their formation. However, the difficulty with identifying boundaries to the host rock, i.e. to distinguish between a fragment inside a quasi-conglomerate and the host rock, could lead to a bias in measurements. Pseudotachylyte veins occur both concordant and discordant to the foliation. One example of a pseudotachylyte network (Figure 4.8) shows that the network boundaries, i.e. the longest and most parallel pseudotachylyte veins,

are parallel to the foliation, whereas the interconnecting veins are discordant and shorter.

The dykes – 'Minor Intrusives' – constitute a major lithology on the headland. Cliffs with the same orientation as the WNW trending dykes are likely to represent dyke walls, where the dyke material has been eroded, or fractures parallel to the dykes. Fractures parallel to dykes were found in several outcrops, especially in areas where dykes are densely spaced, such as the River Mouth south of Àird Ghrèin, and the coast line comprising the small headlands NW of Cleit.

4.6.2 Mapping Strategy

Mapping of pseudotachylyte occurrences in different places in the world has been performed on a range of scales. To the author's knowledge, this is the first time the occurrence of pseudotachylyte was attempted to be mapped on this scale and resolution. Fletcher and Reimold (1989) recorded pseudotachylyte distribution in terms of pseudotachylyte size per locality in Vredefort, South Africa, in an area of approximately 250 x 100 kilometres. A similar strategy, also in the Vredefort impact structure, was applied by Lieger et al. (2009), who recorded brecciation intensity at each of their stations in an area of approximately 40 x 20 kilometres. In roughly the same area, Reimold and Collistion (1994) published estimated abundance of pseudotachylyte in area percentage per 'exposure', but did not define the size of what they counted as an exposure. In the Southern Alps, Di Toro and Pennacchioni (2005) mapped pseudotachylyte veins and cataclasites on an exceptional, glacier polished and freshly uncovered outcrop in an area of 200 m^2 (20 x 10 metres). The detail and scale of their mapping is more comparable to the mapping of outcrops presented in the following Chapter 5.

In the Sudbury impact structure in Canada, Fedorowich et al. (1999) quantified the amount of Sudbury Breccia in a total area of approximately 9 km^2 by conventional mapping techniques that treated the Sudbury Breccia as a lithology. It should be noted that the Sudbury Breccia covers both cataclastic and pseudotachylitic rocks, which are commonly not distinguished (Rousell et al., 2003). A similar concept was applied by the British Geological Survey for the geological maps of the Outer Hebrides (BGS, 1981) on a scale of 1:100 000. Five lithological units and one signature are used to distinguish "Rocks affected by movements on the Outer Hebrides Trust Zone: Gneiss with marked 'cataclastic' fabric; 'Mashed gneiss' (original banding largely destroyed); Gneiss with abundant pseudotachylyte development [signature]; Mylonite; Corodale gneiss: dominatly garnet-pyroxene rock (? meta-igneous) (South Uist)". Of these six categories, only the two pseudotachylyte bearing categories are recorded on Barra.

The scale of the map produced for this study is one order of magnitude more precise than the geological BGS map. In addition, the different modes of occurrence of pseudotachylyte were recorded and defined. The resolution limit of approximately 5 x 5 metres to 10 x 10 metres is insufficient to capture the complex details of the quasi-conglomerate bodies and their potential spacial relationship. To capture some of the pseudotachylyte geometries on the outcrop (meso) scale, a surface photography mapping approach was applied, covering areas of approximately a third of a square metre to a maximum of a continuous area of $2\,m^2$. The data is presented in the following Chapter 5. The strategy of mapping the two dimensional projection of the real surfaces rather than the surfaces themselves complicated the representation of the many vertical outcrops. The mapping of the geometry of quasi-conglomerate zones could potentially be achieved by a surface photographic mapping method at a higher resolution using for example aerial photographs as base maps. Such a surface mapping approach could account for the projection problem encountered when using a topographic projection where vertical surfaces are not represented. At the time of this study this technology was not available to the author.

4.6.3 Relative Occurrence of Pseudotachylyte Modes on the Macro Scale

For each mode of occurrence of pseudotachylyte, that is outcrops containing veins, networks or quasi-conglomerates, a separate macro scale map layer was created from the map (Figure 4.3) which is shown in Figure 4.12. The number of pixels in each colour corresponds to the area covered by that mode. The sum of the coloured pixels of all individual maps represent the total outcrop area of Lewisian gneiss (in black). The area underlain by dykes were not included because they have intruded after pseudotachylyte formation, and are demonstrably younger.

Error Estimate 'A'

An error estimate was performed ('Correction A'), for which a virtual outcrop area of the same extent as the red (quasi-conglomerate) outcrop area with assumed absence of pseudotachylytes was added. Figure 4.13 explains this step. This error estimate is to account for the mapping of vertical outcrops and other systematic biases, such as cognitive biases (Shipton et al., 2019), towards the mapping of pseudotachylyte occurrence. The results of the calculations are shown in Figure 4.14.

Results

The quasi-conglomerate category constitutes the most abundant mode of occurrence (two thirds of the outcrops of Lewisian gneiss) and is followed by networks

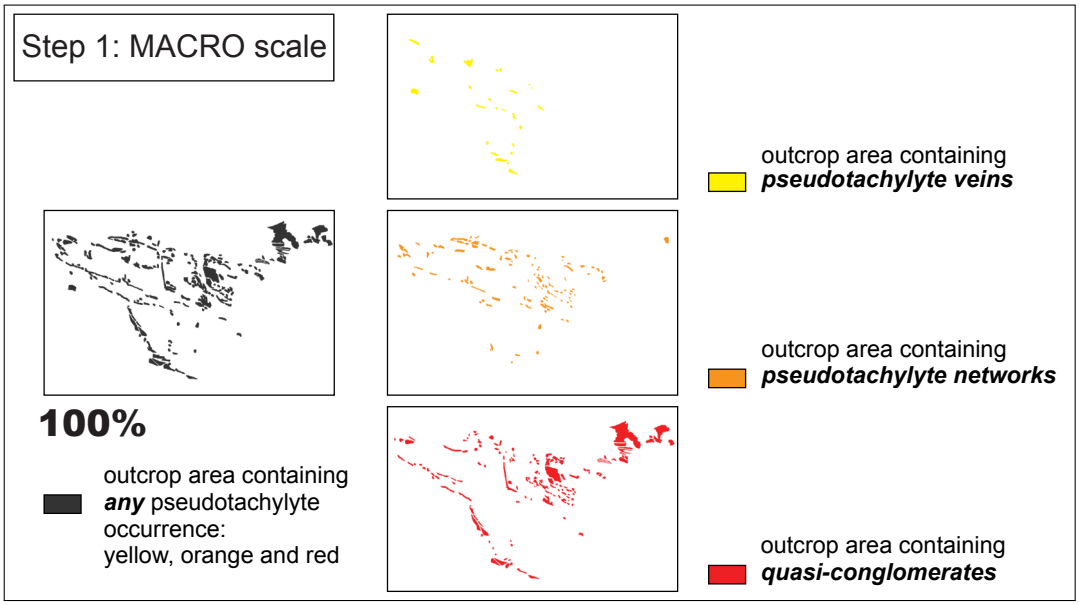

Figure 4.12 – Step 1. – For each pseudotachylyte mode of occurrence (yellow, orange and red) a separate map was made. The areas coloured in each individual map gives the total area of that pseudotachylyte mode of occurrence. The total outcrop area is given by the combination of the yellow, orange and red maps.

(one quarter). The entire outcrop area on Àird Ghrèin is affected by pseudotachylyte development (pseudotachylyte *sensu lato*) and the accompanying deformation. However, from this data no statement can be made about the amount of 'actual' pseudotachylyte in these rocks, that is, the dark aphanitic material between fragments and along veins (pseudotachylyte *sensu stricto*). To quantify the amount of pseudotachylyte sensu stricto, data from a few selected outcrops were collected (meso scale data), which is presented in the following Chapter 5. The two data sets together, the macro and the meso scale, are then used to calculate the amount of pseudotachylyte sensu stricto for the entire headland. The results of these calculations are discussed in Chapter 8.

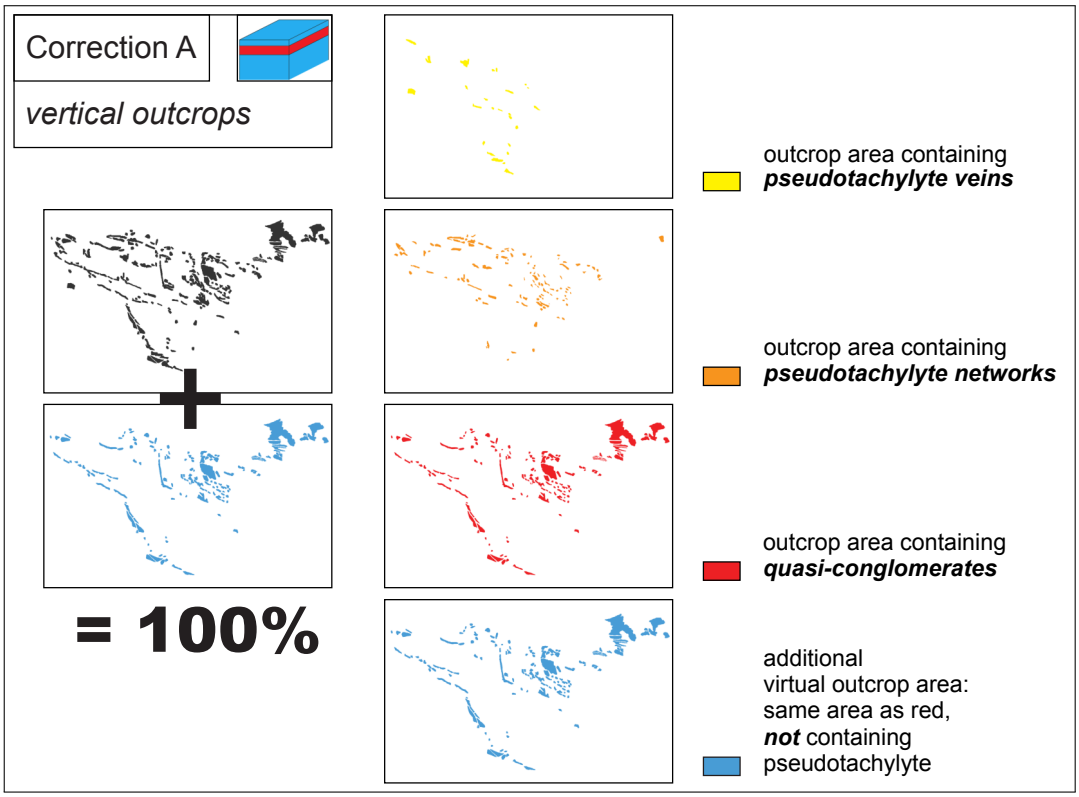

Figure 4.13 – *Illustration of Correction A.* – A virtual outcrop area in blue (no pseudotachylite) is added, its extent being equal to the area mapped in red. Correction A is applied to take into account that a significant number of outcrops are on vertical cliff faces, and other systematic biases.

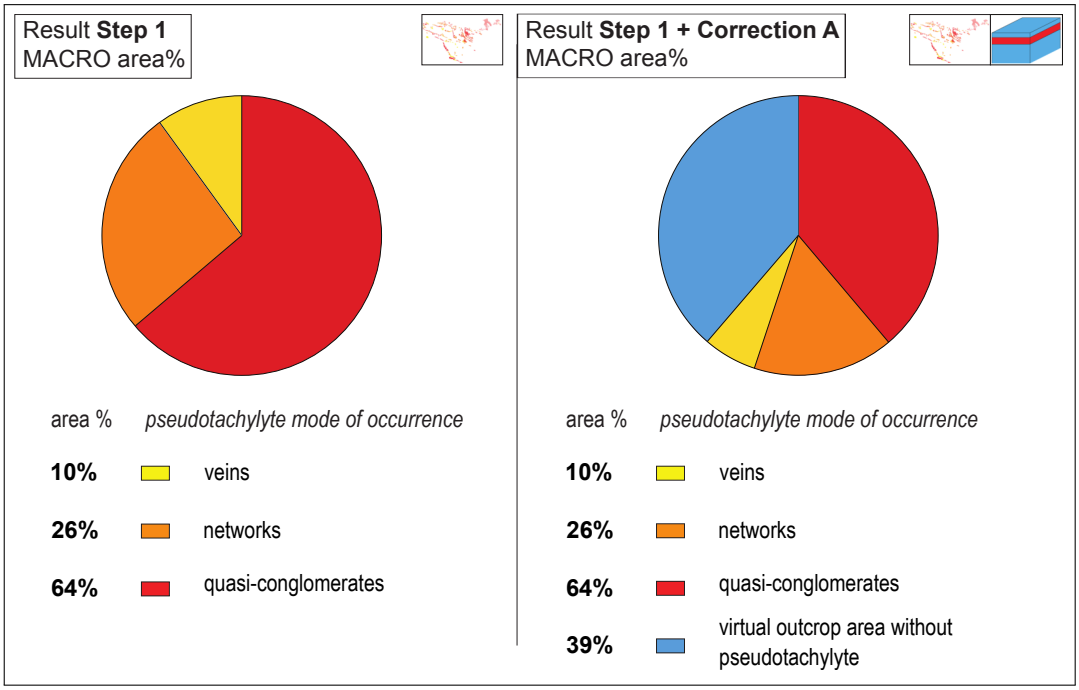

Figure 4.14 – *Results of Step 1 (left hand side) and Correction A (right hand side).* – The area percentages are displayed both in the colour coded pie chart and in the list below. Whereas the results of Step 1 represent the raw data, Correction A adds a virtual outcrop area without pseudotachylyte, see text for explanation.

Chapter 5

Meso Scale: Volume and Structure

5.1 Introduction

The macro scale data (Chapter 4) show that pseudotachylyte (in the following referred to as pseudotachylyte *sensu lato*) occurs in all mapped outcrops on Àird Ghrèin. To quantify the amount of pseudotachylyte *sensu stricto*, the areas of an outcrop that are made up of pseudotachylyte, a representative percentage needs to be established for each mode of occurrence on the map. To facilitate this quantification, outcrop-scale (meso scale) maps were produced in the field. These maps are also used to describe meso scale structures. The meso scale describes what is visible on outcrops in the field by the unaided eye, and ranges from a few metres to a couple of millimetres. The observations focus on the quasi-conglomerate, because the formation of this pseudotachylyte geometry is still an enigma that this study aims to address.

5.2 Setting

Two localities, set within the mapped area on Àird Ghrèin (see previous Chapter 4) were studied in detail in terms of meso structures. These two localities were chosen because of the quality of the outcrops, and to represent the quasi-conglomerates and the networks of pseudotachylytes on the headland. These two localities were chosen because of their exceptionally good surface conditions. Especially the outcrops at Locality 1 allowed for recording of details on the millimetre scale because the surfaces are polished by the tides. The surfaces of many other outcrops were less planar, or stained or covered in lichen, algae or barnacles. The two localities are shown on the map in Figure 5.1. The localities and outcrops are described in detail in Section 5.4.

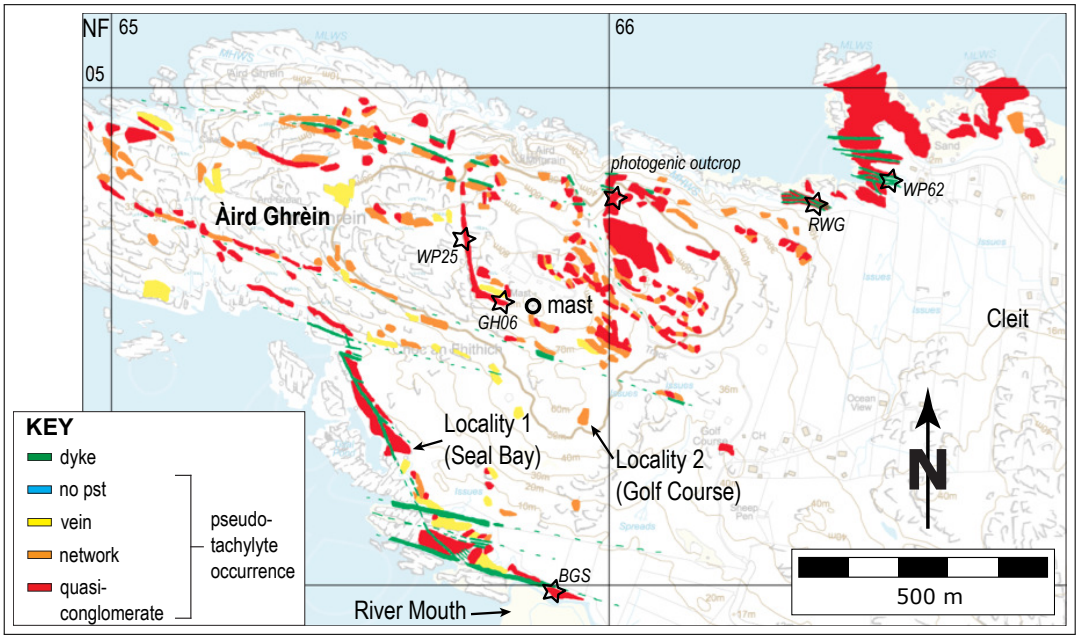

Figure 5.1 – Map of the Àird Ghrèin area. Localities for meso structural analyses are denoted: *Locality 1* (quasi-conglomerate) is located on Seal Bay, *Locality 2* (pseudotachylyte network) is on the Golf Course. A single meso map stems from a location denoted WP25 (see Table A.1 in the Appendix for grid references for all maps).

The Lewisian host rock is variable on the meso scale. Mafic layers of a few centimetres to meter thickness are not uncommon. These layers sometimes form boudins or migmatitic structures. However, in these two localities, the host rock is generally light in colour, which provides a helpful contrast to the dark pseudotachylyte.

5.3 Method

The aim of the meso scale mapping was to produce accurate maps of quasi-conglomerates and pseudotachylyte networks in the 1 : 0.5 to 1 : 5 scale, which distinguish between pseudotachylyte *sensu stricto*, and host rock and host rock fragments. The method is illustrated in Figure 5.2.

5.3.1 Field

Meso-scale structures were traced in the field directly onto printed out photographs. This method enables relatively fast mapping and accurate scaling. Photographs of the rock surface in Locality 1 were taken using a $30 \times 30\,cm$ wire grid (grid spacing $10\,cm$) for scale. In Locality 2, strings were spanned into a grid with $1\,m$ spacing.

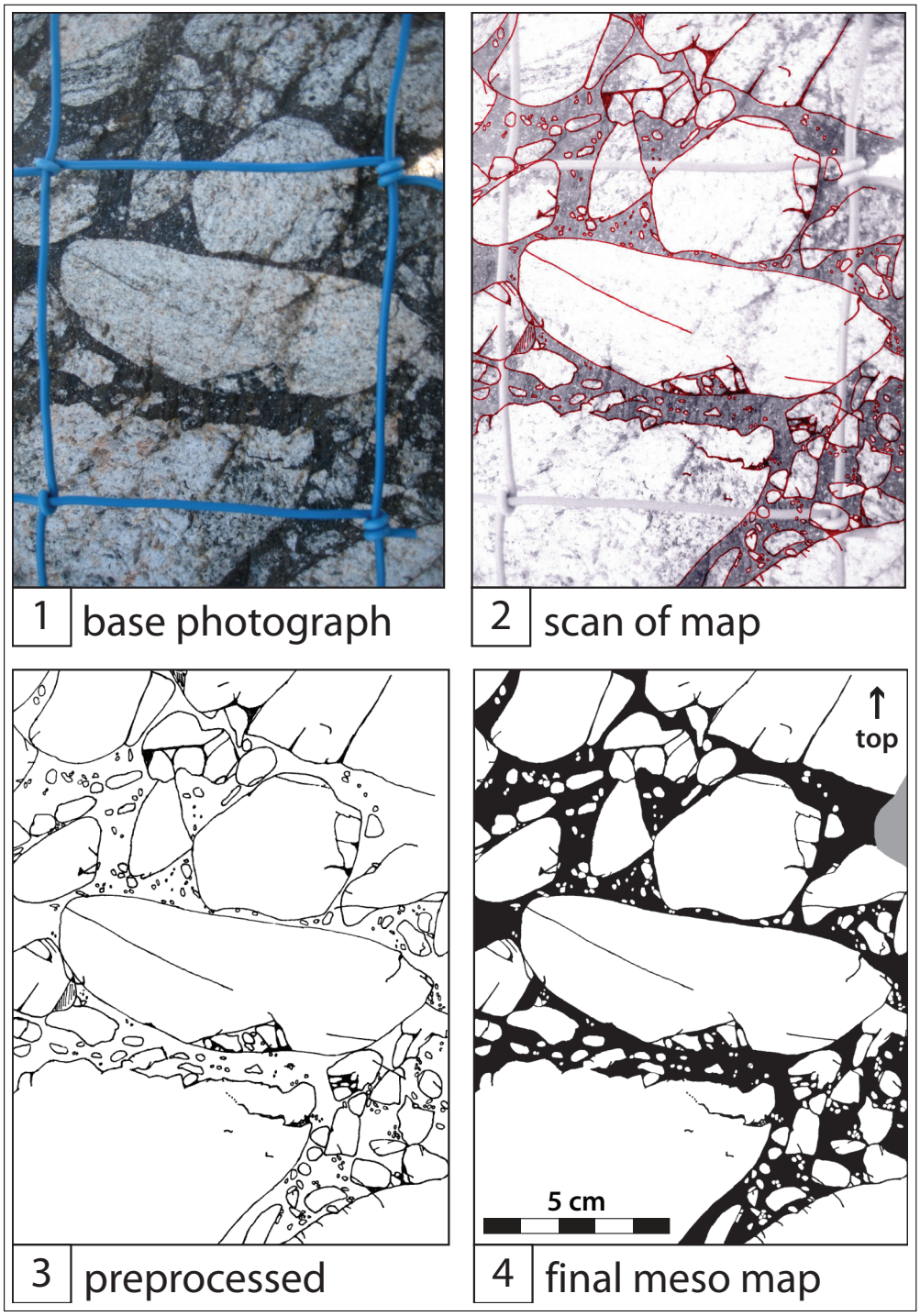

Figure 5.2 – Sequence depicting the stages for meso map production. – (**1**) Photograph of the area to be mapped. Blue wire square is 10 x 10 centimetres. – (**2**) Scan of the printed out base photograph onto which the structures are mapped in the field (in red). – (**3**) Binary image of mapped features extracted from the scan shown in (**2**). – (**4**) Final meso map, black representing pseudotachylyte *sensu stricto*, white are rock fragments, and grey is an area of poor exposure. This map with annotations is again shown in Figure 5.12.

5.3.2 Digitalization

A semi-automated process was used to produce the digitised maps. The traced photographs were scanned, and the scan turned into a black and white image using a suitable threshold. To achieve the most accurate structural details all maps were then refined manually.

5.3.3 Representation

On the digitized maps, white represents host rock and host rock fragments, black represents pseudotachylyte *sensu stricto*, and grey represents areas of no or poor exposure. The pseudotachylyte *s.s.* mapped in black includes unresolved fragments, which are crystalline host rock fragments smaller than few millimetres. Depending on the scale of the meso map, this resolution limit varies between one millimetre to approximately one centimetre.

Because of the scale dependency of mapped features, each map has a reference scale. The reference scale is the approximate extent of the original meso scale map, which is either $10\,cm$, $30\,cm$, or $1\,m$. Several maps were made of the same area using different reference scales. For example, a map covering a $30\,\mathrm{x}\,30\,cm$ area can comprise nine maps of reference scale $10\,cm$. The reference scale also gives a rough guide for the resolution limit of the maps. This means, for reference scale $10\,cm$, the resolution limit is about one millimeter, whereas for the $1\,m$ reference scaled maps the resolution limit is in the order of a centimetre.

5.4 Meso Map Localities and Outcrop Description

A total of twenty-one maps were made, of which, in the following, a few representative examples are shown, described and discussed. The additional maps can be found in Appendix A, and Table A.1 gives an overview of the 21 meso-scale maps, their reference scales, and pseudotachylyte *sensu stricto* area percentages.

5.4.1 Locality 1: Seal Bay

Locality 1 (NF 656 042) is mapped as quasi-conglomerate and is situated in Seal Bay (Figure 5.3), northwest of the River Mouth, where the storm-tidal waves have polished the rock to a nearly perfect surface. This locality is split up into two main outcrops 1A and 1B, which are approximately 20 metres apart. Both outcrops are on the pebbly beach and depending on the tidal action, variably covered with pebbles of centimetres to decimetres in diameter. The rock surfaces are smoothly polished like pebble stones, and are only disrupted by a few fractures. Quasi-conglomerate is very abundant in this area. It can be followed as a zone, starting from the River Mouth, along the high tide line towards North, all the way to the

Figure 5.3 – *Locality 1, Seal Bay, NF 656 042.* The bay is shown on the left hand side. The rock behind is below the high tide line. The western tip of Àird Ghrèin is visible in the background. The main outcrop (Outcrop 1A) is shown at the right hand side. Outcrop 1B is not on the image and located towards the left (south) of the photograph. The photograph is taken at low tide towards WNW, standing on the main quasi-conglomerate outcrop (Outcrop 1A). PET bottle in foreground is 20 centimetres long.

beginning of the headland. Figure 5.4 gives an idea of the surface quality and meso topography of the outcrops of Locality 1.

Outcrop 1A

Outcrop 1A has the most pronounced meso-topography of the three outcrops, with a slightly undulating surface (Figure 5.5). The appearance of the pseudotachylyte in this outcrop very much resembles pebbles embedded in tar.

Outcrop 1B

The appearance of this outcrops reminds of the descriptive terms which have been used by previous workers for rocks in the Outer Hebrides: crushed rock and shattered gneiss. The unique meso topography offered by this outcrop allows a

Figure 5.4 – *Locality 1, Seal Bay, NF 656 042.* This outcrop is nearly perfectly polished by the wave action (pebbles in foreground, left hand side). The meso topography of this locality is pronounced. However, there are many surface areas of approximately $30 \times 30\,cm$ that are quasi planar. The quasi-conglomerate is visible in the foreground at the right hand side, wedges towards the left, where it widens again at the left hand side of the image. Photograph taken towards East. Figure 5.5 is located to the right.

Figure 5.5 – Overview of the part of **Outcrop 1A** where most of the meso maps of this outcrop come from (Locality 1, Seal Bay, NF 656 042). The outcrop surface is curved on the metre scale but rather even on the decimetre scale. The quasi-conglomerate in this outcrop looks like pebbles in tar. The surface slopes towards the observer (dip direction SW). Pen for scale (centre, red cap).

Figure 5.6 – *Locality 1, Seal Bay, NF 656 042.* The surface of **Outcrop 1B** is planar and nearly horizontal up to the pen. The surface makes a step where the massive pseudotachylyte *s.s.* is in the foreground (massive pseudotachylyte *s.s.* wedge slopes towards the observer, and a rounded edge step towards the left of the perpendicular pseudotachylyte just above the wedge. This provides a unique three dimensional view. A schematic block diagram of this outcrop is shown in Figure 5.7. The meso map of this view is shown in Figure 5.9 **C**. Yellow part of the pen is 10 centimetres.

three dimensional view (Figure 5.6) which is shown in the block diagram in Figure 5.7. In the block diagram in Figure 5.7, **A**, **B** and **C** refer to the orientations of the meso maps shown in Figure 5.9, and the corresponding photographs **A** and **B** in Figure 5.8, and **C** in Figure 5.6.

5.4.2 Locality 2: Golf Course

Locality 2 (NF 659 043) is a pseudotachylyte network set inbetween partially grass covered sand dunes on Barra's golf course in the vicinity of *hole number 6*. The outcrop surface is as smooth and fresh as a non-polished rock surface can be. Unfortunately, the surface of the outcrop is not perfectly orientated, that means, the structures are not at ninety degrees to the surface. The outcrop surface dips at 202 / 18. Outcrop 2 is shown in Figure 5.10.

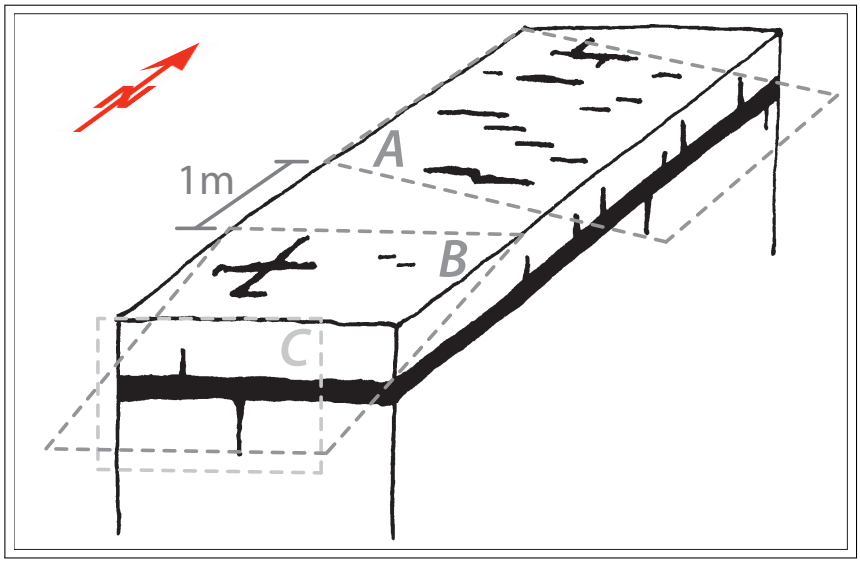

Figure 5.7 – Schematic block diagram of *Outcrop 1B*. **A**, **B** and **C** refer to the meso scale maps in Figure 5.9, and the corresponding photographs in Figure 5.8 (**A** and **B**), and Figure 5.6 (**C**). The surface of the outcrop is nearly horizontal and cuts the massive quasi horizontal pseudotachylyte vein at a low angle. Map **A** is offset from map **B** by approximately 1 metre. Map **A** is slightly inclined towards East. Map **B** includes the step at the pseudotachylyte *s.s.* wedge (Figure 5.6) and is therefore here represented as slightly inclined towards South. Map **C** is the front view, which is here represented as being vertical, however it is non-planar and inclined towards South and covers part of map **B** (the crossed pseudotachylyte veins). Not to scale. *Locality 1, Seal Bay, NF 656 042.*

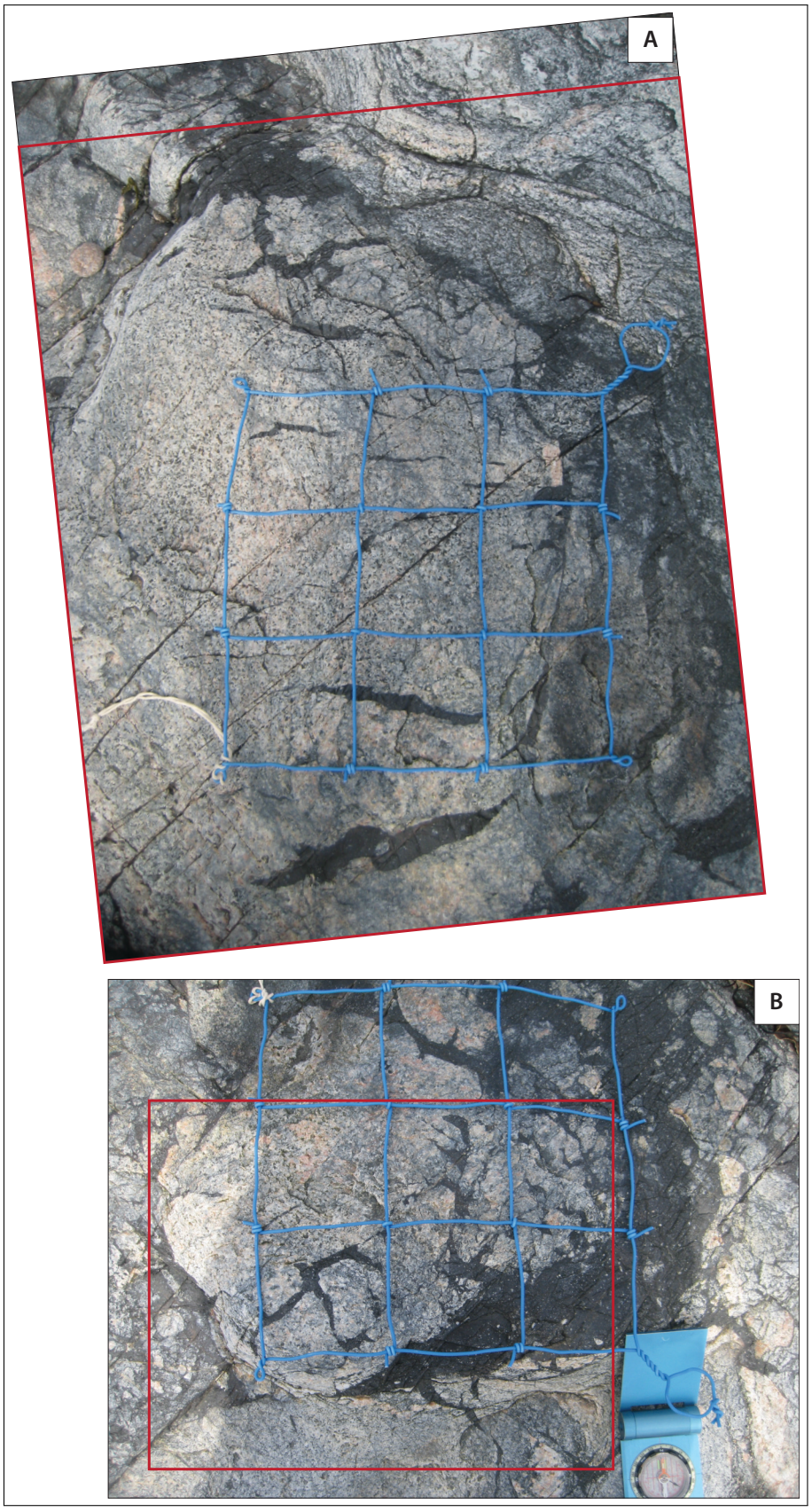

Figure 5.8 – Base photographs for meso maps **A** and **B**, top view of Outcrop 1B. The wire grid is $30 \times 30\,cm$ and oriented parallel to the cardinal directions (top N). The superimposed red rectangles denote the areas covered by the meso maps in Figure 5.9. *Locality 1, Seal Bay, NF 656 042.*

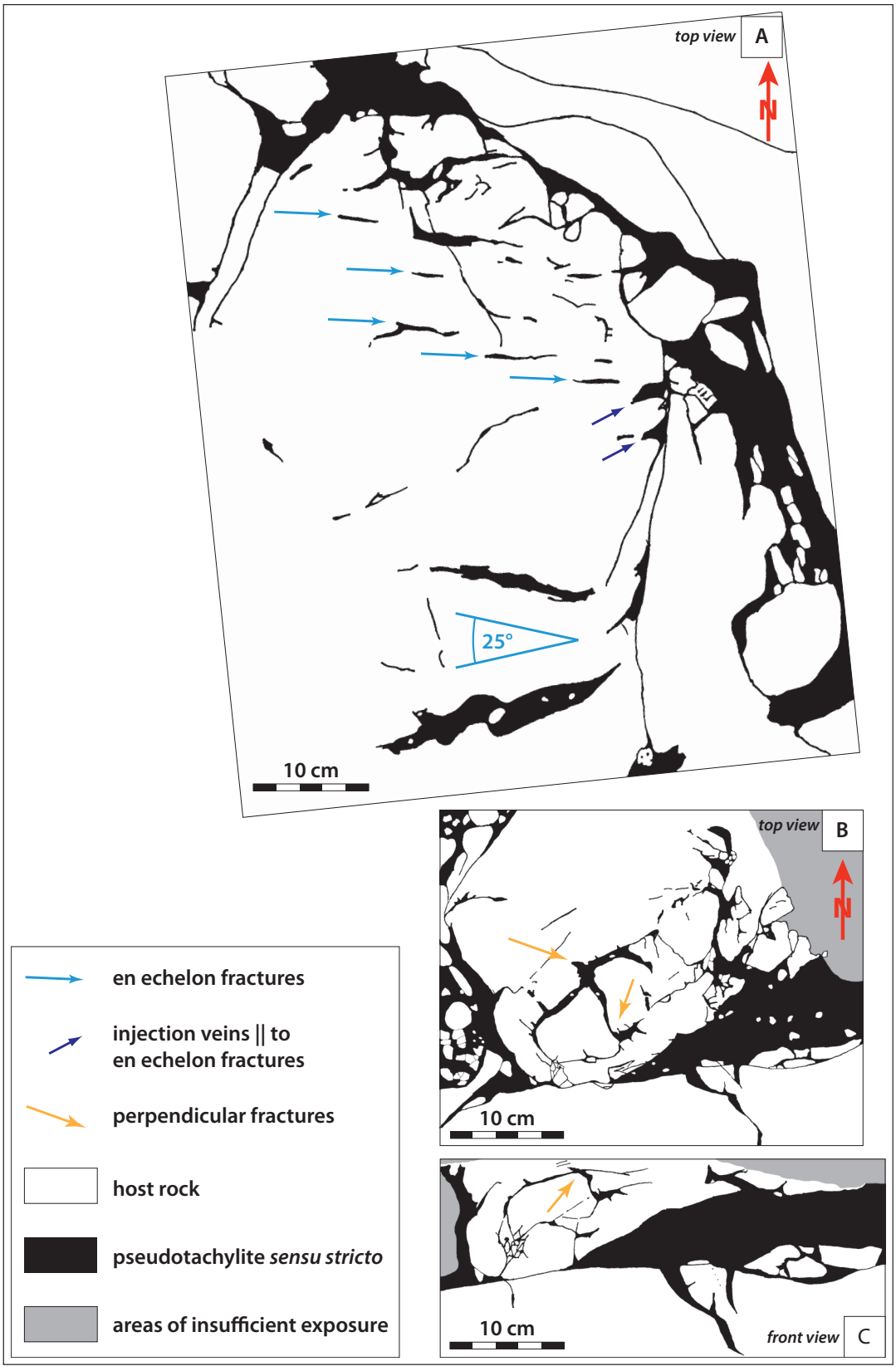

Figure 5.9 – Maps **A**, **B** and **C**, Outcrop 1B. Maps **B** and **C** overlap, map **A** is approx. 1 m towards NW of map **B**. Note the sets of parallel en echelon veins in map **A** (E-W trending). The largest pseudotachylyte vein in the South of map **A** contains rock fragments. This vein is counter-clockwise rotated by about 25° with respect to the en echelon veins. The perpendicular vein set in map **B** is again rotated CCW by about 25° with respect to the large pseudotachylyte vein in map **A**. All these veins are approximately perpendicular to the massive horizontal pseudotachilite vein (see block diagram in Figure 5.7), and are thought to represent injection veins. *Locality 1, Seal Bay, NF 656 042.*

Figure 5.10 – *Locality 2, Golf Course, NF 659 043.* **Outcrop 2** is approximately 6 metres long and 2 metres wide. The pseudotachylyte network boundaries are parallel to the foliation that is marked by darker bands in the schistose gneiss, parallel to the direction into which the photograph was taken. Scale in the foreground is 30 cm long.

5.5 Mesostructural Observations

In the following, the key observations of the meso scale are summarised. Only structures related to pseudotachylytes are described, that means, unless stated otherwise, fractures refers to pseudotachylyte filled fractures, and fragments are embedded in pseudotachylyte.

It should be noted that the observations are based on what is visible on the outcrop surface. The investigated rock surfaces are approximately planar, except in Outcrop 1B, where the suface forms a little hill. The described features are three dimensional, and their orientations and geometries above and below the observable section are generally unknown. This problem is referred to as the *section problem*. For example, the term *fracture* refers to the *fracture's trace* on the outcrop surface. Outcrop 1B is a special case in that it provides a pseudo three dimensional surface. Where the section problem plays a role in terms of interpretation of the feature, its implications are mentioned in the respective paragraph. The figures are shown at the end of the summary of observations (page 87*ff*).

5.5.1 Fracture Shape

The fracture shape describes the observed geometry of a single fracture, that is, the fracture's trace on the outcrop surface. This section describes fracture shapes which were commonly observed on Barra.

Curved Fractures

Curved fractures are smooth on the millimetre scale but not straight on the centimetre scale. Some curved fractures taper off within the rock mass. Curved fractures that do not taper off, i.e. represent fragment boundaries, are **fragment-forming curved fractures**. Due to the generally unknown three dimensional fracture orientation with respect to the outcrop surface, the true angle of curvature cannot be established. However, in any section, the trace of a curved fracture remains curved. Curved fractures were found on nearly all maps. Figure 5.11 shows an example of curved fractures which tapper off, and curved fractures that are fragment forming.

Serrated Fractures

Serrated fractures have a saw-tooth geometry, with a wavelength of millimetres to a couple of centimetres, but with an overall planar direction (on the centimetre to decimetre scale). Serrated fractures commonly originate from a fragment boundary and taper off. At their origin, they may be up to a centimetre wide. In comparison to smooth fractures, serrated fractures are shorter and generally taper

off after a decimetre or less. The observed opening angle (and thus the opening width) of a serrated fracture depends on the angle of intersection between the orientation of the fracture and the outcrop surface. Serrated fractures are rather rare in comparison to other fractures. Figure 5.12 shows an example.

5.5.2 Fracture Arrangement

The fracture arrangement describes how two or more fractures are related to each other, or how a fracture relates to a fragment boundary.

En Echelon Fracture Sets

Opening fractures occur in parallel en-echelon sets with a regular spacing. They have a regular spacing of a few cm, and the longer fractures tend to have a wider spacing. The pseudotachylyte that fills the en echelon fracture may contain rock fragments. En echelon fractures have only been observed in Outcrop 1B (meso map (**A**) in Figure 5.9, and photograph in Figure 5.8). There, they can be correlated with injection veins. Thus they seem to represent the top view of a section that is perpendicular to the injection vein and parallel to the main pseudotachylyte vein.

Perpendicular Fracture Sets

Perpendicular fracture sets meet at close to 90° angles. At the origin (meeting point) of the fractures, the interface of the rock is commonly rounded, giving the pseudotachylyte a four-legged starfish appearance. Further away from the origin, the individual fractures may curve, branch, tapper off, or form more perpendicular fractures. The visible section needs to be close to perpendicular to the perpendicular fracture set, otherwise the fracture set has pairs of two acute and two obtuse angles, and the origin covers a larger area, which make perpendicular fractures more difficult to recognise. Perpendicular fracture sets have most pronouncedly been observed in Outcrop 1B. Figure 5.9 (map **B**) and Figure 5.8 (photograph) show one well developed example. Figure 5.13 shows another example of a perpendicular fracture set that, at one end, shows a curved fracture. Parallel fractures (see below) are sometimes interconnected by perpendicular fractures which may result in rectangular fragments.

Point Indentation Fractures

Point indentation fractures display an origin, from which several fractures branch, but not in a manner as structured as in perpendicular fracture sets. The visible section needs to be close to the rock's interface with the pseudotachylyte to be recognised as such. Point indentation fractures were observed in Outcrop 1B. Figures 5.13 and 5.15 show examples.

Injection Veins

Injection veins are a type of opening fracture that originates from a straight pseudotachylyte vein that is commonly not dominated by opening (shear fracture). Injection veins are described in the literature as veins coming off at a high angle from a pseudotachylyte generation surface (the shear fracture). Injection veins tapper off and are commonly in the order of centimetres up to two decimetres long. The pseudotachylyte in the injection vein may contain fragments. The fracture surfaces are generally planar and can be serrated or curved. The apparent thickness of the opening fracture depends on the angle between the section surface and the injection vein. Injection veins have been observed in Outcrop 1B and Outcrop 2. In Outcrop 1A, injection vein resembling opening fractures occur in fragments. In map **A** in Figure 5.9 and Figure 5.8, injection veins are correlated with en echelon fractures.

Parallel Fractures

Parallel fractures are longer than their spacing and occur side by side. This is in contrast to en echelon fracture sets (see above). Parallel fractures are sometimes opening fractures, but more often very thin and may show offsets (shear fractures). Parallel fractures occur commonly at fragment edges, and sometimes form rectangular fragments when interconnected with perpendicular fractures (see above). Figure 5.14 shows an example of foliation parallel, parallel fractures.

Spall Fractures

At fragment edges, fractures commonly form spalls, which are elongate roughly parallel to the fragment boundary, but curve to reach the fragment boundary at one or both ends, or tapper off. The spalls resemble rock chips that come off when hitting a rock. Spall fractures occur commonly at fragment edges, and sometimes form lanceolate fragments. Where the spall fracture is not through going, the rock forms a finger-shaped headland. This is most commonly observed in Outcrop 1A.

Splaying / Branching

A smooth fracture that branches before it tapers off. The branches may be straight or curved, and they continue into the general direction of the fracture. Compared to the length of the single fracture, its branches are generally short. Branching fractures are not commonly been observed at the field site. Examples are indicated in Figures 5.11 and 5.15.

5.5.3 Fragment Shape

The fragment shape describes the apparent geometry of a fragment.

Rounded Fragments

Fragments are rounded when their surface is not angular. Rounded fragments may have concave surface segments. The shape parameter convexity is the deviation of the fragment's outline from the fragment's hull. Convexity is expressed in a ratio, with 1 being the maximum convexity where no concave segments are present. Most fragments are rounded (e.g. Figure 5.14). Angular fragments have most commonly been observed as in-situ fragments (see below in Section 5.5.4), or where fragments are separated from each other only by millimetre thin fractures.

Irregular Shape of Fragment Boundaries

An irregular shape of fragment boundaries is evident by crenate lobes and cuspate notches. Irregularly shaped fragment boundaries occur in all three outcrops. The general surface of irregularly shaped fragments is rounded, but interrupted by fractures that form lobes and fingers (Figure 5.15). The irregularly shaped fragments often display internal fractures.

5.5.4 Fragment Arrangement

The fragment arrangement describes how neighbouring fragments relate to each other.

In-situ Fragmentation

Some rock fragments are internally fractured. Where these fractures are continuous, they subdivide the fragment into sub-fragments. In-situ fragmentation often forms angular sub-fragments which often show no visible displacement. In-situ fragmentation has been observed in all outcrops. In Figure 5.12, the big fragment in the centre is fragmented at its lower part into sub-centimetre sized fragments, enclosed by a nearly perpendicular fracture pair. These small fragments are both angular and rounded, and they appear to be in the place where they were as part of their host. Through-going spall fractures also form in-situ fragments.

In-situ Fragment Clusters

In-situ fragment clusters are groups of fragments that evidently belong together, given by the rock type, their vicinity, and possibly by their shape (jigsaw puzzle). Based on the geometry of the fragment boundaries and the composition of the fragments compared to the host rock, the pseudotachylyte between the fragments

seems to have replaced parts of a larger fragment, rather than been intruded between the particles. There is no evidence for displacement of the fragments. The individual fragments are generally in the millimetre to centimetre size range. The in-situ fragment clusters give the most pronounced account of poor sorting (see below, Fragment Dispersion). Most angular fragments are in-situ fragments. In-situ fragment clusters were observed in all outcrops. Figure 5.13 shows an example of a massive quartz vein that has been fractured, and most of the fragments seem to fit together like a jigsaw puzzle. Figure 5.16 shows illustratory examples of in-situ fragmentation, which give a poorly sorted appearance to this map.

Rotation of Fragments

Rotation of fragments against each other is most clearly visible by fragments that contain a foliation, and where this foliation is not parallel in all fragments. Rotation is also observable in in-situ fragment clusters. The rotation is thought to be three dimensional, but the third dimension is not visible on an outcrop surface. Rotation of fragments is commonly observed and gives a chaotic appearance to quasi-conglomerates. In some of the fragments labelled with "gneiss" in Figure 5.14, their foliation is indicated by blue lines. These lines are linear but not parallel to each other across the fragments which means that the fragments have been rotated after their formation.

Fragment Dispersion

The fragment dispersion describes the sorting of fragments in terms of size, and the regularity of spacing between the fragments. Due to the three dimensional nature of the problem, even in a perfectly sorted sample, a variability in fragment size is inherent (tomato salad problem). The fragment sizes range from millimetre to over one metre. In-situ fragments cluster, and the spacing between fragments is variable. Often, fragements do not touch (in the visible section), and when they do, they are commonly fragmented to a finer grain size at the point where they touch. There was no layering in terms of size observed. That means the fragment dispersion is heterogeneous and the resulting quasi-conglomerates are not well sorted. Poor sorting is well visible for example in Figure 5.16.

5.5.5 Cross Cutting Relationships

Cross cutting relationships indicate a relative time sequence of the formation of the cross cutting features. For example, a pseudotachylyte vein 1 that is crossed and offset by another pseudotachylyte vein 2, has formed before the second pseudotachylyte vein. The main and most convincing example of cross cutting fractures is from the "photogenic outcrop" (see map in Figure 5.1), on top of the hill East of the mast, which is shown in Figure 5.17).

5.5.6 Quasi-Conglomerate Inside Network, and vice versa

Depending on the scale of observation, and thus the detail investigated, areas of quasi-conglomerate *geometry* were observed within pseudotachylyte network *mode of occurrences*, and vice versa. These quasi-conglomerate geometries were smaller than 10 x 40 centimetres which was set as the limit for a quasi-conglomerate *mode of occurrence*. A zoom into a detail of Outcrop 2 (the pseudotachylyte network), shows a "small-scale quasi-conglomerate" geometry located in a corner where two pseudotachylyte veins meet (Figure 5.18). The meso map in Figure 5.11 (Outcrop 1A) that shows in-situ fragmentation of a fragment, represents a "small-scale pseudotachylyte network" geometry inside a quasi-conglomerate fragment.

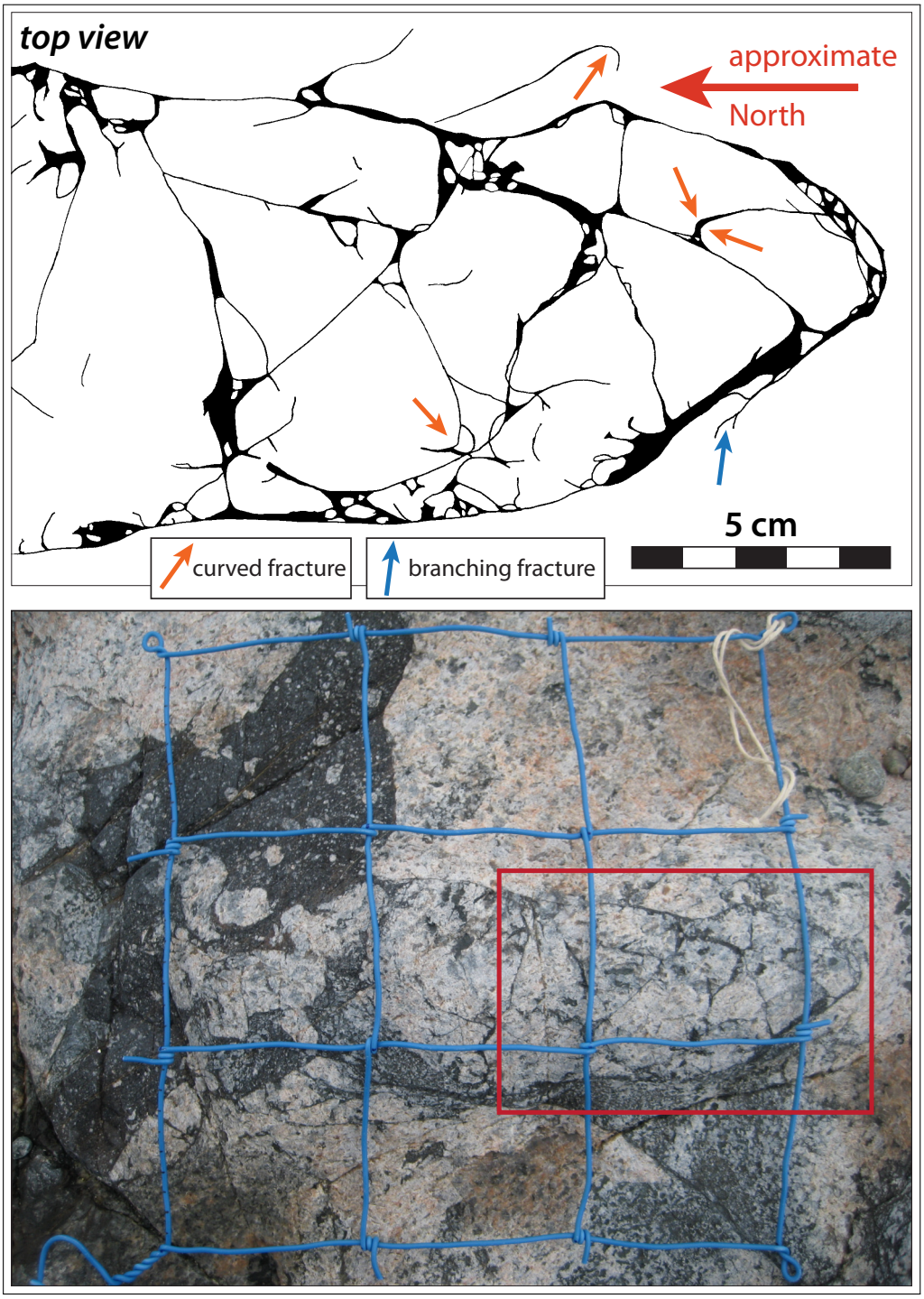

Figure 5.11 – Outcrop 1A, Seal Bay, NF 656 042. Curved fractures, branching fractures and network formation.

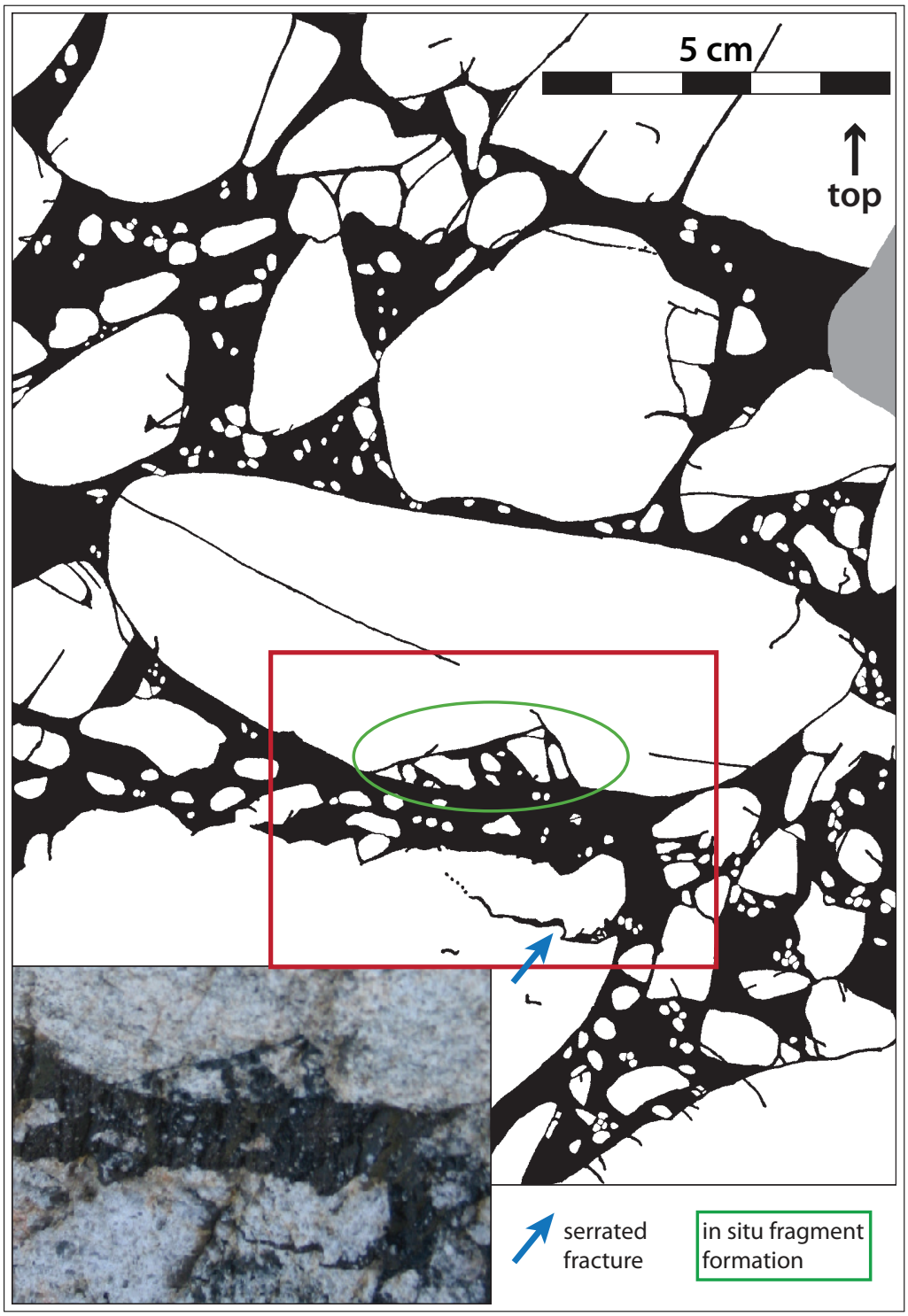

Figure 5.12 – Outcrop 1A, Seal Bay, NF 656 042. This meso map shows examples of serrated fractures and in situ fragment formation. The photograph is outlined by the red box on the map.

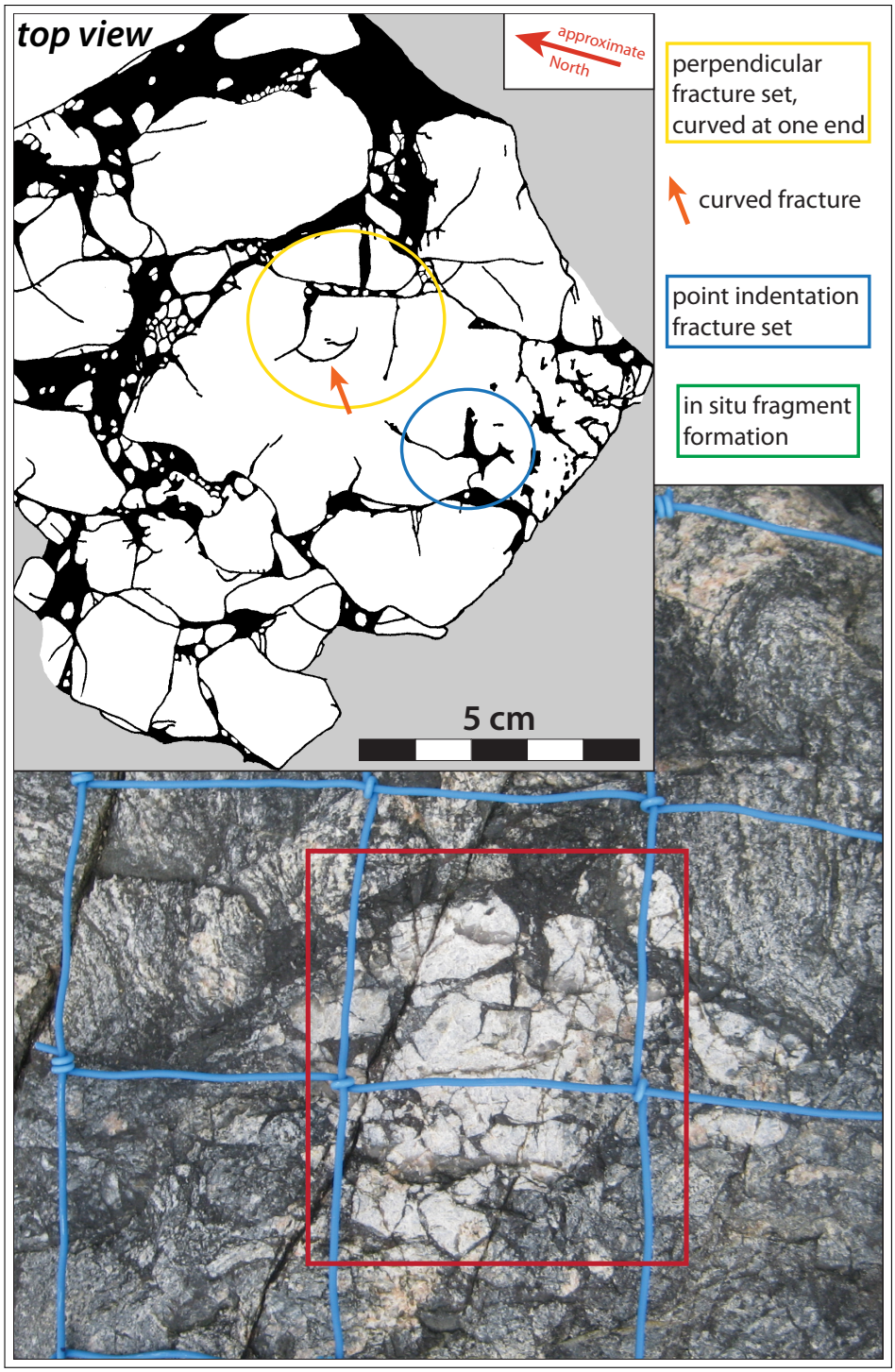

Figure 5.13 – Outcrop 1B, Seal Bay, NF 656 042. This outcrop displays a variety of features: A perpendicular fracture set with a curved fracture, in situ fragmentation and clustering of fragments, and a point indentation fracture set. The blue grid on the photograph has a spacing of 10 cm.

Figure 5.14 – Outcrop 1A, Seal Bay, NF 656 042. This meso map is labelled to indicate two different fragment types: gneiss, where a foliation is visible, and pegmatitic, where foliation is lacking (in the visible section). Not all of the gneissic foliation is aligned parallel which is evidence for fragment rotation. There are parallel fractures and rounded fragments.

Figure 5.15 – Outcrop 1B, Seal Bay, NF 656 042. This small scale meso map shows a point indentation fracuter set, some parallel and perpendicular fractures, and branching fractures. In addition, the yellow areas are transparent with the darker pseudotachylyte shining through from below the gneissic fragments. This hints to structures in the third dimension of this outcrop.

Figure 5.16 – Outcrop 1A, Seal Bay, NF 656 042. Small scale meso map, displaying in situ fragment formation which are present in fragment clusters.

Figure 5.17 – This photogenic outcrop (NF 660 047) shows a cross-cutting relationship indicated by the red arrow which points to a pseudotachylyte vein cutting through adjacent clasts. Clast rotation is visible by rotation of the ngeissic foliation of clasts. The scale at the bottom is 20 cm long.

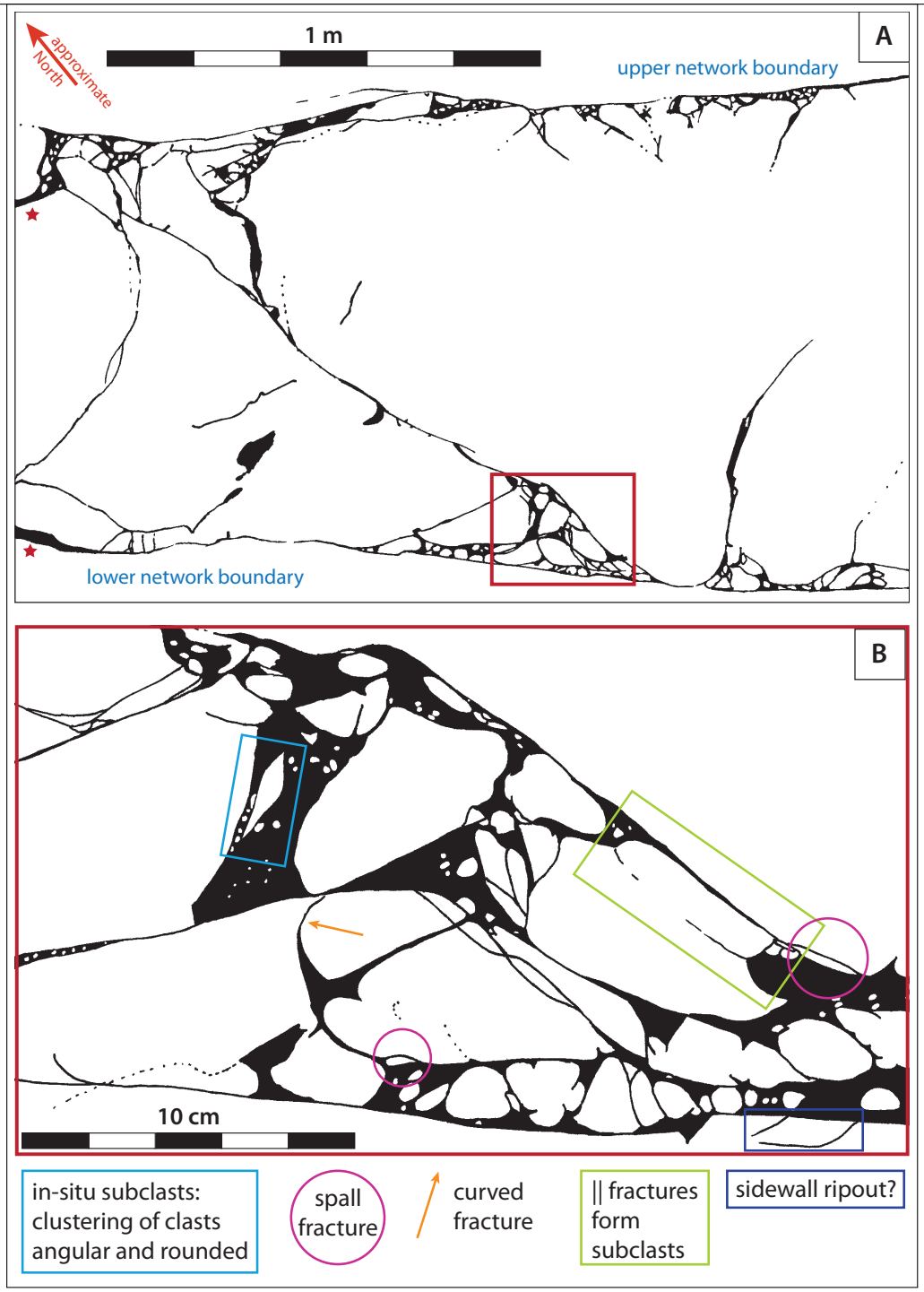

Figure 5.18 – Outcrop 2, Golf Course, NF 659 043. **A** – The pseudotachylyte network from Outcrop 2. The red box indicates the area of the detail shown in **B**. The network is bounded by two subparallel pseudotachylyte veins which have shorter veins come off (injection veins), some of which connect the two bounding veins. **B** was mapped on a separate, detailed photograph. Features visible on this small scale map are clustering of fragments, angular and rounded fragments, curved fractures, spall fracture, a curved fracture which forms a sidewall ripout, and parallel fractures which form a subclast.

5.6 Discussion

The following sections discuss the interpretation of the individual features observed in the quasi-conglomerates, followed by more general observations and a synthesis. A discussion of the formation of the quasi-conglomerates in the context of the literature is located in Chapter 8.

5.6.1 Curved Fractures

A fracture propagates into the direction of the maximum tensional stress (i.e. along the σ_3 trajectory). Curved fractures occur either when (A) a static stress field is applied with the σ_3 trajectory being curved, or (B) the stress field changes dynamically causing deflection of the propagation direction from its original orientation. However, as Kocer and Collins (1998) point out, the fracture formation itself interacts with the preexisting stress field.

Both static (A) and dynamic (B) stress fields, resulting in curved σ_3 trajectories, can be achieved in several ways.

(1) Static loading point indention (A) has been shown in experiments to form Hertzian cone fractures (Frank and Lawn, 1967; Lawn et al., 1974). Hertzian cone fractures produce, as their name suggests, a cone shaped fracture with the narrow end at the indentation surface. Figure 5.19 shows a part of the meso map in Figure 5.12 which shows a fracture set at the fragment boundary that could resemble a section through a Hertzian cone but is not very convincing.

(2) The marked *sidewall ripout* (Figure 5.18) has formed from a free surface with the fracture curving towards parallel to the surface. Sidewall ripouts have been documented by Swanson (1989, 1992) in the context of pseudotachylyte network formation. In point indention experiments they are commonly called "lateral vent cracks" that form upon unloading (B) of after the indentation experiment (Lawn and Swain, 1975; Lawn and Wilshaw, 1975).

(3) During formation of a fracture, the stress field is changed (B) by the propagating fracture (Kocer and Collins, 1998). This intrisic change causes a dynamic stress field that is likely to be different to the preexisting stress field (at fracture initiation). This relaxation induced dynamic stress field can also be caused by fractures in the vicinity that may be forming at the same time.

(4) The interaction with stress waves (extrinsic change) can dynamically (B) change a preexisting stress field (Gross and Seelig, 2011).

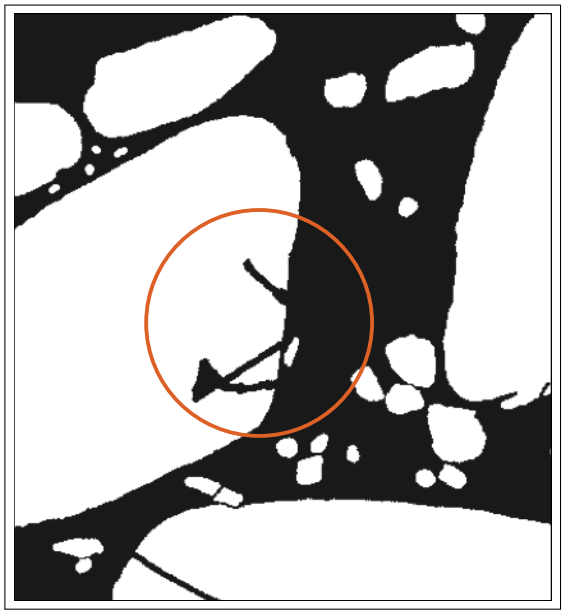

Figure 5.19 – Fracture set that could resemble a Hertzian cone fracture, but is not very convincing: two fractures with similar angles propagating from the surfaec to approximately the same depth into the fragment. Part of Figure 5.12.

(5) Thermal stresses have been shown to produce curved fractures. Bourne (1993) successfully produced oscillating fractures in a homogeneous medium in a quasistatic (A / B) cooling setting.

By which ever means they form, curved fractures are capable of forming rounded fragments (e.g. Figure 5.11).

5.6.2 Serrated Fractures

Serrated surfaces such as seen in Figure 5.15 seem to arise from a curviplanar fracture, from which smaller fractures, emanate at high angles to the main fracture. In this case, they can be compared to perpendicular fractures, where one failure orientation predominantly results in closely spaced but smaller fractures. The serrated fracture in Figure 5.12, which resembles a cartoon image of shark's teeth, appears to have formed as one crack propagating in zigzag manner. This sawtooth geometry might be explained by material heterogeneities, e.g. preferential failure along grain boudaries, or the splitting of a planar fracture into fringe joints and their linkage by cross joints (Hodgson, 1961). Pons and Karma (2010) performed crack growth simultations under mixed-mode I + III conditions in homogeneous material. Their simulations reveal that planar crack propagation is linearly unstable against helical deformations of the crack front. Their mixed-

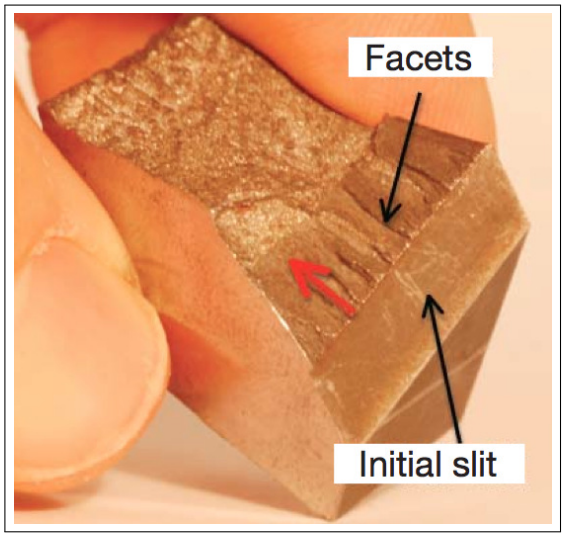

Figure 5.20 – Serrated fractures formed by helical deformation originating from a planar crack. Figure 1a from Pons and Karma (2010).

mode crack (Figure 5.20) evolves into a segmented array of finger shaped daugther cracks which resemble the sawtooth fracture in Figure 5.12. If the sawtooth fracture formed in the same way as described by Pons and Karma (2010), it would have originated from a planar crack that is subsequently deformed in a torsional manner.

5.6.3 Extensional Fractures

En Echelon Fractures and Injection Veins

En echelon fractures are sometimes referred to as "tension gashes". In Outcrop 1B (Figure 5.9) The en echelon fractures seem to have formed perpendicular to the topview plane of observation. The fractures have formed as sets with similar spacing (arrows pointing east) and with the common staggered offset, characteristic of en echelon veins. The en echelon fractures are subparallel (minor clockwise rotation towards north), over the whole large fragment, and, due to the outcrop topography, can be connected to injection veins at the lower interface of the fragment with the main pseudotachylyte vein. The en echelon fractures are thus interpreted to represent injection veins (opening mode I fractures). That means injection veins are formed as en echelon extension fractures in three dimensions, an interpretation supported by Rowe et al. (2012) and Campbell et al. (2020a). Wide extension fractures commonly contain (rounded) clasts. Rowe et al. (2012) note that they found only opening mode offset of clasts which excludes intrusion of clast bearing matrix and suggests clast formation by coalescence of (micro) cracks during mode I fracture formation.

Perpendicular Fractures

Perpendicular fractures that represent extensional fractures (Outcrop 1B, Figure 5.9), are thought to have formed as a result of two of the principle stress axes being extensional and similar in magnitude. There is no evidence for the fractures not having formed simultaneously. To the author's knowledge, orthogonal fracture sets have not been described before to have formed in rocks, except for as sequential sets. They might represent a special case of indentation fractures (see below).

5.6.4 Point Indentation Fractures

Median cracks (radial cracks or hackles) forming during point indentation (Lawn and Swain, 1975; Lawn and Wilshaw, 1975) resemble the crack traces marked as point indentation fractures in Figures 5.13 and 5.15. Both observations of point indention fracture structures in the field are in fragments that appear rather transparent in the outcrop (interpreted as pseudotachylyte sensu stricto shining through a thin and polished fragment layer), therefore they are exhibiting a phenomenon that occurs near the clast surface.

5.6.5 Spall Fractures

Spall fractures occur as fractures parallel to the surface of the fragment, or as a fracture mirroring the surface. They are known from engineering and mining and have already been reported from the pseudotachylytes on the Outer Hebrides by Francis and Sibson (1973). Spall fractures form upon indentation (both impact and static loading) parallel to or parabolically curving towards the free surface. The failure nucleates near the surface of indentation and does not necessarily reach the surface. Considering only the two dimensions of the outcrop surface, the elongate spalls, especially when jammed between the parent and a second fragment, can be explained in this way. Spalls can also be produced by rarefaction waves. A shock waves gets refracted at a material interface, producing a tensional wave which may exceed the tensional strength of the rock (Melosh, 1989; Ernstson et al., 2001; Ren et al., 2011).

5.6.6 Branching Fractures

The propagation of a crack is a multi scale phenomenon (e.g. Buehler, 2010). Ravi-Chandar and Knauss (1984) experimentally investigated the propagation of cracks and documented it with high speed cameras. They find that, at high stress intensity factors, the branching process starts from microcracks that are (initially) parallel to the main crack propagation direction, and a number of cracks attempt to propagate simultaneously. Bourne (1993) find that when crack propagation speed increases, the cracks begin to branch. Dürig and Zimanowski

(2012) performed impact indentation experiments, and also documented the crack propagation by high speed imaging. Their high resolution image sequences show that at some point after initial formation of a relatively wide crack, the crack tip velocity decreases, an effect known as dynamic instability. At this point, the dilational crack collapses (becomes narrower) and branches at its tip. The decrease of crack tip velocity is correlated with a dramatic increase of fracture area production velocity. Sagy et al. (2001) complare experiments on dynamic fracturing in epoxy to branching fractures in dolomite. Their results show a strain rate dependent fracturing style, with lower strain rates producing planar fractures and higher strain rates branching fractures. At even higher strain rate the failure occurs in clusters of tightly spaced and branched fractures, causing local fragmentation of the brittle layer.

It seems that a change of fracture propagation speed (whether increasing or decreasing) can lead to branching of fractures. High, dynamic strain rates are capable of producing branching fractures or even fragmentation of the brittle material through closely spaced fractures.

5.6.7 Cross-Cutting Relationships

Cross-cutting relationships are probably the geologist's safest tool in unravelling the (de)formation history of rocks. However, in the case of pseudotachylytes, the interpretation of cross-cutting relationships is not as globally applicable as in most other cases. Because pseudotachylytes form and solidify in a matter of seconds to minutes (Sibson, 1975), they can show cross-cutting relationships even if produced during a single (macro) event (Dressler and Reimold, 2004). Thus, the significance of a cross-cutting relationship is confined to its (meso) scale of observation. The same should be true for a pseudotachylyte's overprint by mylonitisation. Only one unequivocal cross cutting relationship was observed in the field (Figure 5.17).

5.6.8 Fragment Transport

Transport of fragments has been observed, both lateral (Figure 5.21) and rotational (Figures 5.14 and 5.17). This is suggestive of a shear displacement of the quasi-conglomerate, and mobility of the pseudotachylyte *sensu stricto*. The transport of fragments is likely to induce rounding through abrasion and mechanical wear. The distances of fragment transport appear to be very local (e.g. in the centimetre to decimetre scale).

5.6.9 In-Situ Formation of Fragments

In-situ formation of fragments suggests that fragmentation can occur without significant transport. In some places it seems that pseudotachylyte is replacing

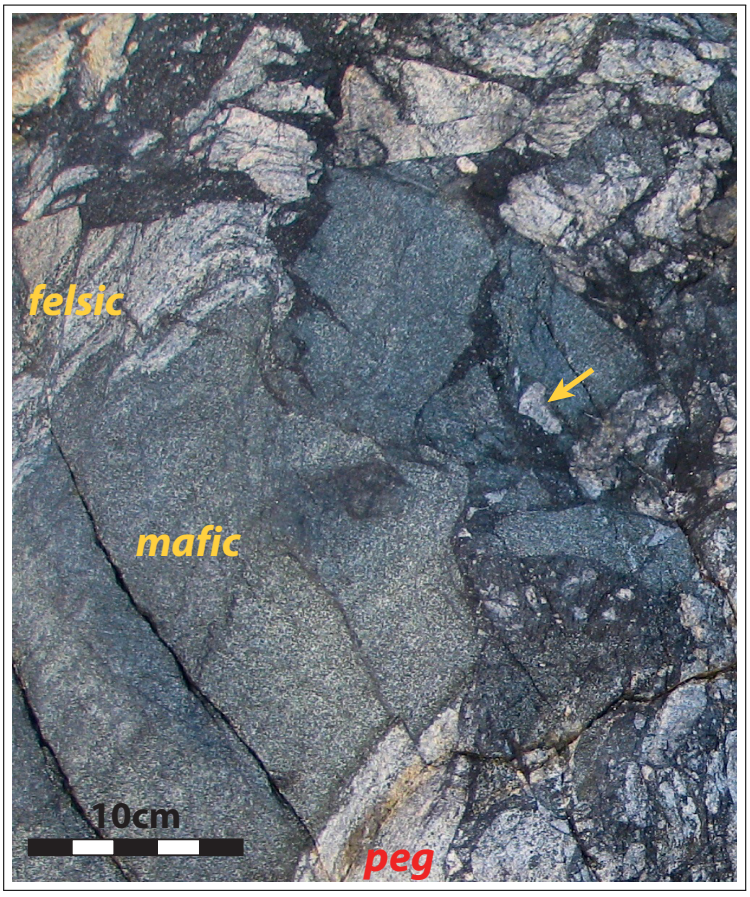

Figure 5.21 – Photograph showing a quasi-conglomerate with felsic, mafic, and pegmatitic (peg) host rock and fragments. The fragments show mixing, for example the felsic (or pegmatitic) fragment indicated by the arrow is surrounded by mafic fragments. Locality 1, near Outcrop 1A, NF 656 042.

the rock rather than having intruded into opening mode fractures, or being locally produced by shear displacement, because there is no evidence of displacement of the host rock. This has also been reported by Macaudière and Brown (1982) who studied pseudotachylytes in anorthosite on Harris. Possibly, very little (and not observable) shear displacement is necessary to produce pseudotachylyte, or the shear displacement took place into a direction that makes its recognition unlikely (i.e. perpendicular to the outcrop surface). Another possibility would be the formation of micro scaled branching fractures, which coalesce and form fragments below the resolution limit, or even produce fragments so small that they melt.

5.6.10 Importance of Scale

The scale is a crucial factor, not only in terms of observability of structural details. A zoom into a detail of Outcrop 2 (the pseudotachylyte network), shows a "small-scale quasi-conglomerate" located in a corner where two pseudotachylyte veins meet (Figure 5.18). The meso map in Figure 5.11 (Outcrop 1A) that shows in-situ fragmentation of a fragment, represents a "small-scale pseudotachylyte network" inside a quasi-conglomerate fragment. These maps were not used for the area calculation, because they are not representative.

5.6.11 General Observations and Synthesis

The general appearance of the gneiss is shattered and crushed, especially in Locality 1 at Seal Bay and other outcrops of quasi-conglomerate. This has been noted as early as 1924 by Jehu and Craig (1924) for places on Barra and smaller islands in its vicinity. The outcrops visually prompt the association of an explosion or a similarly powerful event with high strain rates. High strain rates are also recorded in the branching of fractures. It seemed that the more time was spent looking at these rocks, the more deformation became visible, as for example hairline fractures became visible in seemingly intact rocks and fragments. Suspended host rock fragments are internally deformed and show angular and rounded outlines. Evidence for shear displacement, that is shear along a fault, is markedly absent in the quasi-conglomerates, and no directional indicators such as lineations were found. Many quasi-conglomerate features record dilation, for example in en echelon opening mode fractures, and deformation in situ such as highly fragmented rocks seemingly in situ, or the rotation of fragments. Rotated fragments seem to be more rounded and with less concave outline segments than solely dilational structures of in situ clusters or fragment families. Chilled margins or flow structures have not been observed and the pseudotachylyte *sensu stricto* appears uniform. A cross cutting relationship was observed in only one outcrop on Àird Ghrèin, and the general impression is that the features on the outcrop scale have formed during one single event rather than multiple overprinting events.

A discussion in the wider context of how the quasi-conglomerates may have formed is in Chapter 8. The following sections are dedicated to the quantification of pseudotachylyte on the meso scale. In Chapter 6 micro scale structures are looked at in detail to gain further insights into the formation of these rocks.

5.7 Calculation of Amount of Pseudotachylyte *Sensu Stricto*

Based on the meso scale maps, the percentage of pseudotachylyte *sensu stricto* (black) is calculated for the pseudotachylyte mode of occurrences quasi-conglome-

rate and network (Step 2). A total of 22 meso scale maps were digitised (for the method of digitization see Section 5.3). One meso scale map was not used for the calculation because it had been made for illustration purposes only. A note of this intended purpose had been taken in the field. The meso map that was discarded is map (**C**) in Figure 5.9 on page 79. Its base photograph in Figure 5.6 on page 76 shows that the photograph was not taken at an area representative angle (that would be map (**B**) in Figure 5.9 on page 79), and in the main pseudotachylyte vein, no fragments were represented.

5.7.1 Procedure

Figure 5.22 illustrates the procedure for Step 2. The 21 meso maps were first visually divided into network and quasi-conglomerate geometries, based on the maps, with the aid of photographs and field notes. The grey-scale meso maps were then individually loaded into an open source image analysis software (*ImageSXM*, Barrett, 2013, and *ImageJ*, Schneider et al., 2012). The histogram function was used to count pixels with the three values white, black, and grey, respectively. The grey areas (areas of poor exposure) were subtracted from the total image area. The combined areas in white and black served as the total reference area (100 %). The respective area percentage of white and black was calculated for each individual map.

5.7.2 Results

A total number of 21 meso scale maps were analysed. Four maps represent pseudotachylyte network geometry, and 17 maps represent quasi-conglomerate geometry. These two data sets were analysed separately. The respective data sets were then further divided into *small scale* (10 x 10 cm) and *larger scale* (30 x 30 cm or 1 x 1 m) maps, to evaluate the influence of the map size. The standard deviation σ is calculated by the "unbiased variance" or "$N-1$" method, with the following equation,

$$\sigma = \sqrt{\frac{1}{N-1}\sum_{i=1}^{N}(x_i - \overline{x})^2}$$

where N is the number of maps, x_i is the area percentage of pseudotachylyte *s.s.* of the individual map, and $\overline{x}$ is the mean area percentage of pseudotachylyte *s.s.* for the data set analysed. The mean value represents the average area percentage of pseudotachylyte *sensu stricto* for the respective data set.

Figure 5.23 shows that, for the quasi-conglomerate geometry (with a larger number of maps), the size of the map does not play a role in terms of the mean value (20 % or 19.8 %). The scatter of the data – expressed in the standard deviation σ, also visualized in the histogram – is greater for the smaller scaled

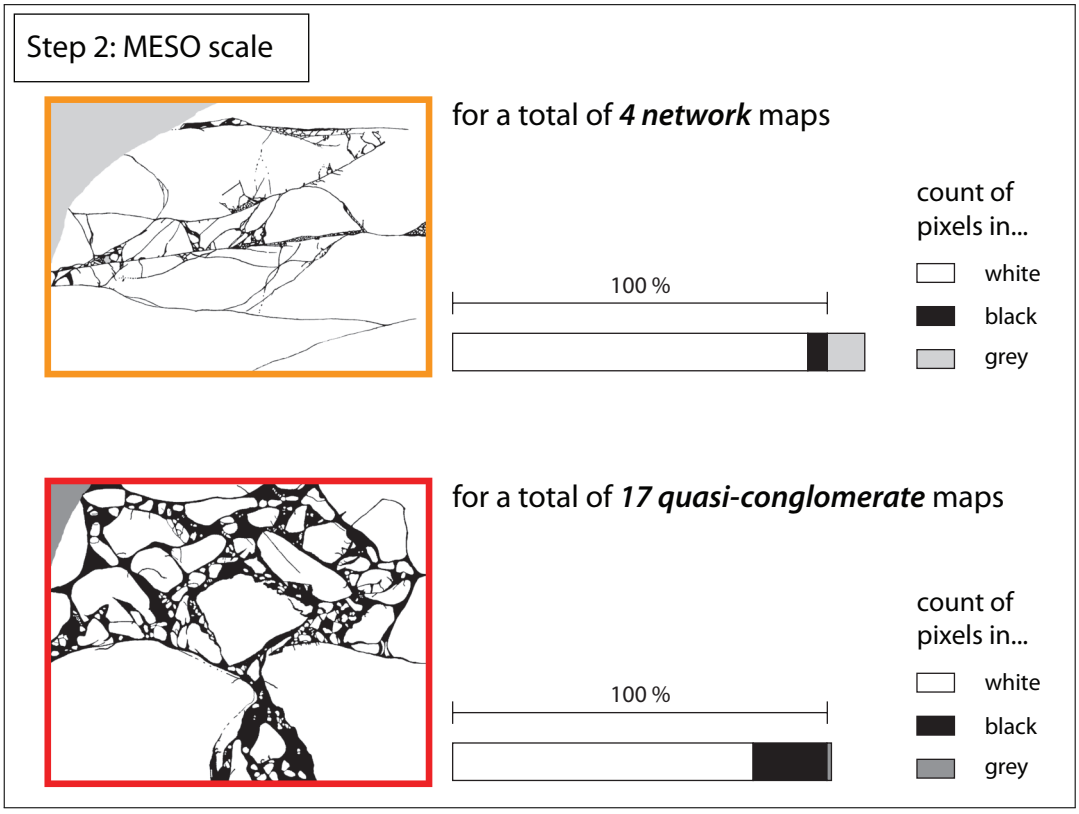

Figure 5.22 – *Illustration of the procedure for Step 2.* – The grey scale meso maps were divided into network geometry and quasi-conglomerate geometry representatives. For each individual map, white, black, and grey pixels were counted. The area covered by white plus black was used as representing 100 % (the total area) of the meso map. Area percentages of black and white were then calculated for each meso map, where black represents pseudotachylyte *sensu stricto*.

maps. The standard deviation for the network maps is below 1. The more detailed (smaller scaled) network map shows a greater area percentage of pseudotachylyte *s.s.* (6.6 %), which is still nearly half the amount of the quasi-conglomerate map with the lowest pseudotachylyte *s.s.* percentage (11.6 %).

5.7.3 Discussion

The small data set of the network maps (N=4) shows very little variance for the three larger scaled maps and is thus thought to be representative, despite the small sample number. The focus on the larger scaled maps is justified by the fact that this data is used to represent the mapped pseudotachylyte mode of occurrence, which covers a mappable outcrop area of 5 x 5 metres. In general, the data is consistet in terms of the mean value for pseudotachylyte *sensu stricto*. Figure 5.24 shows the summary of the results of Step 2. Due to their high length to thickness aspect ratio resulting in a small area, pseudotachylyte veins were not

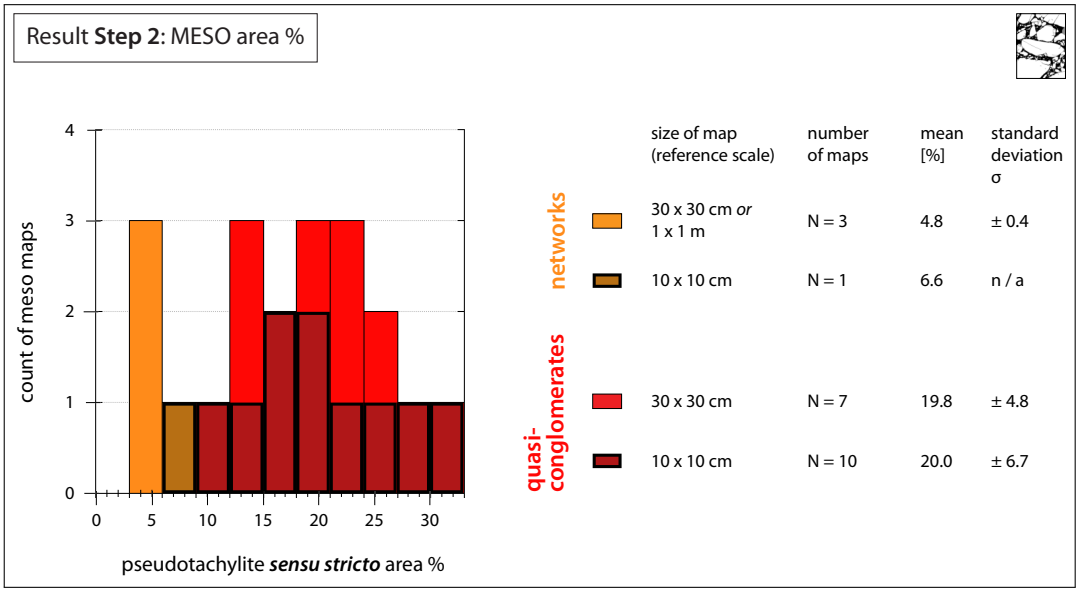

Figure 5.23 – *Results of Step 2. Meso scale, detail.* – The area percentage of pseudotachylyte *sensu stricto* on each meso scale map was calculated. The the maps were grouped into network geometry maps and quasi-conglomerate geometry maps. The groups were further divided into small scale (10 x 10 cm) and larger scale (30 x 30 cm or 1 x 1 m) maps, to evaluate the influence of the map size. In the more meaningful (in terms of number of maps) data set of the quasi-conglomerates, the mean value is the same for both small and larger scale maps, however, the scatter is greater for the small scale maps.

taken into account. Typical pseudotachylyte veins are in the order of millimetres, and less than 2 cm thick. In the case of a 2 cm thick vein with the extent of a whole outcrop (5 m), it would cover 0.004 % of the outcrop area. Because of this negligibly small percentage, pseudotachylyte veins were not considered for the area calculation of pseudotachylyte *sensu stricto*.

In Chapter 8, these results (Figure 5.24) are used to calculate the amount of pseudotachylyte on Àird Ghrèin, integrating the results from the different scales. The following Chapter 6 is concerned with the micro structural observations. In the final section, an estimate is made about how many micro scale fragments would be present in the meso scale pseudotachylyte *sensu stricto*.

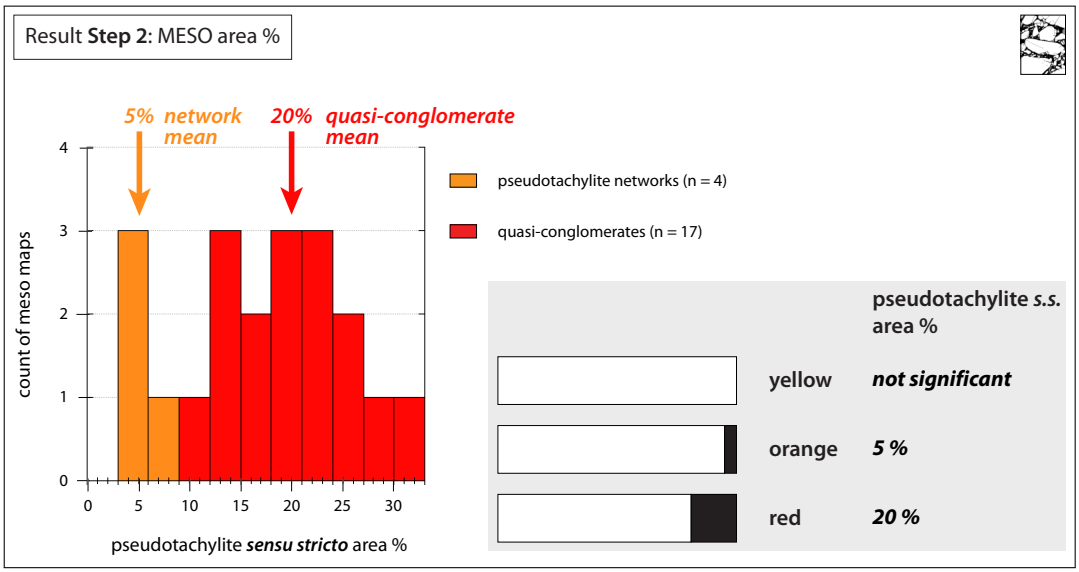

Figure 5.24 – *Summary of the results of Step 2. Meso scale.* – The resulting area percentage of pseudotachylyte *sensu stricto* is the mean value of 5 % for network geometry, and 20 % for quasi-conglomerate geometry. For pseudotachylyte veins (mapped in yellow), the pseudotachylyte *sensu stricto* area is considered to be insignificantly small and equaled to zero.

Chapter 6

Micro Scale

6.1 Introduction

Micro structures allow us to gain insight into processes active during the (de)formation of rocks, which is especially useful in the study of deformation mechanisms. This Chapter focusses on the structural aspect of the micro analysis. Pseudotachylyte *sensu stricto* (Chapter 2) is characterised by a generally dark, aphanitic matrix which is speckled with micro fragments. In thin section, the matrix may exhibit a variation in colour, ranging from transparent to opaque, but generally with a dark brown colour. The colour variation commonly appears in bands or layers, which are often referred to as flow bands or flow structures (Lin, 2008). Micro clasts are ubiquitous and commonly subangular to rounded, which consist mainly of quartz and feldspar. Mafic minerals are generally not found to be present in the matrix as micro clasts.

In the literature on pseudotachylytes in the Outer Hebrides, no report on glass was found. The pseudotachylyte matrix commonly contain plagioclase microcrystallites (laths) that can be up to 200 microns in length (Maddock, 1983), an evidence for rapid crystallization from a clast-ladden melt, without going through a glass phase. Micron to sub-micron grain sizes of matrix minerals are common (Wenk, 1978; Maddock, 1983). "Showers of magnetite" (Maddock, 1983) and other opaques are ubiquitous, both as very fine grained droplets, euhedral grains, and dendritic appearance. Maddock et al. (1987) report vesicles and amygdales, which represent now filled cavities. The authors also report replacement of fragments, however, these have not been found in many samples. Fragments are commonly corroded (Jehu and Craig, 1924), and may show concave fragment sections which Sibson (1975) referred to as embayment structures. Fragments with concave segments have a convexity of $\ll 1$ (convexity defined in Section 5.5.3). The fragments may be monocrystalline, polycrystalline, or polymineralic lithic

(Maddock, 1983). Evidence for cold working, i.e. high strain rate deformation at relatively low temperature has been reported by Wenk (1978).

The structures described in the previous Chapter 5 point to a predominately brittle formation of pseudotachylytes. This micro structural Chapter explores whether the micro structures point to the same conclusion as the meso structural observations or whether these observations and interpretations are scale-dependent. The focus lies on quasi-conglomerates and dilational fractures of pseudotachylytes, in order to better understand their formation. At the end of the Chapter the area percentage of micro fragments in pseudotachylyte matrix is estimated to inform calculations of pseudotachylyte volume in Chapter 8.

6.2 Sampling

All samples were collected from Àird Ghrèin on Barra, from the same field site where the macro scale and meso scale maps come from (for localities see Figure 6.1). The three samples studied in most detail and described below consist of the pseudotachylyte *sensu stricto* of a quasi-conglomerate (Sample A), a terminating pseudotachylyte vein (Sample B), and a pseudotachylyte separating two different rock types (Sample C). In both samples, no shear deformation is evident from visual inspection.

Samples B and C were collected pebbles from Seal Bay. This unconventional sampling collection technique was used for several reasons. Pseudotachylytes are extremely difficult to sample. The most interesting-looking outcrop surfaces, especially quasi conglomerates, are often even to undulating surfaces with few to no open fractures. They are as such impossible to sample with hammer and chisel. The most beautiful outcrops should not be destroyed. Pebbles exhibit a nicely polished surface giving a three-dimensional overview, which makes them perfect for sample selection. Their surfaces are not weathered and they are free from lichen or seeweed. You see what you get! They main drawback is that they are not orientated nor accurately located. From the micro scale observations therefore no conclusions in terms of absolute orientations are drawn.

6.3 Analytical Methods

Several imaging and analytical methods were used to investigate the microstructures in thin sections.

Thin Section Scans: Thin sections were scanned using a slide scanner with and without crossed polarization foils. The scans are used for overview and for the estimation of micro-clast content.

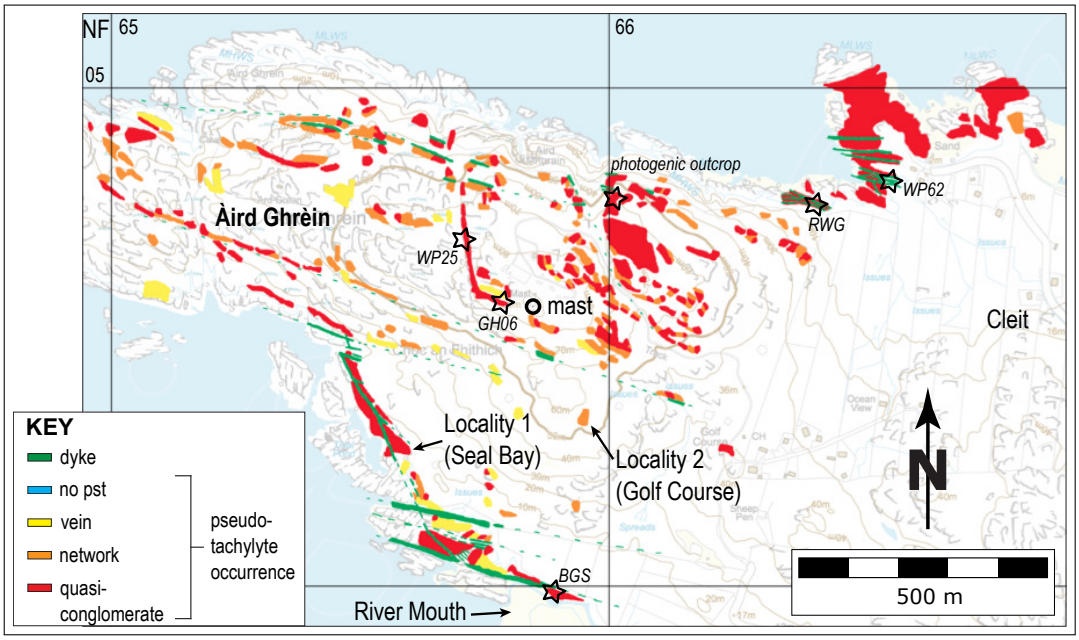

Figure 6.1 – Map of the localities where the samples for this Chapter were collected. Sample A is from an outcrop in the River Mouth, Samples B and C are pebbles collected on Seal Bay.

Optical Microscopy (OM): The thin sections were analysed and photographs taken from optical microscopes. Matrix minerals and some clast mineral grains were too small to identify by optical means.

Electron Micro Probe Analysis (EMPA) and Scanning Electron Microscopy (SEM): The facilities at the Museum für Naturkunde, Berlin, were used for electron microscopy. Semi-quantitative analyses for mineral identification were performed (electron diffraction). This method uses the excitation energies induced by the electron beam, which give an approximate element composition of the analysed area. The analysed volume is depending on the composition of the material, and for rock forming minerals ranges between about 1 μm and 10 μm for normal beam acceleration voltages of 10 to 15 or 20 keV. Thus, the excited rock volume is on average larger than the grain size of minerals in the matrix, which makes interpretation of the results tricky, especially for more complex minerals. The images are backscatter electron images (BSE) that represent different compositions in grey scale: the lighter the phase, the heavier its element components. For example, iron ores are generally white, whereas quartz is shown in a dark grey, feldspars intermediate grey. Fractures or holes are visible in black and may show topography. Due to thin section preparation, not all surfaces are of high quality, that means some areas with the same composition may show different grey values. This is indicated in the figure caption where appropriate.

6.4 Sample Description

6.4.1 Sample A

Sample A is quasi-conglomerate sample from an outcrop at the River Mouth (see map in Figure 6.1). Figure 6.2 shows the outcrop from which the sample derives. The sample is made up mainly of pseudotachylyte *s.s.* that contains a few rock fragments. The thin section (A1) was made from an slab of pseudotachylyte *s.s.* which is adjacent to a fragment. The fragment boundary makes up the upper most end (a few millimetres) of the thin section.

Figure 6.2 – Photograph of the quasi-conglomerate outcrop at the River Mouth. The chisel in the centre of the image lies where Sample A comes from. The chisel is approximately 20 cm in length.

6.4.2 Sample B

Sample B is a pebble sample collected on Seal Bay (see map in Figure 6.1). Figure 6.3 shows a photograph of the cut pebble. The pebble is made up of a gneissose rock that contains a vein of pseudotachylyte which narrows and terminates without tapering off (block in the background centre of the photograph in Figure 6.3). Four thin sections were made of this sample (thin sections B1 – B4). The arrangement of the thin sections is shown in Figure 6.4. The thin sections are divided in two pairs which are perpendicular to each other. B1 and B2 are from the direction towards the termination of the pseudotachylyte vein, whereas B3 and B4 are perpendicular to the first pair. All thin sections are cut perpendicular

to the pseudotachylyte vein.

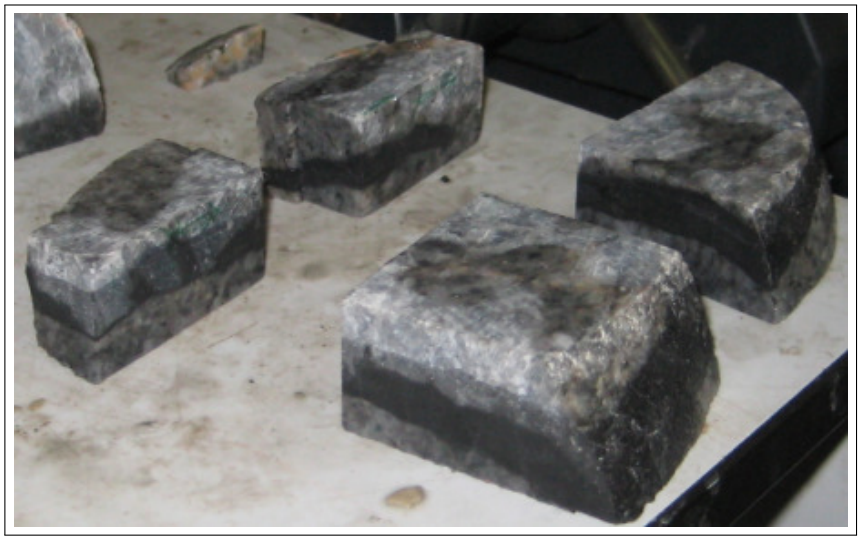

Figure 6.3 – Photograph of the cut pebble of Sample B. The four thin sections are made from the four blocks shown in the photograph.

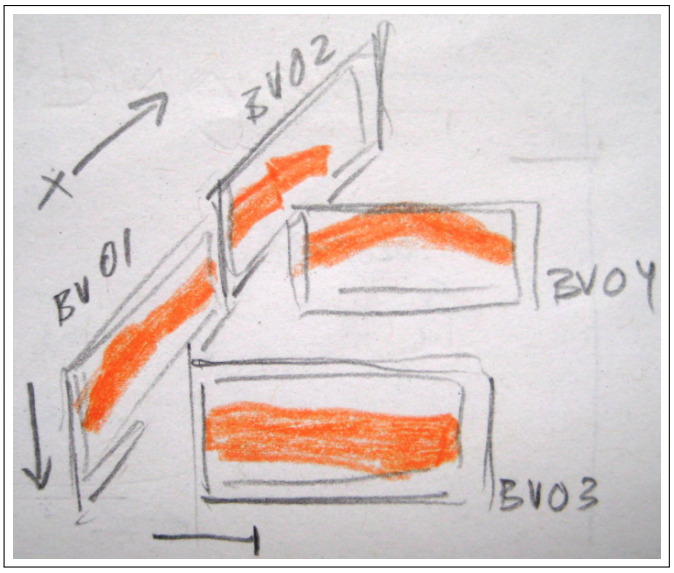

Figure 6.4 – Sketch of the arrangement of the thin sections cut from Sample B. The pseudotachylyte vein is shown in orange. The two sets are perpendicular to each other. The labelling used in the thesis text is a shorter version: BV01 is B1, etc.

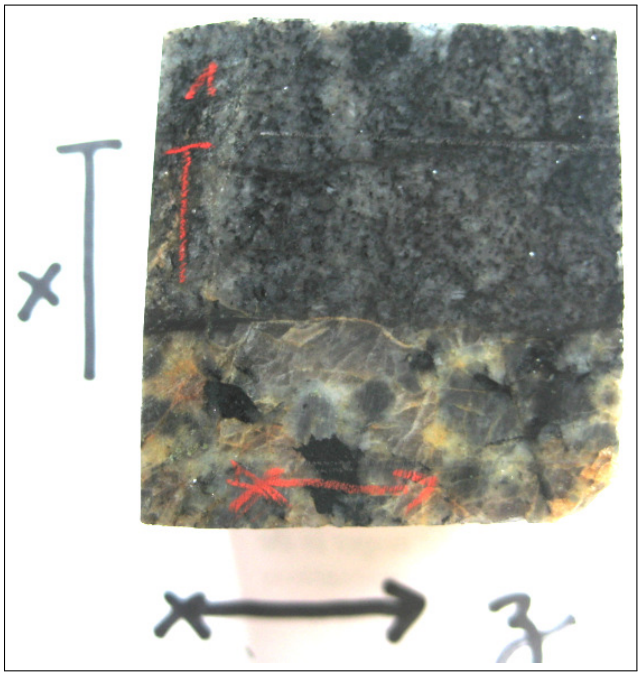

Figure 6.5 – Photograph of the cube cut from Sample C, the side where Thin Section C1 is made from. In the lower part is host rock 1, which is coarse grained, in the upper part is host rock 2, which is finer grained. The two rock types are separated by a pseudotachylyte that is best visible at the left side.

6.4.3 Sample C

Sample C is a pebble sample collected from Seal Bay (see map in Figure 6.1). The pebble is made up of two rock types that are divided by pseudotachylyte. Host rock 1, which is in the lower part, is a coarse grained felsic gneiss. The upper part of the sample is a finer grained gneiss with more mafic minerals (host rock 2). The thin sections make up five sides of a cube. The cube is cut so the bottom and top are parallel to the quasi planar interface of host rock 1 with the pseudotachylyte. Thin Sections C1 – C4 are the four mantle sides of the cube, always with the coarse grained rock on the bottom and the finer grained rock on top. Figure 6.5 shows the side of the cube from which Thin Section C1 derives. Thin Section C5 is from the top of the cube, where a fine pseudotachylyte vein cuts through the fine grained host rock 2 (Figure 6.6).

6.4.4 Samples, Thin Sections and Figures

Table 6.1 shows a list of the thin sections, from which sample they derive, their locality on the map (see Figure 6.1), what was sampled, which analyses have been performed, and which figures show images taken from the thin section.

sample	where	what	thin section	OM	BSE	EDX	Figures
A	*RM*	*pseudotachylite sensu stricto*					*6.2*
			A1	x	x	x	6.10, 6.11, 6.17 – 6.19, 6.14 – 6.25, 6.20, 6.21
B	*SB**	*pseudotachylite vein*					*6.3, 6.4*
			B1	x			6.15
		terminating	B2	x			6.8, 6.9, 6.23
			B3	x	x	x	6.13, 6.12, 6.26, 6.27
			B4	x			
C	*SB**	*pseudotachylite between two host rocks*					*6.5, 6.6*
			C1	x			
			C2	x			
			C3	x			6.28, 6.16
			C4	x			
		terminating	C5	x			6.7

Table 6.1 – List of Samples and Thin Sections.
OM = optical photomicrograph, *BSE* = backscatter electron image, *EDX* = energy dispersive x-ray analysis, *RM* = River Mouth, *SB* = Seal Bay, * = pebble sample.

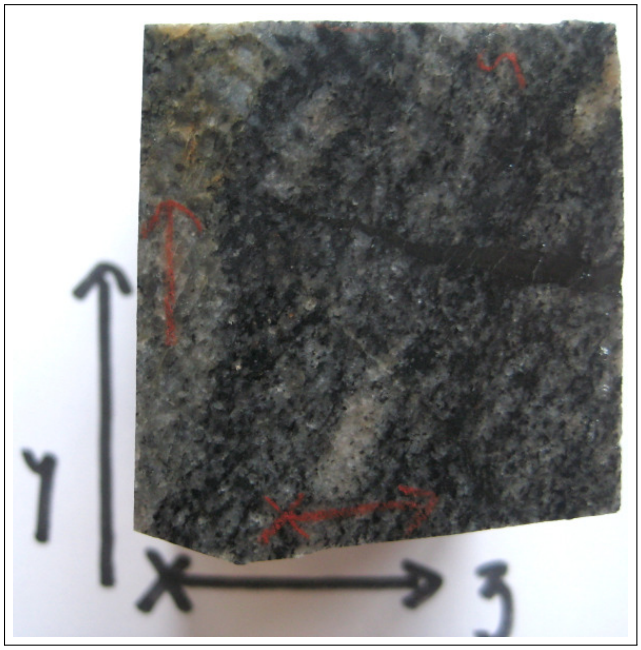

Figure 6.6 – Photograph of the top of the cube cut from Sample C, where Thin Section C5 comes from. A pseudotachylyte vein cuts host rock 2 from the right hand side and tappers off towards the left.

6.5 Microstructural Observations

The micro scale observations are divided into pseudotachylyte host rock and rock fragments, their structural relationship with the pseudotachylyte, and the pseudotachylyte matrix. A discussion of some of the micro structures follows in Section 6.6. The discussion in the context of the macro and meso scales from the previous chapters and the formation of the quasi-conglomerates is located in Chapter 8.

Orientation of the Thin Sections

Thin sections were cut perpendicular to the pseudotachylyte feature of main interest. The thin section might therefore be at an unsuitable angle for proper interpretation of the host rock deformation. The geometrical relationships described and discussed below are as observed in the two dimensions of the thin section (unless stated otherwise), e.g. *parallel* refers to parallel traces of features, and not necessarily to parallel planes.

Pseudotachylyte Terms on the Micro Scale

All samples that were investigated on the micro scale fall under the category of pseudotachylyte *sensu lato*. What was defined as pseudotachylyte *sensu stricto* (pseudotachylyte containing fragments of up to a few millimetres in size) is further divided on the micro scale into pseudotachylyte *matrix* and *micro fragments*. Pseudotachylyte matrix does not include any rock fragments at the scale of observation. This new term is introduced because it is only possible to distinguish between micro fragments and pseudotachylyte matrix by means of microscopy. On the meso scale, this distinction is not possible because micro fragments are too small to be resolved.

6.5.1 Host Rock

Host Rock Composition

The gneissose host rock is granitic to granodioritic in composition with a variability in content of mafic minerals (Figure 6.7). The mafic minerals are biotite and hornblende. The grain size is variable in relatively distinct layers and ranges from about 2 millimetres to about 1 centimetre. In the respective layers, grain size is similar for both mafic and felsic minerals. There are layers that contain little mafic minerals. The grain boundaries are lobate and well interlocked.

Host Rock Deformation

On the micro scale, the term *host rock* is used for the rock that contains or is adjacent to pseudotachylyte. On a larger scale, this might be a rock at a

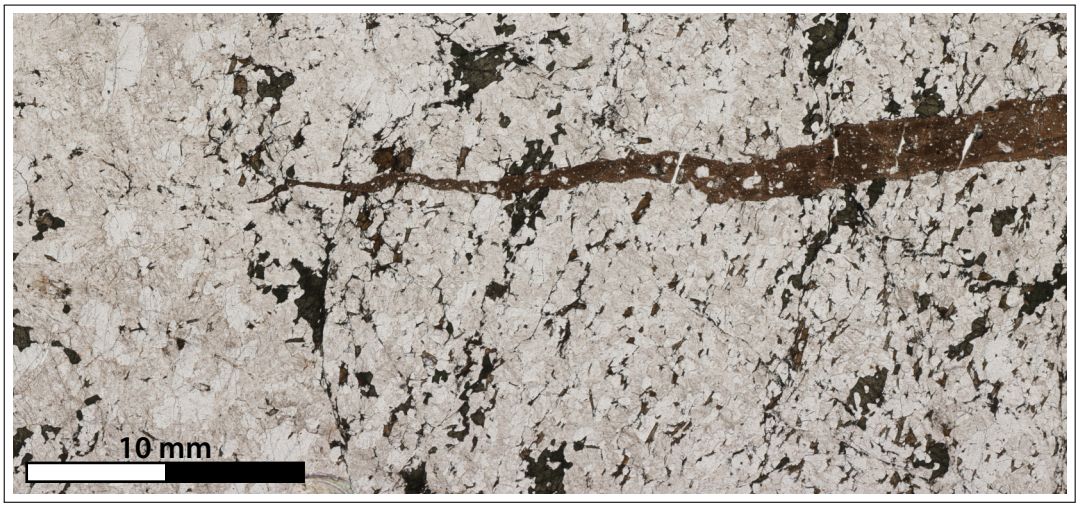

Figure 6.7 – Part of a scan of Thin Section C5 in plain polarized light. Note the variability of content in mafic minerals. The pseudotachylyte vein tappers off and terminates at the transition to the more felsic part of the host rock. The subvertical elongate white parts inside the pseudotachylyte vein are late fractures.

pseudotachylyte boundary, or a host rock fragment that is larger than the thin section area (> 4 *by* $2\,cm$).

Pervasive Deformation: On the thin section scale the host rock of pseudotachylytes is pervasively deformed. The deformation is very prevalent, but not visible on the sample's surface or in plain polarized light, it is only revealed in crossed polarized light (e.g. Figure 6.8). The deformation is characterized by fractures and localised zones of up to a millimetre in thickness, that are made up of grains of much smaller grain size (Figure 6.8 on the next page, and Figure 6.9 on page 117).

Localised Deformation: Cutting through individual thin sections are localised zones of deformation. These *deformation zones* are generally straight on the centimetre scale (sometimes they curve), and they come in several orientations that may vary even on one thin section. Some of the deformation zones are hairline fractures, and all of them cut through the grains of the host rock. The deformation zones are predominantly made up of fractures, which sometimes contain a layer of small (below 1 mm) grains – are predominant. These fractures come in sets, and splay or branch to form composite zones of deformation. Where the zones are thicker than a couple of millimetres, they may contain larger *survivor grains* surrounded by small *recrystallized grains* (Figure 6.9). The fine grained mafic rock is more pervasively cut by localised deformation zones than the coarse grained more felsic rock. The pervasive deformation in localised zones is further discussed in Section 8.2.2.

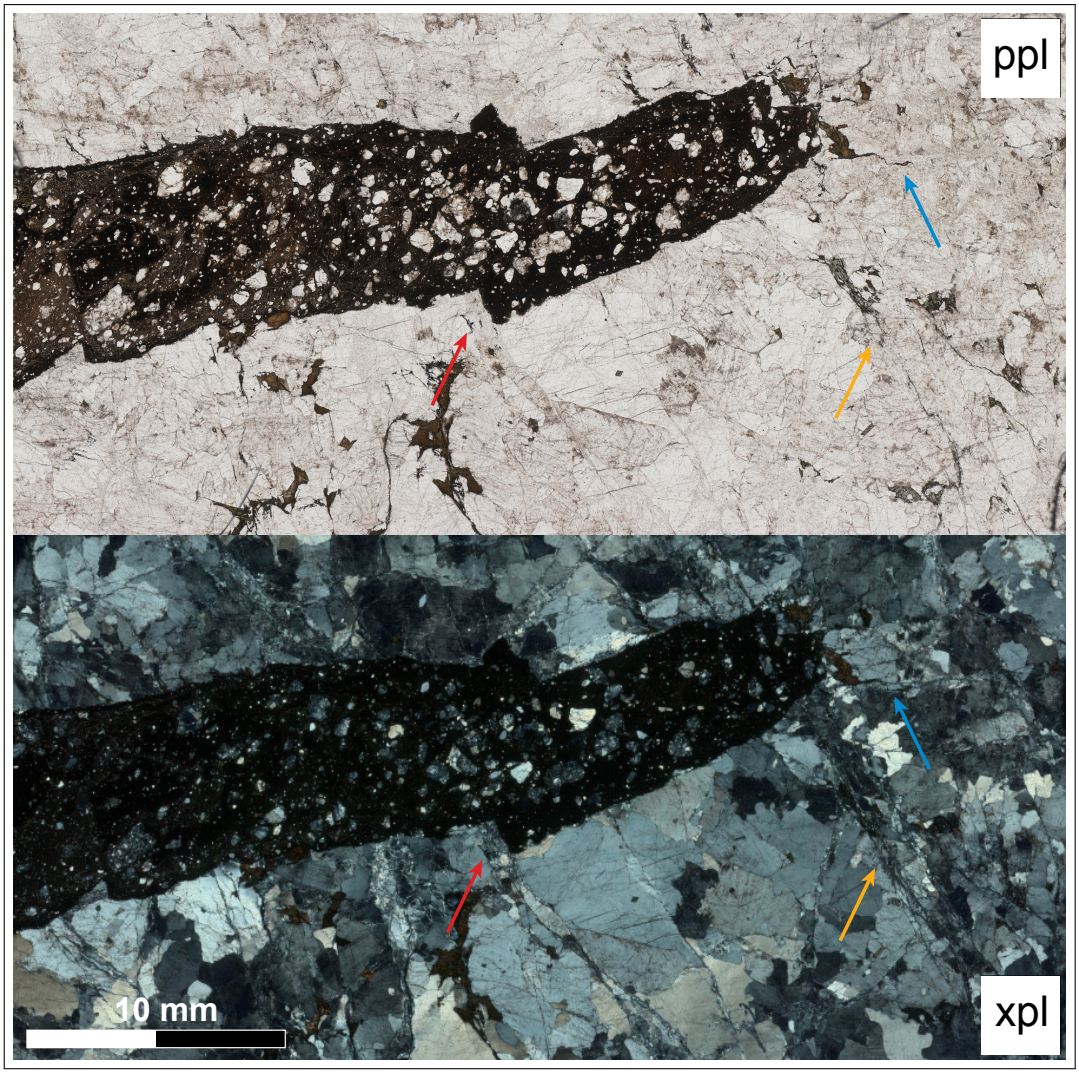

Figure 6.8 – The host rock is pervasively cut by deformation zones and fractures which are barely visibe in plain polarised light. The pseudotachylyte is exploiting a deformation zone (red arrow points to apparent offset). The pseudotachylyte vein appears black and terminates towards the right where it meets the deformation zones indicated by the yellow arrow. The blue arrow points to splaying fractures that continue from the tip of the pseudotachylyte vein into the host. Thin section scan of B2, detail around red arrow shown in Figure 6.9.

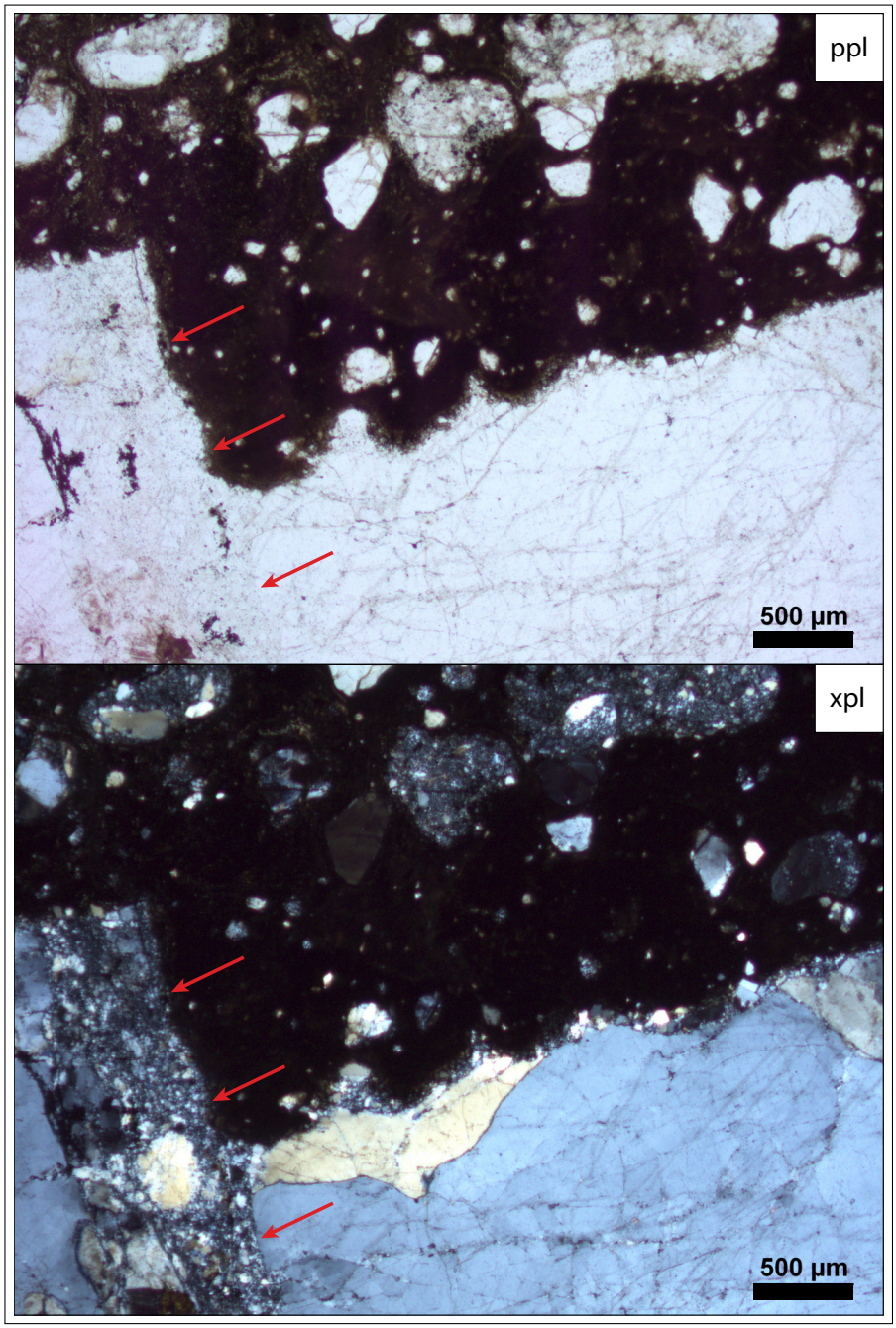

Figure 6.9 – Photomicrographs in plain polarized (ppl) and crossed polarized light (xpl). The red arrows point to a deformation zone exploited by the pseudotachylyte (same as in Figure 6.8, red arrow). Note the concave fragment segments (ppl) along the pseudotachylyte boundary to the host rock in the centre of the image: in xpl it is visible that the structures are made up of smaller grains that are not entirely surrounded by the dark pseudotachylyte matrix. These concave fragments represent plucking structures. It appears that the pseudotachylyte in the right three quarters of the image is exploiting another deformation zone (perpendicular to the one described above) where the fragments that are forming the concave segments are still attached to the host. Similar concave fragment segments are visible in the micro fragments embeded in the matrix. Thin Section B2, thin section overview shown in Figure 6.8.

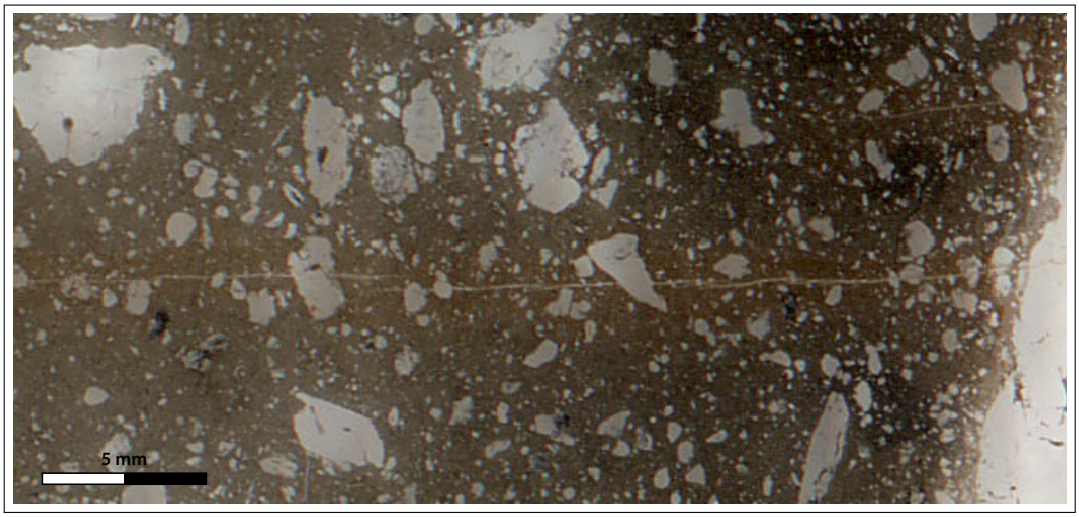

Figure 6.10 – Fractures (here horizontal, but subvertical in the outcrop) with approximately 5 mm spacing cutting through pseudotachylyte and fragments. The pseudotachylyte matrix around the fractures shows a halo of a rusty brown, indicative of fluid infiltration and alteration or precipitation. Part of a scan of Thin Section A1, (ppl), a pseudotachylyte *s.s.* sample.

The host rock deformation in localised zones is characterized by undulatory extinction of quartz (also in lower strain regions), and, predominantly, small grains (micron sized) of quartz and feldspar along intragranular micro shear zones. Larger "survivor grains" with intermediate grain sizes (between the undeformed host rock and the small, micron sized grains) occur in the wider deformation zones. Biotite is often strongly kinked or even more strongly deformed, and often replaced, at least at its rims, by magnetite, titanite and other opaques. The microstructures suggest cataclastic fracturing, with subsequent annealing and recrystallization. Identification of crystal-plastic deformation would require further analyses (i.e. analyses that allow identification of crystal lattice orientation). The microfractures are sealed, and the small grains that make up the deformation zones are not angular but rounded. It needs to be noted that the grain size of these deformation zones is in general too small to be investigated by optical microscopy.

Crosscutting Fractures: A set of fractures, which in places includes evidence of fluid infiltration indicated by a differently coloured halo around the fracture (Figure 6.10), crosscuts all features. These late fractures have been observed in all pseudotachylyte occurrences in this study. However they are more pronounced in larger volumes of pseudotachylyte and occur in regularly spaced sets perpendicular to the pseudotachylyte boundary. Late fracturing of pseudotachylyte gives a distinct weathering pattern.

6.5.2 Structural Relationship between Host Rock (Fragment) Deformation and Pseudotachylyte

Interface: Without magnification aid, the interface between the host rock and the pseudotachylyte has a rather sharp appearance. In particular, larger fragments seem to have well defined boundaries. However, higher resolution reveals that the interfaces are generally less well defined. Sharp edges occur at larger fragments and at straight host rock boundaries. Sharp edges are the least common with biotite, and more often occur with quartz or feldspar. Even at high resolution sharp interfaces are most prevalent in angular micro fragment clusters (e.g. Figure 6.13 on page 124, angular micro fragment cluster are described below in Section 6.5.3).

Commonly, interfaces consist of a layer of fine grained material. The material is made up of small grains as part of the host or fragment, and matrix minerals that are interspersed (Figure 6.9 (felsic host) and Figure 6.23 on page 134 (mafic host)). There seems to be a transition between deformed host rock with inclusion trails, to interface zones with micro metre grain size, to small quartz or feldspar grains with opaques and fine grained green minerals on their grain boundaries, to the dark appearing pseudotachylyte with a higher amount of opaques and mafic (green) mineral, to pseudotachylyte that contains fragments of quartz and feldspar. The transition (and its formation) between host rock and pseudotachylyte is further discussed in the case studies in Section **??** and in Chapter 8.

Alignment with Pseudotachylyte Orientation: The orientation of the deformation zones influences and controls the orientation of pseudotachylyte veins. Generally, parallel deformation zones were found in the vicinity of pseudotachylyte veins. Pseudotachylytes are generally less straight than deformation zones. Often, the pseudotachylyte makes use of a deformation zone by following it. A change in orientation of a pseudotachylyte vein can often be correlated with the pseudotachylyte picking up a deformation zone (Figures 6.8 on page 116, and 6.9 on page 117). The exploitation of pre-existing deformation zones can lead to apparent 'offset' of pseudotachylytes. In areas with this apparent offset, the pseudotachylyte does not show a textural difference to the pseudotachylyte elsewhere, except for that it might show a higher fragment density in these areas.

Termination of Pseudotachylyte: Pseudotachylyte veins that taper off are generally continued by a hairline fracture in the host rock, following the orientation of the pseudotachylyte vein (Figure 6.28 on page 140). The pseudotachylyte termination is characterized by a gradual transition (even if over a short distance in the millimetre range) to a deformation zone that is characterized by grains smaller than the surrounding host rock, i.e. a zone of (micro) cataclasite. On the other hand, some pseudotachylyte veins terminate where the host rock com-

position becomes more felsic (i.e. less mafic minerals) and grain size coarsens (Figure 6.7 on page 115), suggesting an aspect of host rock control. In the one observed location (Thin Section B2, Figure 6.8 on page 116) where pseudotachylyte terminates without tapering off, the host rock is strongly deformed. There, the deformation zones are at high angles to the pseudotachylyte vein, and the pseudotachylyte terminates at a location where deformation zones intersect. In that figure, the pseudotachylyte boundaries are continued by deformation zones in the host rock that splay and terminate within a centimetre, i.e. where they meet the next perpendicular deformation zone.

6.5.3 Micro Fragments

As stated above, clasts that are smaller than a few millimetres are termed *micro fragment*. No micro fragment with mafic mineralogy was found. That means, micro fragments do not contain mafic minerals such as biotite or amphiboles. Micro fragments are componsed of felsic minerals: quartz, feldspars (more commonly plagioclase than alkali feldspars), and rarely zoisite or zircon. Micro fragments range in size from one micron (the minimum observable clast size at this resolution) up to the above defined limit for micro fragments of a few millimetres. Larger fragments occur as well, which are then referred to as fragments or rock fragments.

Rounded Micro Fragments: Most fragments are irregularly shaped with a rounded appearance but complicated shapes (Figures 6.11 and 6.12 on page 122). Rounded fragments often contain concave segments (convexity $\ll 1$; defined in Section 5.5.3).

Angular Micro Fragments: Angular micro fragments are generally found in clusters (or families). The clusters of fragments evidently belong together, given by their mineralogy, their vicinity (generally less than 10 micrometers away from their nearest neighbour), and sometimes by their shape (jigsaw puzzle). The fragments are separated by both straight and curved fractures, which are sometimes only partially open. It seems that the fractures between the micro fragments are not necessarily opening mode fractures but rather replacing the host material (e.g. Figure 6.11 on the following page). Most angular micro fragments are made up of quartz, and the fragments are made up of single grains that are internally undeformed (see below in Section 6.5.3). The formation of these fragment clusters requires a relatively large host rock grain size if they derived from single grains. These fragment clusters were most commonly observed in the vicinity of a pseudotachylyte boundary with its host rock (Figure 6.13) or in the vicinity (or as part) of fragmented quartz micro fragments (Figure 6.14 on page 125). Commonly, the closest host rock mineralogy matches the mineralogy of the fragment

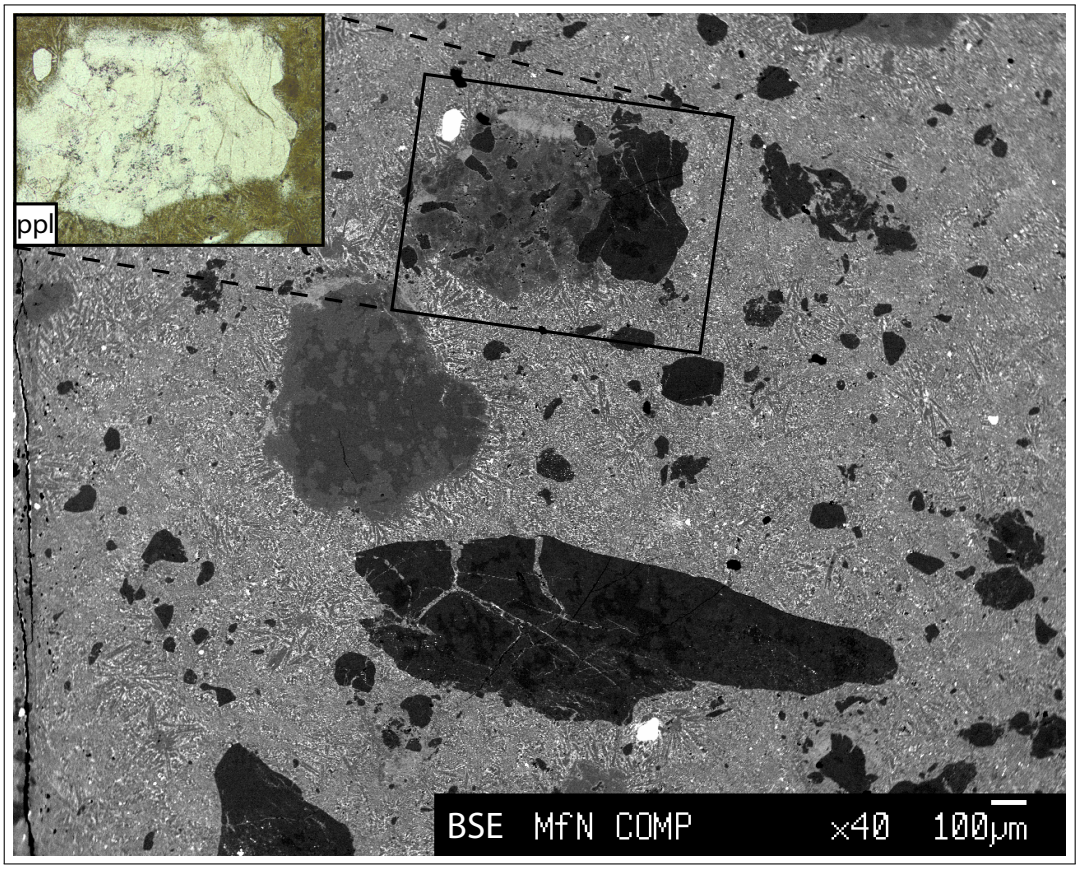

Figure 6.11 – Backscatter electron image of pseudotachylyte s.s. The matrix is light grey speckled. Micro fragments cover a wide size range. Most of them are quartz (dark grey), but feldspar (intermediate shades grey) or polymineralic micro fragments occur as well. The two large white micro fragments are zircon. The inset shows a photomicrograph of what in plain light appears as a rounded micro fragment. Note the many oddly shaped micro fragments, and the pervasive micro fractures inside quartz micro fragments. Figure 6.14 on page 125 shows a detail of the elongate quartz fragment in the lower centre. Thin Section A1. Image taken at the Museum für Naturkunde in Berlin, thanks to the support of Prof. W. U. Reimold and his staff.

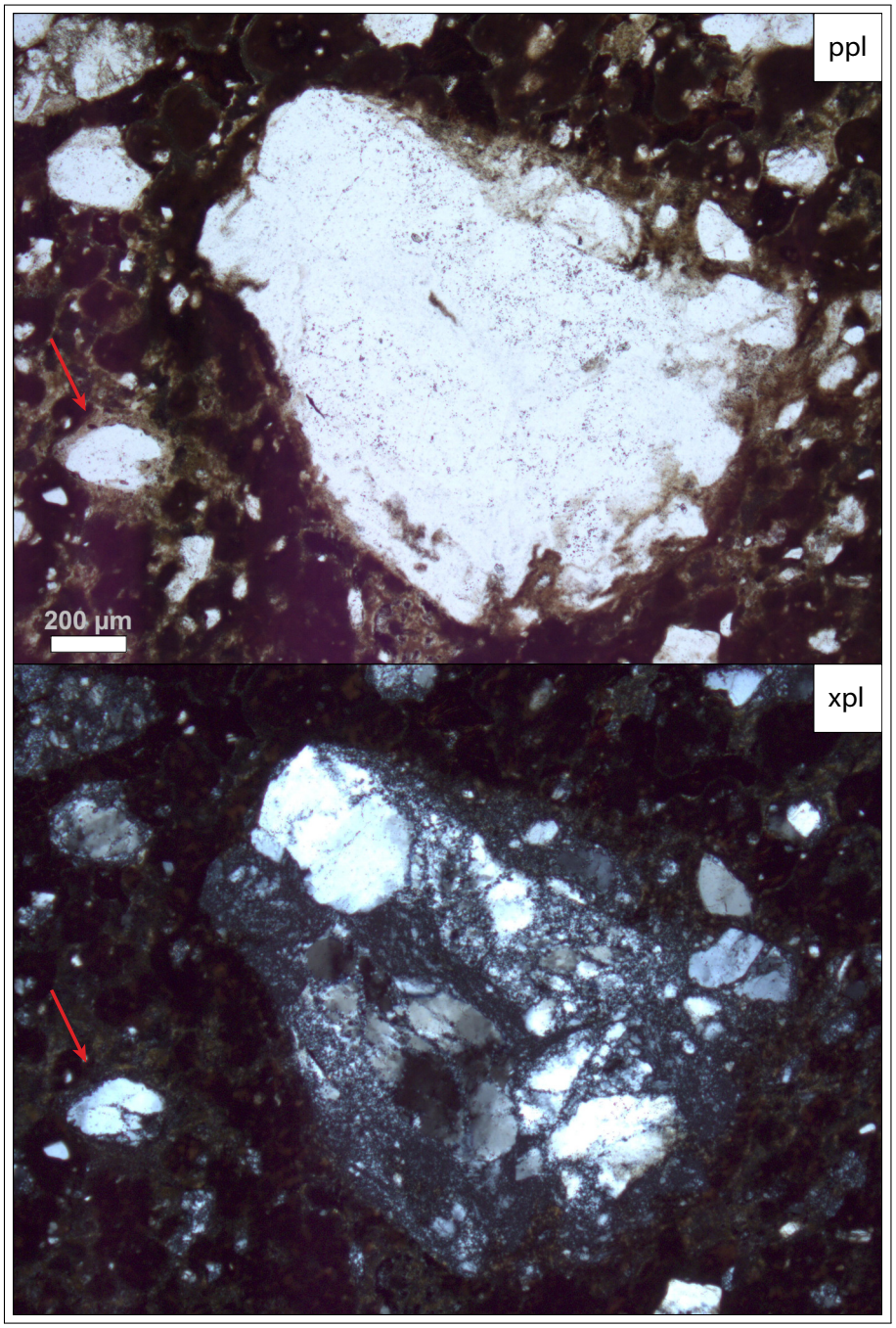

Figure 6.12 – Photomicrographs in plain (ppl) and crossed polarized light (xpl). The fragment in the center is rounded but exhibits a complicated shape with concave fragment segments (ppl). The micro fragment (polycrystalline, probably polymineralic) is composed of larger (up to 400 microns) and smaller grains (below resolution limit). The concave fragment segments occur only in areas with the small grains. The smaller micro fragment on the left (red arrow) also shows a concave fragment segment in ppl. Xpl: the concave fragment segment is due to internal deformation and plucking of the smaller grained material. Thin Section B3.

cluster (Figure 6.15 on page 126). Angular micro fragments are less common than rounded micro fragments.

Curved Fractures

Curved fractures occur both as intragranular micro fractures (Figures 6.15 and 6.16) and as fragment forming fractures (Figures 6.13 and 6.17). Most pseudotachylyte veins show some degree of curvature (e.g. the "wavy" pseudotachylyte veinlet in Figure 6.28 on page 140, and also the pseudotachylyte vein in Figure 6.7 on page 115). Fragments that form by curved fractures may exhibit a pristine rounded shape, including pristine concave boundary segments.

Micro Fragment Internal Structures

The majority of fragments are internally deformed. Micro fragments often consist of small (submillimetre) grains, that sometimes surround larger grains e.g. Figure 6.12). Only a small number of fragments were observed that are made up of only one grain.

Some quartz single grain micro fragments with pervasive micro fracture (cleavage) development have been observed (Figure 6.18 on page 128: their features are discussed in more detail in Section 6.5.3). Some of them contain micro fractures that are straight, occur in several parallel sets, and are decorated by inclusion trails of dark coloured material. The dark coloured material could be identified as magnetite, illmenite and probably an amphibole, but it is possible that other minerals are present too. The identification of these decorating minerals is difficult because the grains are seldomly larger than one micron. Monocrystalline micro fragments that show internal micro fractures often have grain boundaries that are parallel to these internal micro fractures.

Numerous quartz grains, both single grain micro fragments and in the host rock close to the pseudotachylyte boundary, contain inclusions that consist of dark (opaque, rusty brown or greenish) minerals (on BSE images: white spots, e.g. in lower Figure 6.14 on page 125). These inclusions give these grains a "dusty" appearance (Figure 6.20). The inclusions were identified as magnetite, pyrite, and minor illmenite, and one or two green minerals, probably an amphibole, and a pyroxene or epidote (Figure 6.21). Some of the inclusions are geometrically arranged (Figure 6.19 on page 129, and Section 6.5.3).

Polycrystalline and polymineralic micro fragments are the most common micro fragments. They vary in size from several microns to larger than micro fragments (Figure 6.12 on the preceding page). All large micro fragments are

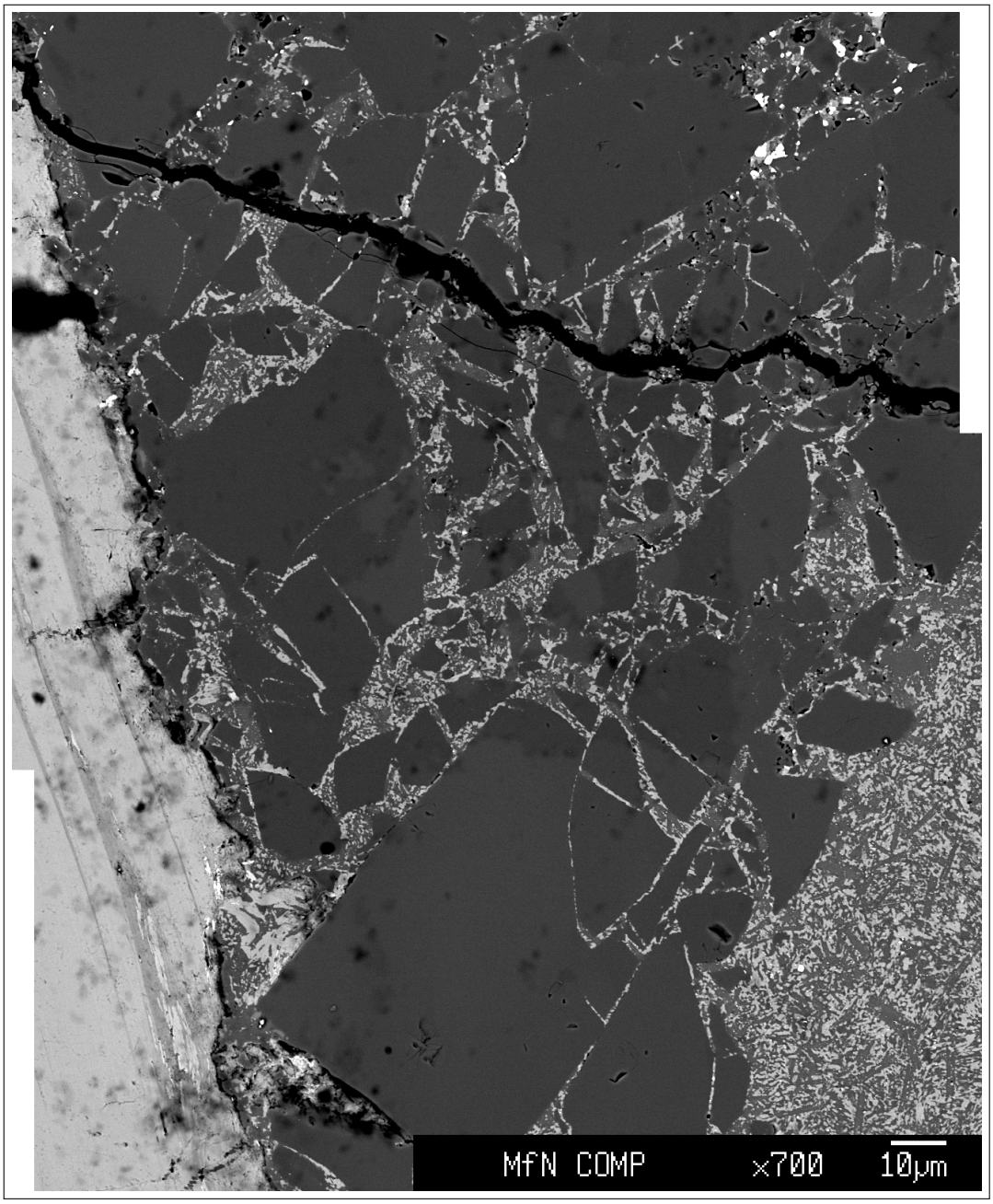

Figure 6.13 – Backscatter electron image of a cluster of angular (monocrystalline) micro fragments. The quartz micro fragments occur in a wide range of sizes down to one micron (possibly smaller). Note curved fractures. In the large quasi rectangular clast at the bottom of the image, the curved fracture produces a concave fragment segment into which the fragments at the top right corner fit. The host at the left hand side of the image is biotite which shows lattice orientation controlled replacement, probably by titanite, at the lower end. Due to thin section preparation, the quartz in this image shows several shades of grey. Thin Section B3. Image taken at the Museum für Naturkunde in Berlin, thanks to the support of Prof. W. U. Reimold and his staff.

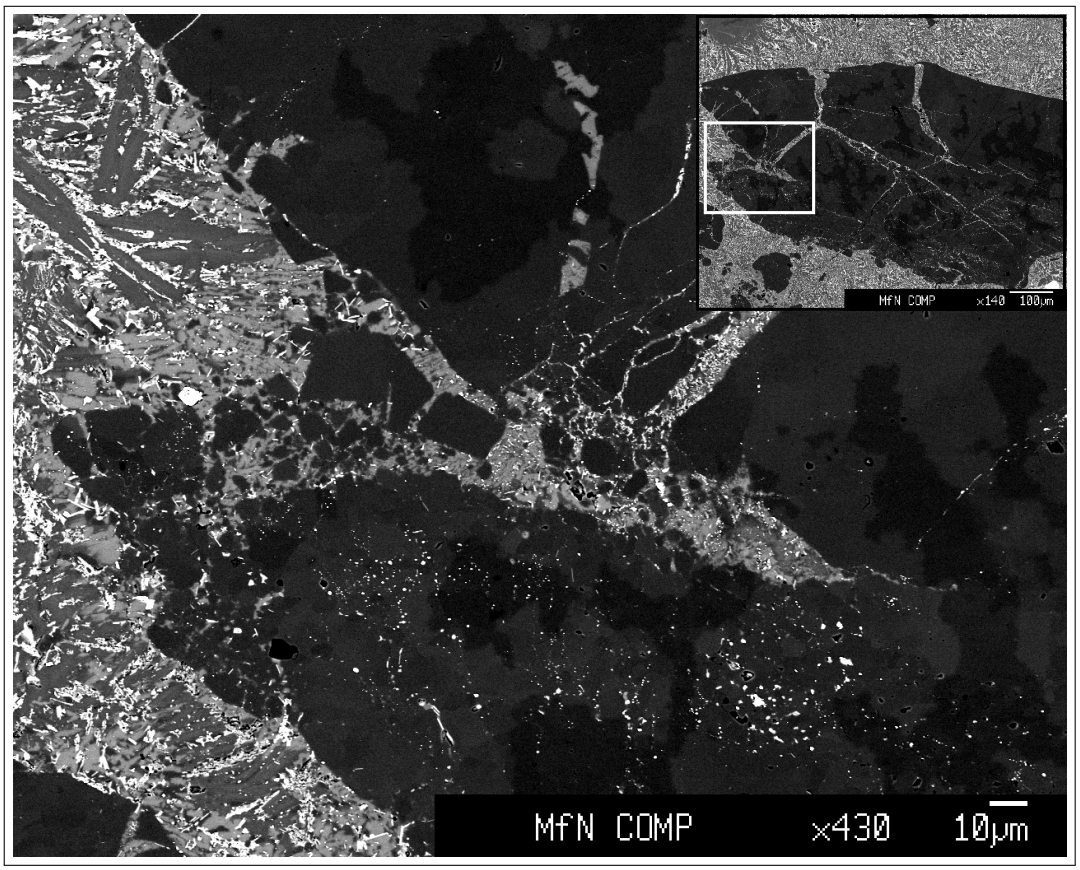

Figure 6.14 – Backscatter electron image of a strongly fractured quartz micro fragment. Different shades of dark grey are due to thin section preparation. The whole quartz micro fragment is elongate but rounded, however, it is composed of numerous and often angular subfragments that are separated from each other by micro factures. Individual fragments that cluster in the "shark's mouth" are in the order of one to twenty microns. In the lower segment, numerous oxide and possibly pyrite inclusions (white spots) are present. The inset shows an overview, inset scale bar is 100 microns. These images are details of Figure 6.11 on page 121. Thin Section A1. Image taken at the Museum für Naturkunde in Berlin, thanks to the support of Prof. W. U. Reimold and his staff.

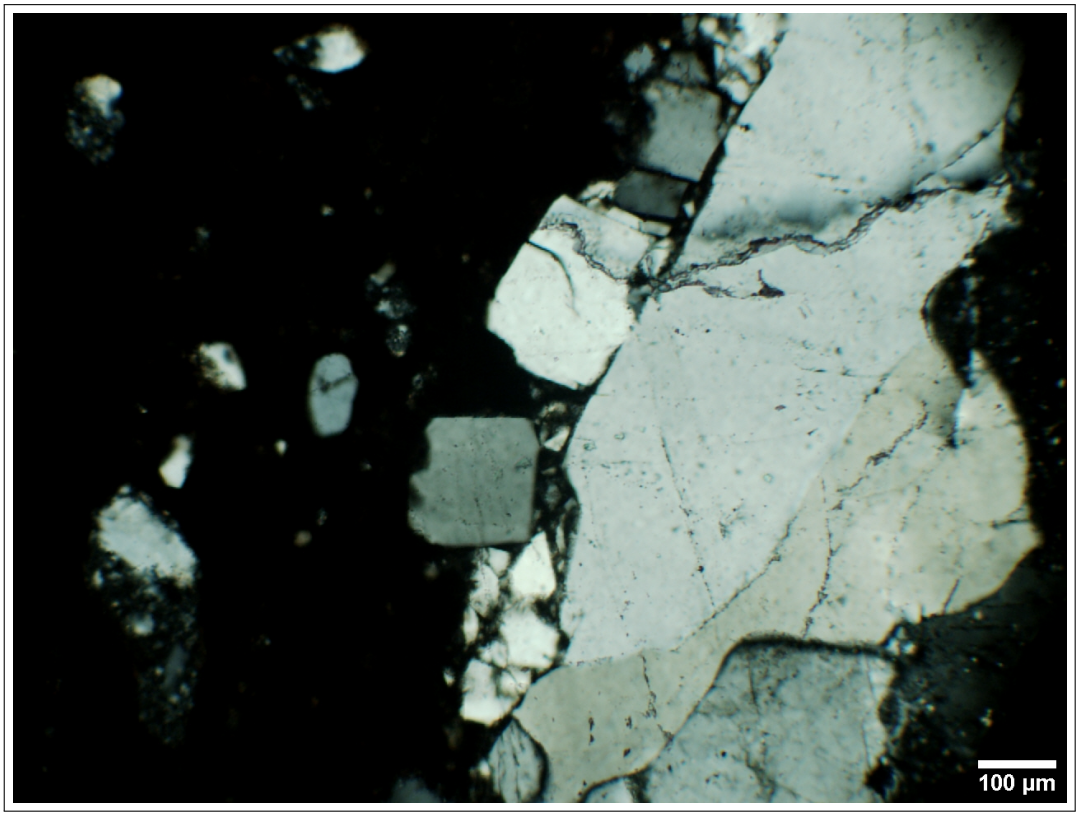

Figure 6.15 – Photomicrograph in crossed polarized light of a pseudotachylyte (left) containing angular and rounded micro fragments. The quartz micro fragments at the interface have not been transported far, as they are still in contact to each other and their host rock (right) in places. Note the curved micro fracture in the quartz fragment just above the centre. Thin Section B1.

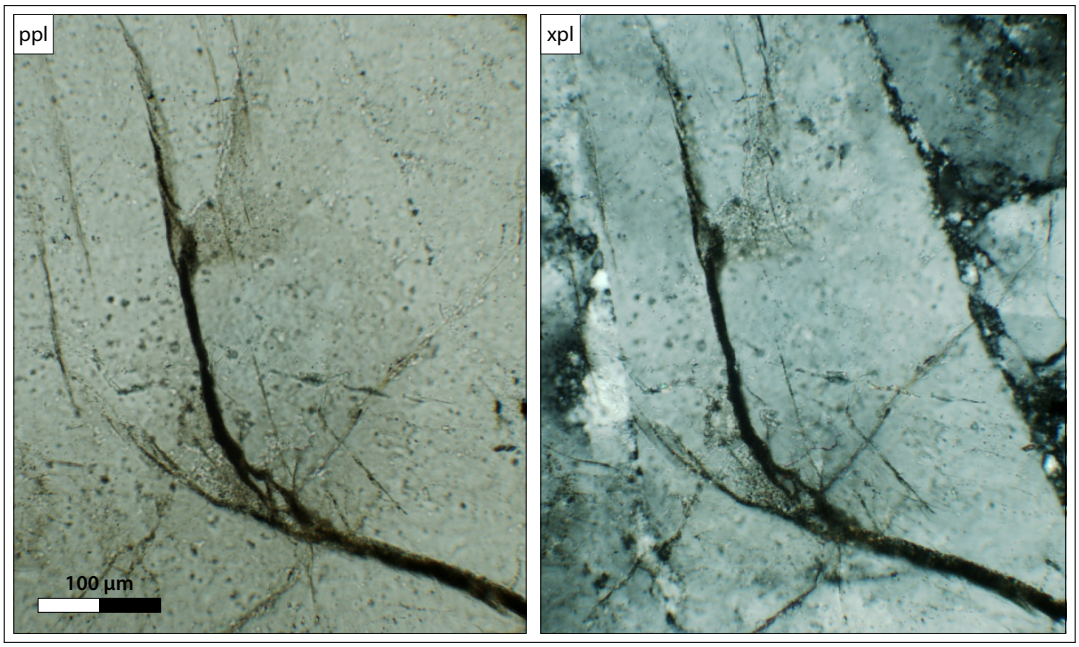

Figure 6.16 – Photomicrograph in plain (ppl) and crossed (xpl) polarized light of a pseudotachylyte micro vein fracture cutting through quartz. Note the micro fragments that occur in the curved segment, where the smaller vein branches off. Thin Section C3.

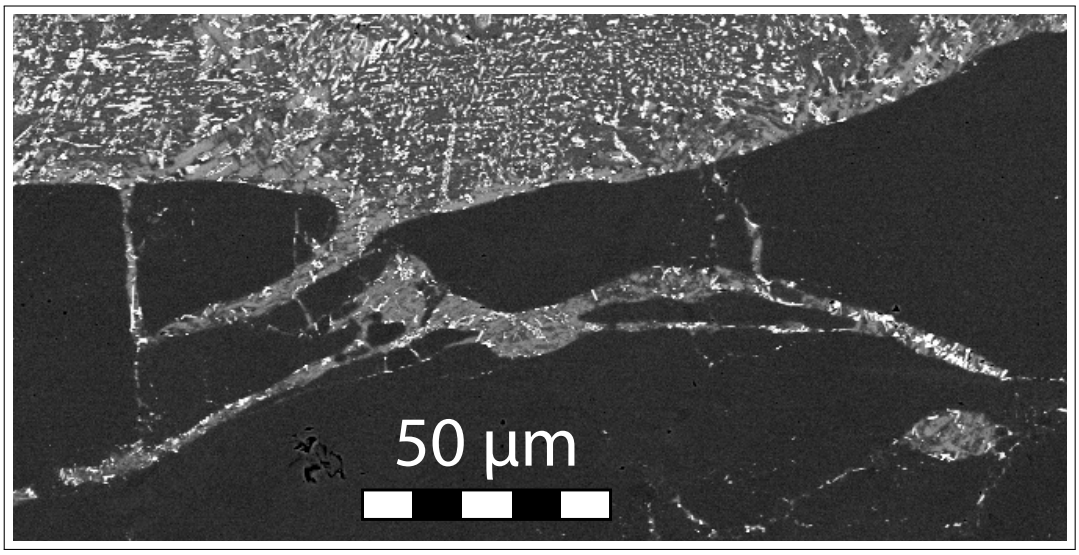

Figure 6.17 – Backscatter electron image of a quartz fragment boundary. The quartz is intensely fractured with several segments of curved fractures. Thin Section A1. Image taken at the Museum für Naturkunde in Berlin, thanks to the support of Prof. W. U. Reimold and his staff.

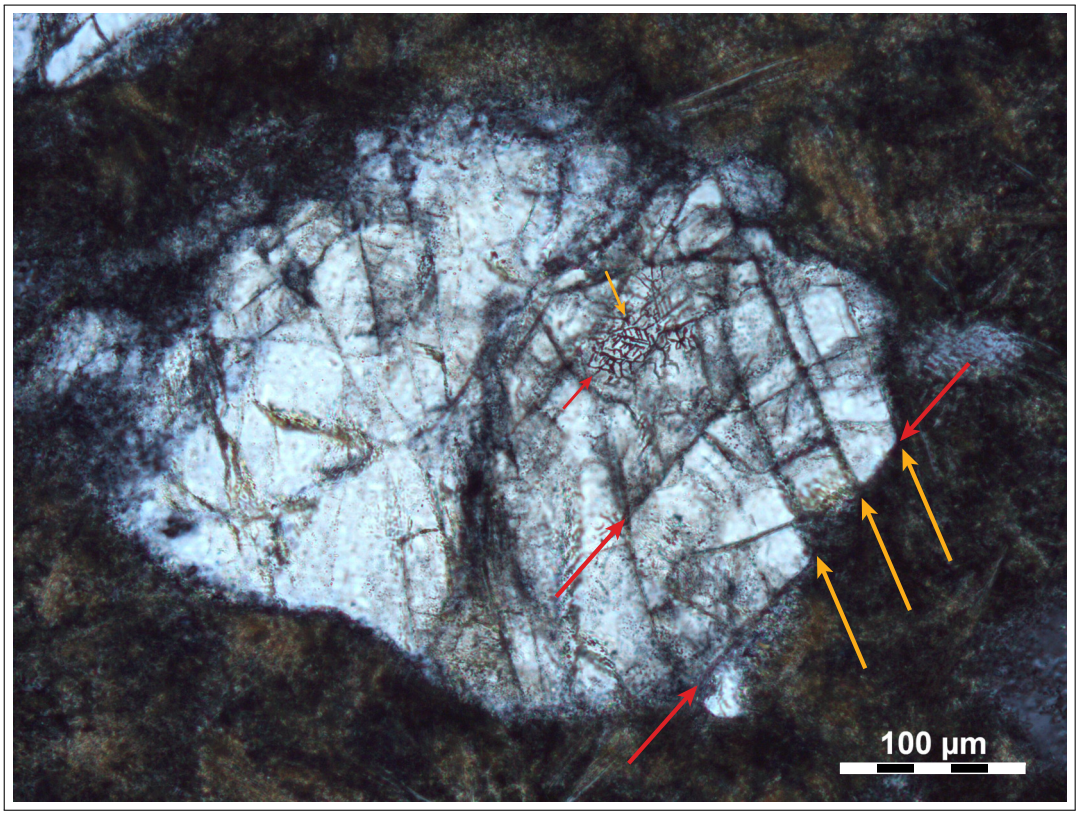

Figure 6.18 – Photomicrograph (ppl) of a quartz micro fragment. The quartz is pervasively deformed by micro fractures with a regular spacing (cleavage, planar fractures) that are decorated with dark inclusions and make up segments of the micro fragment's boundary (large red and orange arrows). The small arrows point to inclusion trails that are parallel to the micro fractures. Both the inclusion trails and the micro fractures seem to be crystallographically controlled. See Figure 6.19 on the next page for a detailed photomicrograph of the inclusion trails. Thin Section A1.

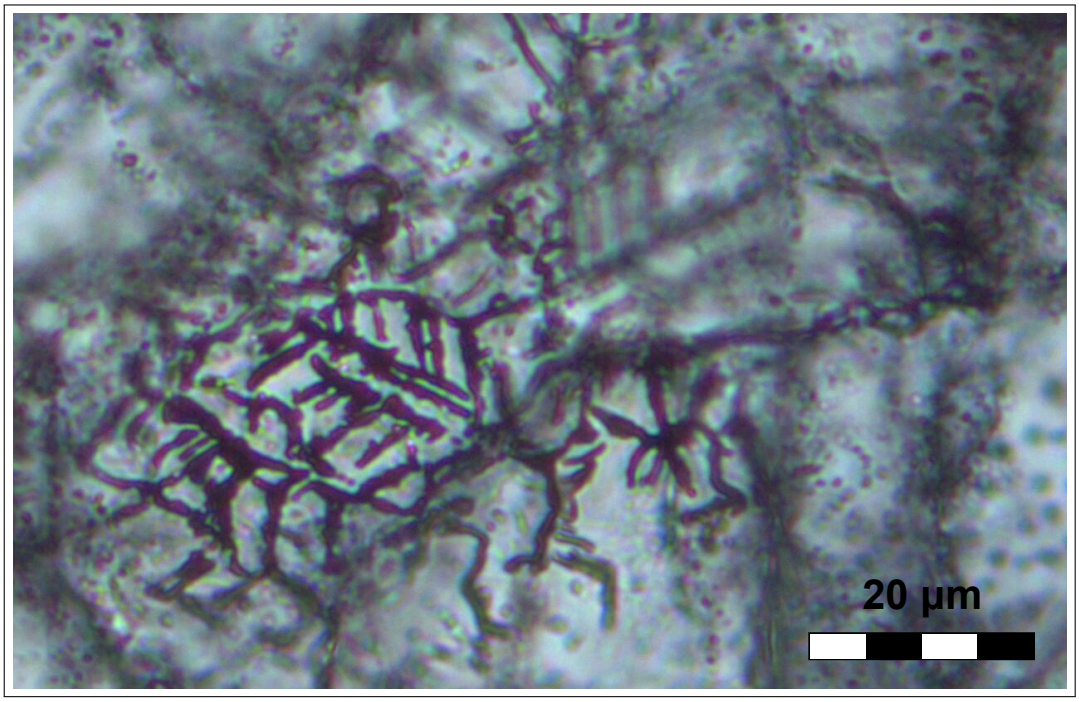

Figure 6.19 – Photomicrograph (ppl) showing part of the quartz micro fragment shown in Figure 6.18. The quartz fragment contains distinct sets of inclusion trails. There is a geometrically arranged set of parallel long inclusion trails that trend top left to bottom right in the figure and shorter inclusion trails that trend at 60 degrees to the long trails. The spacing between the parallel long trails is two or three microns. The trails are all in focus which suggests that they are in one plane that is parallel to the thin section surface – if these inclusion trails were dipping within the thin section the part of the trail that was on focus when the viewer varied the focus depth would short systematically left or right. Thus, measurements of distances and angles are absolute. To the top right of the image another set of similar trails is seem that are out of focus.

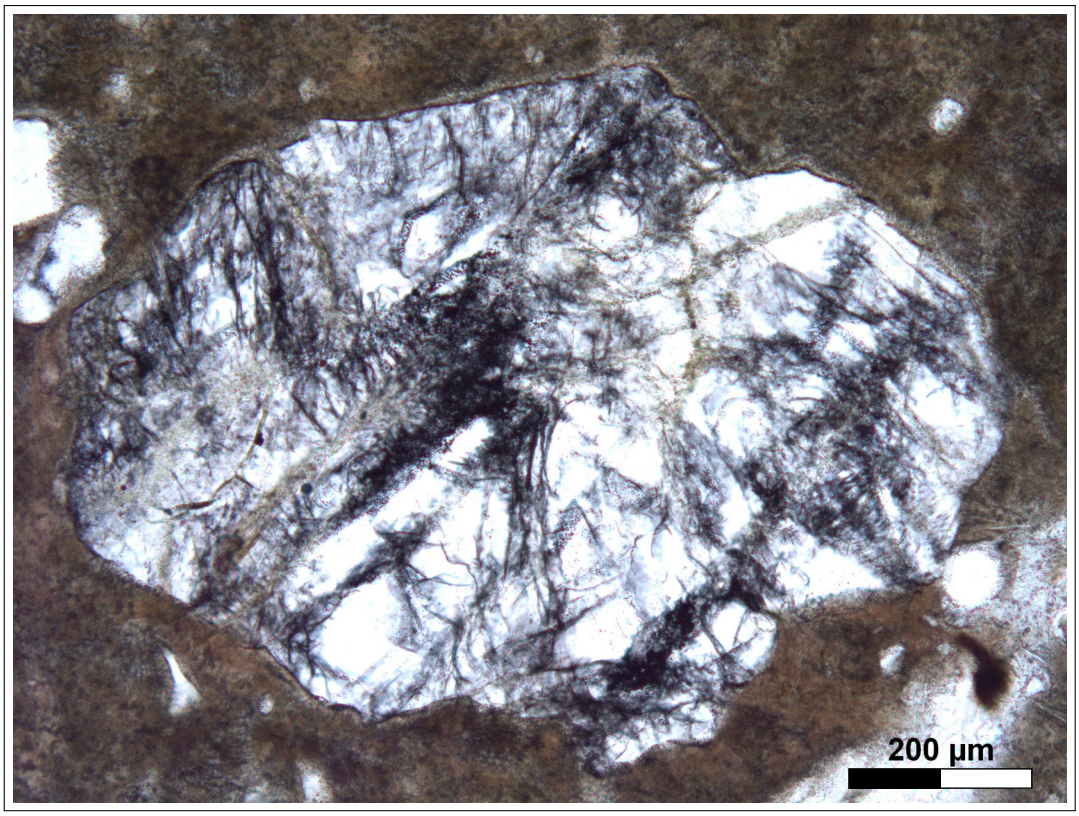

Figure 6.20 – Photomicrograph of a "dusty" quartz micro fragment in pseudotachylyte matrix. Thin Section A1, ppl.

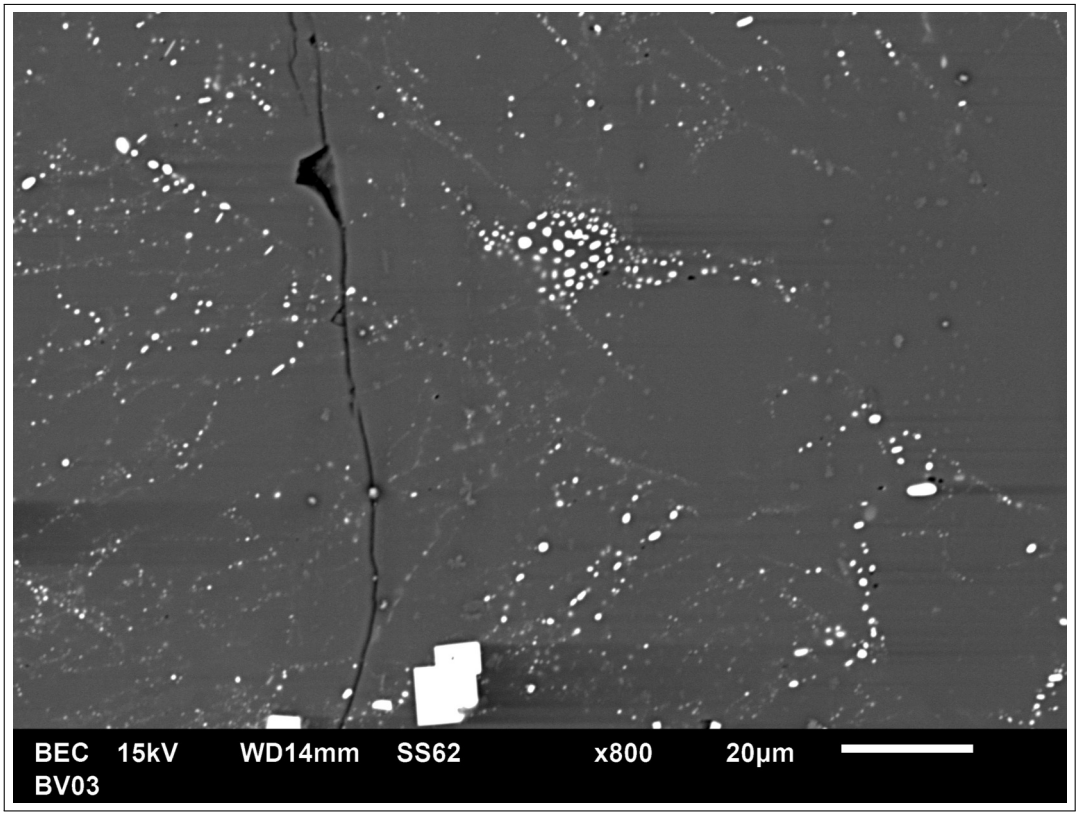

Figure 6.21 – Backscatter electron image of a quartz (grey) micro fragment "with a dusty appearance". The rounded white minerals are magnetite, the squares are pyrite cubes. Some of the magnetite inclusions are arranged in lines that are visible as planar features with the optical microscope. The dark horizontal streaks to the right of white minerals are artifacts due to charging of the sample during imaging. Thin Section A1. Image taken at the Museum für Naturkunde in Berlin, thanks to the support of Prof. W. U. Reimold and his staff.

polycrystalline or polymineralic. They look very much like parts of the deformation zones in the host rock (Figure 6.9 on page 117). Some of them consist of very small grains only (up to about 10 microns in size), others contain larger grains as well. The survivor grains are commonly surrounded by the smaller micron-sized grains. The fragment boundaries are thus made up of these small grains which gives the fragment boundaries a diffuse rather than sharp appearance under the microscope. This is because the small grains are smaller than the thickness of the thin section (25 microns), and between the small grains, matrix minerals of even smaller grain size (up to a couple of microns), are present.

Shock Metamorphic Features

All thin sections were thoroughly searched for planar fractures (PFs) and planar deformation features (PDFs) (Chapter 2), however no unequivocal shock metamorphic features were found. Due to their geometrical arrangement the conspicuous planar fractures and inclusion trails in some quartz grains in thin section A1 seem to be crystallographically controlled. However they have not been indexed by means of a universal stage. Brittle failure of quartz along crystallographic orientations (cleavage) is not common (Bunch and Cohen, 1964). Planar fractures (PFs) in quartz are an indicator for deformation at high strain rates, whether these strain rates are interpreted to be produced by shock deformation depends on the number of PF sets and their crystallographic orientation (Chapter 2). The inclusion trails in Figure 6.19 on page 129 are conspicuous but they do not look like images of PDFs published in the literature. These features are further discussed in the context of formation processes in Section 8.2.3.

Micro Fragment Locality

Generally, micro fragments are found anywhere within the pseudotachylyte. However, their distribution is not homogeneous. Where pseudotachylytes narrow, kink, or terminate, both micro fragments and fragments larger than a couple of millimeters are more abundant (Figures 6.7 on page 115, and 6.8 on page 116). See also case study in Section 6.6.1.

6.5.4 Pseudotachylyte Matrix

The pseudotachylyte matrix is very dark brown to opaque to a more transparent rusty brown, or greenish in plain light (Figures 6.7 on page 115, 6.9 on page 117, 6.10 on page 118, and 6.22 on the following page). In the brown matrices (Samples B and C), a heterogeneous mingling texture has been observed. It consists of spherules of an opaque phase set in a light brown transparent matrix. The two lighter matrix appearances (the mingling texture and the more transparent matrix) occur in streaks or schlieren close to, but not touching, the pseudotachylyte's interface with the host rock. The homogeneously transparent

Figure 6.22 – Photomicrograph in plain polarized light of pseudotachylyte containing micro fragments. The acicular shapes in the matrix are plagioclase laths. They occur in radially structured aggregates in the matrix, and nucleate along boundaries of some micro fragments (mostly plagioclase). Thin Section A1.

brown matrix phase has a very similar appearance to the common fine grained material that surrounds some of the clasts. In the more central parts of pseudotachylyte *s.s.* (i.e. not along its boundaries to the host rock), plagioclase laths in skeletal acicular shape are prevalent (Figure 6.22), which often occur in radial aggregates.

The host rock in the vicinity of the pseudotachylyte plays a role in determining the pseudotachylyte's colour. This can be observed in thin (millimetre) pseudotachylyte veins (Figure 6.28 on page 140) or where pseudotachylyte grades into higher micro fragment densities. The more felsic the host rock, the lighter coloured (and more transparent) the pseudotachylyte. Where pseudotachylyte is in contact with a biotite grain, the pseudotachylyte is darker coloured to opaque (Figure 6.23). This phenomenon is very localised (sub-millimetre range) and discussed in more detail in Section 6.6.2.

The matrix consists of small crystals with a grain size below ten microns, but generally in the sub-micron to micron range (Figure 6.24 on page 135). No glass or flow structures have been observed on backscatter images. The newly crystallised matrix phases are plagioclase, orthoclase, mafic minerals (probably an amphibole,

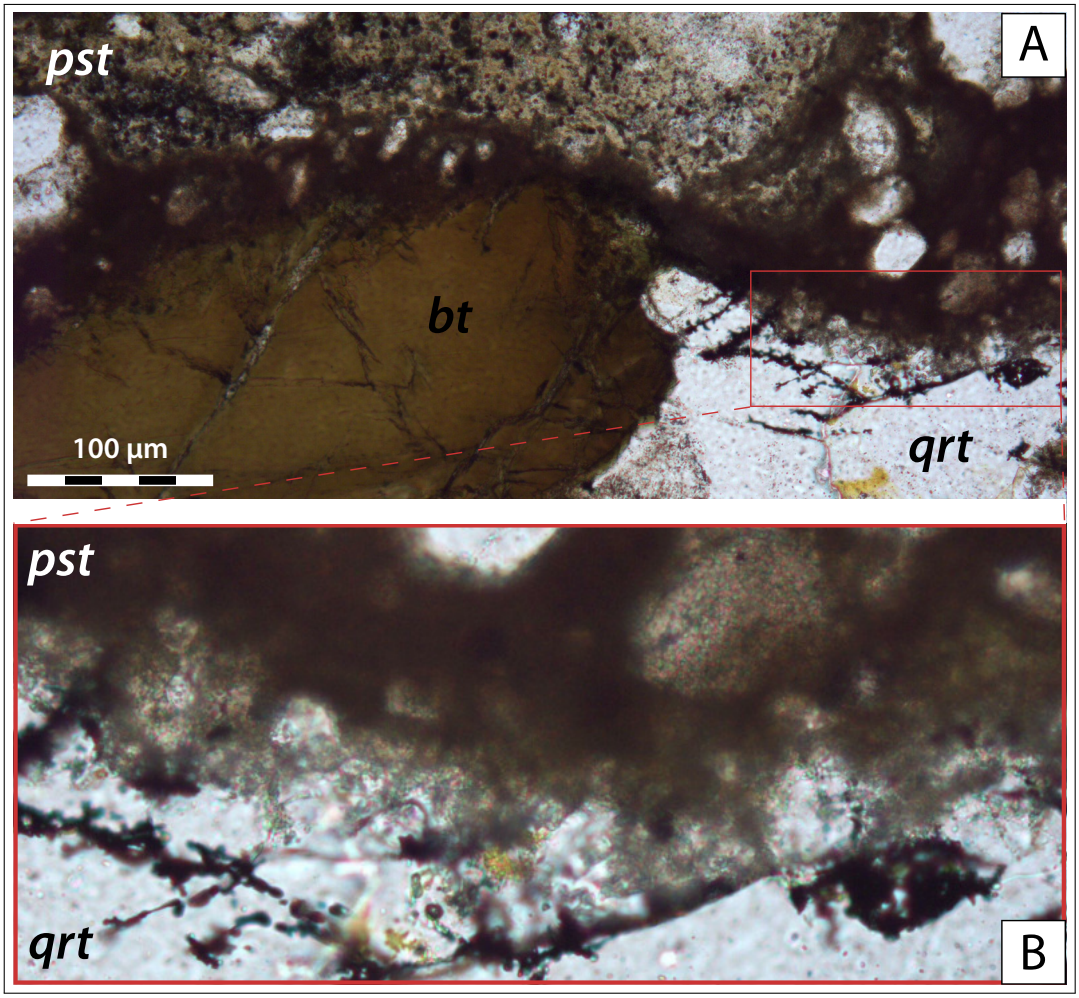

Figure 6.23 – Photomicrographs ppl of the interface between pseudotachylyte (top half of images) and host rock (bottom half of images). Both biotite and quartz do not exhibit a sharp boundary with the pseudotachylyte. The interface is marked by a layer of very dark brown pseudotachylyte, interspersed with fragments (5-20 microns) of a transparent mineral (probably quartz). Biotite and quartz show inclusions of opaque minerals in the vicinity of their boundary to the pseudotachylyte. **B** shows a part of **A** in more detail (red box). **A** Note the heterogeneity of the pseudotachylyte and the high abundance of micro fragments. **B** The dark brown, very fine grained (below 1 micron) matrix is interstitial to fine grained quartz at the interface. *pst* = pseudotachylyte, *bt* = biotite, *qrt* = quartz. Thin Section B2.

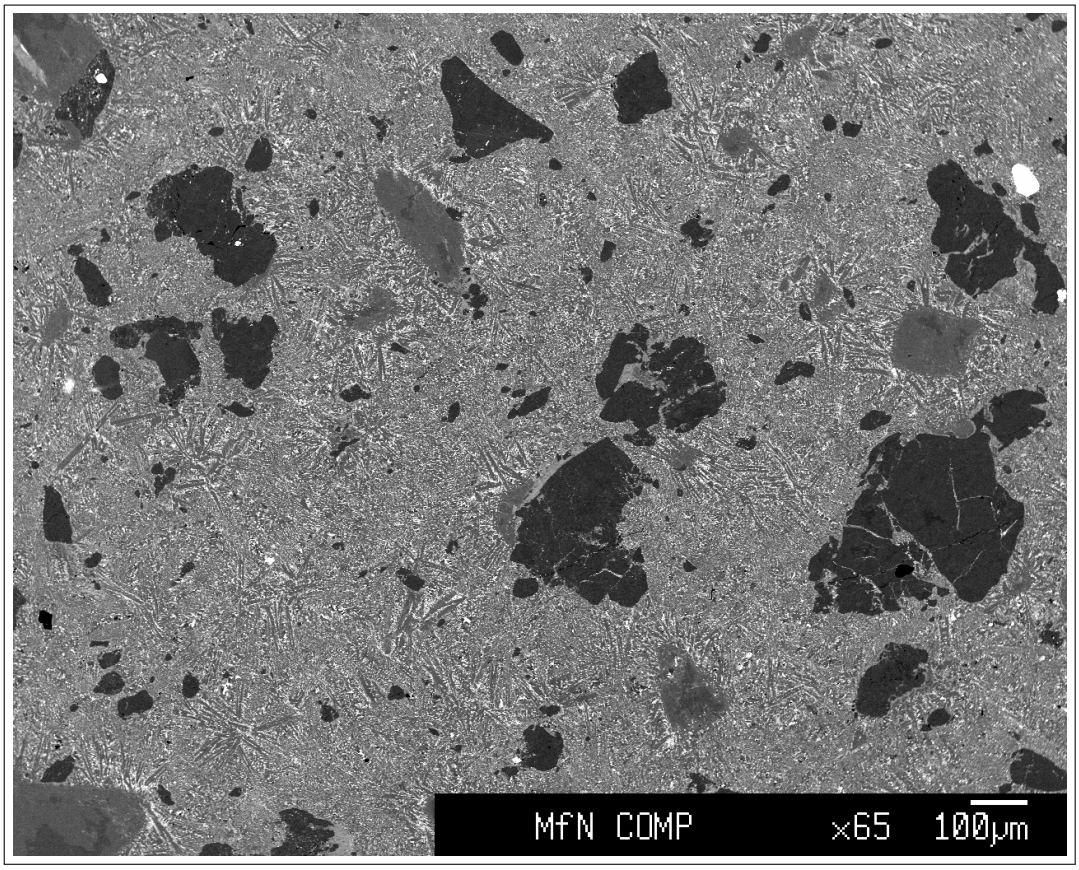

Figure 6.24 – Backscatter electron image of a typical pseudotachylyte *s.s.* without mingling structures. Micro fragments are quartz (dark grey) and feldspars (mainly plagioclase, lighter grey). The elongate micro crystallites are skeletal acicular plagioclase crystals in the matrix. Thin Section A1. Image taken at the Museum für Naturkunde in Berlin, thanks to the support of Prof. W. U. Reimold and his staff.

pyroxene, biotite, and a mineral of the epidote groupe or cordierite), magnetite, other ore minerals including rutile, iron-sulfates (pyrite), and subordinate quartz (Figure 6.25). The exact identification especially of the matrix minerals with a more complex composition is nearly impossible because the rock volume analysed by the electron beam is larger than the matrix mineral size. The larger quartz grains occur as fragments, which are often rounded. Some plagioclase laths grow in radial structures which often originate from rounded (i.e. not angular) plagioclase micro fragments. These laths are up to 10 microns long. They seem to occur in clusters, where as in other matrix areas, plagioclase forms considerably smaller grains. The k-spar develops its platy habitus preferentially next to the large quartz micro fragment and its subclasts. It seems that k-spar would often exist in conjunction with quartz, and plagioclase with a mafic mineral.

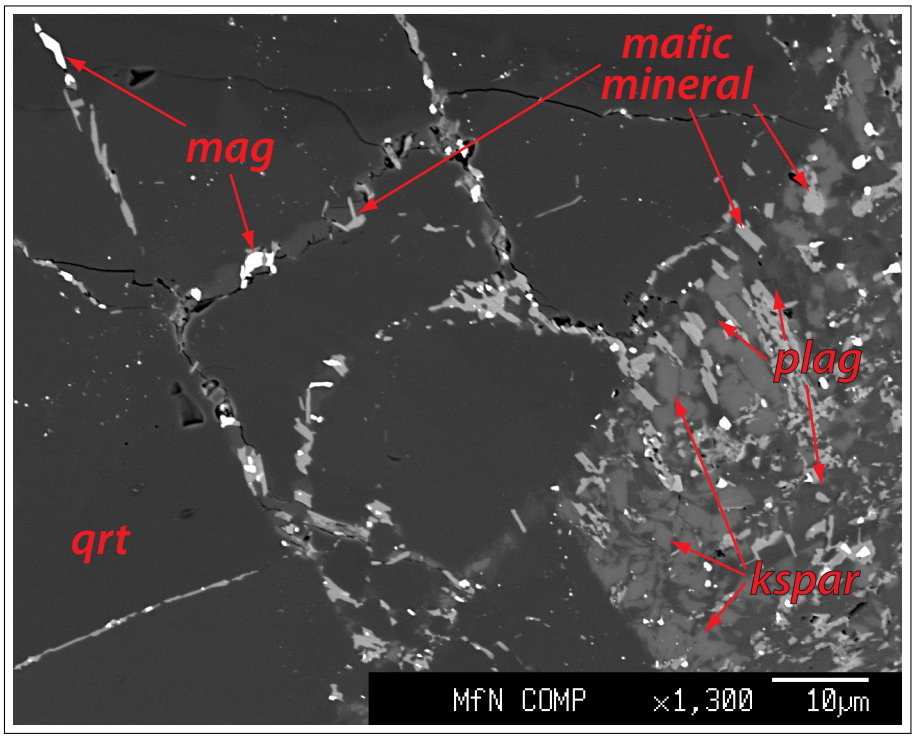

Figure 6.25 – Backscatter electron image of the interface between a micro fractured quartz micro fragment (same as in Figure 6.18 on page 128, area where the yellow arrows are) and the pseudotachylyte matrix. *qrt* = quartz, *mag* = magnetite, *kspar* = k-spar, *plag* = plagioclase. Thin Section A1. Image taken at the Museum für Naturkunde in Berlin, thanks to the support of Prof. W. U. Reimold and his staff.

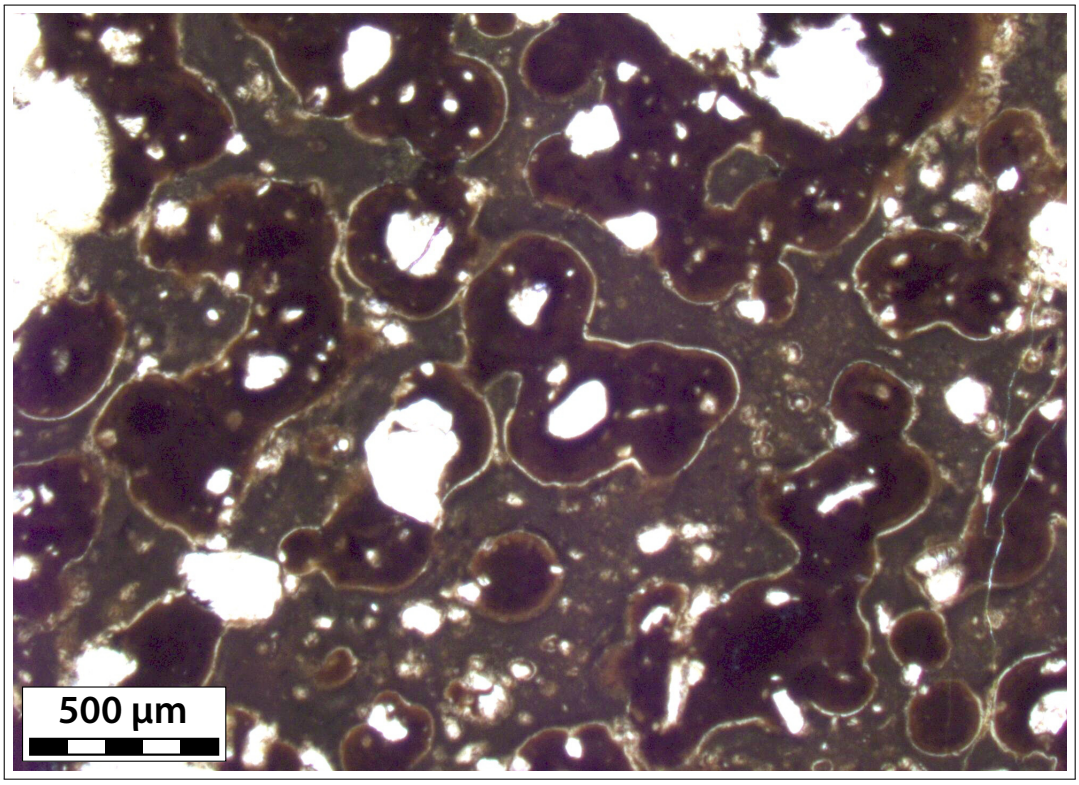

Figure 6.26 – Photomicrograph (ppl) of an area of pseudotachylyte that contains spherules. These spherules generally contain a plagioclase fragment in the core, that is enclosed in a nearly opaque shell that grades into a brown shell. The outermost rim is transparent. The matrix around the spherules is here mainly composed of a green-turquoise mineral (amphibole?), with transparent minerals (feldspar) and an olive green mineral (pyroxene, epidote?). Thin Section B3.

Spherules

In some of the thin sections, spherules were observed in the matrix. They occur commonly in layers or bands, and are prevalent in the larger pseudotachylyte veins in Sample B. These bands are part of the flow or mingling structures described above. The spherules are approximately 150-400 microns in diameter (Figure 6.26). Quartz fragments may be present within spherules but their presence doesn't seem to affect the spherule structure, and they seem to be inertly overgrown.

The spherules most commonly form around plagioclase fragments of a few tens of microns in size, from which plagioclase laths grow in radial manner (Figure 6.27 on the next page). Interstitious to the plagioclase laths is a submicron sized matrix of mafic minerals, potassium feldspar and ore minerals such as iron-sulfates, magnetite and titanium oxides such as rutile and illmentite. This inner shell is about 20-40 microns thick. The outer shell is similar in composition and thickness

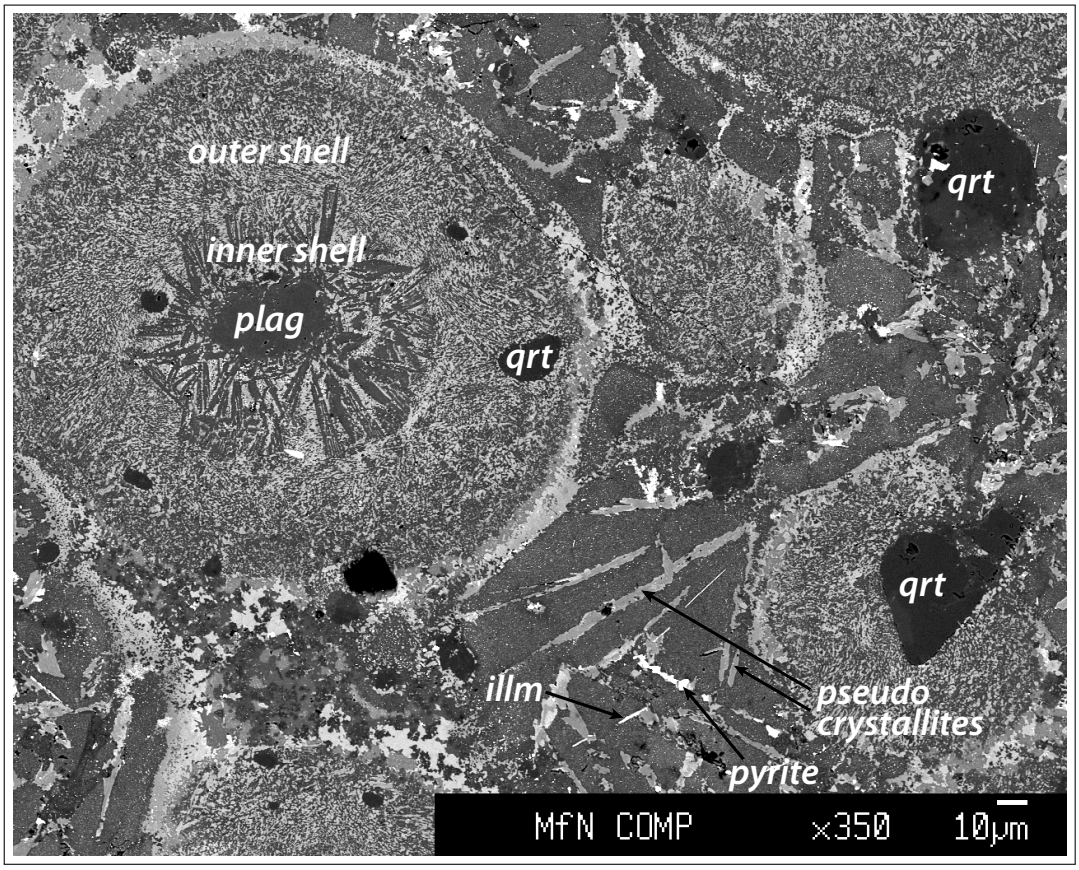

Figure 6.27 – Backscatter electron image of spherules. The spherule on the left hand side shows a plagioclase (plag) micro fragment core from which skeletal acicular plagioclase micro crystallites originate. Quartz (qrt) is inertly overgrown. Pseudo-crystallites occur interstitially to the spherules. Pyrite and illmenite (illm) are abundantly present in spherules and within the interstitial pseudo crystallites. See text for further explanation. Thin Section B3. Image taken at the Museum für Naturkunde in Berlin, thanks to the support of Prof. W. U. Reimold and his staff.

(slightly thicker), but different in texture: the plagioclase does not exhibit laths and the texture is more homogeneous (equigranular) in terms of grain size and shape. The two shells together are dark brown. Towards the outer surface of the outer shell, plagioclase is more abundant. The outer shell is rimmed by a couple of microns thick k-spar rim. This outer rim is not continuous and not present around all spherules. In places, this k-spar rim is followed by an outermost rim that is probably made up of an epidote group mineral, or another silicate mineral such as a pyroxene or amphibole. EDX analyses were not conclusive due to the small grain size of the minerals, their skeletal habitus containing numerous inclusions especially of oxides, and the mineral variability.

In some areas, the spherule matrix consists of pseudo-crystallites of up to 70 microns in length (Figure 6.27). The pseudo-crystallites exhibit a habitus but are not made up of a single crystal (and potentially more than one mineral). There are four phases that can be distinguished in BSE images: two in white, one in light grey and one in darker grey. The nearly white phase with acicular habitus is illmenite (Ti-Fe-oxide). The white phase that did not develop an idiomorphic habitus is pyrite (iron-sulfate). The light grey phase with elongate shape might be a pyroxene (aegirin-augite?), or possibly an amphibole, which occurs together with an even lighter grey phase that could not be identified. The darkest grey is an albite-rich plagioclase speckled with submicron grains of other minerals (probably predominantly oxides). Some spherules have a bromium-silicate core, which is formed of lath shaped micro crystals that grew in a parallel habit.

6.6 Micro Structural Synthesis

6.6.1 Case Study: "Wavy Veinlet"

The pseudotachylyte in Figure 6.28 can be divided into three parts with a more or less gradual transition. The three parts are illustrated in the sketch in Figure 6.29 on page 141 (lower half, stage 2) and from left to right with respect to the image are (A) the vertical pseudotachylyte vein, (B) the horizontal and dark wavy veinlet, and (C) the second half of the veinlet which is brown, less dark and includes the tip. Figure 6.28 **C** and **D** zoom into its tip (C) in Figure 6.29. The veinlet shows a gradual transition from cataclasite at its tip (C) to an opaque pseudotachylyte (B) which is indistinguishable by optical means from the larger pseudotachylyte vein (A). In the left half of the veinlet (B), the two sides of the veinlet fit seemingly perfectly to each other, and the grains on either side wall seem to match orientation roughly. In the right half of the veinlet (C), well visible at the very tip (Fig 8.23 C and D), the two sides don't seem to match. The veinlet's colour between the two red lines resembles the brown of the biotite under plain polarised light and the size of the area (C) is similar to the size of the biotite grains in the host rock, suggesting that this part of the veinlet may have replaced biotite in situ. Under crossed polarised light, the shape and the actual extent of the veinlet become apparent, and the cataclastic nature of the very tip. Mingling structures or flow structures indicate the material within the veinlet was behaving as a fluid. Quartz fragments of various size line the sidewalls and the tip, and the mixing of those fragments with the brown fluid originating from the biotite is incomplete. It seems the wavy left hand side of the veinlet (B) connects, as an open mode fracture, the left vein (A) and the right hand side of the veinlet (C) (stages 1 and 2 in Figure 6.29).

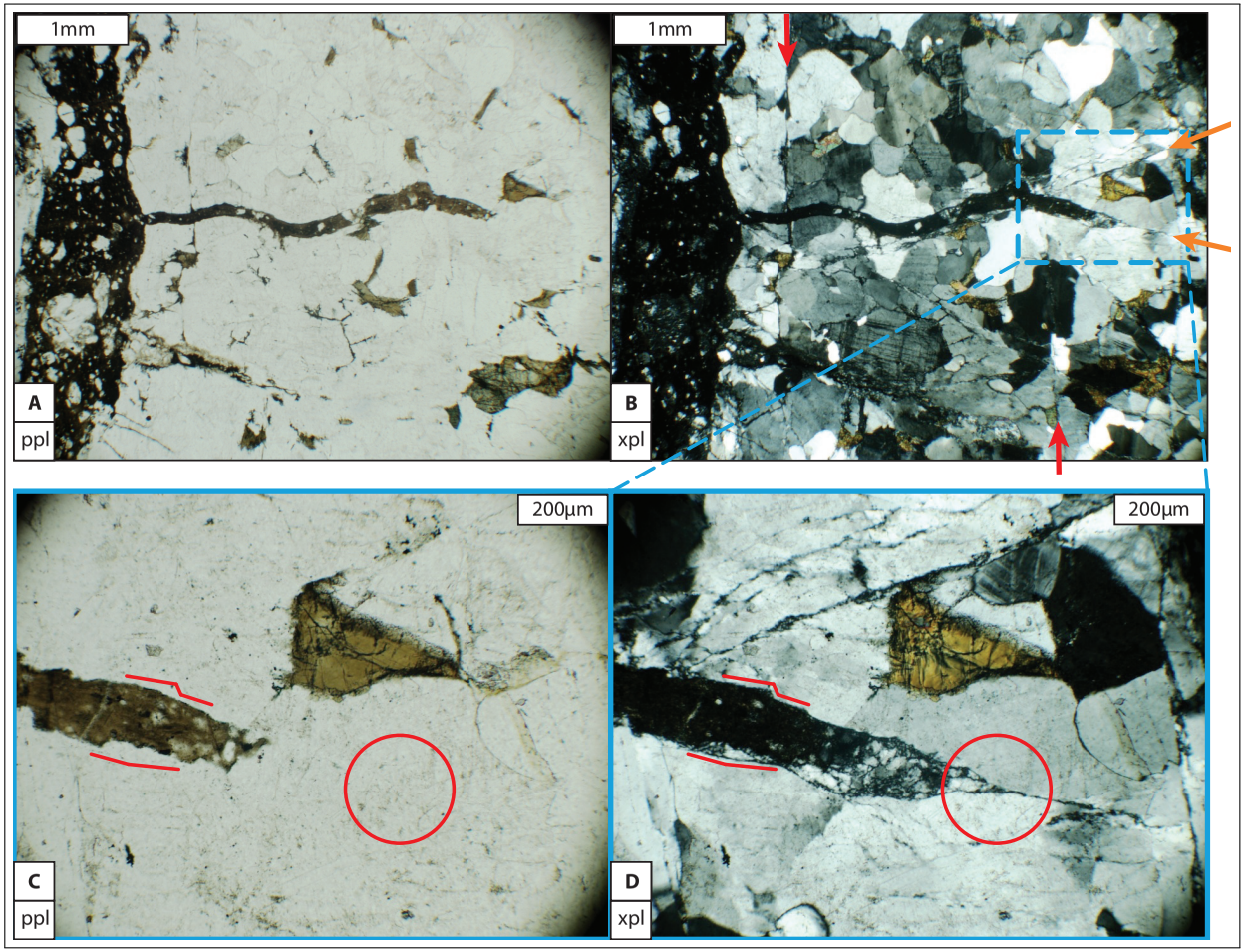

Figure 6.28 – A wavy pseudotachylyte veinlet originating perpendicular to the main pseudotachylyte vein (left hand side of **A** (ppl) and **B** (xpl)). The veinlet is opaque at its origin and gradually becomes lighter in colour. In **B**, the red arrows point into the direction of fractures that are parallel to the main pseudotachylyte vein. The orange arrows indicate a fracture set that is parallel to the segments of the pseudotachylyte veinlet in the centre of the images. **C** (ppl) and **D** zoom into the tip of the pseuodtachylyte veinlet, which grades into an aggregate of fine grained quartz before it tappers off into an annealed fracture. Note the difference in observability of the pseudotachylyte and its accompanying deformation in ppl (**C**) and xpl (**D**). Thin Section C3. This pseudotachylyte veinlet is discussed as a case study in more detail in Section 6.6.1.

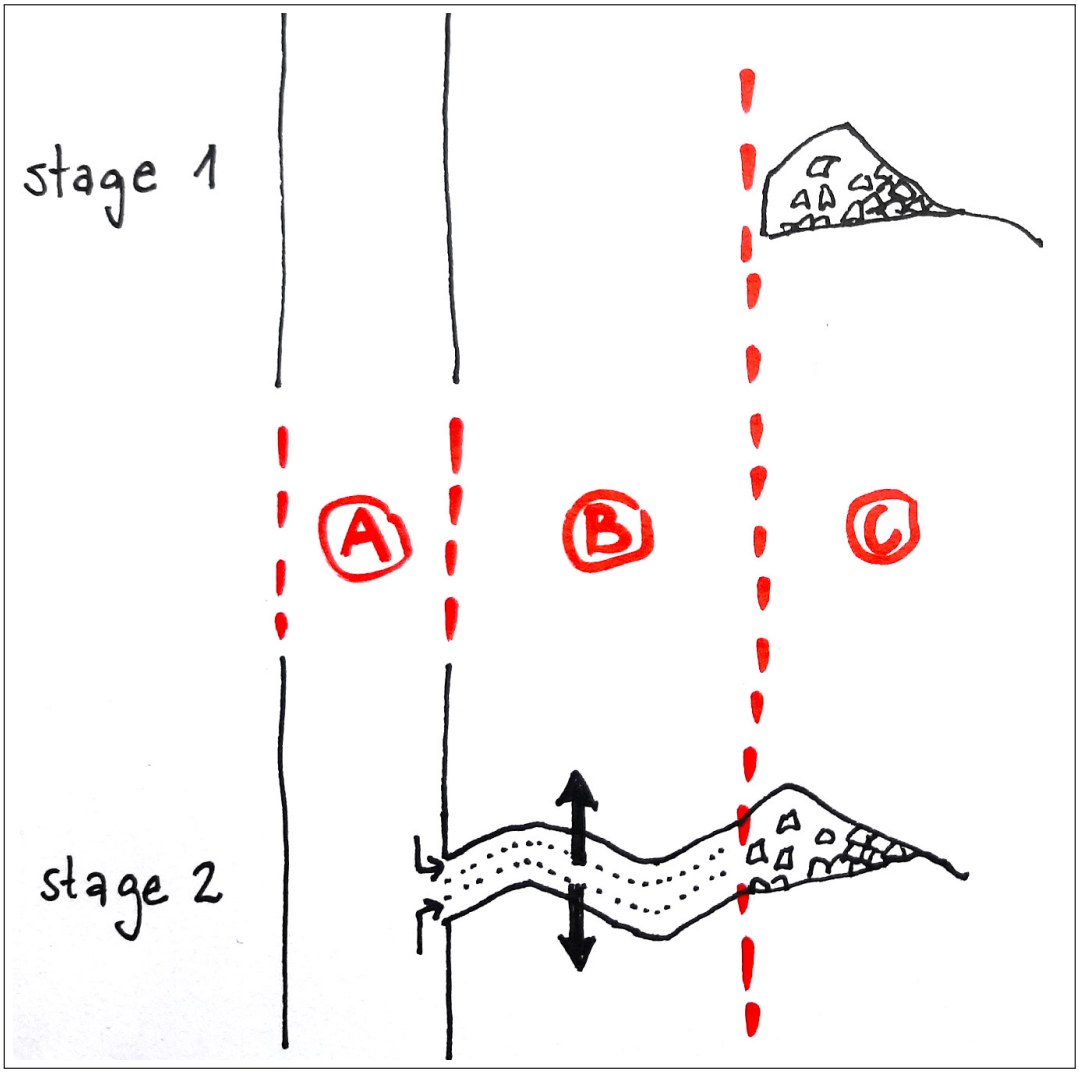

Figure 6.29 – Interpretation of formation of the wavy veinlet in two stages, based on Figure 6.28: (**A**) is the pseudotachylyte vein on the left, (**B**) is the wavy part of the veinlet, and (**C**) is the tip, consisting of quartz cataclasite.See text for further explanation.

6.6.2 Initial Stage of Pseudotachylyte Formation: Difference for Biotite and Quartz

Figure 6.30 shows strongly deformed and partly replaced biotite in the centre of tentacle-like opaque veinlets branching into the surrounding quartz grains. Some of the veinlets contain quartz fragments. Despite the strong deformation of the surrounding felsic minerals (visible in xpl), the veinlets in this Figure are opaque and single phase, that means – in contrast to Figure 6.31 – they do not display any mixing or mingling structures. The biotite in the centre of the micro feature is still optically identifiable as a biotite. This image is from the same thin section as Figures 6.28 and 6.31 and illustrates the initial formation of pseudotachylyte at a biotite grain.

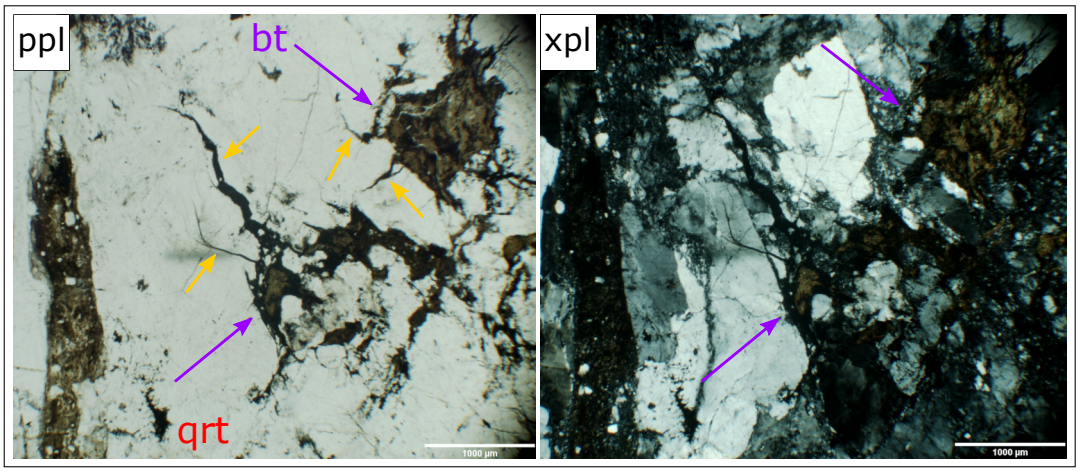

Figure 6.30 – Initial step of pseudotachylyte formation in situ on biotite (purple arrows), producing an opaque (black) matrix which intrudes into tentacle-like fractures (yellow arrows) in the surrounding quartz (qrt) grains. Note biotite deformation where it is still recognisable.

Figure 6.31 shows a deformation microstructure from the same thin section as the veinlet (Section 6.6.1), but in a more felsic host rock. In plane polarised light the quartz grain on the left hand side appears intact, colourless and transparent, with a change in relief from the increased number of grain boundaries, whereas in crossed polarised light the extent of the deformation both within and outside the grain becomes evident. Most of the very fine grained matrix (right hand side, appearing dark in crossed polarised light) is transparent in plane polarised light, and it is not possible to tell whether the grains are fragments, recrystallised fragments or crystallised microcrystals. Especially along the grain boundary of the large grain on the left hand side the matrix is darker (bottom and upper half of the image). The colour change is visible when the grain boundaries are decorated (also e.g. Figures 6.12 on page 122, and 6.25 on page 136). Wenk et al. (2000) found similar microstructures of cataclastic 'debris' along fractures (their Figure 9b). The very fine grained felsic (here quartz) material has formed in situ, and

gradually been infiltrated by, and mingled and mixed with a darker fluid originating from mafic minerals (Figure 6.30). The photomicrographs in Figure 6.31 illustrate the initial stages of pseudotachylyte formation in a felsic environment. Deformation / cataclasis of such a host rock leads to the formation of fragments with a variety of grain sizes such as visible in the right hand side of the lower two rows (**C** to **G**) in Figure 6.31. The occurrence of angular micro fragments down to (sub-)micron size (e.g. Figure 6.32) suggests that they did not form in an environment that favours their melting, because very small grains with a high surface to volume ratio melt preferentially. These angular micro fragments have only been observed in the vicinity of host rock or fragments. Angular fragments and quartz cleavage, have only been observed inside the pseudotachylyte. This suggests that their formation is related to pseudotachylyte formation.

In plane polarised light, a gradual transition was observed in many occasions from transparent fragment (or host rock mineral), to a coloured but still transparent mix of small fragment grains with matrix minerals, to the dark pseudotachylyte (e.g. Figure 6.31). Darker matrix material seems to intrude along grain boundaries of the very fine grained aggregates along host rock or of polymineralic aggregates, and disaggregate ("pluck") or suspend grains (or smaller aggregates) in the matrix. The disaggregated small fragment grains may then melt, or be incorporated into or dispersed in the pseudotachylyte matrix, possibly forming the flow structures (Section 6.6.3) containing more transparent material. This process of disaggregation by intrusion along grain boundaries can explain both fragment size reduction (comminution), the formation of concave fragment segments or irregularly shaped fragments, and rounding of fragments.

EMPA images shown in Figure 6.32 **A**, **B** and **C**, reveal biotite (bt_1) being replaced (blue arrows) by an aggregate of tiny (approx. $1\mu m$) grains of titanite, biotite (bt_2 with a different composition) and iron oxide. The newly formed aggregate is dark: titanite contains iron which gives it a darker colour, iron oxides are opaque and biotite dark coloured. Quartz, on the other hand, breaks up into angular, transparent fragments, some smaller than $1\mu m$ (red arrows). The biotite does not simply 'melt' as by equilibrium contact melting. Biotite breakdown occurs both at the contact with the pseudotachylyte (pst) (Figure 6.32 **A** and **C**) and at a distance from the contact (also Figure 6.30). This was also noted by Kelley et al. (1994) who found that the mechanism of argon loss in their biotites in contact with and in the immediate host rock of a pseudotachylyte from the Outer Hebrides was *not* volume diffusion, but a mechanism which seems to sample all areas of a grain simultaneously. They speculate that the mechanism could be similar to that which occurs during stepped-heating experiments in the laboratory, which occurs at temperatures in excess of 600-800°C and leads to a breakdown of the biotite lattice.

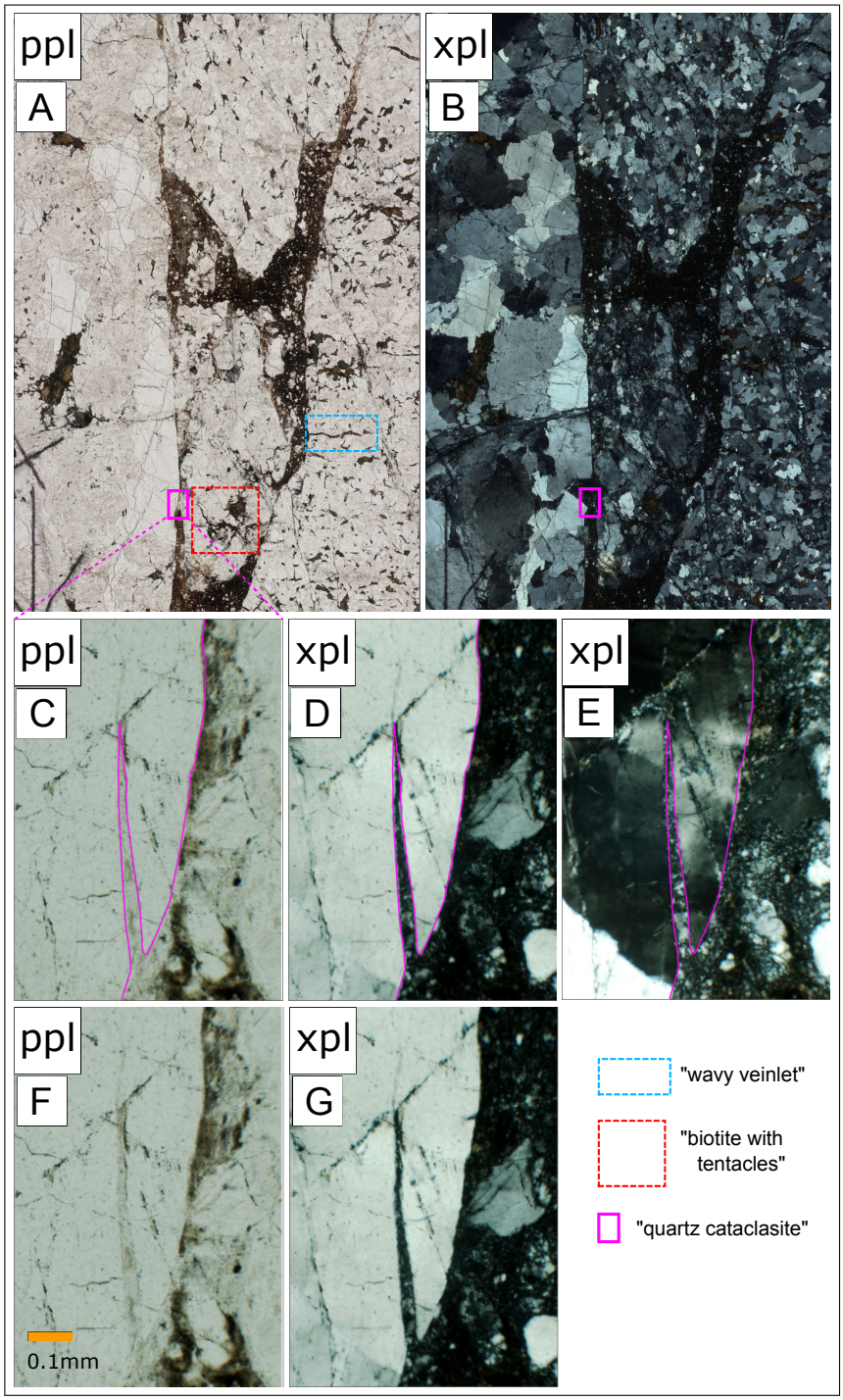

Figure 6.31 – Top two images (A and B) are thin section scans with the pink rectangle indicating the area of the photomicrographs (C – G) below. Ppl left three images, rest xpl. A quartz grain (left) in contact with a cataclasite–pseudotachylyte. The extent of the deformation in the quartz grain is barely visible in ppl. Thin section is 40 mm long, orange scale bar in bottom right is for all 5 photomicrographs (C - G). The two xpl images (D and E) in the middle row are taken at different angles and later rotated back.

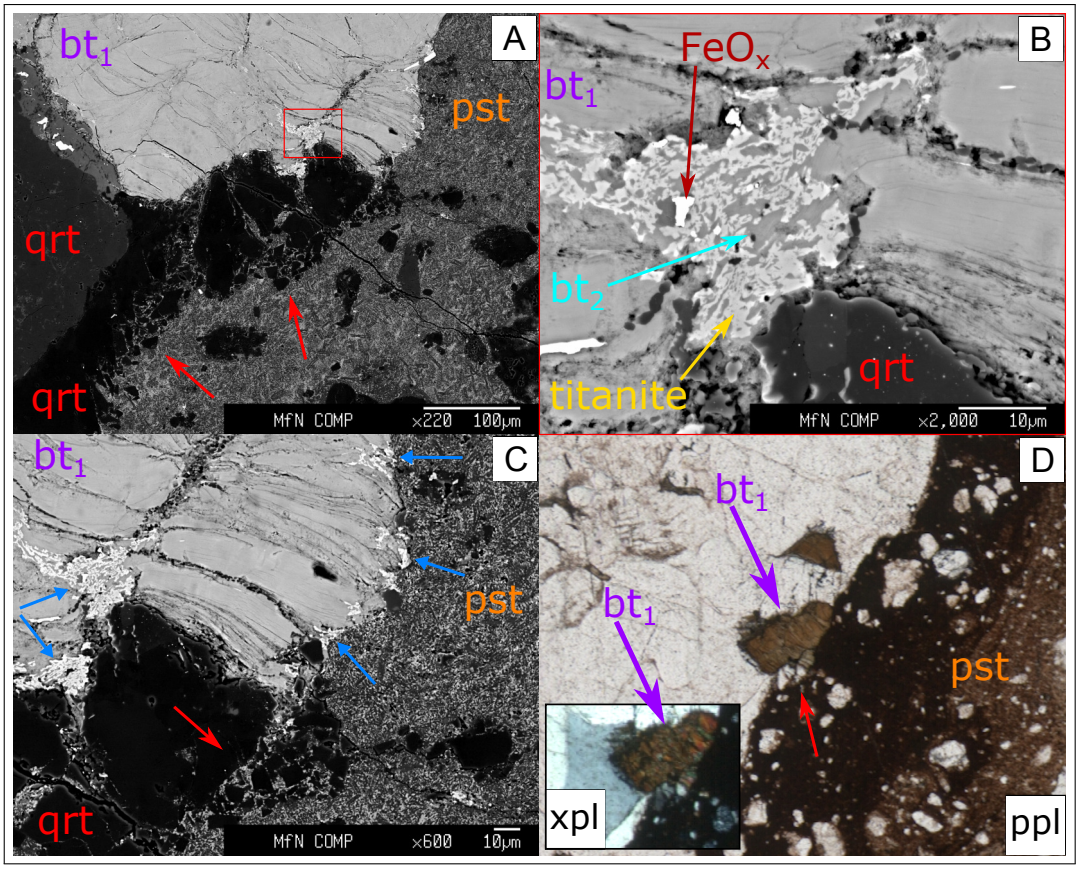

Figure 6.32 – EMPA image of the same area with three different magnifications **A**, **B** and **C** (area of interest indicated by red box in **A**). Bottom right (**D**): overview ppl and xpl images. Pseudotachylyte (pst) in contact with host rock biotite (bt_1) and quartz (qrt). The red arrows point to cataclastic fragments of the quartz. The fragments are still near the host grain. Biotite is replaced by very small (around $1\mu m$) crystallites of iron oxide, a new biotite (bt_2) with different composition, and titanite. Biotite breakdown and replacement (blue arrows) occurs both at the contact to the pseudotachylyte and at a distance to it. The biotite deformation is visible as domains, by wavy lines on EMPA images, variable pleochromism in plane polarised light and non-uniform appearance in crossed polarised light. First three images taken at the Museum für Naturkunde in Berlin, thanks to the support of Prof. W. U. Reimold and his staff.

6.6.3 Mingling Structures

Figure 6.33 **A** shows the same area of a thin section scan as in **B** but with the exposure changed to reveal pseudotachylyte internal structures. The optically very dark, even opaque appearing pseudotachylyte in **B** shows a wide variability in colour in **A**. Chaotic schlieren or flow structures are visible. The lighter phase is thought to have formed by disaggregation of transparent minerals, whereas the darker phase is thought to originate from the mafic mineral content of the host rock. The implications of this interpretation is discussed further in Section 8.2.3.

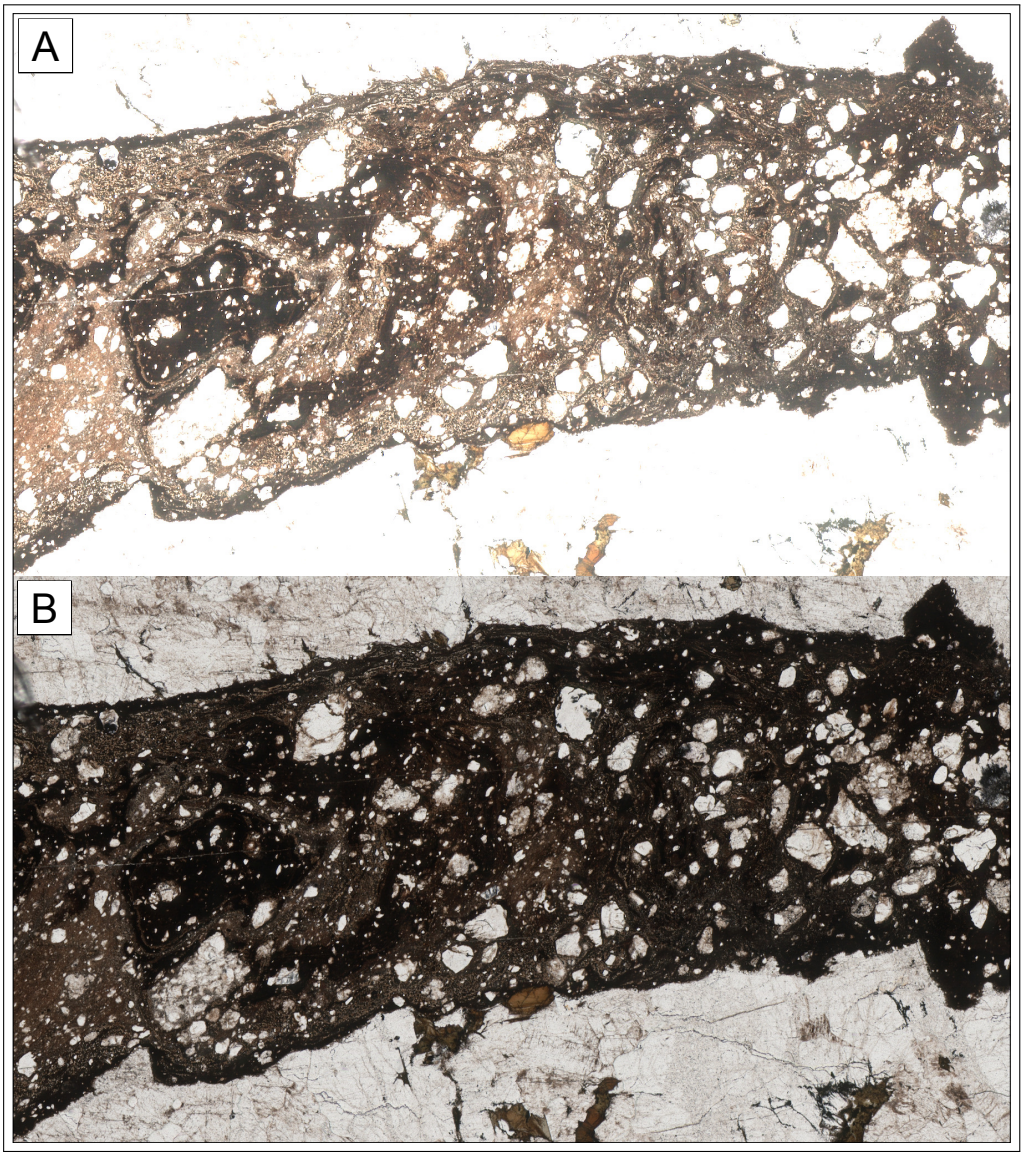

Figure 6.33 – Scan of a thin section of a pseudotachylyte vein at two different exposures in ppl. **A** reveals mingling structures which are barely noticeable in **B**. Part of Figure 6.8 on page 116.

6.6.4 Synthesis and Deformation Sequence

The observations presented suggest the following sequence of events in the formation of the Barra pseudotachylytes. The initial stage of pseudotachylyte formation occured by in situ deformation of the rock (in zones, potentially originated at points), producing a (granular) fluid. Two separate processes seem to have acted to transform differnt mineral types: Mafic minerals were replaced ('melted', but seemingly not by simple contact melting), Figure 6.30; felsic minerals disaggregated along preexisting grain boundaries and formed micro fragments through fracturing, Figures 6.28 and 6.31. This effectively forms a mafic liquid with felsic particles (some of which may be extremely small) - a granular fluid. It is possible that some of these felsic particles are transformed to and incorporated in a genuine liquid through contact melting, friction and/or attenuation. This has not been observed in this study, and would require TEM-scale observations of an unaltered sample. It is possible that no pseudotachylte would form in the absence of mafic minerals, and the veinlets would have been filled entirely with felsic derived cataclasite and potentially silica gel.

The difference in deformation mechanism of the protolith minerals resulted in a strongly localised manifestation of the fluid matrix, ranging from end member quartz fragments (transparent, cataclasite) in felsic rich areas of the samples to end member breakdown and replacement of mafic minerals such as biotite (opaque, 'melt'). Patches of transformed minerals link to form the throughgoing veinlets (Figure 6.28). Linkage of transformed minerals would have been promoted by the varying mechanical properties of the mineral phases acting to concentrate stress, the likely volume increase in the mafic mineral transformation, as well as the 'far-field stress', leading to veinlets with consistent geometries.

Continued deformation of the rock and fluid matrix led to mingling of the locally produced fluids, resulting in optically and/or geochemically visible flow structures, comminution of fragments (both through disaggregation and fracturing), potential fragment alignment, and mixing. With further deformation, the fluid matrix became more homogeneous, fragments were more (homogeneously) spaced, which may result in a lack of mingling structures due to mixing, and subsequently smaller (pseudo-) crystallites in the matrix once crystallised. At the same time, the initial processes continued to be initiated, which is evident by coexisting cataclasite (angular fragments). This may have led to the observed cross cutting relationships and mingling of newer and older fluid. The granular fluid was likely to be supercooled and crystallisation hindered mainly by continued motion. The absence of unequivocal shear displacement indicators suggests a deformation process with insignificant finite shear. Some of these observations and interpretations leading to the hypothesis of this deformation sequence are discussed in the context of the literature and in more depth in Section 8.2.3.

6.7 Estimate of the Amount of Pseudotachylyte *Matrix* versus Pseudotachylyte *Sensu Stricto*

In the previous Chapter 5 which was concerned with the meso scale, the amount of pseudotachylyte *sensu stricto* was calculated. On the micro scale, a further distinction to pseudotachylyte *matrix* can be made by taking into account the amount of micro fragments (Figure 6.34). The proportion of pseudotachylyte matrix was estimated from a pseudotachylyte vein which appeared clast-free in hand specimen. Semi-automated image analysis was performed on a single thin section scan.

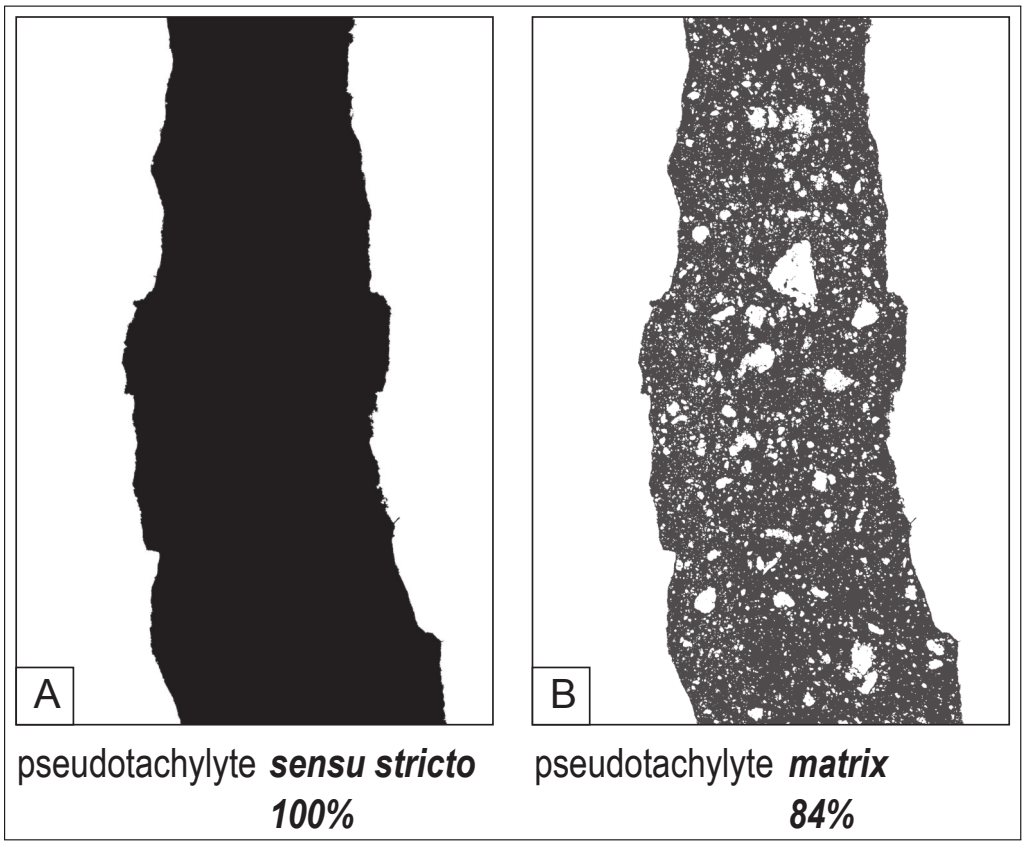

Figure 6.34 – Illustration of the difference between (**A**) pseudotachylyte sensu stricto in black and (**B**) pseudotachylyte matrix in dark grey. The two binary images are based on a thin section scan. The width of the pseudotachylyte vein is approximately 1 centimetre at its narrow (top) end. Host rock and micro fragments are represented in white. Procedure and calculation explained in the text.

6.7.1 Procedure and Result

The thin section was scanned in plain polarized light (Figure 6.35 **A**) and the image contrast optimised to facilitate differentiation between pseudotachylyte and

host rock and fragments. The result was converted into a grey scale image and thresholded to create a binary (black and white) image (**B**). The interface between the host rock and the pseudotachylyte was manually refined where mafic (dark) minerals that are part of the host rock were in contact with the pseudotachylyte. The host rock on either side was then masked with white (**C**) to have in black the pseudotachylyte matrix. The extent of pseudotachylyte *sensu stricto* is obtained by masking the white host rock on either side and filling the pseudotachylyte with black (**D**). For this rough estimate, no manual refinement was performed inside the pseudotachylyte vein. If the number of black pixels in **D** (pseudotachylyte *sensu stricto*) equals 100% then number of black pixels in **C** results in 84% of pseudotachylyte matrix and 16% fragments (Figure 6.34). The results of the pseudotachylyte calculations and estimate on the different scales which are presented in this Chapter and the previous two are combined and discussed in Section 8.1.

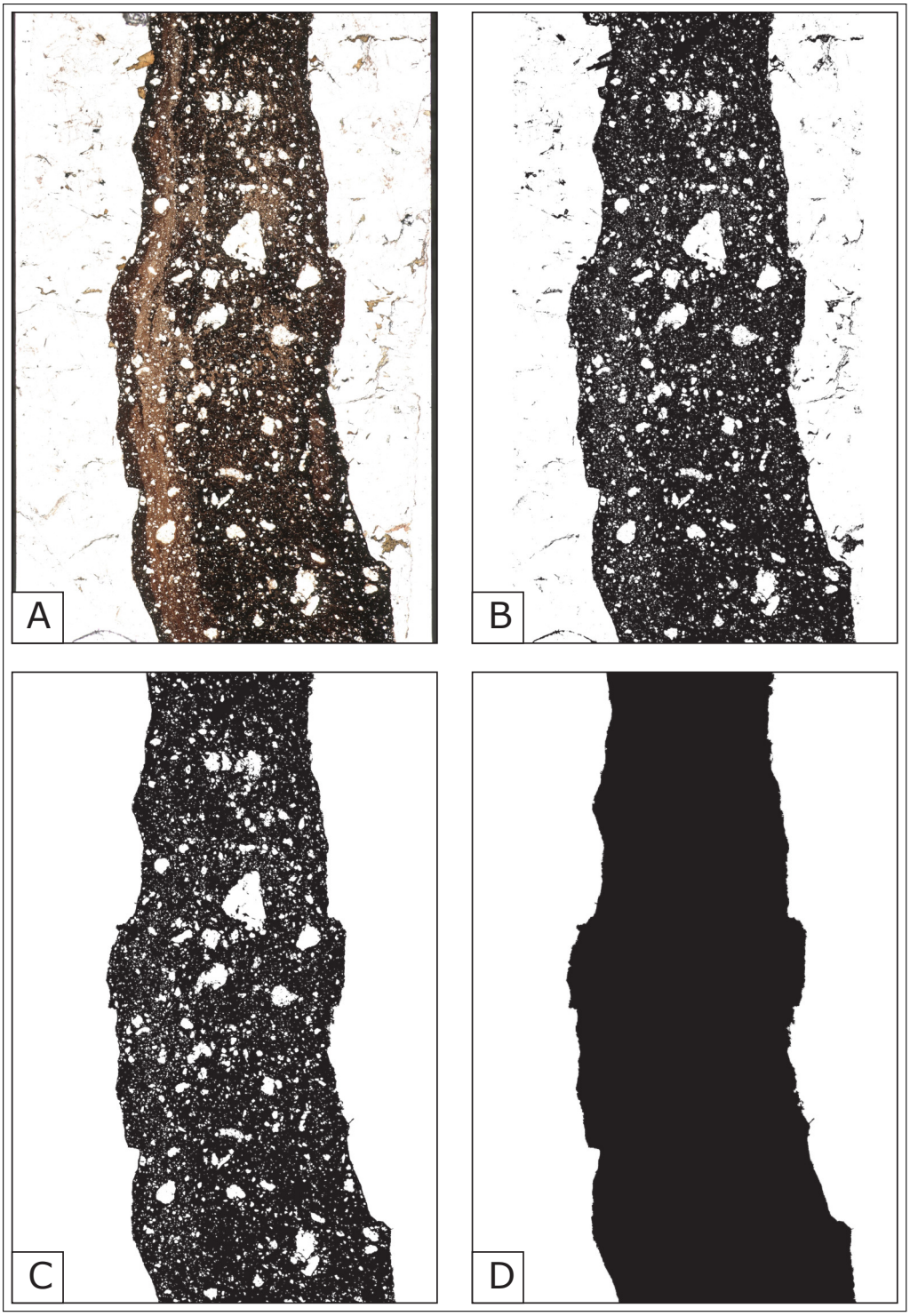

Figure 6.35 – Image processing procedure leading to the binary images showing in black the pseudotachylyte *matrix* (**C**) and pseudotachylyte *sensu stricto* (**D**). See text for explanation.

Chapter 7

Isotope Geochemistry

7.1 Introduction

It is generally assumed that pseudotachylytes form in "dry" crust and under "dry" conditions (e.g. Wenk, 1978, and references therein, but the review paper by *cf.* Sibson, 2003, and references therein) included papers that suggested pseudotachylytes may also form in water-rich rock (Sibson 2003 and refer therein). The question whether there was any fluid present or not during pseudotachylyte formation is relevant for stress calculations, and also because deformation mechanisms are influenced by the presence of fluids (e.g. Moecher and Sharp, 2004). Measurement of readily soluble isotopes, especially of hydrous elements, can provide a direct proof for this assumption. Loss of argon, a volatile element, has been recorded for pseudotachylytes (Reimold et al., 1990; Thompson et al., 1998) and Sherlock et al. (2009), even though the latter interpret their results in a different way (see discussion in Chapter 8).

A question that arose in the field is the role of the presence of Minor Intrusives (BGS, 1981). They account for a considerable percentage of the mapped area on Àird Ghrèin (Chapter 4). Isotope geochemistry is able to show whether there is evidence for a relationship between these dykes and the pseudotachylytes, and whether any fluids associated with the dyke intrusions would have used the pseudotachylytes as pathways. The data have been collected and interpreted to inform whether or not the pseudotachylytes have formed in a system closed to fluids. The data have not been collected for age dating.

Isotope data for the pseudotachylytes, gneiss and the dykes, may be used and interpreted beyond this study, for example in terms of geochronology, metamorphic history, provenance studies, and crustal contamination of the intrusives. The Rb–Sr system was chosen because it is sensitive to metamorphic effects already

of a few hundred degrees, especially when fluids are present. Sr–Nd data are used for mixing models of crustal contamination of mantle rocks. Meyer et al. (2009) published a detailed trace element and isotope study from igneous rocks and Lewisian Gneiss on Rum. The igneous rocks of Rum are geometrically related to the analysed dykes of the BPIP (British Paleogene Igneous Province) on Barra and are thought to have intruded contemporaneously.

To the author's knowledge, this is the first study of the Sm–Nd and Rb–Sr isotope systems applied on pseudotachylytes of the Outer Hebrides. Studies from other regions have used Rb–Sr to attempt dating a pseudotachylyte formation event (e.g. Magloughlin, 2003).

7.2 Radiogenic Isotope Systems

Radiogenic (parent) isotopes decay with a specific half life into another isotope (the daughter). Certain radiogenic isotopes have got a half life which is suitable to date rocks, or to distinguish a source or mixing relationships of rocks. This is especially the case if the daughter isotope is stable. The use of this techinque has been helped by the advance of technology, especially precise measurements of very small fractions of elements.

7.2.1 Basic Assumptions

Three assumptions are inherent to isotopic age dating methods: (1) The isotopic evolution of the source is known, (2) the emplacement of the samples took place in a short time and during one single event, and (3) the parent / daugther ratio, and the occurence of their reference isotopes, was not modified by subsequent events.

7.2.2 Rb–Sr and Sm-Nd Systems

The two systems Rb–Sr and Sm–Nd were used because the elements Rb and Sm occur as trace elements in a wide variety of silicate rocks (Potts, 1987). These two systems allow interpretation in terms of absolute age dating, mixing relationships of rocks, and how closely related the analysed rock is with a reference such as depleted mantle. Rb, Sm and Nd are incompatible elements, which means that they prefer to reside in partial melts or in late liquids resulting from progressive fractional crystallisation (Winter, 2010).

7.2.3 Model Ages and Geochemical Signature

Model ages are not to be confused with rock formation ages. Applying age models means that an initial composition of a magma source of the respective model is

assumed.

A commonly used model is called the CHUR bulk Earth which stands for *Chondrite uniform reservoir*. The CHUR bulk Earth is an estimate of the average chondrite (isotope) composition by DePaolo and Wasserburg, 1976 (Winter, 2010). Chondritic meteorites are thought to represent undifferentiated material of the solar system, representing a composition before planets formed.

The *Depleted Mantle model* seems to be more accurate espercially for rocks younger than Archean age (Winter, 2010). It assumes a composition of the residue that remains after a basaltic melt has been removed from a peridotite.

Model ages based on Neodymium radiogenic isotope data may correspond to a specific crust formation age. The ages correspond only if (A) the Nd ratio (often expressed as ε_{Nd}, see Section 7.2.5 below) of the sample was at some point the same as the depleted mantle (model composition), which is presumed to be their source; and (B) the sample did not experience contamination during differentiation from the depleted mantle.

In most cases, the model ages represent a mixing of material which differentiated from the mantle at different times (Arndt and Goldstein, 1987). This is the case for the Lewisian Gneiss, which is rather heterogeneous in terms of origin, age and composition of protoliths (Whitehouse, 1989).

The model ages are used as a representation of the data to illustrate the relationship, or lack thereof, of the analysed samples. These results are not claimed to constitute actual ages.

7.2.4 Sm – Nd

^{147}Sm decays to ^{143}Nd with a decay constant of $\lambda_{\mathrm{Sm}} = 6.54 \times 10^{-12}$ a^{-1}. This corresponds to a half life of $t_{1/2} = 106 \times 10^{9}$ a (Potts, 1987). The long half life makes this system employable for an age range of 60 Ma and older. ^{144}Nd is the stable isotope, which is not involved in the decay process and is therefore used as reference. Sm and Nd occur in silicate minerals and the method is used for whole rock analyses (Potts, 1987).

7.2.5 $\varepsilon_{\mathrm{Nd}}$ Values

The differences in isotopre ratios for Nd are small. Therefore the term $\varepsilon_{\mathrm{Nd}}$ has been introduced to express the degree of Nd enrichment. $\varepsilon_{\mathrm{Nd}}$ is defined as

$$\varepsilon_{\mathrm{Nd}}(t) = \left[\frac{(^{143}\mathrm{Nd}/^{144}\mathrm{Nd})_{sample(t)}}{(^{143}\mathrm{Nd}/^{144}\mathrm{Nd})_{CHUR(t)}} - 1\right] \times 10\,000$$

where:

t = time,

and the CHUR bulk Earth $^{143}\mathrm{Nd}/^{144}\mathrm{Nd} = 0.0512628 - 0.1967 \cdot (e^{\lambda t} - 1)$.

A positive $\varepsilon_{\mathrm{Nd}}$ for a rock implies that it was derived from a depleted mantle source, and negative $\varepsilon_{\mathrm{Nd}}$ indicates that the rock was derived from a crustal source, once the values have been corrected for time.

7.2.6 Rb – Sr

^{87}Rb decays to ^{87}Sr by β-decay. The stable reference isotope is ^{86}Sr. The half life of ^{87}Rb is $t_{1/2} = 48.8 \times 10^9$ a (Potts, 1987). The Rb–Sr system is applicable for a wide range of samples because the elements are abundant, in REE terms speaking. The Rb and Sr elements are sensitive to metamorphic effects, already starting at a few hundred degrees Celcius (Potts, 1987). Compared to Sm and Nd, Rb and Sr are more mobile because they are readily soluble in hydrous solutions (Okrusch and Matthes, 2005).

Rb substitutes for K in some important rock forming minerals such as potassium feldspar, muscovite and biotite, in the order of tens of ppm. In granitoid rocks, Sr normally occurs in the range of several hundred ppm, and substitutes for Ca.

7.3 Method

The samples were prepared and analysed at the Scottish Universities Environmental Research Centre (SUERC), East Kilbride, Scotland. For measurements and ion separation from whole-rock powders, the standard method was followed, modified after Potts (1987).

7.3.1 Sample Preparation

Whole rock samples were ground using a steel mill (the pseudotachylyte was harder than the agate mill). Approximately 300 mg of rock powder was digested in a sequence of HF – HNO_3 – HCl solutions. Element concentrations were determined by isotope dilution using an enriched tracer (spike) prior to ion separation. The spikes were ^{149}Sm and ^{145}Nd, ^{84}Sr, and ^{87}Rb, respectively. Ion exchange columns were used for ion separation.

7.3.2 Analyses

The isotope ratios were measured in the thermal ionization mass spectrometer (TIMS). The samples are loaded as a solution onto a tantalum filament and heated under vacuum. By applying a potential to the filament the ions are extracted into the mass spectrometer.

7.3.3 Data Processing

For the data processing, two excel spreadsheets were used: Sm–NdV4.01.xls and Rb–SrV4.02.xls, both written by Rob Ellam (Ellam, 1998a,b). The input consists of the sample weights and the TIMS measurements, and the output comprises isotope ratios, their standard errors, ε-values, and model ages.

7.4 Samples

7.4.1 Sample Localities

Samples were collected in the Greian Head area on Barra. Figure 7.1 shows a map with the localities of the samples.

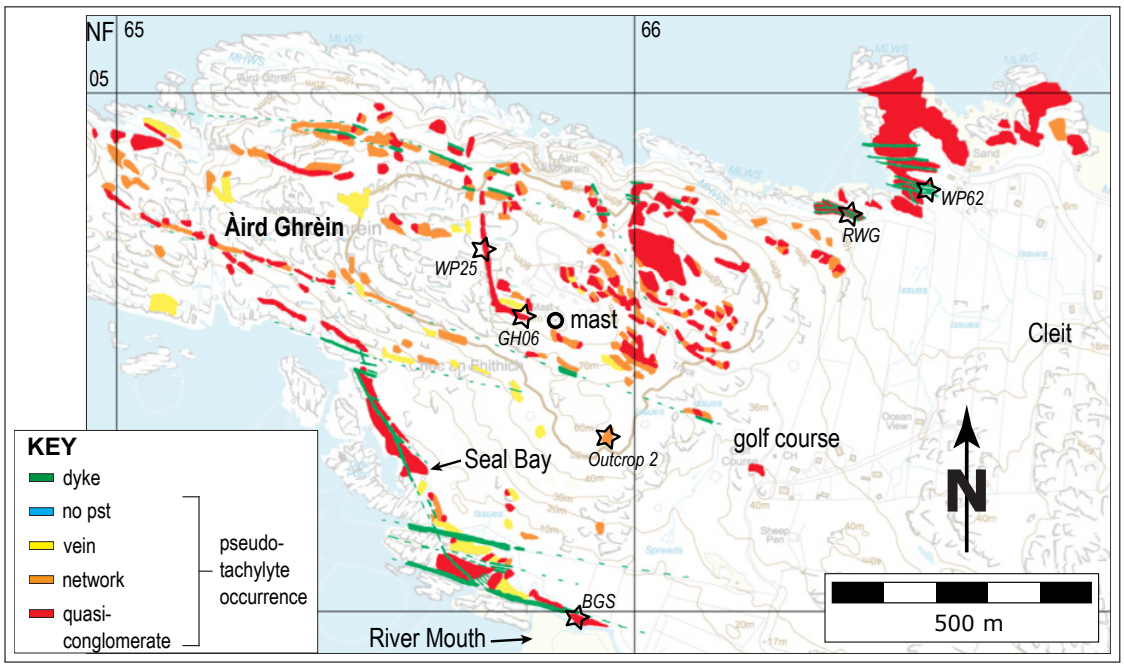

Figure 7.1 – Map of Greian Head showing sample localities for isotope analyses.

7.4.2 Sample Description

Twelve samples were analysed in total, consisting of five samples from dykes, five from pseudotachylyte matrix and two gneiss samples (one small clast, and one large clast). The pseudotachylyte samples consist of pseudotachylyte matrix only, with no lithic clasts, however small clasts of up to 1 mm grain size may have been present. Figure 7.2 shows photographs of the samples used for isotope analyses. Analyses were carried out on the bulk rock. Table 7.1 gives an overview of the samples and their origin.

Note that several samples originated from the same handspecimens: H071 and H072 are from the same hand specimen RWG02, and H074 and H075 are both from handspecimen WP62. H078 is a dyke chilled margin attached to a pseudotachylyte (H073 and H077) containing clasts (H079), all from handspecimen RWG10 (see Figure 7.2).

Sample	*Rock Sample*	*Description*
H071	RWG 02-2 A	dyke (width 20 cm)
H072	RWG 02-2 B	dyke (width 20 cm)
H074	WP62-03 A	dyke centre (width 2.5 m)
H075	WP62-03 B	dyke centre (width 2.5 m)
H078	RWG 10 C	dyke margin
H073	RWG 10 B	three bits of pst matrix in qc, a few cm from a dyke wall
H077	RWG 10 A2	pst in qc, a few cm from a dyke wall
H080	WP62-04	pst matrix directly at a dyke wall
H081	BGS 01	pst matrix in bits from a qc
H082	BGS 02 D	pst matrix in bits from a qc
H079	RWG 10 D	small clast of gneiss in qc, directly at a dyke wall
H083	GH 06 A	large clast of gneiss

Table 7.1 – The isotope samples and their corresponding rock sample labels, their description and origin. Samples are grouped in dykes, pseudotachylytes and gneiss, respectively. *pst* = pseudotachylyte; *qc* = quasi-conglomerate.

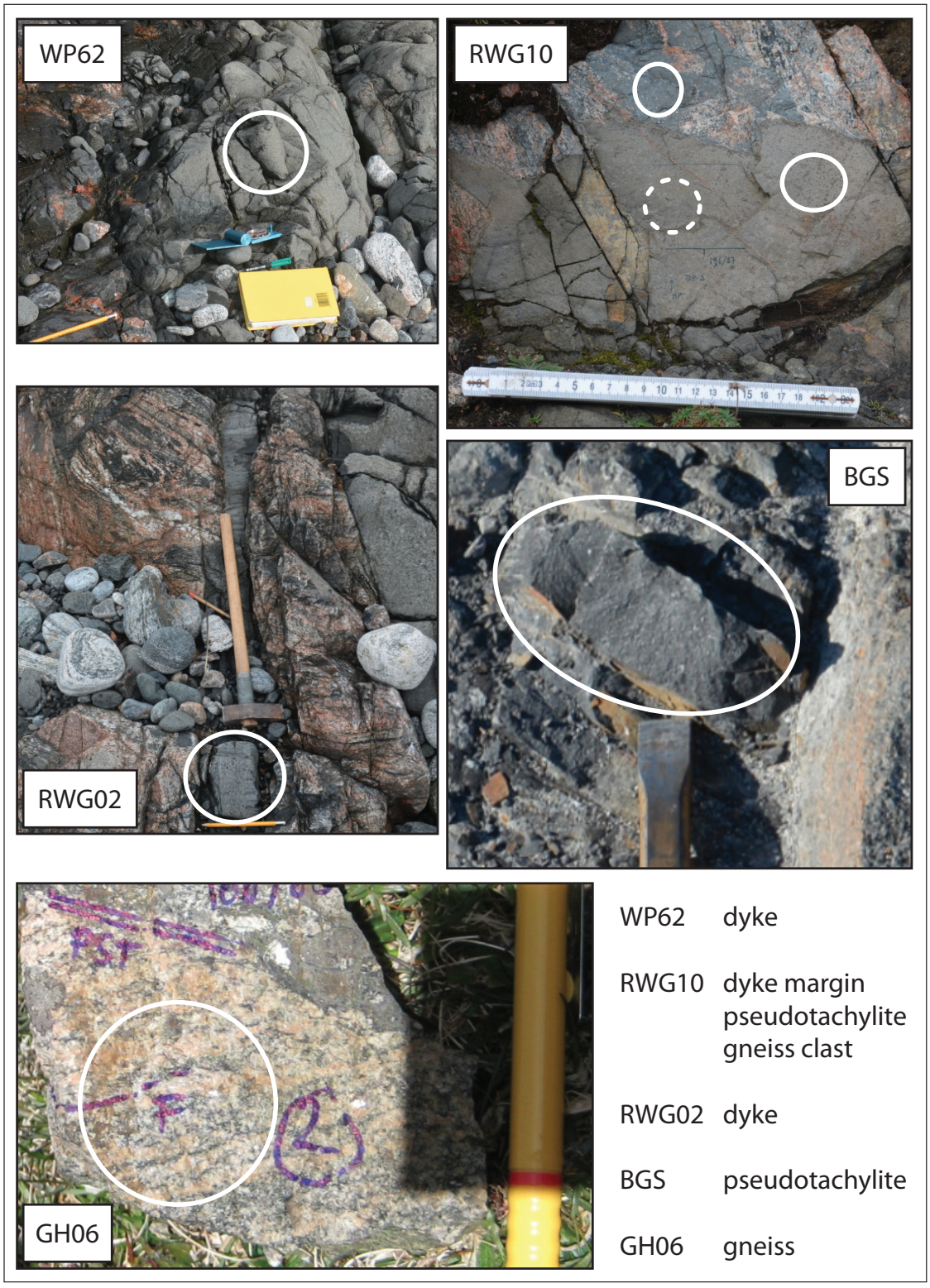

Figure 7.2 – Photographs of samples used for geochemical analyses.

7.5 Results

The results of the isotope measurements (ratios) are displayed in Table 7.2 on page 162.

7.5.1 Sm–Nd Isochron for Gneiss and Pseudotachylytes

Figure 7.3 shows the isochron for the Sm-Nd measurements of the gneiss and pseudotachylyte samples. The R^2-value of the linear best fit function to the data for both rock types is close to 1 which suggests that the Sm and Nd ratios stems from a single population. This means the gneiss and pseudotachylyte are indistinguishable with regards to their Sm-Nd values. This means that the system in both rock types remained closed to Sm and Nd since their formation.

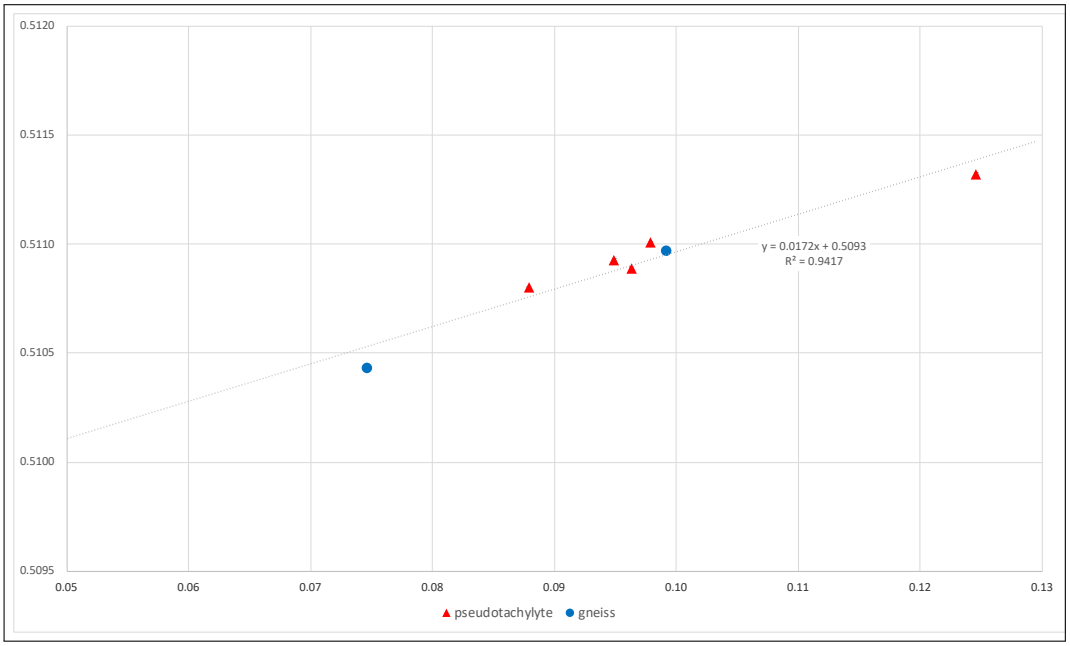

Figure 7.3 – Sm–Nd data and linear best fit for the pseudotachylyte and gneiss samples. The error horizontal error bars are smaller than the symbols. The age calculated with the linear best fit function yields an age of 2.62 Ga for the pseudotachylytes and gneiss samples combined (Winter, 2010).

7.5.2 Model Ages

Figure 7.4 shows the model ages which were calculated using the Depleted Mantle model. From this diagram, the samples can clearly be divided into two groups: (A) the younger dyke samples and (B) in the green band the pseudotachylyte matrix and the gneiss samples. The 60 Ma reference is the approximate age of the British Paleogene Igneous Province (BPIP). The magmatism on Rum and

other areas of magmatism in the vicinity (i.e. NW Scotland) are considered to be part of the BPIP.

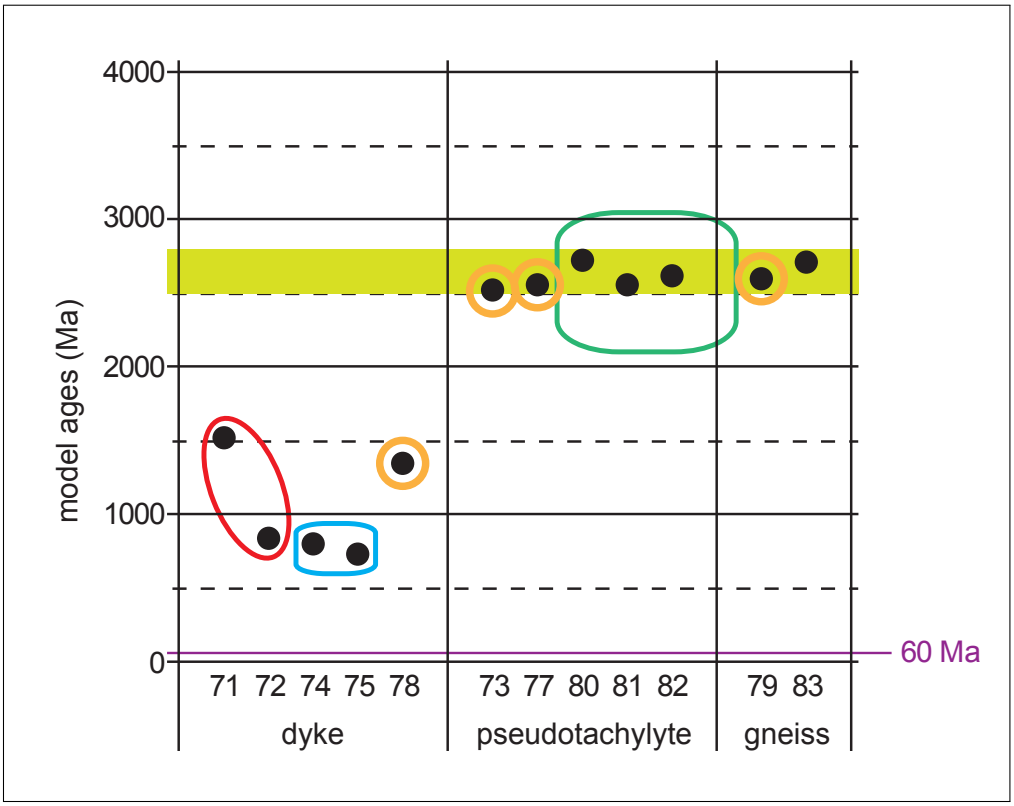

Figure 7.4 – Depleted Mantle model ages for the samples analysed. Data points in the same coloured circle derive from the same hand specimen. The age band between 2.5 and 2.8 Ga is the expected age of the Lewisian Gneisses (e.g. Wheeler et al., 2010). The 60 Ma reference line corresponds approximately to the magmatism of the British Paleogene Igneous Province (BPIP). Standard errors are smaller than the symbols.

7.5.3 ε_{Nd} Values

In figures 7.6 and 7.5, the ε_{Nd} values for the gneiss and pseudotachylyte samples, and the dyke samples, respectively, are plotted against their model ages.

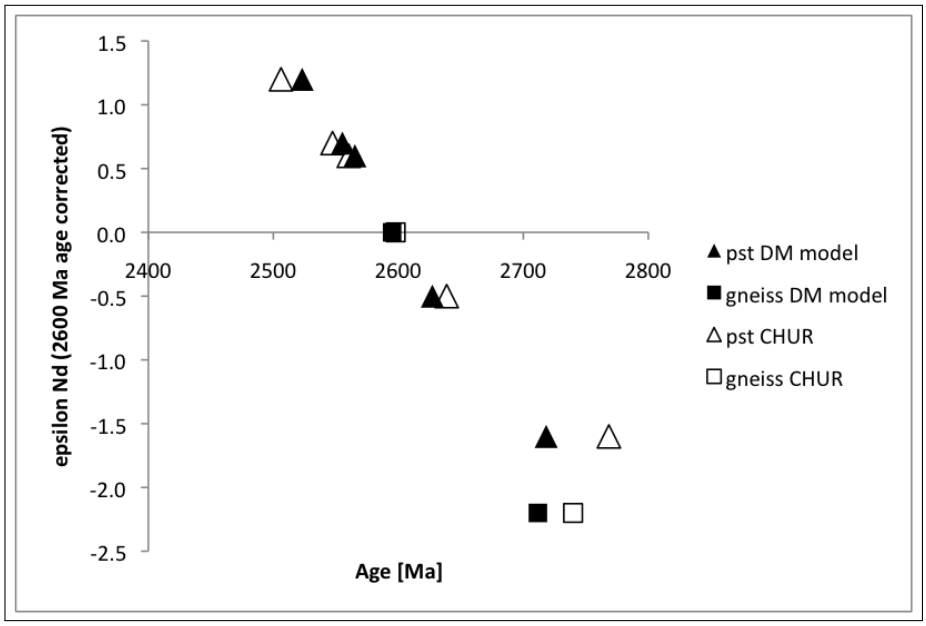

Figure 7.5 – ε_{Nd} values corrected for 2.6 Ga of pseudotachylyte samples (triangles) and gneiss samples (squares). The model ages are calculated using the depleted mantle (DM) model, solid symbols, and the CHUR bulk Earth, open symbols. Error bar are smaller than symbols.

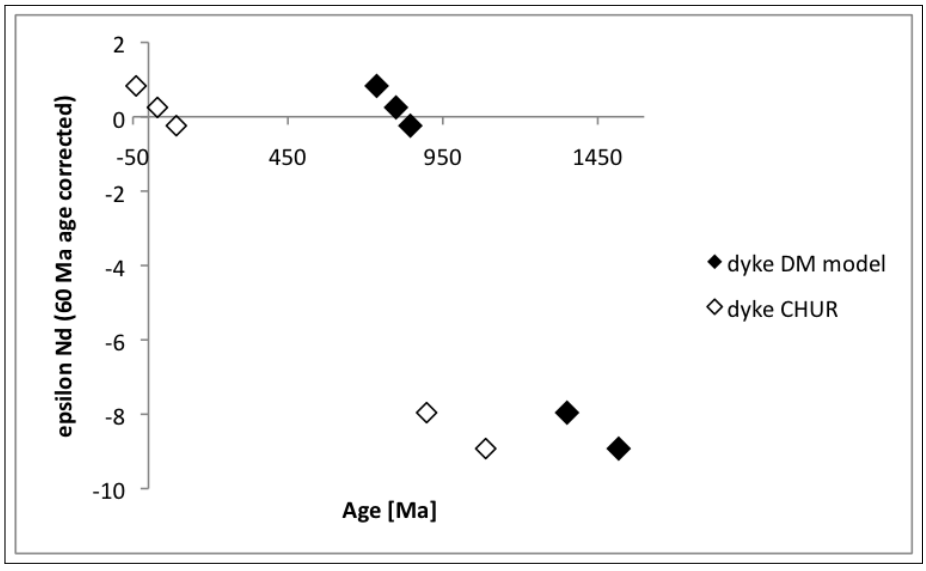

Figure 7.6 – ε_{Nd} values corrected for 60 Ma of dyke samples. The model ages are calculated using the depleted mantle (DM) model, solid symbols, and the CHUR bulk Earth, open symbols. Error bar are smaller than symbols.

Sample	$^{85}Rb/^{87}Rb$	1σ Error	$^{87}Sr/^{86}Sr$	1σ Error	$^{143}Nd/^{144}Nd$	1σ Error	$^{149}Sm/^{147}Sm$	1σ Error	
H071	0.1771214	0.000005	0.706558033	0.000011	0.512154	0.0000037	3.626851	0.0006	
H072	0.2422774	0.000007	0.706564708	0.000013	0.512601	0.0000037	2.606696	0.0004	
H074	0.2743034	0.000051	0.706213869	0.000013	0.512626	0.0000037	3.304803	0.0002	dyke
H075	0.2907898	0.000007	0.706029824	0.000013	0.512655	0.0000079	3.63629	0.0003	
H078	0.0909924	0.000005	0.707886771	0.000013	0.512201	0.0000042	2.746657	0.0001	
H073	0.8302794	0.000040	0.723723322	0.000014	0.511006	0.0000037	5.414272	0.0002	
H077	0.5994756	0.000007	0.722267833	0.000012	0.510928	0.0000057	4.490964	0.0002	
H080	0.5096991	0.000086	0.724537384	0.000021	0.511321	0.0000042	4.190758	0.0001	pseudtachylyte
H081	1.1319641	0.000074	0.730730654	0.000015	0.510800	0.0000042	3.271909	0.0001	
H082	n/a	n/a	0.733376*	0.000013	0.510890	0.0000042	6.918968	0.0001	
H079	0.7745589	0.000182	0.715857523	0.000014	0.510968	0.0000042	14.03031	0.0006	
H083	n/a	n/a	0.744350*	0.000013	0.510431	0.0000036	5.181398	0.0002	gneiss

Table 7.2 – Results of the isotope ratio measurements and their standard errors (no age correction applied). 1σ errors correspond to measurements of the analyses only and indicate very high precision of the data.
* The Sr measurements are influenced by Rb and therefore a correction is applied to the original Sr measurements. For samples H082 and H083, Rb measurements are not available and therefore no correction has been applied. For all other samples, the Rb corrected Sr ratio was $\leq 1.8\,\mathrm{E}^{-06}$ higher than the not corrected ratio. This means, most likely, the correction would only affect the last digit of the values given.

7.6 Discussion

For all interpretations the small sample numbers need to be taken into account.

In terms of the Rb, Sr and Nd ratio results, the samples can be divided into 2 distinct groups: group (A) the dykes, and group (B) the pseudotachylyte and gneiss samples. The dyke samples show much less variety than the samples of group (B) (Table 7.2). The model ages for the gneisses and pseudotachylytes are much more consistent than the model ages of the dykes (Figure 7.4).

7.6.1 Pseudotachylyte and Gneiss

The Lewisian gneiss is not a homogeneous rock which means that variations are expected. The variability of the pseudotachylyte data may be explained by heterogeneities of its parent rock.

The pseudotachylyte data and gneiss data are fairly indistinguishable. This suggests that isotope systems remained closed during the formation of the pseudotachylytes and therefore the formation of the pseudotachylytes occurred under dry conditions. The data here supports findings from previous work using different methods (e.g. Campbell, 2016). No melt differentiation took place during the formation of the pseudotachylytes. The pseudotachylyte matrix reflects the composition of the gneiss and not a partial melt thereof.

The model age is the age at which the system closed. It may be the formation age or the age of metamorphism. The gneiss and the pseudotachylytes fall into a model age range of between 2.52 and 2.72 Ga, with a combined Sm–Nd isochron age of 2.62 Ga (Figure 7.3), which is a possible age range for Lewisian Gneiss (e.g. compilation in Kinny et al., 2005). Given the small number of (Gneiss) samples and the intention of these analyses, further interpretation of this data is outwith the scope of this study.

7.6.2 Dykes

The dykes do not show a single model age and vary between 736 Ma and 1517 Ma. Even the results of samples 71 and 72, which originate from the same handspecimen, differ by 672 Ma. The samples are bulk rock analyses and are likely to contain clasts originating from the host rock. Thus the variation can be explained by crustal contamination of the magma during emplacement. Petrographic and structural interpretation of thinsections should confirm that. Clast formation by dykes was observed in the field.

Even though the dykes do not give the 60 Ma model age, it is very likely that the dyke intrusions of Barra are related to magmatism of the NAIP (pers. comm. Kathryn Goodenough).

7.6.3 Sr/Nd in the Regional Context

Figure 7.7 shows the data Sr and Nd data of this study from Barra, and data for intrusives and host rock of Meyer et al. (2009) from the Isle of Rum. The isotope ratios of Meyer et al. (2009) are corrected for 60.5 Ma, according to the time of emplacement of the Rum Igneous Centre. The data of this study is corrected for 60 Ma. The 60 Ma age correction applied has not altered the data significantly: uncorrected symbols of the same size would still touch the age corrected symbols. There is no Rb data available for two samples (one pseudotachylyte, one gneiss), their data points are indicated by symbols plus grey arrows. The arrows point into the direction in which the symbols would move if Rb data was available.

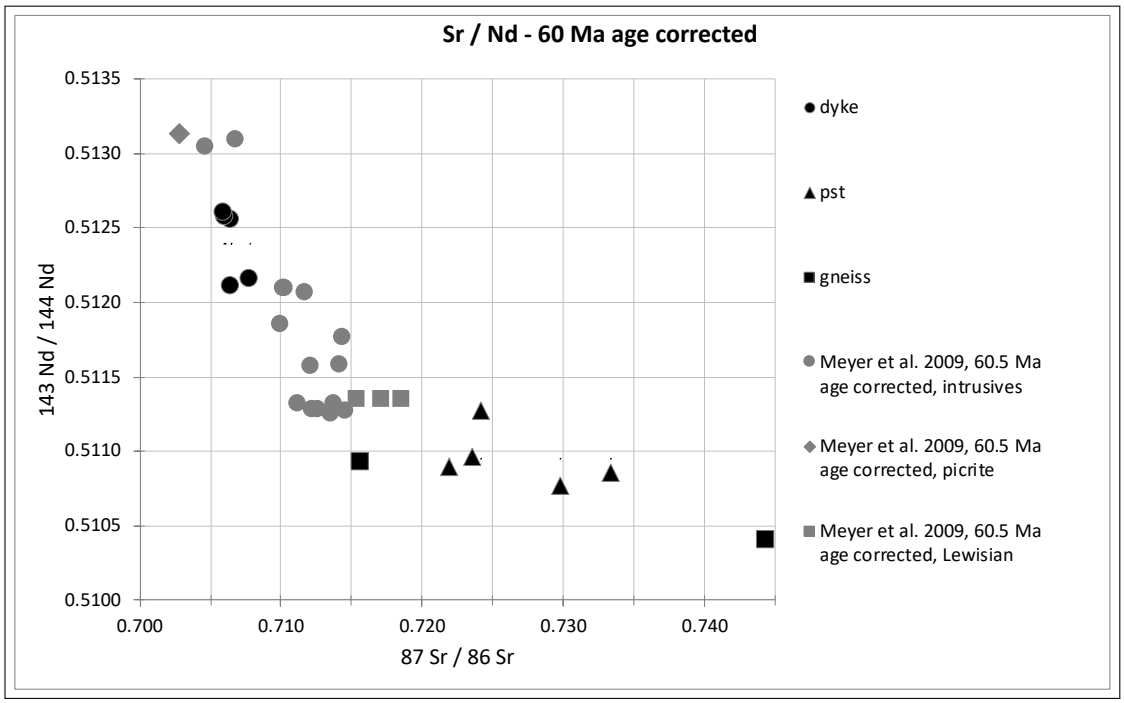

Figure 7.7 – Sr and Nd ratios of Barra (this study) in black, and in grey of Rum (Meyer et al., 2009). The data of this study is corrected for 60 Ma, except for the two samples (missing Rb data) where the possible influence of a correction is indicated by the grey arrows. Standard deviation error bars lie within the symbols.

The Barra intrusives fall on line with Rhum intrusives (circles). For both Barra and Rhum, the Lewisian and gneiss data groups in the lower right of graph. The Rhum (grey) and Barra (black) data are distinct but not far out.

The dyke data from both Barra and Rum (circles) fall around a mixing line (Meyer et al., 2009) between a picrite (diamond data point in the upper far left representing a "pure intrusion") and the Lewisian Gneiss (data points with lower Nd ratios). This suggests that the isotope values of the dykes represent a mixing of mantle magma and Lewisian Gneiss. This means the intrusion of the NAIP dykes was not accompanied by fluids which would likely have altered the isotope signatures away from the mixing line. This means the intrusions took place well below the surface. The data does not point to metasomatism which means there was no connecting network to surface waters and the intrusions were potentially not overlain by an ocean. Because they plot closer to the picrite, the crustal contamination of the Barra dykes should be of lesser extent than the crustal contamination of the intrusives on Rum.

The pseudotachylyte data lies within gneiss data. This indicates a closed system for the formation of the pseudotachylytes. The scatter in the Sr ratio of the gneiss and pseudotachylyte matrix samples is likely to indicate variation in the origin of the gneisses. The Lewisian exhibits great variations in Sr content (e.g. Whitehouse, 1989), given its long and complex history.

Later deformation did not reset the sensitive Rb/Sr system. The system remained closed, and no fluids or metamorphism altered the chemistry.

7.7 Conclusions

The data presented here adds nicely to the regional data pool of scarce isotope data.

The Sm and Nd isotopes were not fractionated during the formation of the pseudotachylyte. In terms of isotope signatures, the pseudotachylytes cannot be distinguished from the gneisses. The results show that the pseudotachylytes have formed in a closed system which is provided by a dry crust. This is common for the formation of pseudotachylytes (e.g. **?** and references therein). The large amount of pseudotachylyte can therefore not be explained by a fluid assisted process.

The model ages for the pseudotachylytes are not inconsistent with the known regional geological history (e.g. MacDonald and Goodenough, 2013).

The method was successful in showing that the pseudotachylyte isotopes remained unaffected by the later dyke intrusions in terms of isotope exchange. The later intrusions have not remobilised the pseudotachylytes. There are two distinct

phases of 'melt' rock formation: (1) the pseudotachylytes, and (2) a much later injection of dykes.

The isotope results of the dykes represent a mixing of the NAIP magma with the host gneiss. No fluid influx and metasomatism took place during the NAIP intrusions. This could mean that this area was potentially not overlain by an ocean.

Chapter 8

Discussion

8.1 How Much Pseudotachylyte is there on Barra?

8.1.1 Rationale

As stated in Chapter 1, Melosh (2005) argued that it is impossible to generate very large volumes of pseudotachylyte from frictional shear heating along faults alone. In the literature, the distinction is therefore commonly made between tectonic, friction-induced 'small' *fault pseudotachylytes* and 'bigger' *off-fault pseudotachylytes* occurring in larger impact structures (e.g. Sibson and Toy, 2006; Reimold, 1995). But of course size is relative: in the context of a fault, a 4 cm-thick pseudotachylyte has been described as "massive" by Rowe et al. (2005). Given that the combination of pseudotachylyte abundance and the 'size' of individual pseudotachylyte bodies cropping out may be one of the ways of discriminating between origins it is important to develop a methodology that will allow researchers to reliably compare volumes (inferred from outcrop area) of this rock type between field sites. In this section the data from the one square kilometre mapped area of Àird Ghrèin presented in Chapters 4, 5 and 6 are used to estimate the amount of pseudotachylyte within the headland, and investigate ways that such estimates can be made robust enough to compare between sites.

8.1.2 Method of Calculations

Outcrops at Àird Ghrèin were categorised into three modes of occurrence of pseudotachylyte (*pseudotachylyte sensu lato (s.l.)*) to create a km-scale map (macro scale, see Chapter 4). A fourth colour was assigned to outcrops without pseudotachylyte; however, this case did not occur in the area mapped on Àird Ghrèin. The area percentage of each unit was calculated in Step 1 (Chapter 4).

> Colour A – red – Quasi-conglomerate occurrence of pseudotachylyte with a minimum area covered of 10 x 40 cm.
>
> Colour B – orange – Pseudotachylyte veins in abundance or fracture networks.
>
> Colour C – yellow – Lewisian Gneiss with thin pseudotachylyte-filled fractures.

Specific outcrops were mapped with grids to quantify the amount of actual pseudotachylyte (*pseudotachylyte sensu stricto (s.s.)*) on the meso (metre) scale, Step 2 in Chapter 5. A micro scale scan of a thin section was used to estimate the amount of fragments in a hand specimen of pseudotachylyte that appeared clast-free to the naked eye (Chapter 6, *pseudotachylyte matrix*). These clearly defined and scale dependent terms (in italics) were introduced for clarity. In the literature, a distinction is commonly not made.

For the mapping of pseudotachylyte occurrence, and in particular the occurrence of quasi-conglomerate, no standardised methodology is available. Previous authors have presented estimates, which are discussed in Section 8.1.5. Here, a new method is presented for using maps from separate outcrops to make estimates of overall pseudotachylte outcrop area that should be transferrable to other field sites and therefore permit more robust comparisons of occurrence from multiple sites.

Combining Macro, Meso and Micro Scales

Step 3 combines the macro scale data and meso scale results. Based on the results from Step 2 (meso scale), each macro scale mapping unit (Step 1: A – red, B – orange and C – yellow) was assigned a respective ratio (a, b or c) of [pseudotachylyte sensu stricto] to [host rock and fragments]. The result is presented as the area (%) of pseudotachylyte sensu stricto for the total of Lewisian gneiss outcrops on Àird Ghrèin (Figure 8.1). The final step integrates the amount of pseudotachylyte that appears aphanitic and clast-free in hand specimen that is actual pseudotachylyte matrix material into the results from Step 3.

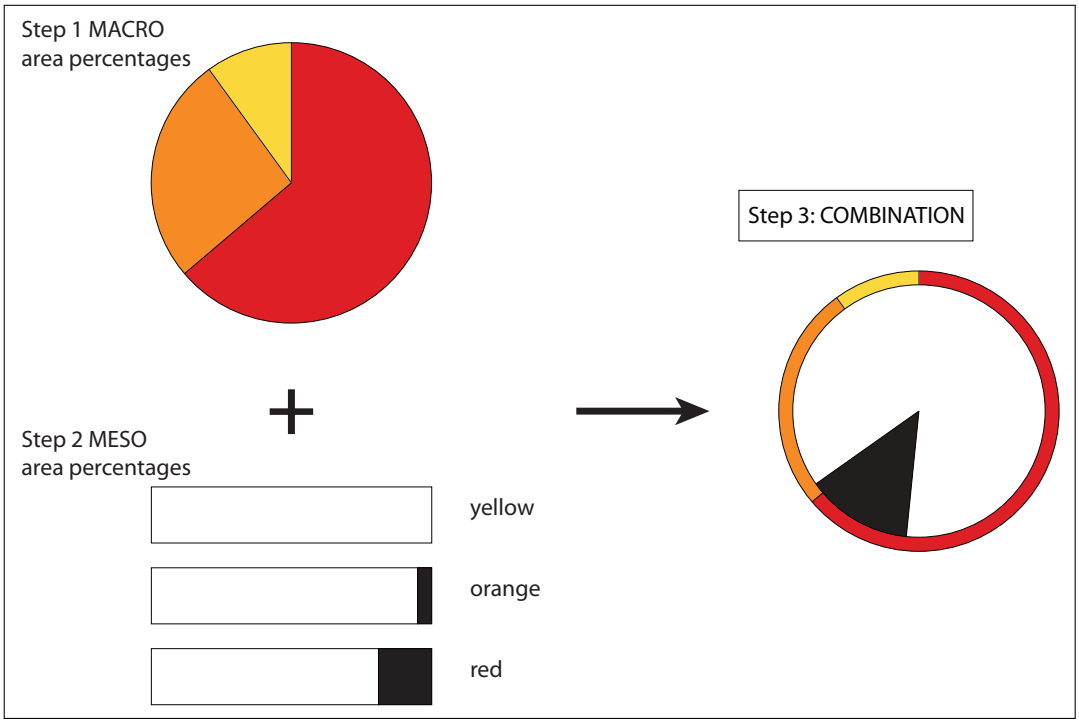

Figure 8.1 – Illustration of Step 3. – The macro area percentages obtained in Step 1 for each of the pseudotachylyte modes of occurrence is represented in the colour coded pie chart (top left). – Below, the column chart shows the ratio of pseudotachylyte sensu stricto (black) to host rock and fragments (white) for each of the pseudotachylyte modes (yellow, orange, red) as obtained in Step 2. – In Step 3, the ratios of Step 2 were applied to the percentages of Step 1. The result is shown in the black and white pie chart. The full circle represents the entirety of Lewisian gneiss outcrops in the macro mapped area. The section in white stands for Lewisian gneiss, both unaffected by pseudotachylyte development, and as host rock and fragments. The section in black represents the outcrop area of pseudotachylyte sensu stricto. The contribution of the quasi-conglomerates (red), and pseudotachylyte networks (orange) towards the pseudotachylyte sensu stricto section is shown by the black section's overlap of the respective colour.

The calculations can be expressed in a number of formulae with scale dependent parameters:

Macro scale, area of **pseudotachylyte s.l.** proportion, fraction of T, with $T = A + B + C + D$ (from macro map, Section 4.6.3):

- T total area of mapped outcrops of Lewisian Gneiss
- A quasi-conglomerate (red)
- B networks (orange)
- C veins (yellow)
- D no pseudotachylyte (blue, was never found to occur in the 1 km^2 mapped area)

Meso scale, area of **pseudotachylyte s.s.** proportion, (black from meso maps, Section 5.7.2):

- a quasi-conglomerate
- b network
- c veins (insignificant volumetric contribution and therefore omitted in calculation[1])

Micro scale, area of **pseudotachylyte matrix** proportion, fraction of (image analysis thin section, Section 6.7.1:

- m matrix in macroscopically clast free pseudotachylyte

The following formulae give the mathematical solution for each step, providing results for pseudotachylyte (PST) *sensu lato* (s.l.), pseudotachylyte *sensu stricto* (s.s.) and pseudotachylyte *matrix* proportions.

Amount of **pseudotachylyte sensu lato**:

$$PST\,s.l. = A + B + C + D \tag{8.1}$$

Amount of **pseudotachylyte sensu stricto**:

$$PST\,s.s. = A * a + B * b \tag{8.2}$$

Amount of **pseudotachylyte matrix**:

$$PST\ matrix = m(A * a + B * b) \tag{8.3}$$

[1]Typical pseudotachylyte veins are in the order of millimetres, and less than 2 cm thick. A 2 cm thick vein with the extent of a whole outcrop (5 m by 5 m) would therefore cover 0.4% of the outcrop area.

8.1.3 Errors and Uncertainties

An error estimate was presented in Chapter 4 (Correction A) to account for mapping of vertical cliffs and other biases towards the mapping of pseudotachylytes (Section 4.6.3). For the method's nested approach an additional error estimate, 'Correction B' has been performed to account for the size of the actual pseudotachylyte s.s. area with respect to the size of a mappable outcrop.

Vertical outcrops

Many pseudotachylyte outcrops are on near-vertical cliffs which are not represented on a map. A topographical map is a two-dimensional projection which systematically under-represents non-horizontal surface areas of the real world, to the extreme of being devoid of vertical surfaces and overhangs (introducing a physical bias, Shipton et al., 2019). The pseudotachylyte occurrences are partly controlled by the gently dipping foliation. Therefore, the best outcrops are on near-vertical sections, which can, conventionally, not be mapped. A practical solution in the field was to map them anyway, pretending that they were horizontal surfaces. This error affects mainly the quasi-conglomerates. If a unit to be mapped were (1) thick enough or orientated to cross-cut contour lines, and (2) its three-dimensional habitus predictable, a cross section could be constructed. However, neither of these prerequisites are not met for the pseudotachylytes at hand. Ideally a surface mapping technique would be used such as lidar scanning or drone photogrammetry, to capture the 3D aspects of he outcrop. However, neither were available during this PhD, thus the current representation was developed. (n.b. Àird Ghrèin is exceptionally windy and even if a drone had been available, it would have taken an expert pilot to capture high quality photographs). The error estimate ('Correction A') is presented in Section 4.6.3, and the results shown below (Section 8.1.4 on 174).

Pseudotachylyte Geometry vs. Mode of Occurrence

The areas mapped in red (quasi-conglomerate *mode of occurrence*) on the macro scale map do not always consist of solely the quasi-conglomerate *geometry* in the outcrop on the meso scale (Figure 8.2). The definition of the quasi-conglomerate mode of occurrence was designed for macro scale mapping: if an outcrop of mappable size (5 x 5 to 10 x 10 metres) contained a patch of at least 10 x 40 centimetres of quasi-conglomerate geometry, it falls under the category of quasi-conglomerate mode of occurrence and is mapped in red. Thus, the extent of the quasi-conglomerate geometry can vary from as little as the above mentioned minimum definition, to the entire outcrop. Because the meso scale maps are representative of the geometry, Correction B is applied to translate between the two scale dependent definitions. Correction B redefines the red signature from quasi-conglomerate mode of occurrence into quasi- conglomerate geometry. Ta-

ble 8.1 shows several estimates of the area percentage of the quasi-conglomerate in a mappable outcrop. Indicated are the values used for B_{min} and B_{max}.

***Correction B**: scale translation factor*		outcrop size		
		5 x 5 metres	10 x 10 metres	
actual quasi-conglomerate size	10 cm x 40 cm	***0.16 %***	0.04 %	$\boldsymbol{B_{min}}$
	50 cm x 5 m	10 %	2.5 %	
	25 cm x 5 m	***5 %***	1.25 %	$\boldsymbol{B_{max}}$
	50 cm x 10 m	20 %	***5 %***	

Table 8.1 – *Selected values for the scale translation factor of Correction B.* – Depending on the size of a mapped outcrop in red (quasi-conglomerate *mode of occurrence*), the area percentage covered by the quasi-conglomerate *geometry* depends on the quasi-conglomerate's actual size. This table shows in area percent, how much of the mapped area is actually quasi-conglomerate *geometry*. The scale translation factor of 5 % is used as a conservative value for Correction B_{max}, whereas the value of 0.16 % serves as a lower limit for Correction B (Correction B_{min}).

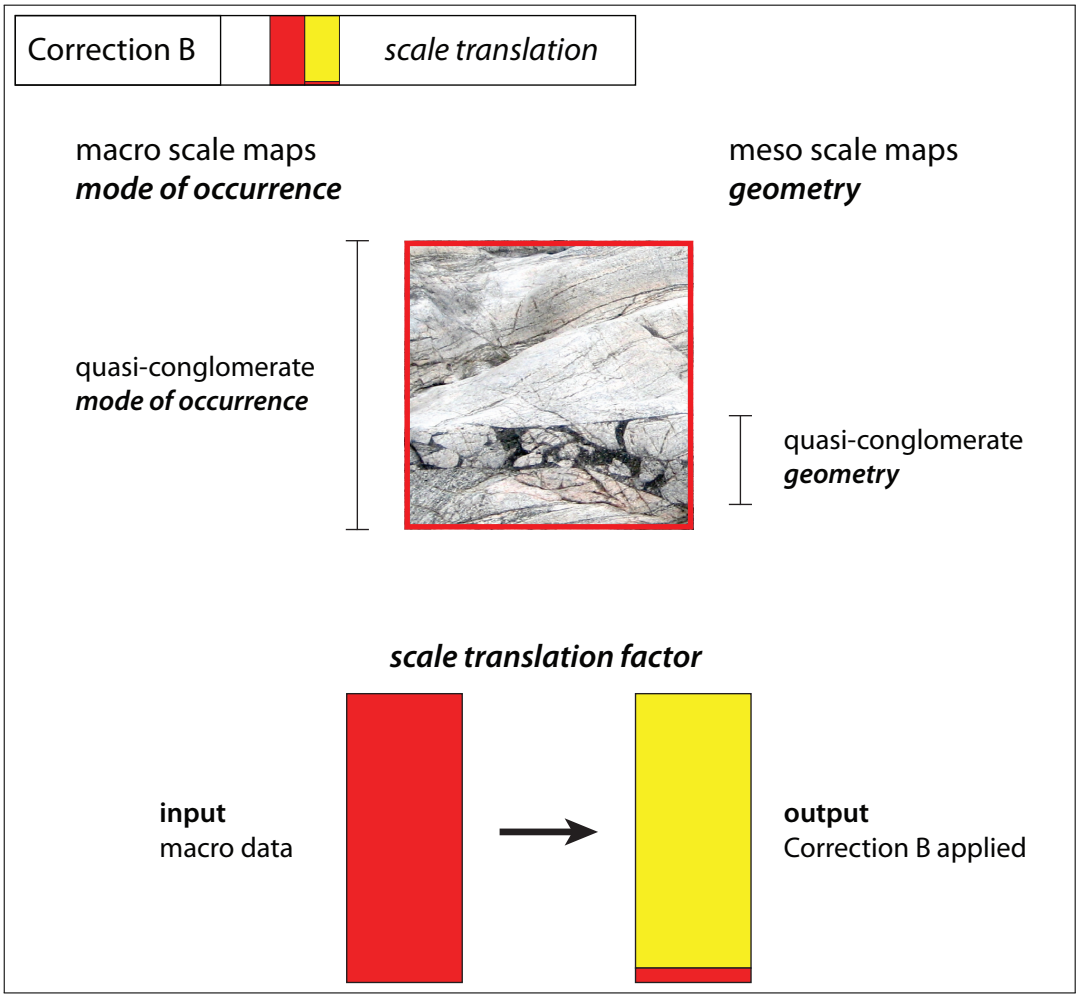

Figure 8.2 – *Illustration of the scale translation problem and Correction B.* – An outcrop mapped in red (macro scale) records that it contains quasi-conglomerate. However, the extent of the quasi-conglomerate might be smaller than the mapped outcrop area, as for example in the image shown. Correction B redefines the red signature (from the macro scale definition of quasi-conglomerate *mode of occurrence*) into the meso scale representation of quasi-conglomerate *geometry*.
Note: the photograph is used for illustration purposes and does not represent a whole outcrop area of 5 x 5 metres.

8.1.4 Results

Macro scale – The maps of the respective scale were used to calculate the pseudotachylyte area for Àird Ghrèin with the following results. Approximately two thirds (64%) of the outcrop area was mapped as quasi-conglomerates, a quarter (26%) was mapped as networks and 10% as single veins. No outcrops were observed without any pseudotachylyte. Taking into account the error estimates for the vertical cliffs (Correction A, Section 4.6.3), 39% of the outcrop area map as quasi-conglomerate, 16% as networks, and 6% as veins.

$$\begin{aligned} \text{Total outcrop area} = \text{A} + \text{B} + \text{C} &= 1 \\ \text{A} &= .64 \\ \text{B} &= .26 \\ \text{C} &= .10 \\ \text{D} &= 0 \end{aligned}$$

$$\begin{aligned} PST\,s.l. &= A + B + C \\ &= 1 \text{ or } 100\% \end{aligned} \quad (8.1)$$

Correction A – Area of pseudotachylyte sensu lato corrected with Correction A, with $|D|_{\mathcal{A}} = |A|_{\mathcal{A}}$:

$$\begin{aligned} \text{Total outcrop area} = 2\text{A} + \text{B} + \text{C} &= 1 \\ A_{\mathcal{A}} &= .39 \\ B_{\mathcal{A}} &= .16 \\ C_{\mathcal{A}} &= .06 \\ D_{\mathcal{A}} &= .39 \end{aligned}$$

$$\begin{aligned} PST\,s.l._{\mathcal{A}} &= A_{\mathcal{A}} + B_{\mathcal{A}} + C_{\mathcal{A}} \\ &= .61 \text{ or } 61\% \end{aligned} \quad (8.1)$$

Meso scale – The network outcrop covering approximately 2 m^2 yields 5% of pseudotachylyte, whereas the quasi-conglomerate outcrop consists of 20% pseudotachylyte in average on mapped areas of 30 x 30 cm (Section 5.7.2). Combining the results from the macro and the meso scale, 14% of the outcrop area is pseudotachylyte sensu stricto.

Meso scale results:

$$a = .20$$
$$b = .05$$

$$\begin{aligned} PST\,s.s. &= A * a + B * b \\ &= .14 \text{ or } 14\% \end{aligned} \quad (8.2)$$

Correction B – Area of pseudotachylyte sensu stricto:

Correction B factors:

$$\mathcal{B}_{min} = 0.0016$$
$$\mathcal{B}_{max} = 0.05$$

$$\begin{aligned} PST\,s.s.\ (\mathcal{B}_{min}) &= A * \mathcal{B}_{min} * a + B * b \\ &= 0.013 \text{ or } 1.3\% \end{aligned} \quad (8.2)$$

$$\begin{aligned} PST\,s.s.\ (\mathcal{B}_{max}) &= A * \mathcal{B}_{max} * a + B * b \\ &= 0.019 \text{ or } 1.9\% \end{aligned} \quad (8.2)$$

Corrections A and B – Area of pseudotachylyte sensu stricto:

$$\begin{aligned} PST\,s.s._{\mathcal{A}}\ (\mathcal{B}_{min}) &= A_{\mathcal{A}} * \mathcal{B}_{min} * a + B_{\mathcal{A}} * b \\ &= 0.008 \text{ or } 0.8\% \end{aligned} \quad (8.2)$$

$$\begin{aligned} PST\,s.s._{\mathcal{A}}\ (\mathcal{B}_{max}) &= A_{\mathcal{A}} * \mathcal{B}_{max} * a + B_{\mathcal{A}} * b \\ &= 0.012 \text{ or } 1.2\% \end{aligned} \quad (8.2)$$

Micro scale – Image analysis revealed 84% pseudotachylyte matrix for the analysed vein which appeared clast free in hand specimen. Factoring in the micro scale clasts that were not distinguished on the meso scale results in an estemated 12% of the entire mapped area being composed of pseudotachylyte matrix.

Micro scale result:

$$m = .84$$

$$\begin{aligned} PST\ matrix &= m(A * a + B * b) \\ &= .12 \text{ or } 12\% \end{aligned} \tag{8.3}$$

Corrections A and B – Area of pseudotachylyte matrix:

$$\begin{aligned} PST\,matrix_{\mathcal{A}}\ (\mathcal{B}_{min}) &= m(A_{\mathcal{A}} * \mathcal{B}_{min} * a + B_{\mathcal{A}} * b) \\ &= 0.007 \text{ or } 0.7\% \end{aligned} \tag{8.3}$$

$$\begin{aligned} PST\,matrix_{\mathcal{A}}\ (\mathcal{B}_{max}) &= m(A_{\mathcal{A}} * \mathcal{B}_{max} * a + B_{\mathcal{A}} * b) \\ &= 0.010 \text{ or } 1.0\% \end{aligned} \tag{8.3}$$

8.1.5 Discussion

This is the first time an estimate of pseudotachylyte area has been made based on multi scale mapping. Table 8.2 shows published area percentages for pseudotachylyte in other locations. It is striking that for none of the numbers published is the method made explicit: all reports simply refer to an 'estimate' (Camacho et al., 1995; Reimold et al., 1985; Fletcher and Reimold, 1989; Reimold et al., 1994). Reimold et al. (1994) for example merely state: "The spatial distribution of pseudotachylite in the Vredefort Dome was assessed by estimating the areal percentages of breccia at more than 600 exposures, most of them located within the core." The map showing their results lacks a scale for the stations where pseudotachylyte occurrence was recorded (Figure 8.4). Lieger et al. (2009) explain their method of recording breccia intensity for outcrops (and refer to an unpublished, and now unavailable thesis for more detail). Their method does not record an area percentage. The focus of their study lies on the systematic structural analysis of the pseudotachylyte brecciation in the entire Vredefort Dome. The area covered by their study is approximately 55 x 25 km (from measuring the map in their Figure 4). Figure 8.3 compares the results of this study with the data from the literature (Table 8.2). Only one fault-related occurrence was fund in the literature (the thrust fault reported in (Camacho et al., 1995). The bottom three rows in Figure 8.3 show data from the Vredefort impact structure. This graph illustrates how important a reference scale and publication of the methodology is, including a definition of what is estimated.

Author	*Location*	*Published percentage of pseudotachylyte*	*Scale*	*Method*	*Setting*
This study	Barra	pst s.s.:1-14% pst s.l.: 61-100%	<cm resolution, 1 km^2, 100 m elevation	Nested multi-scale mapping	
Camacho et al., 1995	Woodroffe Thurst, Australia	4% in a 1 km thick zone* with ultra-mylonites	*km*	n/a, estimate	thrust
Reimold et al., 1985	Vredefort Dome	0.4% over entire granitic basement	*approx. 1000 km^2*	Surface proportion estimate, method not explained	impact
Fletcher and Reimold, 1989	Vredefort, Master Bedding Fault	30 up to 65%	n/a, (likely dm or m)	n/a, method refers to unpublished PhD thesis 'in preparation', University closed 2004	impact
Reimold and Colliston, 1994	Vredefort Dome and Witwatersrand Basin	Outcrops with >5%	n/a, *(likely dm or m)*	Area percentage estimate, method not explained	impact
Lieger et al., 2009	Vredefort Dome		*cm–m in approx. 1000 km^2*	Breccia intensity method briefly explained, refers to calibration in unpublished diploma thesis	impact
Fedorowich et al., 1999	Strathcona Embayment, Sudbury	4.7% (varying from 2 to 8%) Sudbury Breccia (which includes cataclastic breccias)	7 km^2	"Outcrop mapping using conventional techniques", 1:2500 airphotos for control	impact

Table 8.2 – Published pseudotachylyte area percentages and mapped extent. Publications are included only if they made clear that the quasi-conglomerate geometry occurs, however, the geometry might not be distinguished for the area estimate. The scale is printed in italics where an educated guess by the author of this study was possible.
*According to Lin et al. (2005), the individual pseudotachylytes in the Woodroffe thrust do not exceed centimetre thickness which means they would not qualify as quasi-conglomerates.

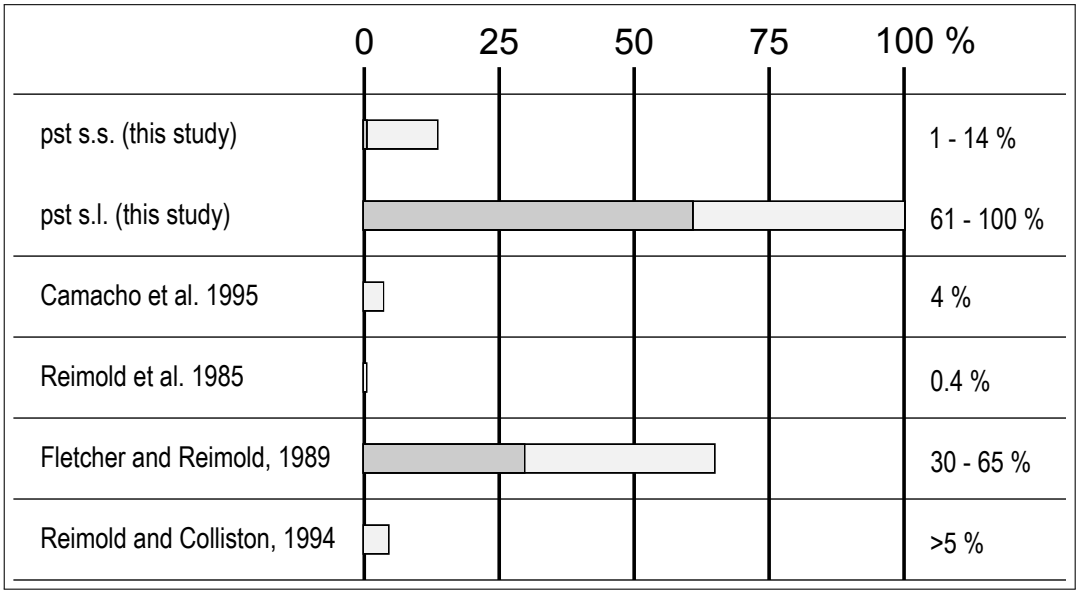

Figure 8.3 – Pseudotachylyte with quasi-conglomerate geometry: Results from this study and the literature. Where available, minimum estimates are shown in darker gray. Note the bottom three rows are data published from the Vredefort impact structure. Refer to Table 8.2 for locations.

'Volume' versus 'Area'

The pseudotachylyte occurrence for this study has been mapped as two dimensional areas on all scales. On the meso and macro scales, the pseudotachylyte areas were mapped onto a two dimensional area (map), even if in reality they were undulating surfaces and therefore three dimensional (see also Section 8.1.3). It became evident that in the literature on pseudotachylyte occurrence (Table 8.2) the terms *area* and *volume* are, in a physics sense, commonly used incorrectly. The term *area* seems to be used to refer to a geographical location, whereas *volume* refers to a lithology or rock volume that does not fulfil the criteria for a lithology (such as e.g. pseudotachylytes or mylonites). The physics definition of volume – meaning the three dimensional extent of an object – stands in contrast to the use of the same word in a more literary meaning, where volume can refer to "an amount or quantity of something, especially when great" or the "fullness or expansive thickness of something [...]" (Oxford University Press, 2020). It must be in this sense that Camacho et al. (1995) report on "an unusually large volume of pseudotachylyte", but describe their findings in percentage of "pseudotachylyte veining" or one dimensional measures (cm). Also Fletcher and Reimold (1989) state that a fault "contains large volumes of pseudotachylite" and mention that the "pseudotachylite [is] comprising up to 30% of the volume of the zone". Their indications of methodology do not suggest that true three dimensional volumes were taken into account. Reimold and Collistion (1994) however estimate "the

areal percentages of breccia", and Fedorowich et al. (1999) report on percentage of exposure of Sudbury Breccia in a defined area, and indicate the width of zones. The term volume therefore is frequently used in a geo-poetic sense, in the manner of a geological version of preciseness.

Applying this Method to other Sites

- Classification or categorisation of the outcrops must be repeatable. Quantitative information should be given about 1) the sampling area (the area of the outcrop window used), 2) the definition of the category (% area covered estimated by eye e.g. Reimold et al., 1994; Shipton and Cowie, 2003, or applied from a calibration set (this study). Optimal sample window size varies as the characteristic length scale of the network (Andrews et al., 2019 and references therein).
- Consideration of how to account for geometrical bias in the expression of the rocks – i.e., are exposures of the quasi-conglomerates biased towards cliff sections (due potentially to a foliation-control) and therefore under-sampled on a map – surface mapping will help here where the surface area of coverage can be extracted from a mapped surface, rather than from a map (vertical projection of the geometry) as in the present study.
- Consideration of the bias in outcrop – i.e. at Àird Ghrèin the sub-vertical dyke walls present almost perfect outcrops, whereas flat surfaces are very often grassed over, and at best are draped with lichen, which obscures the details. This is especially important when thin veinlets are the dominant structure.

The data from Àird Ghrèin are within the range of reported volume estimates for the Vredefort and Sudbury impact structures. However, none of the other studies reported how exactly they made their estimates. Future studies should ensure that their method of estimating volumes is clearly presented, and is reproducible. In the absence of such metadata it is difficult to compare between sites.

From these volume calculations and by analogy with other sites, it is highly likely that the pseudotachylytes on Àird Ghrèin are not fault-related. The theory (McKenzie and Brune, 1972; Melosh, 2005), previous observations (Francis and Sibson, 1973) and the data presented in this study (Chapter 4, 5 and 6), show that the pseudotachylytes in the quasi-conglomerate geometry on Àird Ghrèin are not fault related (Chapter 1). Therefore, evidence for other origins must be examined.

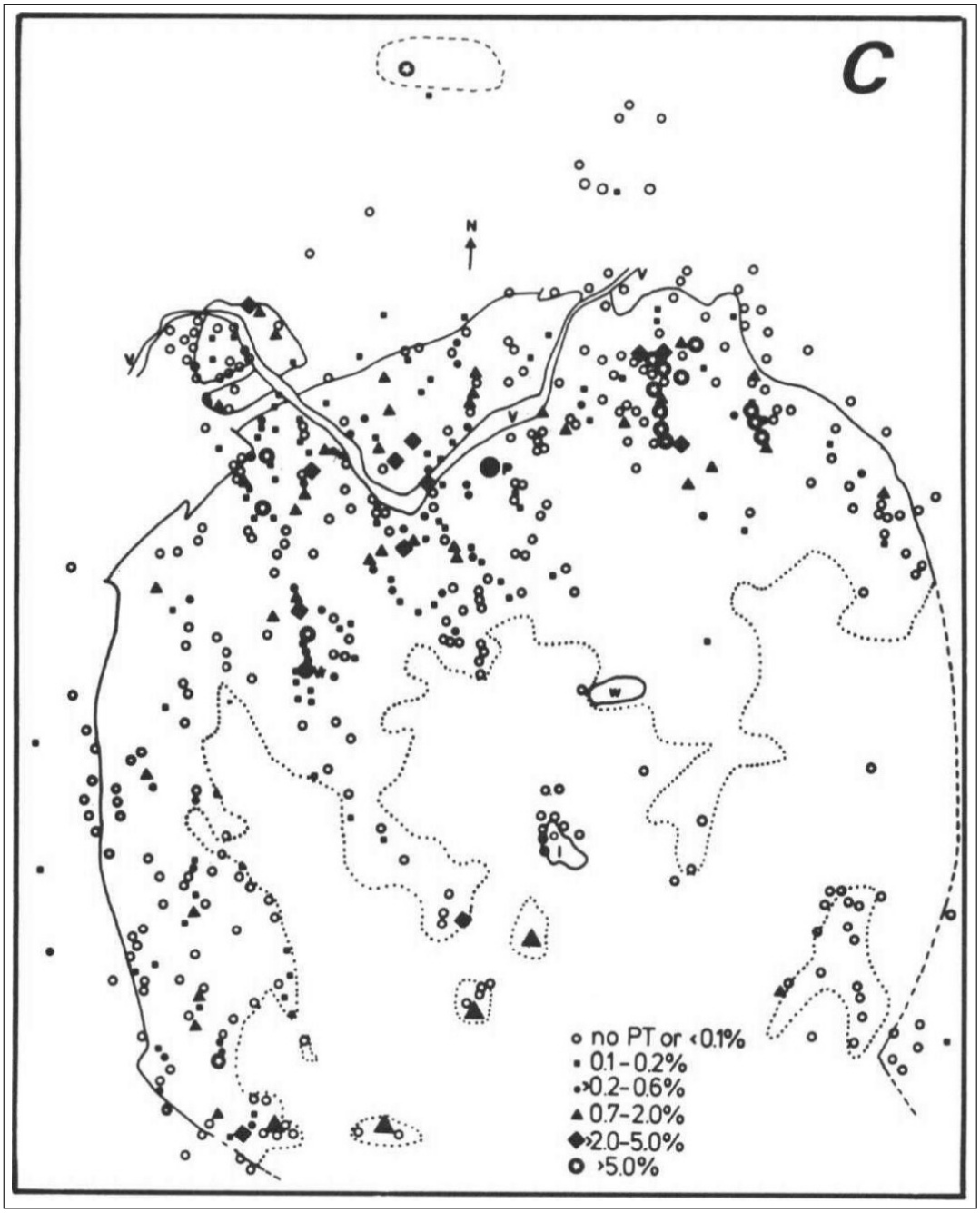

Figure 8.4 – Figure 2C in Reimold and Collistion (1994). "Estimated abundances (in area%) of pseudotachylite at about 570 measurement stations in the core and collar of the Vredefort Dome. P = Parys, Vr = Vredefort, I = Inlandsee, w = wherlite intrusion, PT = pseudotachylite, V = Vaal River. The dotted line separates outcrop-rich gneiss terrane and Karoo-covered (in the south) terrane. The solid line marks the core-collar contact (solid, where exposed, dashed, where covered) by Karoo or alluvium and, hence, inferred."
Note the lack of scale both of the map and of the 'measurement stations', inhibiting comparison to other sites or methods.

8.2 Evidence for the Origin of Pseudotachylytes on Barra

This section lays out the evidence for the origins of the Barra pseudotachylytes, combining evidence from this study with previously published evidence.

8.2.1 Age

Determining the age of the pseudotachylytes would offer insights into the paleo geographical setting, facilitate correlation of the Barra formation event(s) with other sites, and help constrain the conditions of formation (depth, in situ stress, ambient temperature). Several attempts have been made to date the pseudotachylytes of the Lewisian, both on the mainland and on the Outer Hebrides, with variably conclusive results. This study did not attempt to date the pseudotachylytes on Barra. The isotope data collected for Chapter 7 served to determine whether the pseudotachylytes had formed within an open or a closed system with regards to the elements analysed, which serves as an indicator of whether fluids were involved or not. The following paragraphs summarise the findings from the published literature. It should be noted that all samples presented in the literature bar one are from outwith the Àird Ghrèin field area of this study.

There is no conclusive age for these quasi-conglomerates on Barra. The age of the pseudotachylytes of the Outer Hebrides Fault Zone (OHFZ) can be bracketed by structural geological evidence (Chapter 3) between 1.7 Ga (Laxfordian metamorphism of the Lewisian Gneiss) and 250 Ma (Stornaway Beds containing conglomerates with pseudotachylytes: Storetvedt and Steel, 1977). Because the OHFZ is not significantly offset by the NW-SE trending shearzones on South Harris which are of Paleoproterozoic to Grenville age, Macinnes et al. (2000) infer that the OHFZ is younger than Grenvillian (c. 1000 Ma). However Imber et al. (2002) find evidence that they are significantly offset and thus infers an initiation of the OHFZ during the late Laxfordian or early Grenvillian. On the Mainland Piper and Poppleton (1988)'s paleomagnetic studies constrain the formation of the pseudotachylytes to c. 1500 (Laxfordian metamorphic events and pegmatites) to c. 1000 Ma (overlying Torridonian Sediments). The method applied by Piper and Poppleton (1988) involves recovering the primary remanence in ferromagnetic minerals (very fine grains formed in conjunction with the pseudotachylytes, Chapter 6) and compares the direction of magnetism with the predicted path of the palaeofield direction with respect to the sampling area between the time limits defined by geological evidence. Piper and Poppleton (1988) analyse samples from all major islands in the Outer Hebrides for palaeomagnetic dating of pseudotachylyte formation in the Lewisian complex. They interpret their data sequence from their 'Southern Zone' on Lewis to be most probably coeval with deposition of the Stoer Group (which hosts the Stac Fada member) around 1200 Ma ago.

On Barra, Piper and Poppleton (1988) investigate five different sites, however none of the samples are from the exact study area. The samples from the Uists and Barra give results which are more complex to interpret. The results plot in two different groups, with some samples plotting in both groups. They seem to roughly correlate with a late Laxfordian event (around 1500 Ma) and a Caledonian event (around 430 Ma). However, it is not clear how a later uplift (i.e. post-Caledonian) of several kilometres, a potentially related tilt, and sinistral strike slip movement of almost 100 km as proposed by Piper (1992) would affect these results. It is worth pointing out that attempts to date other pseudotachylyte occurrences have come across similar difficulties. Carporzen et al. (2005) suspect that some of their pseudotachylyte samples from Vredefort which show high natural magnetic remanence (an observation also stated by Piper and Poppleton (1988) for their samples from the Outer Hebrides) have been hit by lightning, and therefore show aberrant directions. In that sense Carporzen et al. (2005) justify discarding over 25% of their samples. Nakamura and Iyeda (2005) analyse samples of pseudotachylytes from the Sudbury impact structure and find that the petrology of the protolith controls the magnetic petrology of the pseudotachylyte and thus its reliability of paleointensity record.

Kelley et al. (1994) publish laser-probe $^{40}Ar/^{39}Ar$ data from one sample of a pseudotachylyte vein and its host rock from Grimsay (island between North Uist and South Uist). The sample stems from the OHFZ and featured in a number of publications (Maddock, 1983, 1986; Maddock et al., 1987; Maddock, 1992). Despite a wide variety of ages ranging from 425 to 2350 Ma Kelley et al. (1994) settle on their young age of 430±3 Ma. The older ages are interpreted to be influenced either by alteration (zones of paler colour identified during the experiment), or, it is suggested that close to the contact with the host rock the ages are older due to argon diffusion from the host rock or partially outgassed clasts, i.e. represent a mixing age. An age of 430±3 Ma is coeval with the Moine thrusting on the Scottish Mainland. Kelley et al. (1994) note that measurements of biotite profiles near the pseudotachylyte margin do not display diffusion-loss curves, as would be expected by a heat conduction-induced Argon loss. The authors propose two different models to explain the anomalous intragrain age profiles: (1) The biotite grains had a domain structure on a scale less than the laser pits and (2) the mechanism of argon loss was not volume diffusion, but rather a mechanism that sampled all areas of the grain simultaneously. A small domain size would require the uniform development of defects in order to explain their results. Either of the two models suggest a process different to heat conduction from a planar source caused by friction induced heating.

Sherlock et al. (2008) analyse samples from the Scottish Mainland between Gairloch and Loch Maree, from crush zones in Lewisian gneiss containing pseudotachylyte. The samples from the Mainland Lewisian pseudotachylytes give

ages in the range of 1690 to 823 Ma (plus error). The authors go on to justify a selection of dates between c. 1000 and c. 900 Ma to be the age of these pseudotachylytes, with ages of millions of years apart even within a single pseudotachylyte sample.

Sherlock et al. (2009) analyse a total of 6 samples from the footwall of the OHFZ. One of the samples stems from Àird Ghrèin on Barra, the other five samples are from the islands further North. The measurements result in host rock ages ranging from 7.6 Ga for 3 adjacent measurement spots (which is earlier than the age of the solar system!) to 544 Ma, with the pseudotachylytes from the current field site somewhere in between. Some measurements reveal younger ages for the host rock than for the pseudotachylytes, and some 'clasts' yield ages younger than the surrounding matrix material. Nonetheless, the authors claim that they were able to discern three separate periods of pseudotachylyte formation: c. 1900 Ma (Lewis), c. 1300–1200 Ma (Barra and South Uist), and c. 700 Ma (Barra, South Uist and North Uist). They also state, however that "None of the dated samples can be related conclusively to the Outer Hebrides Fault Zone."

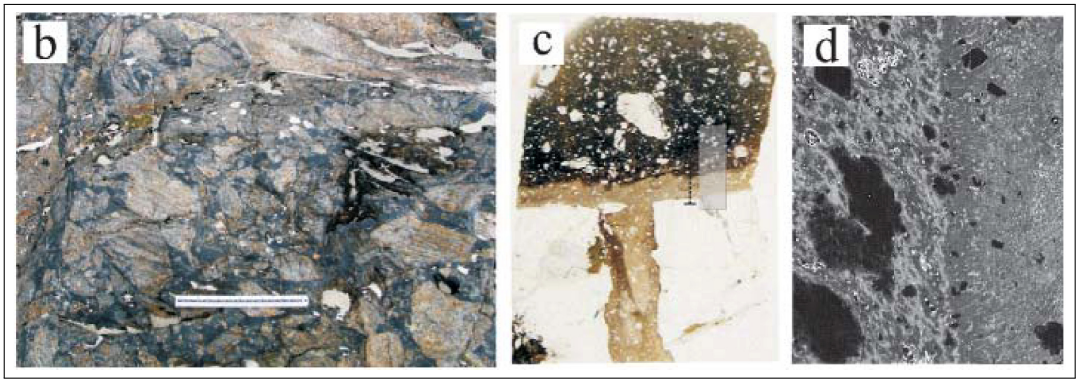

Figure 8.5 – Part of Figure 3 in Sherlock et al. (2009) – Photograph with 30cm ruler for scale is a 'representative section of outcrop' from which the Barra sample was taken. Photograph of a thin section 2cm wide of the Barra sample; grey box and black line indicate the positioning of the UV laserprobe traverse. SEM image 500μm wide showing the boundary between the dark and light pseudotachylyte phases.

Sherlock's sample from Barra is a quasi-conglomerate sample (Figure 8.5). Other than the observation that the dated samples stem from areas of two different colours no structural evidence is provided that would support the interpretation of their results of two separate pseudotachylyte forming events 500 to 600 Ma apart shown in Figure 8.6 indicated by the orange line and pink box, respectively. Figure 8.5 shows on the left hand side a "[r]epresentative section of outcrop from which [the Barra] sample was collected (ruler 30cm [...])". Neither

the outcrop photograph, the accompanying sketch of the outcrop, nor the text indicate evidence for a sequence of at least two pseudotachylyte forming events by which the sample would have been affected. On the contrary, Sherlock et al. (2009) state that "[t]here are no cross-cutting features or deformation of clasts residing at the boundary between the two types [of pseudotachylyte]." In the centre, the figure shows a photograph of the thin section with a width of 2cm (transmitted light and plane polarised light assumed, but not stated) with the "grey box and black line indicate the positioning of the UV laserprobe traverse". It should be noted that the lighter coloured pseudotachylyte (lower part of the image) is the 'younger' pseudotachylyte. On the right hand side of Figure 8.5 is an SEM image with a width of 500μm showing the interface between the lighter (left) and the darker (right) pseudotachylyte phases. The authors state that "[t]here are no cross-cutting features or deformation of clasts residing at the boundary between the two types [...]". Yet they conclude: "The [...] technique has allowed the identification of narrow, seismically reactivated margins on pre-existing pseudotachylites in Barra and North Uist, which would otherwise have remained undetected."

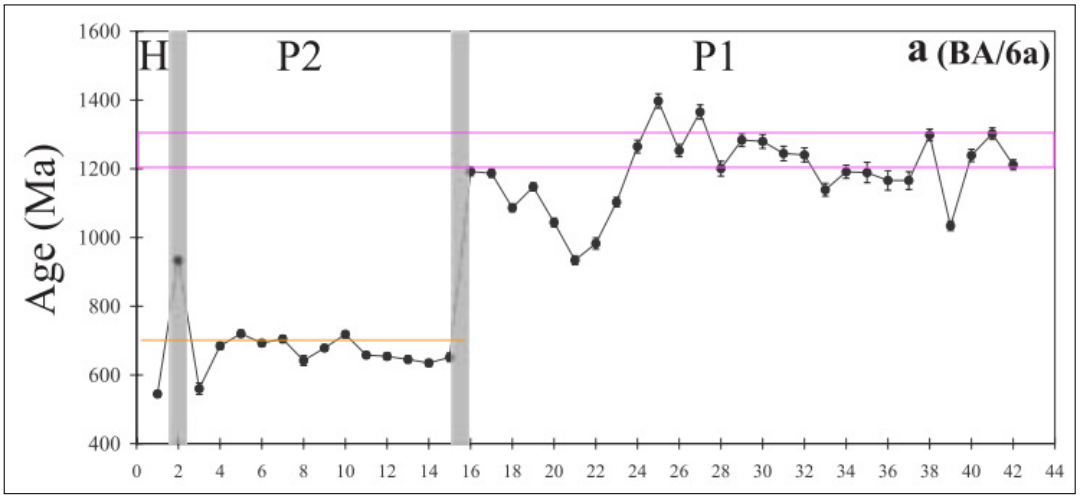

Figure 8.6 – Figure 8a in Sherlock et al. (2009) – The x-axis is the distance times 20μm. Results for the sample from Àird Ghrèin. The host rock (H) gives a younger age than the pseudotachylyte P2 (first data point) and P1 (second data point). The pink box brackets the age for the P1 1300-1200 Ma event and contains 15 out of 27 data points within their error margins (note, this is a 100 Ma bracket for a single, only seconds lasting event). The orange line lies at the P2 700 Ma event, including 4 out of 13 data points within their error margins.

Sherlock et al. (2008) state that given the wide range of resulting ages, the data "demonstrate that the Ar-isotope heterogeneity in pseudotachylite, [...] is beyond the resolution of the IR laserprobe $^{40}Ar/^{39}Ar$ dating technique." Sherlock et al. (2008) explain that a general problem with the $^{40}Ar/^{39}Ar$ dating method is that if the resolution of the laser probe beam is too low (that is the beam size

larger than the homogeneous domain), the beam may release argon from surrounding minerals (such as clasts in the pseudotachylyte matrix) during analysis and spoil the result. The size of the laser beam can be varied, but for more accurate results enough argon needs to be released. Sherlock et al. (2008) create pits of 75μm diameter, and Sherlock et al. (2009) use three different approaches with the smallest beam size being 20μm. The amount of clasts in the pseudotachylyte matrix is significant (16% in the analysed example in Chapter 6, Figure 6.34) and clast sizes smaller than 20μm common (e.g. Figure 6.13 in Chapter 6. The presence of clasts in pseudotachylytes is known to provide geologically ambiguous ages from $^{40}Ar/^{39}Ar$ analyses (e.g. Reimold et al., 1990; Müller et al., 2002; Di Vincenzo et al., 2004; Kirkpatrick et al., 2012). This signifies that clasts are not completely outgassed or in equilibrium with the matrix (O'Brien and van der Pluijm, 2012). Warr et al. (2007) developed a method to use this drawback to their advantage and date both the host rocks and the pseudotachylyte by measuring not only the argon, but also combining the results with measured (micro) clast percentage. The measurements are then extrapolated to both 0% and 100% of pseudotachylyte matrix, to find the pseudotachylyte and host rock age, respectively. The method was subsequently successfully deployed with reproducible results by O'Brien and van der Pluijm (2012) to date pseudotachylytes in Canada. However, not taking into account this microstructural information, interpretation of $^{40}Ar/^{39}Ar$ data on pseudotachylyte is, at its best, speculative.

Cross-cutting relationships were rarely observed on Àird Ghrèin outcrops. They were never observed in the big bodies of quasi-conglomerates, with the exception of one subvertical pseudotachylyte vein cutting across several clasts inside a quasi-conglomerate with no apparent displacement (see Figure 5.17). In none of the detailed studies of quasi-conglomerates for Chapter 5 was any evidence found for clasts that would indicate reactivation i.e. deformed, pseudotachylyte clasts inside younger pseudotachylyte matrix. A colour variance in pseudotachylyte in thin section similar to those observed by Sherlock et al. (2009) is observed (e.g. in Figure 6.33). This colour variation is clearly a mingling structure, i.e. two phases with a difference in matrix texture (composition, size, habitus and arrangement of micro-crystallites), amount of clasts or variation in clast size. Mingling and flow structures are discussed further below on page 196.

A geochemical study by O'Callaghan and Osinski (2019) show the heterogeneity of a pseudotachylyte from the Outer Hebrides in terms of the elements Mg and Si (Figure 8.7). Unfortunately, it is not clear what their third image displays and if under plain polarised light there would be a difference in colour of the two discerned pseudotachylyte phases A and B. O'Callaghan and Osinski (2019) suggest that "[t]he two simplest explanations are that these two phases either represent separate tectonic events and/or that they represent the melting of different host rocks." One of the most common observations of pseudotachylytes

is that ferromagnesian phases of the protolith are most susceptible to formation of pseudotachylyte matrix, whether that is because of their lower melting temperature or their lower fracture toughness in comparison with more silicate-rich minerals or a combination of the two (compare to "biotite with tentacles" in Section 6.6.2). A third simple explanation is therefore that melt B is indeed a later pseudotachylyte phase, and it is relatively enriched in Si because of the preferential and therefore early breakdown of ferromagnesian minerals forming phase A (see also subsection 'Microstructures' below on 195). However, O'Callaghan and Osinski (2019) make it clear that phase A and phase B have both formed during the same tectonic event. Complete mixing of the two phases is unlikely given the short duration of the fluid state of pseudotachylytes. A forth simple explanation is that without knowing the exact and full three dimensional structure of both the protolith and the pseudotachylyte vein system we don't know whether for example a big ferro-magnesian mineral grain fed, and has now been entirely replaced by, the 'tensile veinlet' of pseudotachylyte phase A. O'Callaghan and Osinski (2019) conclude that without dating the phases A and B, the different hypotheses cannot be distinguished. A combined and critical analysis of microstructures and dating techniques such as $^{40}Ar/^{39}Ar$ could indeed be of great value to help unravel the history of such pseudotachylytes.

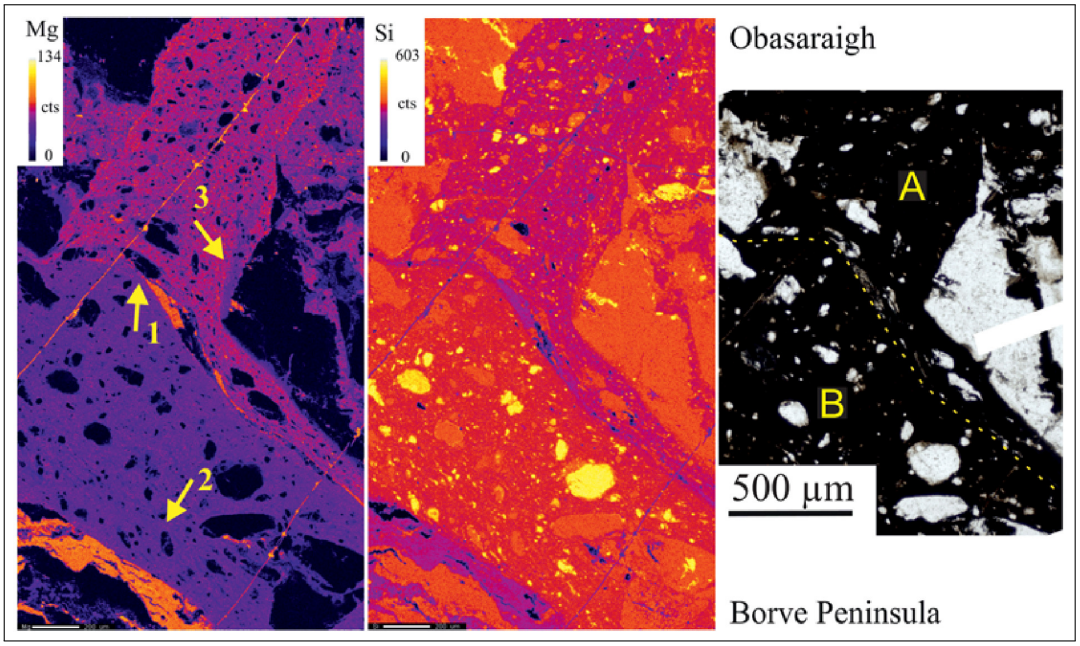

Figure 8.7 – Part of Figure 8 in O'Callaghan and Osinski (2019) – "Electron microprobe wavelength-dispersive spectrometry element maps of Mg and Si in pseudotachylyte veinlets [...]". It is assumed the third image is a photomicrograph, however the image is not mentioned in their publication.

8.2.2 Field-Scale Structure

The quasi-conglomerates on Àird Àird Ghrèin are ubiquitous and generally foliation-controlled (Chapter 4). Where they are exceptionally well exposed, the zones show thinning and thickening along strike (e.g. Figure 5.4 shows an undulating outcrop surface at Seal Bay on which the quasi-conglomerate thins into a narrow band, and then thickens). Some of these zones can be followed for a few hundred metres. Given the nature of the outcrop, it is problematic to identify stepping and splaying, to distinguish between clast and host rock, and to grasp the three dimensional structure and therefore the extent and continuity of these zones due to the size of patches of exposure. This study was not able to conclusively show that the quasi-conglomerate zones are tabular on the scale of the whole headland.

The complexity of the quasi-conglomerate structures and the quasi-conglomerate's relationship with their host rock has been demonstrated for other quasi-conglomerate occurrences. Figure 8.8 shows an outcrop of quasi-conglomerate on two perpendicular walls of a quarry in the Vredefort impact structure. The photograph illustrates the complex and unpredictable three-dimensional shape of the quasi-conglomerate. The apparent thickness on the corner is approximately 2 m, whereas at a distance of less than 2 m from the corner towards South, the quasi-conglomerate is absent in the plane of observation. The quasi-conglomerate is hosted by a strongly deformed (fractured) host rock. Despite that, there is a sharp and clear boundary observable between the quasi-conglomerate and its host rock. Very similar observations have been made on Àird Ghrèin too, however on less ideal (and photogenic) outcrop surfaces.

Figure 8.9 shows a quasi-conglomerate on a wall 2 - 2.5 m high in a different quarry in the Vredefort impact structure. The pink arrows point to clasts of such a large scale that, on a smaller outcrop surface, could easily be mistaken for the in-situ host rock. The orange arrow points to an indicator that the quasi-conglomerate continues beyond the area of the photograph. This illustrates that the size of the outcrop will bias the observation, with smaller or less ideal outcrops potentially leading to a smaller extent of quasi-conglomerate recorded.

Because the quasi-conglomerates on Àird Ghrèin are foliation parallel there are no offset markers to gauge potential shear displacement. For the quasi-conglomerates, no evidence was found for shear fabrics related to the pseudotachylyte formation such as mylonites or S-C fabrics, as observed elsewhere for smaller vein pseudotachylytes (e.g. in quartzite (Bestmann et al., 2011), or tonalite (Di Toro et al., 2005)). The deformation of the Lewisian gneiss is pervasive throughout the whole headland. The characteristic Lewisian fabric is gneissose with mafic layers up to a metre thick sometimes displaying migmatitic boudins (Fig-

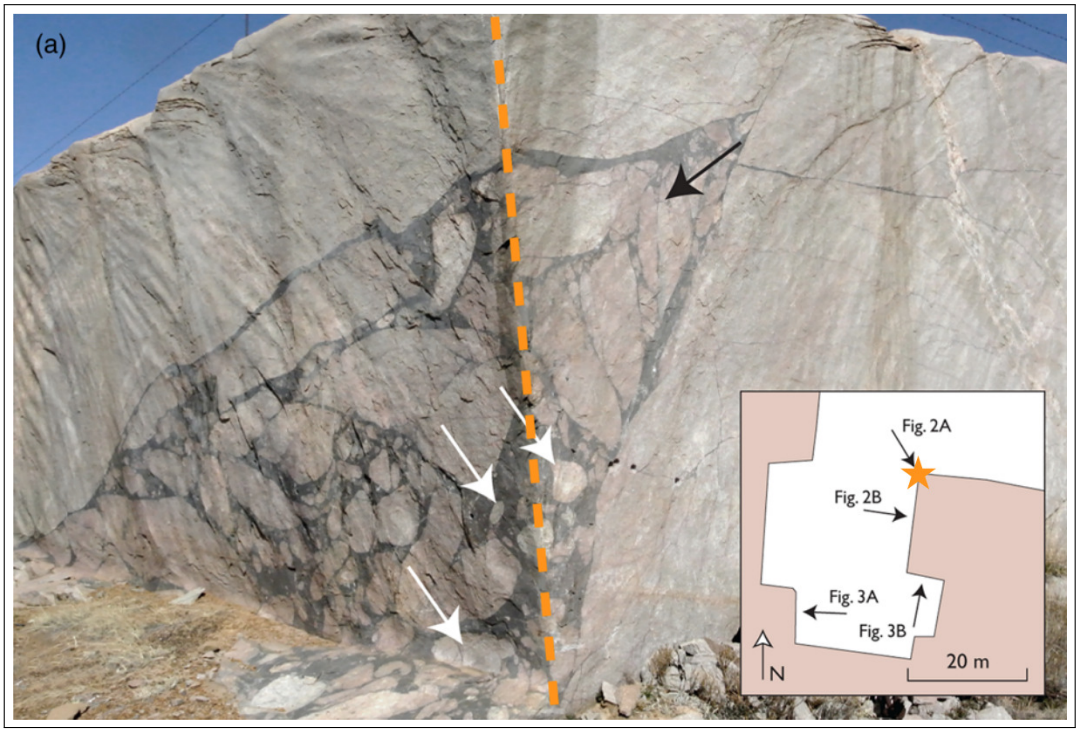

Figure 8.8 – Part of Figure 2a in Garde and Klausen (2016), with annotations added in orange. – Esperanza Quarry in the Vredefort impact structure, height of quarry wall is 3.5 m. The photo shows the view of two perpendicular quarry walls, the corner between them highlighted by the orange dashed line and the orange star. The image illustrates the complex three-dimensional structure of quasi-conglomerates and the change in apparent thickness within short distance. The quasi-conglomerate thins out into a fracture above the black arrow.

ure 5.21). On Àird Ghrèin, the cataclastic or crush rock fabric is ubiquitous but most often subtle. In places, the host rock fabric appears macroscopically intact, and only upon smaller scale investigation can the deformation be seen. Garde and Klausen (2016) found similar pervasive deformation in the vicinity of metre-scale quasi-conglomerate outcrops in the Esperanza Quarry in the Vredefort dome. Figure 8.8 shows one of their examples of what they call the dendritic fracture network. Other examples are shown in their Figures 3 and 4 (Garde and Klausen, 2016). Jehu and Craig (1924) describe the dendritic fracture network on the Barra isles as "penetrat[ing] the rock mass [...] in complicated reticulations often of extreme tenuity ramifying through the mass in intrusive fashion." The photographs (Figures 8.10 and 8.11) from Mohr-Westheide et al. (2009) illustrates how difficult these fracture networks are to identify in the field even in a perfectly polished and fresh cut rock. Even on these images, of a light coloured homogeneous and dry host rock with an even and flat surface, the fracture networks (some of which are pseudotachylyte-filled) can barely be made out. For the more heterogeneous Lewisian gneiss which is often covered in lichen or algae,

Figure 8.9 – Part of Figure 4a in Garde and Klausen (2016), annotated with pink and orange arrows. – Salvamento Quarry in the Vredefort impact structure, height of quarry wall is 2-2.5 m. Photograph showing a quasi-conglomerate with various clast sizes and matrix component. Pink arrows point to large clasts which could easily be mistaken for the boundary of the quasi conglomerate on a smaller outcrop surface.

and frequently wet, the bias will be against picking up on these small fractures. Because they offer nearly polished surfaces, a lot of the more detailed (meso scale) mapping on Àird Ghrèin was done in the tidal outcrops of Seal Bay. Already in 1819, MacCulloch, held back by wind and weather, noted: 'a future geologist will be fortunate if he is not compelled to leave much unseen, and to supply somewhat from conjectures.' (in Jehu and Craig, 1924).

Garde and Klausen (2016) note that the dendritic fracture network at Vredefort is exploited by the pseudotachylyte. Pseudotachylyte exploiting micro fractures has also been noted by Mohr-Westheide et al. (2009) in a Vredefort quasi-conglomerate (e.g. their photo in Figure 8.10). The widespread deformation of the rock on the Outer Hebrides has led to the usage of the term crush rock (e.g. Jehu and Craig (1924); Francis and Sibson (1973)). Extensive crush zones have been noted by Jehu and Craig (1924) giving an example for Sandray where "the whole thickness of the crushed gneiss cannot be less than 800 feet [over 240m]."

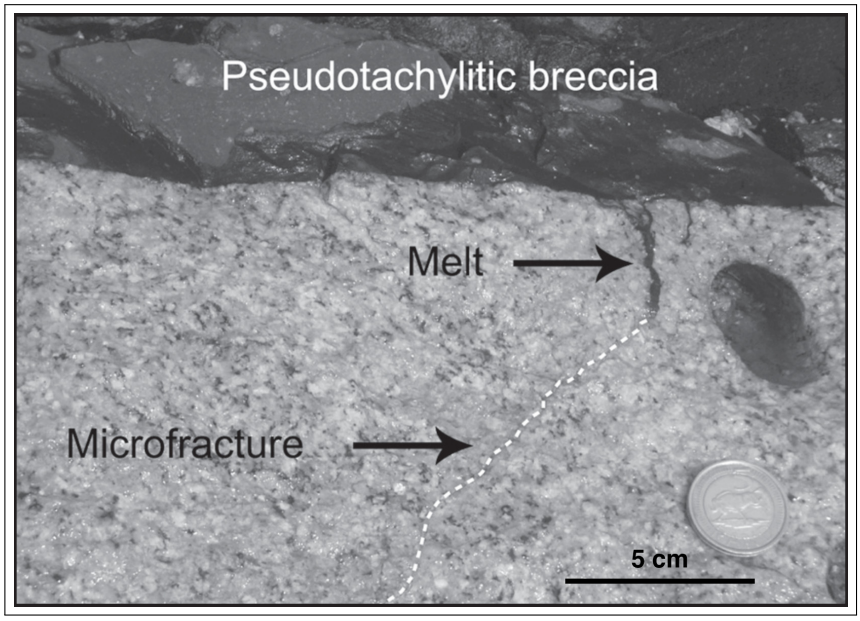

Figure 8.10 – Figure 13 in Mohr-Westheide et al. (2009) – Pseudotachylyte (Melt arrow) exploiting a Microfracture.

Transport and Displacement

The question whether clasts and pseudotachylyte matrix have been transported, and if yes how far, is of great interest. Considerations of the thermodynamics of cooling of small volume melts shows that long distance transport (decimetres) of matrix (and therefore clasts) should not be possible (McKenzie and Brune, 1972; Melosh, 2005) because any melt formed solidifies within seconds Dixon and Dixon (1989). In the impact literature, primarily around the Vredefort impact structure, this question has been posed in the context of the origin of the pseudotachylyte matrix. It has been suggested that the pseudotachylyte matrix may be melt which derived from the impact (shock) melt and was then injected into the host rock (e.g. Lieger et al., 2011). In the context of 'tectonic' pseudotachylytes, the interest lies in determining displacement and mechanisms of formation. In both geological contexts, the answer can help shed light on the process responsible for the formation of pseudotachylytes.

On Àird Ghrèin, evidence has been found for both transport and displacement of clasts, but never more than centimetres to decimetres. Figure 5.21 shows a quasi-conglomerate with both mafic and more felsic clasts. This limited magnitude of material transport is in agreement with findings from Mohr-Westheide and Reimold (2011) from the Vredefort dome who report at most 20 - 25 cm of clast transport on a 3 m by 1.5 m surface. Clasts are frequently rotated (rotational

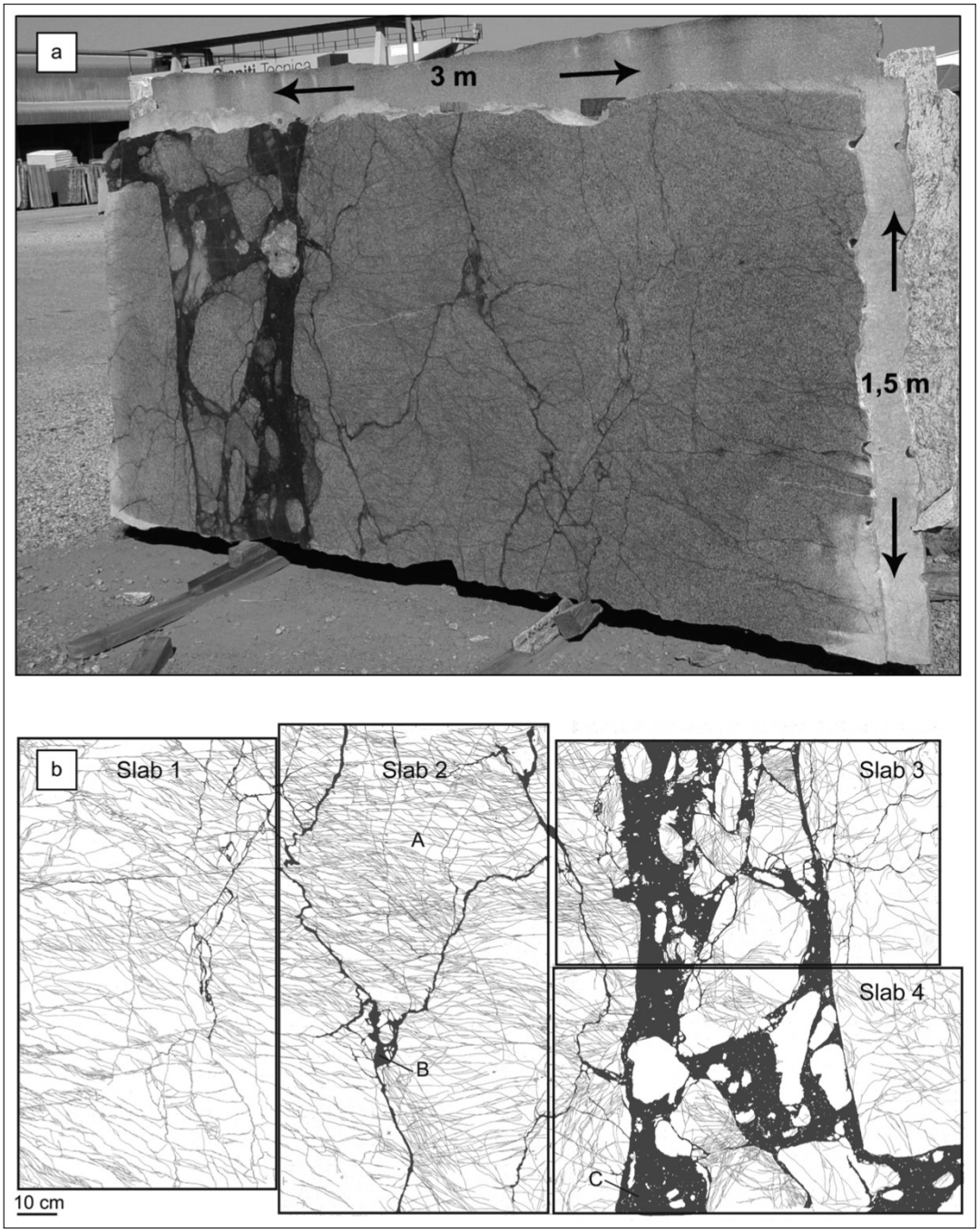

Figure 8.11 – Figure 3 in Mohr-Westheide et al. (2009) – a) Polished 3 x 1.5 m granite slab from the Vliegenkraal or Esperanza dimension stone quarry in the western part of the Vredefort dome. (b) Traced structures of the granite slab.

displacement) to variable degrees away from the host rock foliation orientation

(e.g. Figure 5.14). No indicators of shear direction are present in pseudotachylytes (i.e. no lineations), in addition to the absence of markers of shear displacement. These absences make it impossible to determine whether the plane of observation (the outcrop surface) is indicative for any apparent displacement observed, and therefore, no attempt has been made to quantify the displacement. This is in agreement with the geochemical findings of O'Callaghan and Osinski (2019), who conclude: "The mixing model results indicate that the pseudotachylyte at all three locations [on the Outer Hebrides] was derived from the melting of the proximal lithologies. However, the mixing and homogenization of the melts, combined with petrographic observations such as aligned fragments, suggests that the pseudotachylytic melts did not form purely in situ and that a degree of transportation took place, although the exact transport distances cannot be determined from this study."

Jigsaw Pattern and Clast Families

On the outcrop scale, in-situ fragment clusters were observed (Chapter 5), which represent the most pronounced evidence of poor sorting of clasts in the quasi-conglomerates. The clusters often consist of angular fragments and at times seem to fit together in a jigsaw pattern c.f. Woodcock and Mort (2008), e.g. in Figure 5.13. This was also observed by Lieger et al. (2009) (Figure 8.12), and by Dressler and Reimold (2004); Mohr-Westheide et al. (2009), for quasi-conglomerates in the Vredefort structure. Other clasts have been broken into daughter fragments which are surrounded by pseudotachylyte. The original, generally rounded shape of the parent clast can still be traced. In this study, no attempt has been made to fit the jigsaw pieces back together. Garde and Klausen (2016) note that the amount of pseudotachylyte appears to correlate with the size reduction and rounding of the daughter fragments.

Rounding of fragments

It has been shown that formation of primary round clast segments is possible by curved fractures (Chapter 5, e.g. Figure 5.11 and exploitation of tabular fracture sets (Chapter 6, e.g. 'wavy veinlet' in Figure 6.28). Secondary rounding of clasts requires an additional process of comminution. Lieger et al. (2009) demonstrate the presence of a shape fabric in a quasi-conglomerate in the Vredefort impact structure. More angular fragments are closer to the margin of the pseudotachylyte body than more round fragments (Section 6.6.1), or occur in clast families (Section 5.5.4). This observation was also made by Garde and Klausen (2016). Lieger et al. (2009) speculate that the fragments in the more central parts have remained in a hot pseudotachylyte melt for longer and are therefore more rounded, a similar explanation as given by Sibson (1975) for the rounding of clasts. On the other hand, Garde and Klausen (2016) suggest that cataclasis can result in rounding of the clasts. The microstructural observations (Chapter 6) of this

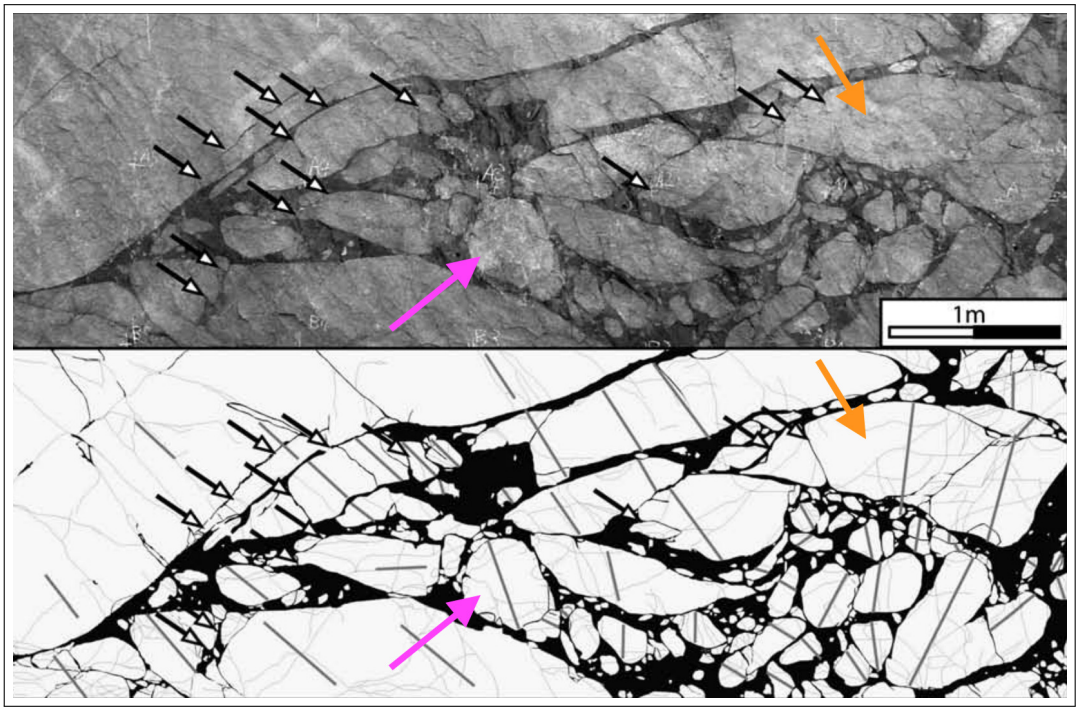

Figure 8.12 – Part of Figure 8 in Lieger et al. (2009) (annotated) – Quasi-conglomerate from the Vredefort impact structure. The arrows point to clasts which appear whole on the photograph. On the map it is evident that these clasts are both fractured (grey lines) and broken up into daughter fragments which are separated by pseudotachylyte.

study are indicative of cataclastic rounding including disaggregation (in the sense of Bestmann et al. (2011), Section 6.6.2 and 8.2.3) for the quasi-conglomerates on Àird Ghrèin (see also Section 8.2.3).

Progression

The preferential occurrence of angular fragments both close to the host rock Lieger et al. (2009); Garde and Klausen (2016), and as daughter fragments of larger parent clasts, point to a similar process for the formation of clasts both from the protolith, and the formation of smaller clasts (i.e. comminution of clasts). The following succession for the formation of quasi-conglomerates is therefore proposed and illustrated in Figure 8.13: (1) Cataclastic, pervasive deformation (blue lines) of the protolith (green lines) and the formation of pseudotachylyte (red) along pre-existing features (veins). (2) Rounding of rock fragments and increase in amount of pseudotachylyte goes hand in hand, formation of loose clasts. (3) Enough pseudotachylyte matrix surrounding the clasts facilitating rotation and further rounding. (4) At the same time, clasts continue to form and deform in the manner of the (1) – (3) sequence, forming smaller clasts, first

in clusters or family groups (2), and later disaggregating and rotating (3). It is suggested that this sequence is continuous, with all previous stages being initiated and continued throughout the process. Such a progression is for example captured in Figure 5.11.

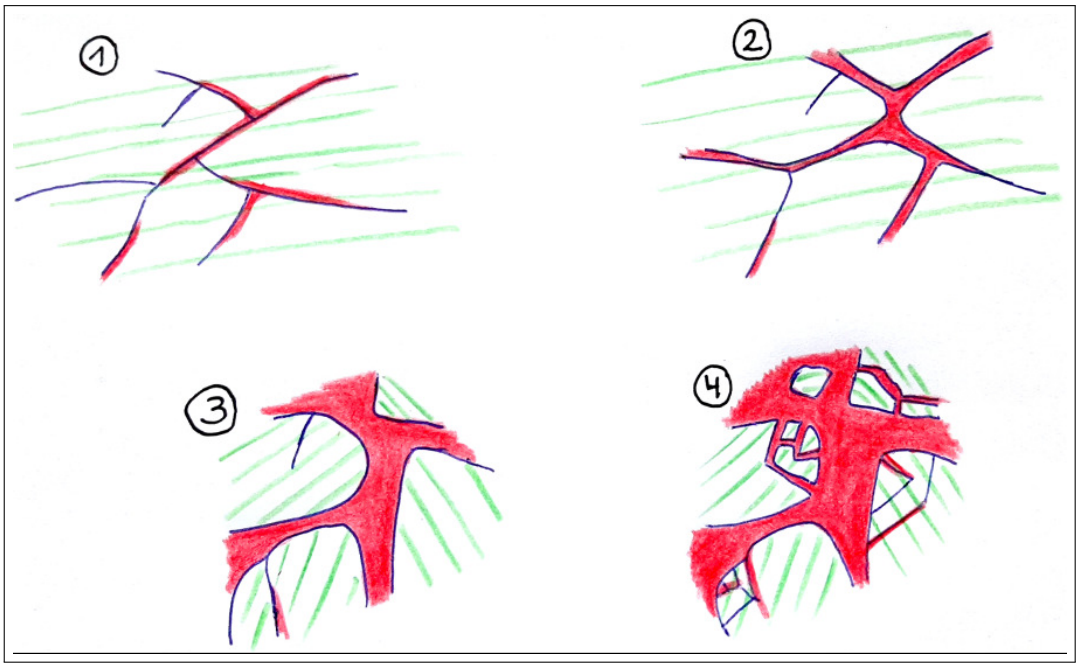

Figure 8.13 – Sequence of quasi-conglomerate formation: (1) Pseudotachylytes form along a pervasive fracture network in the protolith. (2) The pseudotachylyte increases as the protolith decreases and clasts get rounder. (3) Enough pseudotachylyte surrounds the clasts to facilitate their rotation. (4) At the same time, pseudotachylyte forms along fractures in the clasts, forming in situ clusters of angular fragments. Note: foliation trace for illustration of rotation mainly – as has been shown the foliation does to an extent control the orientation of pseudotachylyte veins and fractures.

Fractal – Sequence (1)–(4) on All Scales

A fractal distribution of clasts has been demonstrated for the outcrop and the micro scale of pseudotachylytes in impact settings (Hisada, 2004; Rousell et al., 2003), in tectonic settings (micro scale only) (Pittarello et al., 2008; Di Toro et al., 2009; Shimamoto and Nagahama, 1992), and in high velocity friction experiments (Tsutsumi, 1999). The observations of this study suggest that this sequence and its continuation (i.e. all previous stages being continued to be initiated throughout the process) represents the chronology at all scales of this study: from the macro scale to the meso scale and the micro scale.

8.2.3 Microstructure

The host rocks of pseudotachylytes are pervasively deformed. The ubiquitous deformation discussed in the section above for the field scale has also been shown for the micro scale (e.g. Section 6.5.1). The microfractures are difficult to identify in the field, especially on rough outcrop surfaces. Thin section analyses reveal arrays of tabular deformation zones in the host rock, some of which are exploited by the pseudotachylyte (e.g. 'wavy veinlet' in Figure 6.28). In plain polarised light, as in hand specimen or in outcrop, the host rock often appears undisturbed (e.g. Figure 6.7 or 6.8, and Garde and Klausen (2016). Ultracataclastic areas and regions of high clast density of a pseudotachylyte vein are not identifiable in plain polarised light (compare the red outline and circle in Figure 6.28). Microfractures are easier to identify when they are decorated by material of a contrasting colour. The difficulty to identify pseudotachylytes in the field (c.f. Kirkpatrick and Shipton, 2009) is enhanced by the 'apparent intactness' of the host rock down to the micrometre scale.

Shape and Microstructures of Fragments

In accordance with the host rock, the micro scale fragments in the pseudotachylyte matrix are internally strongly deformed. Deformation is apparent in different ways. Parts of fragments are made up of small (micron sized), potentially recrystallised grains, often in conjunction with larger, detrital grains (Figure 6.12). This has also been reported from fragments in pseudotachylytes from Vredefort (Mohr-Westheide et al., 2009; Lieger et al., 2011; Reimold et al., 2016) and Sudbury (Lafrance and Kamber, 2010). Fragment shapes are irregular and especially the larger fragments are often lobate. This shape has been referred to as 'embayment structures' (Sibson, 1975; Lin, 1999, 2008) and used as evidence for melting of pseudotachylytes and estimation of the melting temperature (Sibson, 1975). In the thin sections analysed it was found that more commonly than single grains with concave segments (i.e. displaying an apparent fragment convexity markedly smaller than 1), irregular grain shapes are associated with lithic or polycrystalline fragments. Rather than melting, the apparent 'embayment structures' therefore represent plucking structures, that is, a disaggretation of fragments (Bestmann et al., 2011).

Single grain fragments of quartz show fractures which may be crystallographically controlled. Figure 6.18 shows an example of two sets of these planar fractures. Numerous inclusions give the grains a dusty appearance (Figure 6.20 and 6.21. The high abundance of sulphides and oxides and especially of ferromagnetic minerals is a common pseudotachylyte attribute (e.g. Piper and Poppleton, 1988; Camacho et al., 1995; Nakamura et al., 2002; Kirkpatrick and Rowe, 2013). These minerals decorate intra grain fractures of both fragments and in the host rock, and often occur in the host rock in conjunction with biotite being

in contact with pseudotachylyte (Figure 6.23). The relatively high mobility of the constituent elements seem to facilitate the formation of these ore minerals. It is the presence of those dark coloured phases, in combination with the small grain size of the matrix material, which make pseudotachylytes dark and visible in the field. The dark colour can potentially help distinguish pseudotachylytes from ultra-cataclasites in the field which often appear as a slightly lighter colour. More angular fragments occur close to the wall rock (Section 8.2.2), and in freshly micro fractured fragments (e.g. Figure 6.13 and 6.14). This observation is common for pseudotachylytes and has served as evidence for frictional melting (e.g. Lin, 1999).

Many authors who studied the fate of fragments in pseudotachylyte assumed a monocrystalline and isotropic fragment (Sibson, 1975; Lin, 1999, 2008; Ray, 1999, 2004; Bizzarri, 2014). Their general conclusion is that frictional heat (then present as latent heat in the molten matrix) melts the fragments and is responsible for their rounding. Lin (2008) compared several pseudotachylytes and cataclasites in terms of roundness of fragments. He finds that in pseudotachylytes, a significant amount of fragments have a roundess of > 0.4, whereas in cataclasites all fragments exhibit a roundness of < 0.4. However, the micro fraction of fragments in cataclasites is monocrystalline (Figure 7.9 in Lin, 2008), whereas the majority of micro fragments in pseudotachylytes in the samples at hand are polycrystalline or polymineralic. Bestmann et al. (2011) find that pseudotachylyte matrix intrudes along grain boundaries of the very fine grained (1 micron) grain aggregates that make up the fragments in their pseudotachylyte veins. In this way, the polycrystalline grain aggregates (fragments) disaggregate. That means not only cataclasis, but also other grain size reducing deformation mechanisms (e.g. subgrain rotation deformation) may provide a small enough starting grain size for successful pseudotachylyte formation. The formation of micro fragments which constitute polycrystalline grain aggregates could therefore be facilitated primarily through disaggregation of deformation zones along micron sized grain boundaries, a process that seems to be capable of creating genuinely rounded fragments, with genuinely concave fragment segments.

Mingling Structures

As presented in Section 6.6.4, the pseudotachylyte matrix goes through a three stage evolution of (1) locally derived ultra cataclastic (felsic) material and replacement of biotite (mafic) to (2) flow structures which represent mingling to (3) mixing where no flow structures can observed.

Flow structures (or sometimes called textures) represent an intermingling of (at least) two phases which are characterised by a difference in geochemical composition, grain size of the matrix, homogeneity of the matrix, micro-crystallite

habitus, and/or clast size and amount of clasts (Figure 6.33 in Chapter 6). Flow structures are commonly observed in pseudotachylyte veins and injection veins (e.g. Kirkpatrick and Rowe, 2013). They seem to be not reported upon from larger pseudotachylyte bodies, i.e. quasi-conglomerates, (evident from the text and figures in Garde and Klausen, 2016) and in this study have not been found in the thin sections consisting of clast poor quasi-conglomerate rich in pseudotachylyte s.s. (i.e. the area of an entire thin section without host rock). However, such textures were found in veins and near the host rock in samples from pseudotachylyte in Vredefort (Lieger et al., 2011). This absence of flow structures in samples rich in pseudotachylyte s.s., or far from the host rock, could be due to it representing a more advanced state of deformation, where more time was available for the mixing of fluids with potentially different compositions. Better mixing could also have an influence on the crystallisation of micro-crystallites in the matrix. In the investigated thin sections, no pressure shadows (Garde and Klausen, 2016), quenched margins, alignment of fragments, or aligned growth of matrix minerals were apparent. These observations suggest crystallisation of the matrix under hydrostatic stress conditions and with limited element mobility. The radial geometry of the micro crystallites that crystallise as part of the matrix originates on micro fragments in the samples at hand. Spherulitic and dendritic crystals form when the ratio of diffusion to growth is small (Lofgren and Hargraves, 1980), because the incubation period for homogeneous nucleation is not available. These features are traditionally interpreted as due to high cooling rates (e.g. Wenk et al., 2000), however they could also occur by crystallisation from a supercooled fluid, as the increased temperature is generally inferred from a temperature required to melt the replaced minerals in an equilibrium situation. Wenk et al. (2000) note that morphologic zoning of micro crystallites of smaller size at the margin indicates higher cooling rates in comparison to the centre, which means that the crystallisation is likely primary and not the result of subsequent devitrification. O'Callaghan and Osinski (2019) report aligned micro-fragments in their flow structures (their figure reproduced in Figure 8.7), however they did not support their observation by quantitative means. Flow structures have been used as evidence for melt, intrusion, and an incomplete mixing of two melts (e.g. Kirkpatrick and Rowe, 2013; O'Callaghan and Osinski, 2019). Flow structures may form by mingling of two phases and can be formed in both general shear and pure shear. It should be noted that in the Sudbury impact structure, the part of the Sudbury Breccia that is categorised as cataclastic is the one that shows flow structures in the outcrop (meso) scale, whereas the pseudotachylyte-bearing Sudbury Breccia (the one which resembles the quasi-conglomerates of this study, and in Vredefort) lacks flow structures at the outcrop scale.

Transport vs. In Situ Replacement

In situ cataclastic deformation and comminution have also been commonly observed by Garde and Klausen (2016) in the host rock surrounding Vredefort pseudotachylytes. They note that the rock appears little affected by deformation in the field and under a handlens, which has also been observed in this study (Section 8.2.2). On the micro scale, Garde and Klausen (2016) note that the pseudotachylyte matrix records the transition from solid to liquid: "Gradual transitions are observed from micro-cataclastic and variably fluidized material into material that displays flow textures and contains new, tabular crystallites of K-feldspar, plagioclase and platy biotite too small to be visible with optical microscopy" and contains numerous, tiny cataclastic fragments of quartz. Lafrance and Kamber (2010) interpret the small subgrains of quartz, which they observe in the pseudotachylyte and cataclastic Sudbury breccias, to have formed first within their host rock and subsequently incorporated in the breccia as fragments where they underwent further cataclasis and abrasion. The descriptions from both Vredefort (Garde and Klausen, 2016) and Sudbury (Lafrance and Kamber, 2010) match the observations of this study both on the meso and on the micro scale.

In the Vredefort pseudotachylytes, similar pseudotachylyte colour dependence on the host rock colour have been observed as presented in Section 6.6.2. Mohr-Westheide et al. (2009) find that in some cases, when a thin pseudotachylyte veinlet crosses from quartz or plagioclase rich to a more K-feldspar rich host rock, the veinlet changes colour promptly from black to red. Dressler and Reimold (2004) had noticed a similar abrupt colour change when thin pseudotachylyte veins crossed from a grey gneiss (pseudotachylyte dark grey or black) to an aplite vein (pseudotachylyte light coloured). Their chemical analyses (EMPA) of three veins show that only the thinnest vein (0.5 - 1 cm) matched the immediate host rock, and the two thicker veins (2 - 3 cm and 3 - 5 cm, respectively) showed some mixing. The veins analysed by Dressler and Reimold (2004) are two orders of magnitude thicker than the 'wavy veinlet' (Figure 6.28) for example. Dressler and Reimold (2004) conclude that in situ fusion may be responsible for the formation of many thin pseudotachylyte veins in the central parts of an impact crater, a process they name "flash replacement melting". Both this study and the studies from Vredefort suggest that the in situ replacement can be observed in the very thin pseudotachylyte veins. The element maps published by O'Callaghan and Osinski (2019) can be interpreted in this light. Their 'tension fracture' (top half in Figure 8.7) shows a different matrix composition in terms of Mg and Si to the matrix in the bottom half of the images. The matrix in the 'tension fracture' may represent the very local protolith composition which may differ to the composition of the protolith of the matrix in the bottom half, creating two matrix phases. The composition of the protolith may also differ to the composition of the immediate host rock of the pseudotachylyte.

Shock Features

No unequivocally identifiable shock features were found in any of the thin sections analysed in this study. The two sets of planar fractures (Figure 6.18) record high strain rates, which are not unique to shock deformation and would only be shock indicative if there were three sets and at low crystallographic index. The crystallographically controlled quartz microstructures discussed in Section 6.5.3 (Figure 6.19) are conspicuous. The following observations are in line with planar deformation features (PDFs), e.g. Stöffler and Langenhorst, 1994: The micro structures occur as three sets of parallel, optical discontinuities, are decorated with a dark phase, and occur in planes with a spacing of the individual features somewhat variable between 2 and 10 μm. The features seem to be linear rather than planar but arranged in planes (as evident under a transmitting light optical microscope). Decoration of PDFs is a secondary feature which forms by annealing of the amorphous lamellae of non-decorated PDFs and is very common for PDFs in autochthonous and parautochthonous impact rocks (Stöffler and Langenhorst, 1994). However, they do not look like PDFs in comparison to published images of PDFs (Figure 8.14) and from personal communication with W.U. Reimold (2016). PDFs are a diagnostic impact feature (Chapter 2), however they are rarely recorded from clasts in quasi-conglomerates or pseudotachylytes (Reimold, 1995). To the author's knowledge, no systematic investigation of the Lewisian Gneiss on Barra to look for PDFs has been performed so far. It has been stated that no evidence for shock has been found in the samples analysed (e.g. Sibson, 1975; Sherlock et al., 2009; Campbell, 2016). However, the OHFZ is regarded as the type locality for tectonic pseudotachylytes (O'Callaghan and Osinski, 2019), and therefore it seems likely that a researcher's focus would not lie on looking for shock diagnostic features. This facilitates a motivational, confirmation and even physical bias towards not finding shock diagnostic features (Shipton et al., 2019). Further aspects of the spatial occurrence of shock metamorphic features is discussed in Section 8.4.

8.2.4 Geochemistry

The geochemical isotope analyses of the Lewisian Gneiss host rock, the pseudotachylytes, and the minor intrusives show that the pseudotachylytes formed in a closed system. The incompatible elements Rb, Sr and Nd readily leave the system when fluids are available. The derivation of pseudotachylyte from its local if not adjacent host rock has been shown for major elements and trace elements in a recent study by O'Callaghan and Osinski (2019). The scatter of the data presented in this study, and especially in the Sr ratio (e.g. Figure 7.7) can be explained by mixing of the different host rock lithologies as seen in Figure 8.15. The difference of the curves between the Tonalite Gneiss and the Granite-Gneiss is approximately an order of magnitude. The pseudotachylyte samples in this study were pseudotachylyte s.s. rich, clast free, and flow structure free pseudotachylyte,

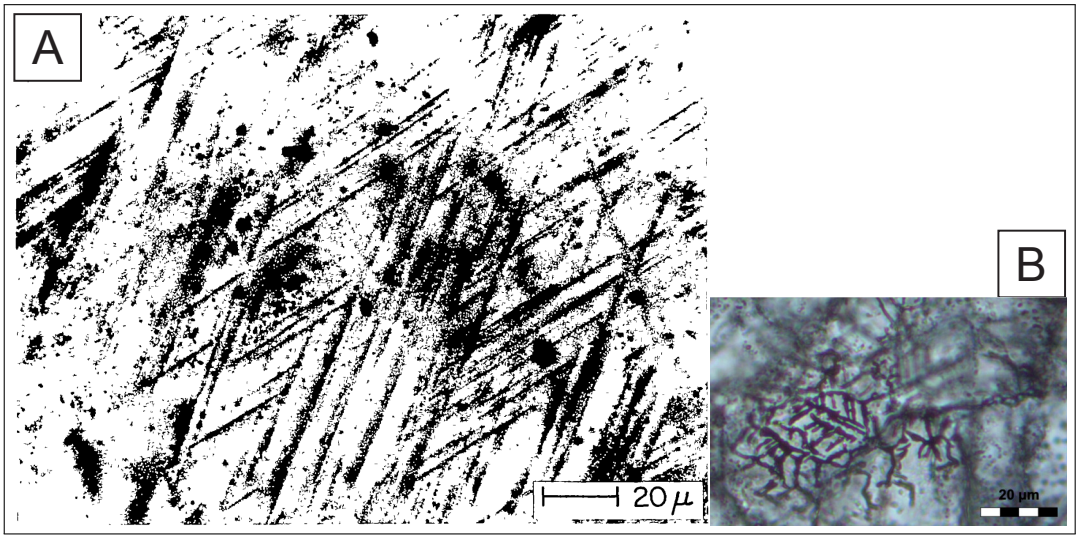

Figure 8.14 – (A) Figure 17 in Stöffler and Langenhorst (1994): "Decorated PDFs parallel to $\{10\bar{1}3\}$ in quartz of a gneiss clast (sample S 379) from the suevite of Zipplingen, Ries crater, Germany, plane polarised light [...]." – (B) Reproduction of Figure 6.19 with decorated enigmatic planar features.

which suggests that mixing was advanced.

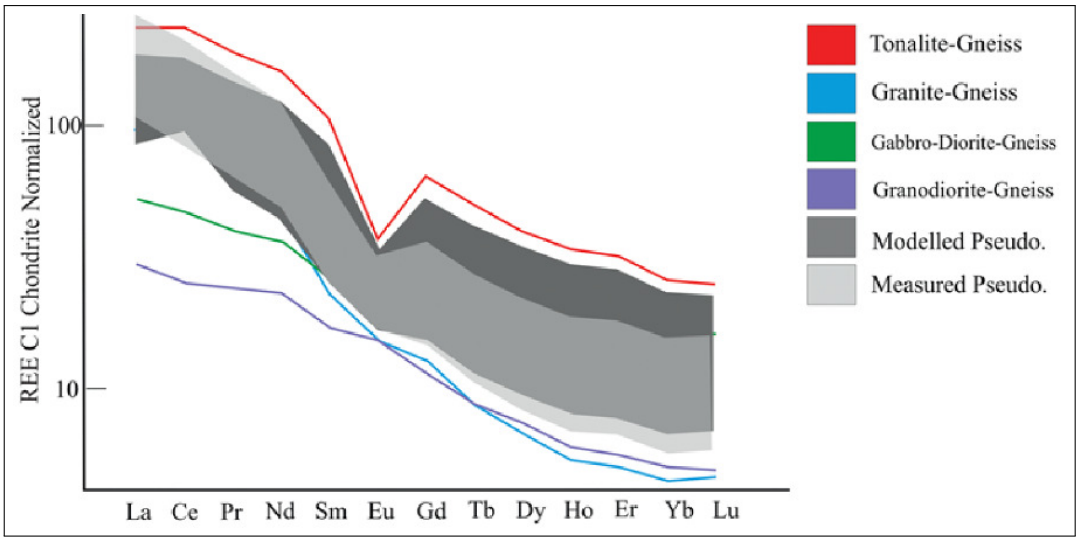

Figure 8.15 – Figure 7b in O'Callaghan and Osinski (2019): "Rare earth element chondrite-normalized diagrams (Sun and McDonough, 1989) of the host lithologies, with the shaded areas representing the measured pseudotachylyte samples and modelled pseudotachylytes produced by the mixing model. [...]". Sample from Borve Peninsula on Barra, approximately 3 km South of Àird Ghrèin.

The pseudotachylytes were also not affected by the later intrusion of the dykes of the minor intrusives. The dykes are on a mixing line between the Picrite and the Lewisian Gneiss (Figure 7.7), which suggests that there was no interaction with surface water. This indicates that the intrusion of the dykes around 60 Ma occurred well below the surface and probably not sub-oceanic, or at least not in contact with sea water. That implies that Barra was still buried at the time of dyke intrusion and major uplift and erosion took place between the beginning of the Paleogene and now.

To the author's knowledge, no analyses of elements have been published to date on the pseudotachylytes on Barra that suggest a meteoritic component, such as the siderophile Ni, Co, Cr, Au, or the platinum group elements (Ru, Rh, Pd, Os, Ir, and Pt) (French and Koeberl, 2010). These elements would not be expected to be found in pseudotachylytes generated at impact structures, but of rocks melted directly by the impact (Chapter 2). These impact melt breccias may visually resemble pseudotachylyte breccias, however their matrix has formed as a shock melt and may contain a meteoritic component (e.g. Dressler and Reimold, 2004). Meteoritic elements (e.g. elevated Ni/Cr), shock-induced micro structures (PDFs), and the shock-pressure mineral reidite have been found in the Stac Fada member of the Stoer Group on the Scottish mainland (Reddy et al., 2015) which is interpreted as an impact ejecta layer (Amor et al., 2008, 2019). The Stac Fada member has been dated at 1177 ± 5 Ma (Parnell et al., 2011) and has previously been interpreted as a volcanoclastic layer (e.g. Young, 2002) which is still favoured by some authors (Osinski et al., 2011). The Stac Fada member is discussed in more detail in Section 8.4.

8.2.5 Volume

It has been shown in Chapters 4 to 6 and above in Section 8.1 that the extent of deformation, and the amount of pseudotachylyte on Àird Ghrèin is pervasive and ubiquitous. The quasi-conglomerates make up a considerable amount of the rock mass on the headland (up to 14% of the mapped surface area), and are thicker than even the largest of the documented tectonic occurrences of pseudotachylyte at the Woodroffe thrust in Australia (pers. comm. N. Mancktelow, 2015). The amount of pseudotachylyte matrix present on Àird Ghrèin cannot be explained by melt produced by frictional heating which is limited to smaller veins (Melosh, 2005).

8.3 Revisiting Pseudotachylyte Generation Processes

Since MacCulloch's journeys along the West coast of Scotland in the late 19th century, when the 'flinty crush rock' of the Outer Hebrides were first described (Jehu and Craig, 1924), our understanding of 'pseudotachylytes' has progressed

significantly. One of the questions which is still debated is whether large pseudotachylyte bodies form by a different process than the thinner, 'tectonic' pseudotachylytes, or whether the processes are fundamentally the same.

Large volumes, that is pseudotachylyte bodies over 50 centimetres thick that appear to have formed during one continuous event are rare (Sibson and Toy, 2006). The literature search resulted in a handful of occurrences apart from the quasi-conglomerates on the Outer Hebrides: the Vredefort pseudotachylyte type locality (Shand, 1916; Reimold and Gibson, 2005), the Sudbury Breccia (e.g. Thompson and Spray, 1996; Rousell et al., 2003), the Ivrea pseudotachylytes in the Alps (Techmer et al., 1992; Garde et al., 2015), the Woodroffe Thrust pseudotachylytes (Camacho et al., 1995; Lin et al., 2005) and the pseudotachylytes from the Tertiary East Greenland volcanic rifted margin (Karson et al., 1998; Curewitz and Karson, 1999). The first two are associated with the two largest impact structures on Earth and are unique in both size and extent of pseudotachylytes. From the very limited information given in some of the literature, Vredefort and Sudbury appear to be the only other reported occurrences where metre-thick pseudotachylyte bodies can be followed over tens or hundreds of metres, as they are at Àird Ghrèin.

The distinguishing element between pseudotachylytes and other rock types that demonstrate outcrop-scale features such as injection veins and rounded clasts in a matrix, such as ultracataclasites, is the type of matrix. Whereas ultracataclasites have a cataclastic matrix (which may or may not have recrystallised), an additional process is at work for the formation of pseudotachylytes. The process has been described as explosive (Shand, 1916), but more often as melting (e.g. Sibson, 1975) and is most commonly ascribed to the heat production caused by frictional displacement, with cataclasis being an essential precursor (e.g. Spray, 1987, 1995). There seems to be consensus about the formation of the pseudotachylyte geometries that record a shear displacement along a fault, i.e. the classic 'single jerk' pseudotachylyte (Di Toro and Pennacchioni, 2005) which provide evidence for seismic slip (Cowan, 1999), and their associated injection veins which are thought to act as a sink for the matrix produced on the shear interface (Rowe et al., 2012). It is the pseudotachylyte geometries which lack the evidence for shear interfaces that represent the enigma. The 'friction melt' pseudotachylytes are commonly referred to as 'tectonic' pseudotachylytes – in contrast to 'impact' pseudotachylytes. Thanks to Sibson (1975)'s seminal publication, the Outer Hebrides has become the type locality for friction melt or tectonic pseudotachylytes, an association implicitly hinted to by numerous papers and explicitly stated by O'Callaghan and Osinski (2019). This, however, has led to the conclusion that large volumes of pseudotachylytes are not unique to impact settings, because they occur also in major fault zones – referring to Sibson (1975) and the OHFZ (e.g. French, 1998). This results in the circular argument that the large pseu-

dotachylytes, specifically the quasi-conglomerates on the Outer Hebrides, do not present an impact criterion, because large pseudotachylytes occur also in tectonic environments, that is, in the OHFZ.

There are three main hypotheses of the process of formation of pseudotachylytes: friction melting, seismic shaking and decompression melting (including other formation processes only available during impact cratering). It is worth briefly revisiting these processes to unravel the origin of the Barra pseudotachylytes.

8.3.1 Frictional Melting

In the recent literature, it seems established that frictional melting on faults and shear zones is the predominant process of formation of 'tectonic' pseudotachylyte (e.g. Spray, 1995; Mitchell et al., 2016. The process requires a frictional contact and a shear displacement along that contact. A displacement (slip) velocity in the order of 1 m/s is sufficient to produce melt (Sibson, 1975; Spray, 1992; Niemeijer et al., 2011). The classical geometry of these friction melt pseudotachylytes is shown in Figure 8.16. In theory, pseudotachylytes produced by frictional melting should not exceed a thickness of 1 cm (McKenzie and Brune, 1972), and it has been found that in nature most pseudotachylytes are thinner than 5 cm (literature compilation in Sibson and Toy, 2006). 'Tectonic' pseudotachylytes commonly show a finite displacement (e.g. Sibson, 1975), which has been used in calculations of earthquake source parameters (e.g. Sibson, 1975; Di Toro et al., 2005, 2009 and referencess therein; Campbell et al., 2020b). However, finite displacement might not equal total displacement if the slip is not unidirectional. In a series of experiments with granite rocks on a linear friction welding apparatus Spray (2016) finds that melting may occur by oscillatory slip, in absence of finite displacement. Spray (2016) also noted that in addition to the central melting zone, a "subsurface comminution / fractured zone" formed on either side. Comminution in the form of cataclasis is an important precursor for friction melting (Spray, 1992, 1995, 2010). In that sense, both cataclasis and melting processes are active to a varying degree in pseudotachylyte formation (e.g. Wenk et al., 2000). By definition, the geometry of quasi-conglomerates is different to the one shown in Figure 8.16 (Chapter 2 and 4), and their thickness exceeds the frictional melt limit of both theory and field observations. Sibson (1975)'s original idea of quasi-conglomerate formation is a progressive shear displacement on two bridging faults, where a dilatational jug acts as a sink for the melt from the pseudotachylyte generation plane (e.g. Curewitz and Karson, 1999). The viscosity required for a melt transport of 1 metre is equivalent to the viscosity of fresh motor oil (Melosh, 2005), which is unlikely even in the absence of clasts and fragments. Thus, the 'tectonic pseudotachylyte' sense of a frictional melting during shear displacement along a fault is highly unlikely to be the process of formation of

the quasi-conglomerates on Barra, due to their size and lack of evidence for shear displacement.

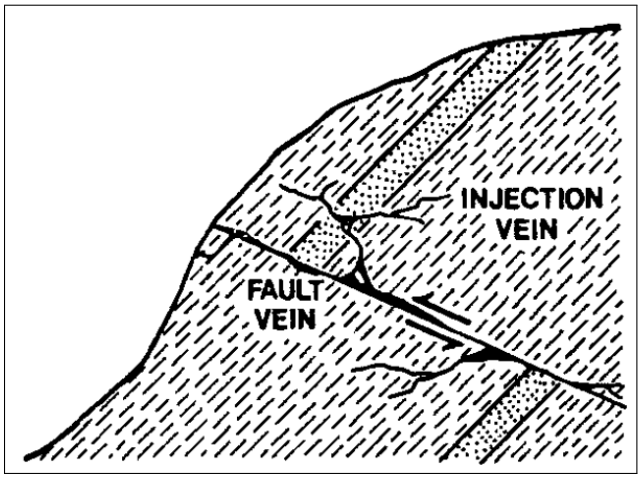

Figure 8.16 – Figure 2a in Sibson (1975) – sketch of the classic 'single jerk' pseudotachylyte geometry of a fault vein with displacement and injection veins.

8.3.2 Seismic Shaking

The process of seismic shaking is based on the theory by Melosh (1979, 1996) on acoustic fluidisation. The theory suggests that acoustic waves (high frequency seismic waves with a wavelength of metres or less) are scattered and preserved in a damaged fault zone of up to 20 m thickness (Melosh, 1996). The pressure wave may exceed the overburden (or ambient) pressure and allow for movement on an otherwise 'sticky' fault (Melosh and Ivanov, 1999). This behaviour of the material resembles a Bingham fluid, i.e. a non-linear rheology (Melosh and Ivanov, 1999), which means up to a certain yield stress, the material behaves like a rigid body, whereas above the yield stress the behaviour is that of a viscous fluid. Brune et al. (1993) perform laboratory experiments of stick-slip movements on foam rubber blocks. They suggest that dynamic fluctuations of the normal stress on a fault may be responsible for slip. Their observations indicate significant vibrations normal to the interface, causing separation during slip. Numerical modelling results by Ben-Zion (2001), shown in Figure 8.17, illustrate particle velocities at a given time for a rupture (thick black line) along a horizontal material interface with the rupture propagating to the right. The arrows indicate particle velocities in the material resulting in a dilatational stress field at the rupture front on the right, the source of the (pressure) wave, and compression on the left, rear end of the rupture. This process creates a tensional stress field in the material represented in the upper left quadrant of the image. If the tensional stress exceeds the tensional strength of the material, dilatational failure occurs in situ, at a

distance from the fault (Mitchell et al., 2011). The approaches of Melosh (1979, 1996) on one hand and Brune et al. (1993) and Ben-Zion (2001) on the other hand differ in terms of the location of the source of the pressure waves with respect to the damage zone, and whether such a damage zone is pre-existing or not. They share however the commonality of an oscillating pressure wave which results in a dynamic tensional stress field significantly reducing the normal stress.

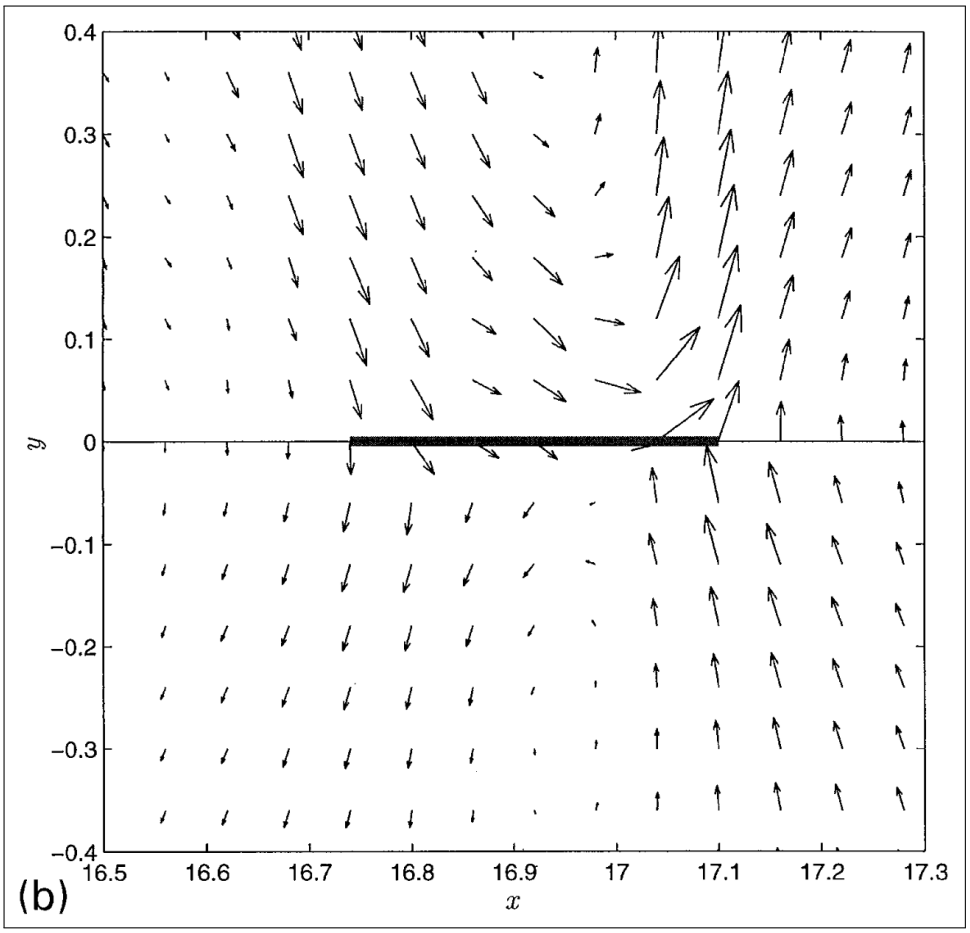

Figure 8.17 – Figure 5b in Ben-Zion (2001) – "Particle velocities at a given time for rupture along a material interface [...]. The slipping region is marked by the thick segment on the fault and is propagating to the right. The existence of a material contrast across the fault produces an asymmetric motion in the different media [...]."

Coseismic in situ cataclasis along active faults, but at a distance to the fault and not due to fault movements themselves, has been reported for a number of faults. These 'off-fault' zones of deformation which resulted in zones of pulverised rock are known for example from the San Andreas Fault (Dor et al., 2006; Wechsler et al., 2011), the Arima–Takatsuki tectonic line in Japan (Mitchell et al., 2011),

the Borcola Pass fault zone in the Italian southern Alps (Fondriest et al., 2012), and the Insubric line in the Alps (Garde et al., 2015). Pulverisation occurs in the absence of shear displacements within a few hundred metres of the faults. Garde et al. (2015) propose that the pseudotachylytes of the Ivrea-Verbano Zone have formed in the same manner alongside cataclasites near the Insubric line. Garde et al. (2015) suggest that the high-frequency, near-source seismic waves radiated during an earthquake may be responsible for the damage, as these "waves exert a series of rapid, in-situ, deviatoric stresses comprising compression, tension and torsion". High frequency seismic waves are strongly attenuated and scattered (Kanamori and Rivera, 2006). The attenuation of the waves means their energy is translated into damage and heat (Garde and Klausen, 2016). Rock failure causes non-linear attenuation of seismic waves (Roten et al., 2014; Sleep, 2014; Sleep and Erickson, 2014). Mitchell et al. (2011) conclude that their observations of pulverised rocks in a damage zone of up to 200 m wide – which generally lack significant shear strain, grain fragment rotation, wear and rounding of fragments – suggest that the rocks have shattered in situ, and that the protolith was subjected to strong tensional stresses.

Table 8.3 lists observations which have been used to described pseudotachylytes in quasi-conglomerate geometry by Garde et al. (2015); Garde and Klausen (2016), and in this study. The process of formation of pseudotachylytes (quasi-conglomerates) in the Ivrea-Verbano Zone (Garde et al., 2015) and the Vredefort impact structure (Garde and Klausen, 2016) has been interpreted to be seismic shaking.

Observations	*Garde et al. (2015) and/or Garde and Klausen (2016)*	*this study*
MICRO STRUCTURES		
Cataclastic deformation and comminution predominantly in situ and by pure shear	x	x
Simple (or general) shear subordinate and localised	x	x
Pseudotachylyte matrix represents and may display a gradual transition: intense microcataclasis of solid – fluidised material – fluid	x	x
Pseudotachylyte matrix may display flow structures	x	x
Mineral dependent deformation process: brittle, plastic, melting	x	x
Contact between host or clast may appear sharp in the field and hand specimen but gradational in microstructural detail	x	x
Round fragments of feldspar and the absence of biotite in the comminuted parts	x	x
Wide variety of micro structures		x
MESO STRUCTURES		
Intense and pervasive brittle microdeformation in all internal clasts and wall rocks, including rocks which in the field and under a hand lens appear to be little affected by such deformation	x	x
Intimate relationship between dendritic fracture network in host rock and pseudotachylytes	x	x
Blocks suspended in ultracataclastic or pseudotachylyte matrix and/or fracture systems	x	x
Progressive cataclasis of floating blocks	x	x
Size reduction of clasts, rounding and comminution ('jigsaw pieces' too small)	x	x
Larger amount of pseudotachylyte material where lithic blocks are more processed by rounding and size reduction	x	x
Sometimes rotation of clasts	x	x
Absence of chilled margins	x	x
Absence of significant displacement of the wall rocks along bounding fractures or other fractures, i.e. absence of faulting	x	x
Interior of clasts commonly intensely affected by arrested microcataclasis, which is difficult to see at outcrop scale	x	x
Clast families exhibiting rounded exterior and more angular interior margins	x	x
Matrix mostly produced in situ and not injected	x	x
Injection veins occur, but volumetrically insignificant, and over short distances	x	x

Table 8.3 – Observations which characterise pseudotachylytes in quasi-conglomerate geometry by Garde et al. (2015), Garde and Klausen (2016), and this study.

Seismic shaking occurs during earthquakes from slip on a fault, and as part of the impact cratering process after the passage of the shock and rarefaction waves. A significant difference between the two geological settings is the type of failure. An earthquake is characterised by slip on a fault plane, producing shear waves and pressure waves, whereas impacts, much like explosions, radiate compression waves which are theoretically isotropic (e.g. Lowrie, 2006). In forensic seismics, these characteristics are used to discriminate explosions from naturally occurring earthquakes (e.g. Walter, 2009). Earthquakes and impacts (or explosions) exhibit distinct source type characteristics, reflected in the seismic waves they radiate, which can be expressed in terms of shear component (T) and volume change component (k) in a Hudson source type plot (Hudson et al., 1989), Figure 8.18. The diagram is split into three zones divided by the dotted lines, representing explosions (or impacts), earthquakes and implosions (Figure 8.19).

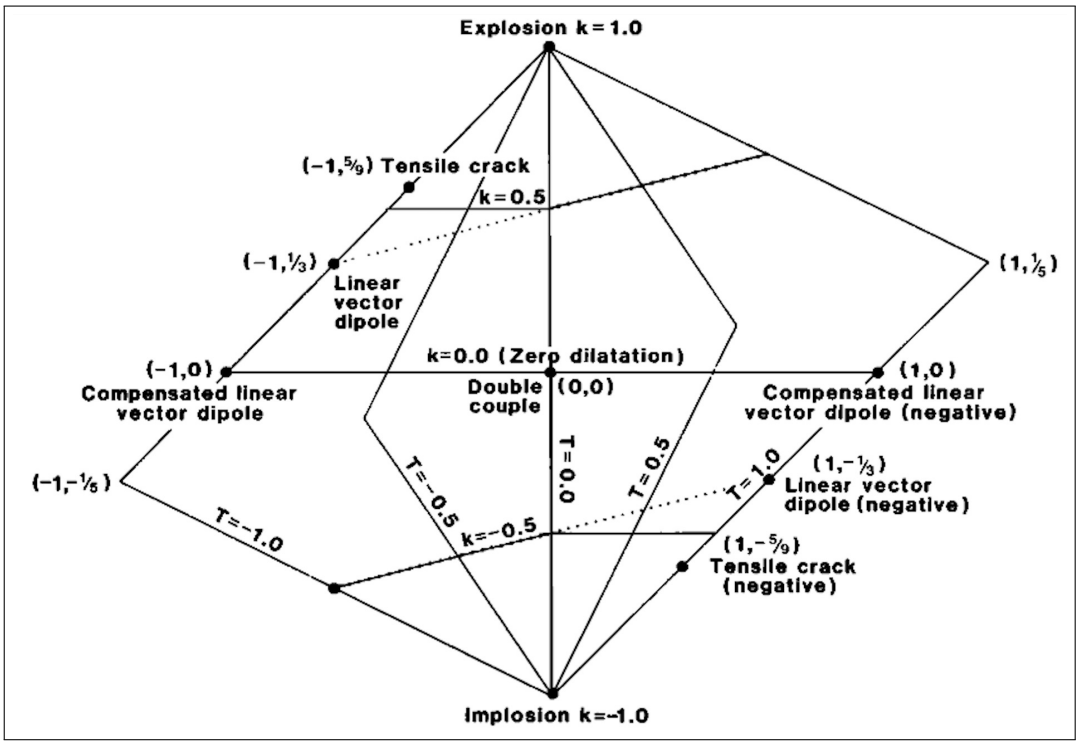

Figure 8.18 – Figure 3 in Hudson et al. (1989) "Equal-area source type plot, showing key points and the positions of key source types in terms of (T, k) coordinates. The dotted lines denote the zone within which modal surfaces exist in the P wave radition pattern. Outside this zone, P radiation is all of the same polarity: positive and negative in the upper and lower regions, respectively."

A tectonic fault type pseudotachylyte which records a single slip during an earthquake (e.g. Di Toro et al., 2005) should record deformation that plots in the central part of the diagram, (i.e. little or no volume change). Garde et al.

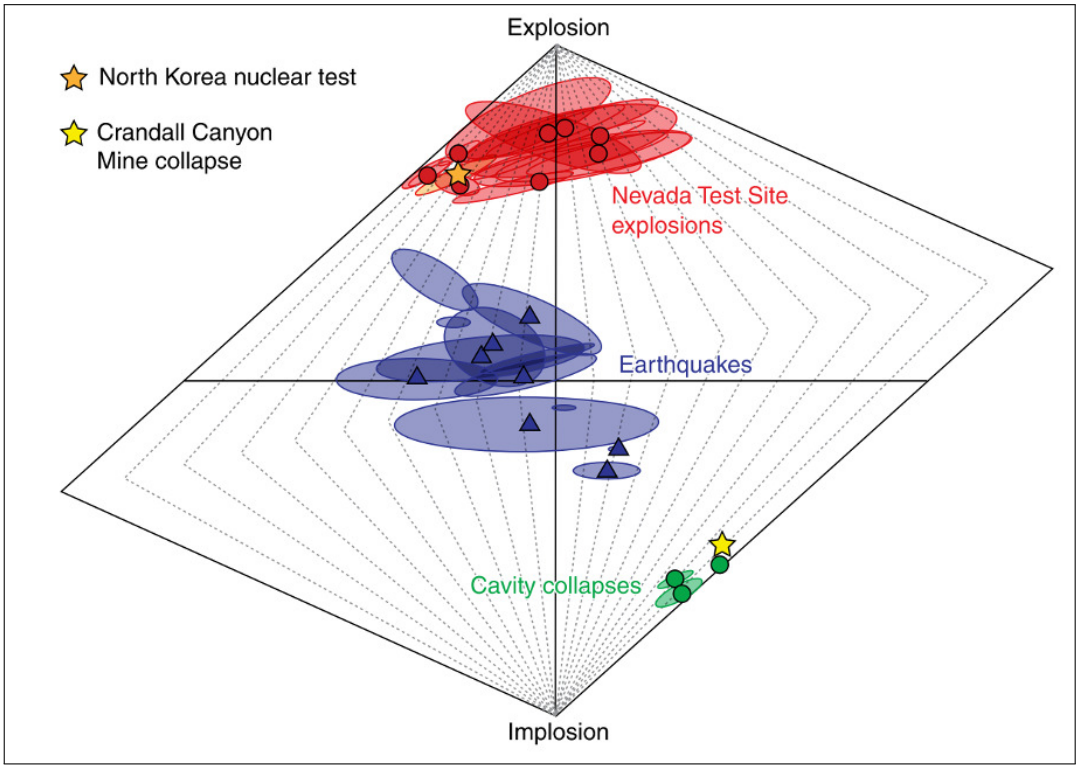

Figure 8.19 – Figure in Walter (2009) – Example of a source type plot showing data plotting in the three different regions (which are separated by dotted lines in Figure 8.18).

(2015) argue that the pure shear deformation constituting the shear geometry of off-fault pseudotachylytes, such as the ones of the Ivrea-Verbano zone, can be explained by oscillations caused by seismic waves radiated from slip on a fault, as at a distance to the fault the seismicity can be approximated by a wave front. The authors emphasise the validity and occurrence of ordinary shear zones in the area, which suggests an overall general shear setting, i.e. features of both pure and simple shear. Figure 8.19 shows for the examples Walter (2009) plotted that indeed the earthquakes yield a volume change component, i.e. not all of them are situated on the horizontal line.

The shear geometry caused by explosions or impacts is isotropic and pure shear and the volume change intrinsic ($k \neq 0$). These events plot on the apices of the diagram. A geographical area with rocks recording predominantly dilatational, pure shear deformation, and with noted absence of shear displacement on slip surfaces, should therefore point towards an explosion, implosion or impact. An analysis of structures in this shear versus volume change space could potentially help unpick the two geological settings in the future.

8.3.3 Pseudotachylyte Formation as Part of the Impact Cratering Process: Decompression Melting, Shock Melting and Impact Melt Pooling

According to e.g. Reimold et al. (2017), there are two different kinds of decompression melting that have been proposed that can only occur in impact structures. Melting due to decompression immediately after shock compression is sometimes referred to as 'shock compression melting'. Decompression melting upon the formation and collapse of the central uplift in larger impact structures has been advocated for Vredefort by Mohr-Westheide and Reimold (2011); Reimold and Koeberl (2014); Reimold et al. (2017). The process is explained in Figure 8.20 and follows the same principles as decompression melting on a mid-oceanic ridge, for example. Garde and Klausen (2018) argue that the process would not be fast enough to produce the amount of pseudotachylyte seen in the Vredefort dome.

Lafrance and Kamber (2010) state that the origin of the Sudbury Breccia "is widely attributed either to shock melting and cataclasis during propagation of an impact shock wave, or to frictional melting and cataclasis during large slip displacements along crater collapse superfaults". The first process of shock melting is, like Reimold's decompression melting, limited to the shocked volume of the rock and might be what Dressler and Reimold (2004) called 'flash replacement melting'. However, the shocked volume is generally limited to the central uplift of a large impact structure (see distribution of shock metamorphic features, later in Section 8.4.5, e.g. Figure 8.37, and also Spray and Thompson, 1995), and thus cannot explain pseudotachylyte occurrence outwith the shocked volume. Spray (1997)'s superfault hypothesis was based on remote observations from extra-terrestrial impact craters and proposed to be responsible for the annular occurrence of pseudotachylyte rich zones in the Sudbury impact structure. The required displacement of hundreds of metres on these superfaults has however not been demonstrated anywhere on Earth to date. It should be noted that in the light of Spray (2016)'s experimental results of oscillatory friction (with a significant total displacement, however lacking finite displacement, see Section 8.3.1), and potentially in combination with seismic shaking, the superfault hypothesis could explain the localisation of deformation. Last but not least it has been proposed that the pseudotachylyte matrix is impact melt (the melt that forms due to the impact shock at the contact to the projectile) which has intruded into the brecciated crater floor Riller et al. (2010); Lieger et al. (2011). A (trace) component of indicative meteoric elements could therefore be expected.

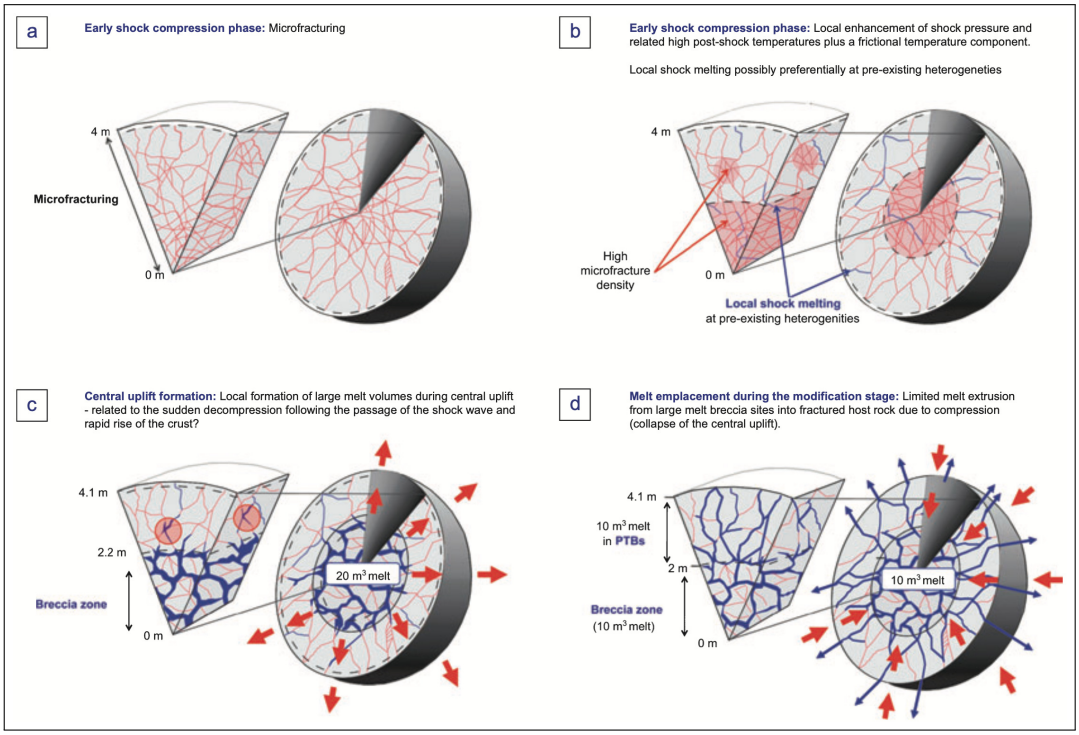

Figure 8.20 – Figure 6 in Mohr-Westheide and Reimold (2011) explaining their interpretation of 'Decompression Melting'. PTB stands for pseudotachylitic breccia, a term used in that research group for pseudotachylytes which cannot be explained by frictional melting. "a–d) Schematic half-sphere model for illustrating hypothetical PTB formation during different stages of impact cratering (see Chapter 2). a) Contact / compression stage; microfracturing, cataclasis, and b) generation of shock veins. c) Excavation stage; formation of massive melt breccias by decompression melting. Red arrows indicate dilation. d) Modification stage; emplacement of centimeter-wide injection veins off larger breccia zones / veins. Blue arrows indicate direction of melt flow in response to contraction, which, in turn, is schematically indicated by red arrows."

8.4 Likely Origin of Barra Pseudotachylytes

The above sections have shown that there is a genuinely 'vast' amount of pseudotachylyte s.s. on the Àird Ghrèin headland on Barra (Section 8.1). The occurrence of quasi-conglomerates is unlike 'tectonic' pseudotachylytes and resembles in its expression on the micro scale and on the meso scale the quasi conglomerates found in the two largest impact structures currently known and exposed on Earth, the Vredefort and the Sudbury impact structures (Section 8.2). Section 8.3 describes and discusses the processes which have been proposed for pseudotachylyte formation. The following sections discuss some aspects of the formation of the quasi-conglomerates on Barra, the likely process of formation, and investigate if they could have formed during an exogenic impact event, rather than during an endogenic tectonic event.

8.4.1 The Amount of Energy

A simple calculation gives a rough estimate of how much energy it would take to melt 1% of the total volume of Àird Ghrèin – the (conservative) amount of pseudotachylyte s.s. (Section 8.1). The following equations and most numerical values are based on Wenk et al. (2000). The amount of energy E_m required to melt a unit mass of rock is

$$E_m = (C_p \Delta T + H)\rho V \tag{8.4}$$

where C_p is the specific heat at constant pressure, ΔT is the difference between the melting temperature and the ambient temperature, H is the heat of fusion, ρ is the density and V the volume of rock. It should be noted that the values in brackets in Equation 8.4 are all based on equilibrium measurements, whereas the formation of pseudotachylytes is a non-equilibrium process. Assuming a ΔT of $1000°C$, $C_p = 800\,J\,kg^{-1}\,°C^{-1}$, $H = 7 * 10^5 J\,kg^{-1}$, and $\rho = 2800\,kg\,m^{-3}$. The volume V is calculated by the area covered on Àird Ghrèin ($1\,km^2 = 10^6\,m^2$) multiplied by the elevation (approximately 100 m) and multiplied by 1% (representing the results of the calculations from Section 8.1) yielding $V = 10^6 * 10^2 * 0.01 = 10^6\,m^3$. This volume calculation assumes that the pseudotachylyte area percentage calculated in Section 8.1 is representative for the volume percentage. In their calculations, Wenk et al. (2000) do not state explicitly how they arrive at the volume from their measured pseudotachylyte areas, and it seems the same assumption has been made (a similar approach seems to be used by Reimold et al., 2017). This results in a melting energy required to melt the pseudotachylyte volume on Àird Ghrèin of $E_m = 4.2 * 10^{15}\,J$. A smaller temperature difference, e.g. $\Delta T = 500°C$ would result in $E_m = 2.1 * 10^{15}\,J$.

Melt energies of the order of $10^{15}\,J$ are the same order of magnitude as that released in a magnitude 7 earthquake (British Geological Survey), yet a magnitude 7 earthquake typically extends over a rupture area of 1000 km^2 (e.g. Konstantinou, 2014). If this calculation is correct, then the same amount of energy has been concentrated in an area 3 orders of magnitude smaller. In comparison, $10^{15}\,J$ is comparable to 10% of the impact energy of a 100 m diameter rocky asteroid after entering the atmosphere (calculated using the web-based software *ImpactEarth!* by Collins et al., 2005). There is little evidence for the Barra pseudotachylytes having being generated in multiple episodes. While this does not prove that the entire volume was generated in a single event, these calculations show that if they had been, the energies required must have been similar to those in an impact event rather than an earthquake. An alternative way of looking at it is that if the pseudotachylytes had been generated in multiple earthquakes, they would have been generated in 31 magnitude 6 earthquakes or 1000 magnitude 5 earthquakes.

Moment Magnitude	*name / location*	*year*	*approx. rupture duration*
7.6	Chi-Chi, Taiwan	1999	30 s
7.9	Denali, Alaska	2002	70 s
8.3	Tokachi-oki, Japan	2003	40 s

Table 8.4 – Moment magnitude and rupture duration for three very large earthquakes.

If that was the case it seems strange that no evidence of cross cutting relations are observed.

8.4.2 Duration of Event: Earthquake Rupture vs. Impact Seismicity

Mitchell et al. (2011) propose that the repeated occurrence (several but separate events) of ruptures on a bimaterial interface, such as shown in Figure 8.17, characterised by strong dynamic reduction of normal stress and at the same time high strain rates, are likely to produce pulverised rocks as observed as off-fault damage zones. The rupture duration is the time during which seismic waves are produced and it gives an indication of the time available for the formation of and the deformation in the fault and damage zone. The duration of an earthquake rupture depends on several factors, but three examples published in Olson and Allen (2005) provide an order of magnitude for very large earthquakes:

The duration of an impact cratering event is largely dominated by the duration of the modification stage which is the stage after the passage of the shock wave. Melosh and Ivanov (1999) calculate the timescale for a final impact crater diameter range of 10 to 100 km is 10-30 seconds as a lower limit (if the material was strengthless). They suggest the upper limit is the time it takes for the impact melt to solidify, which is in the order of several minutes. Numerical modelling by Ivanov (2005) comes to the same conclusion – an example of a 100 km diameter final crater takes just over 5 minutes. The modification stage is characterised by the collapse of the transient cavity and therefore large scale movement of rock masses. During this stage, seismic waves are continued to be radiated, scattered, and produced. The duration scales with the size of the transient cavity and thus the size of the final crater diameter. This means that the formation of the Vredefort impact crater, and the formation of the Sudbury impact crater, both over 100 km diameter, are likely to have taken longer than 5 minutes. Comparing the duration of an earthquake with the duration of an impact cratering event shows that the large impact cratering events take in the order of several minutes, whereas the rupture of large earthquakes takes in the order of a minute or less.

In quasi-conglomerate type pseudotachylytes, there is evidence for a progressive and iterative development with the following elements (Lafrance and Kamber, 2010; Garde and Klausen, 2016), which can be divided into two groups of three:

- Fracturing
- Cataclasis
- Comminution

- Abrasion
- Block/clast rotation
- Frictional melting

The second three elements require relative and independent movement of rock fragments, which can only occur following the first three. Pulverised rocks on the other hand show evidence only for the first three (e.g. Dor et al., 2006). The progressive deformation observed in quasi-conglomerate type pseudotachylytes requires a seismically active time span during which the intense, high frequency oscillations and high strain rates are maintained. As shown above, the modification stage of impact cratering provides a relatively long sustained setting for seismic shaking. Smaller occurrences of 'off-fault' pseudotachylyte, i.e. smaller quasi-conglomerates such as those described by Garde et al. (2015), are likely to occur also during earthquakes. It should be noted that not only does the duration of the events differ in the two geological settings, but also other factors, such as the source of the energy, the amount of energy dissipated, the way the energy is translated, the kind of strain at the source, and the strain rate, some of which will be discussed below.

8.4.3 Seismic Shaking – is it shaken?

The observations which have been interpreted to indicate seismic shaking and have been compiled from the literature and listed under Section 8.3.2 match the observations made in this study (Table 8.3). In fact, seismic shaking is the only one of the proposed processes that does not contradict any of the observations – such as the lack of shear displacement, the absence of faults, or the size of the quasi-conglomerates.

Thus, the most likely process of formation for the quasi-conglomerates on Barra is seismic shaking due to energy input from an impact event. It should be noted that Francis and Sibson (1973) previously stated that the pseudotachylytes on Àird Ghrèin seem to be parallel in strike but not on the fault plane of the OHFZ, and the question was raised on whether the two could be associated or not.

Furthermore, this study supports the suggestion that seismic shaking could be responsible for the formation of other off-fault pseudotachylytes (e.g. Garde and Klausen, 2016, 2018).

In tectonic settings, seismic shaking produces pulverised rocks (Section 8.3.2), or cataclasites with subordinate pseudotachylytes (Garde et al., 2015) adjacent to but outwith fault zones. The size of the individual pseudotachylytes of the Ivrea-Verbano zone is not stated by Garde et al. (2015), however judging from the text and the field photographs, the occurrences are in the range of centimetres to decimetres, and from field observations from the authors own field trip to the site in 2006 the area covered about 1-2 square metres at most. The pseudotachylytes on Barra are undoubtedly larger than the ones in the Ivrea-Verbano zone. The quasi-conglomerates of Barra share many similarities with the Vredefort pseudotachylytes and the Sudbury breccias (e.g. Section 8.2). The total area of quasi-conglomerate outcrops seems to be larger in the two documented impact structures, however with field data from one square kilometre from one island, constrained in part by the island locality, significant uncertainty remains as to the maximum extent of the Barra pseudotachylytes. These two comparatively well documented cases are the two largest impact structures known and exposed on the current land surfaces, and it could be expected that the size and total volume of quasi-conglomerates would scale with the size of an impact crater, as the pseudotachylyte volume is thought to scale with the earthquake magnitude (e.g. Wenk et al., 2000).

8.4.4 Quasi-Conglomerates and Similar Breccias in Impact Structures

Large occurrences of pseudotachylytes, i.e. quasi-conglomerate geometry are not common and are only documented for the two largest exposed impact structures, in Sudbury and Vredefort. Reimold (1995) note that: "Even in large impact structures, such as the 100 km Manicouagan, the 17 km Lappajiirvi, and the 24 km Ries structures, only small pseudotachylite veinlets have been recognized." The available data and study cases to compare to the quasi-conglomerates on Barra are therefore limited to two other localities. It should be noted that in the impact literature, the distinction between cataclastic and ultra-cataclastic breccias and pseudotachylytes is not always made. The term Sudbury Breccia for example explicitly contains all of the above (Reimold, 1995; Rousell et al., 2003; Grieve et al., 2008) and only a few authors make the distinction (e.g. Rousell et al., 2003). Even though this might be hindering some analyses, comparison and discussion, it is a useful approach in the field, and it bypasses the usage of genetically defined terms, such as the problematic definition of pseudotachylyte. Reimold (1998) observe that in the tectonic literature the term 'pseudotachylyte' is commonly used with a genetic definition of a friction melt process of formation and suggest the usage of the non-genetic term 'pseudotachylitic breccia'. The strong association

of cataclastic breccias with pseudotachylytes has been documented both in this study and in the literature (see sections above), and Rousell et al. (2003) suggested that the Sudbury Breccia pseudotachylytes may have formed in a similar manner to the clastic breccias, that is, possibly by acoustic fluidisation.

The impact related pseudotachylytes and breccias, that is pseudotachylytes which are not directly associated with a fault (i.e. pseudotachylitic breccias in some of the Vredefort literature, Reimold, 1998), are found to be parautochthonous. That means they are located within the impact structure and are part of the rock mass that has been subject to dislocation and movement, however not to ejection. Figure 8.21 gives an overview over the different rock units in a complex impact crater with central uplift. In a simplified approach, the parautochthonous rock mass experiences two directionally different movements. It moves outwards during the formation of the transient cavity (1. thrusting), and back towards the centre during the modification stage (2. normal faulting). The central uplift forms as part of the 'back towards the centre' movement with reverse faulting and subsequent normal faulting collapse

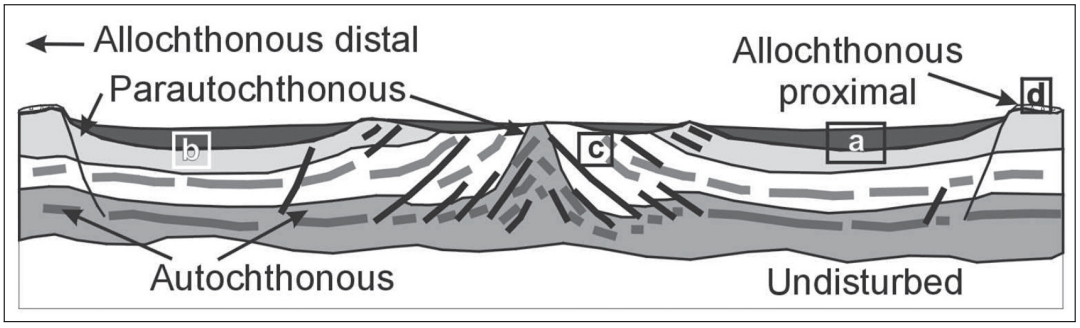

Figure 8.21 – Figure 7.2 in Grieve and Therriault (2013) – Schematic cross section of a complex crater showing their definition of allochthonous, parautochthonous and autochthonous rocks. Parautochthonous are all the rocks which have moved (and are therefore deformed), but have not left the crater.

Various studies approach the parautochthonous rock mass differently. From a numerical modelling point of view, a degree of homogeneity needs to be assumed, and some detail is lost due to constraints in terms of data volume. The concept of acoustic fluidisation and therefore seismic shaking has been found to be an important element to explain the reduced rock strength of the parautochthonous rock mass during the modification stage (Grieve et al., 2008; Ivanov, 2005). Gravitational forces alone are not able to explain the final structures. The vibrations allow the rock mass – on a crater scale with a grid spacing of several hundred metres (Ivanov, 2005) – to behave like a non-Newtonian viscous fluid (Melosh, 1996). Figure 8.22 shows a numerical model of the crater forming process of a

crater with 100 km diameter. The largest grid distortion occurs in the central region, in the area which eventually forms the central uplift, but the deformation towards the rim is also striking.

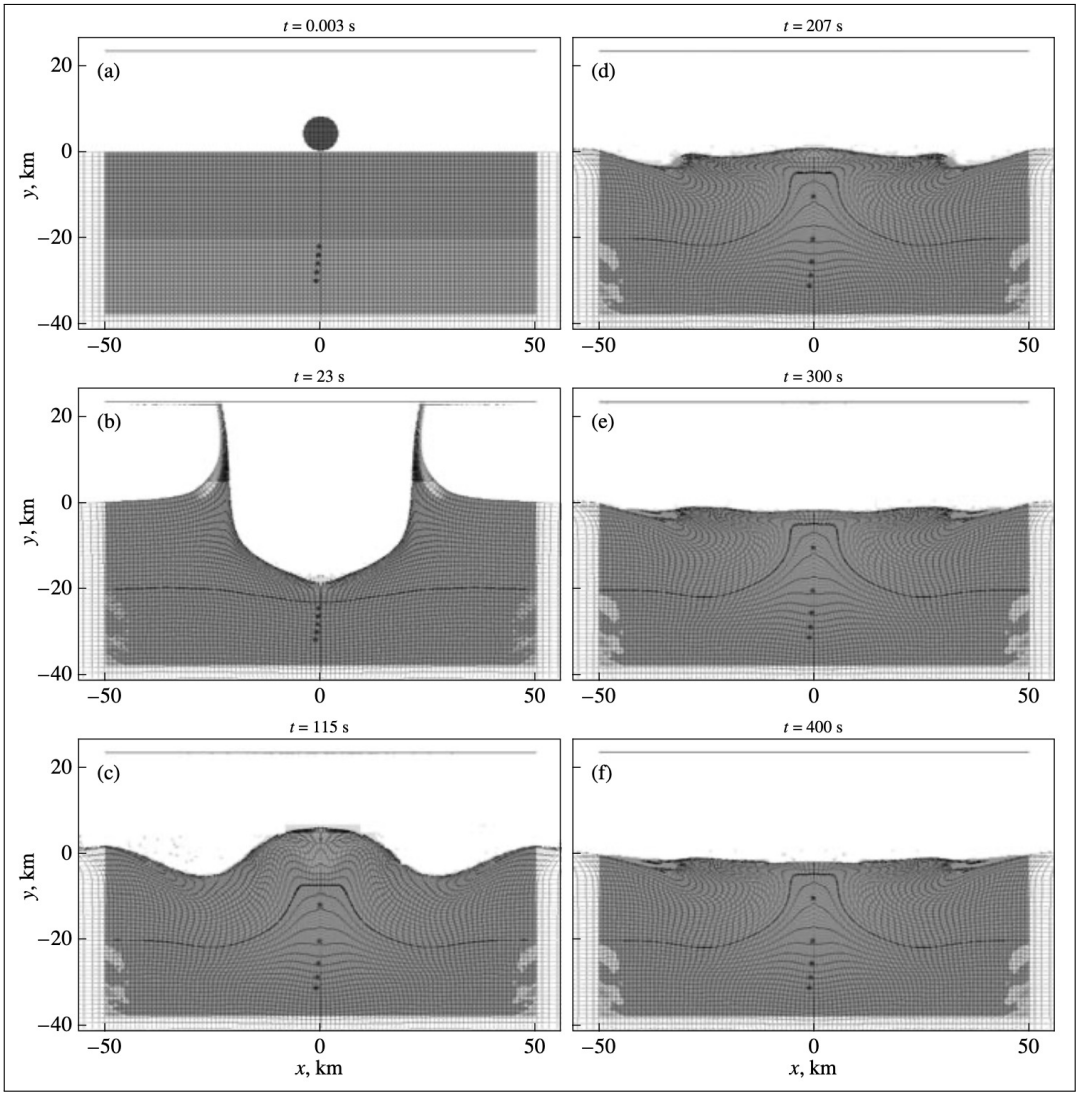

Figure 8.22 – Figure 6 in Ivanov (2005) – "Sequence of events during the formation of the model Popigai crater: (a) the initial positions of a spherical projectile and a layered target; (b) the 23th second: the transient cavity of the crater reaches its maximum depth of about 19 km; (c) the 115th second: the collapse of the transient cavity (the uplift of rocks in the center through the rim collapse) gives rise to a transient hill up to 5 km in height, the deep rocks under the crater rise above the level of their original burial; (d) the 200th second: the transient hill spreads in the field of gravity, while the deep rocks stop due to the restoration of normal internal friction, the speed of the near-surface spread reaches 200 m/s; (e) the 300th second (5 min after the impact): the motion is close to a stop; (f) 400 second after the impact: the crater assumes a stable final shape."

Grieve et al. (2008), in an approach combining field, seismic and borehole data from the three largest impact structures (Vredefort, Sudbury, Chicxulub) find that the parautochthonous rock mass moves in discrete packages of several kilometres in size. For Chicxulub, the seismic data suggests that these blocks would be in the order of 10 km near the rim and get progressively smaller towards the inner peak rim where they are approximately 5 km (Figure 8.23). Comparing this model to the numerical and geophysical solution presented by Ivanov (2005) in Figure 8.24, where the deformation appears strikingly more homogeneous. It appears that the deformation of the parautochthonous rock mass occurs in localised zones, however facilitating a homogeneous and pervasive deformation.

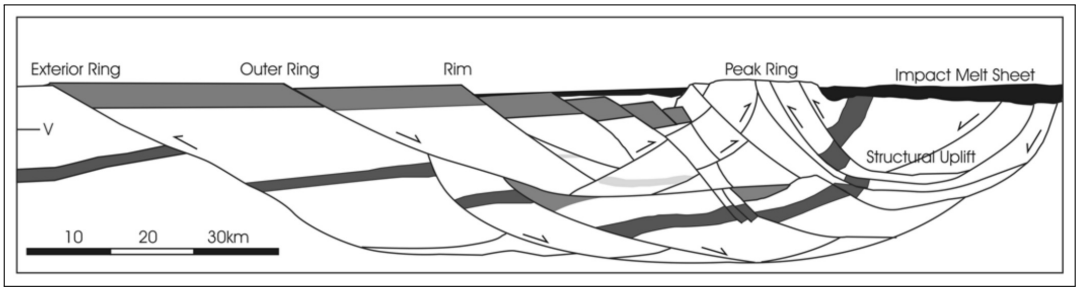

Figure 8.23 – Figure 16 in Grieve et al. (2008) – Schematic cross section: terrestrial ring basin, no vertical exaggeration. Combining data and observations from Vredefort, Sudbury and Chicxulub. 'V' indicates the implied current erosion level of the Vredefort impact structure. Note that the listric faults join at approximately 20 km depth.

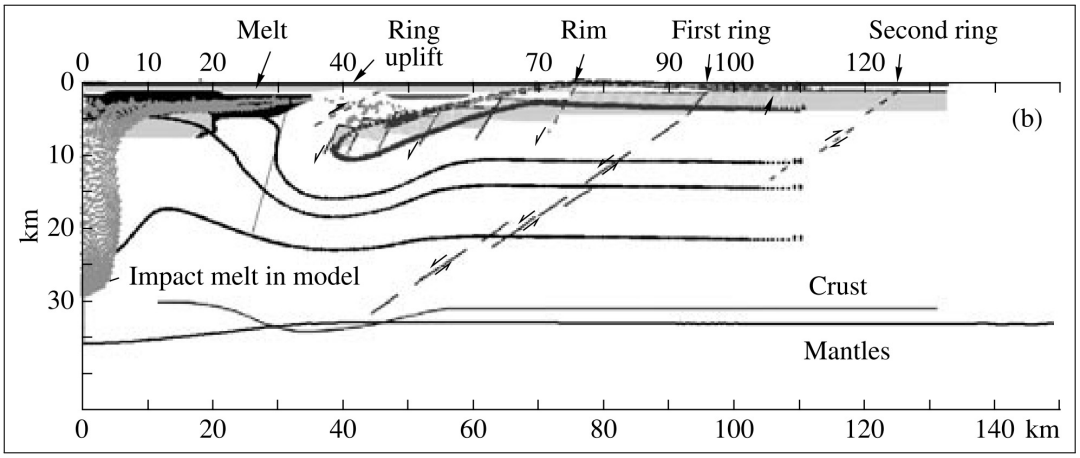

Figure 8.24 – Figure 9 in Ivanov (2005) Cross section of the Chicxulub modelled crater superimposed on a model constructed from geophysical data (Morgan et al., 1997; 2000). The solid lines at depths below 30 km indicate the crust–mantle boundary in the computation and on the geophysical profiles.

The parautochthonous rock mass deforms by directionally opposite movements, i.e. the initial outward thrusting is followed by the normal, inward faulting. The formation of the central uplift is part of the inward movement, which is followed by a collapse. It has been documented that in some cases, the deformation exploits structures that have formed during an earlier stage of the cratering process, both in the largest impact structures (Grieve et al., 2008; Lafrance and Kamber, 2010) and smaller complex craters (Osinski et al., 2005; references in Lafrance and Kamber, 2010). Figure 8.25 shows a schematic geological map of the Vredefort impact structure with the trace of some of these 'thrust faults' (Grieve et al., 2008) highlighted in red. The stars and blue lines represent pseudotachylyte occurrences as documented by Killick and Reimold (1990) and Lieger et al. (2009). The pseudotachylyte occurrences can be divided into the occurrences in the central uplift (circular structure in the bottom right of the map), and a SW-NE trending zone, roughly 30 km wide and extending over at least 150 km, which is situated towards the rim of the impact structure. The majority of the 'thrust faults' (red lines) are aligned and occur in this same zone.

For the Sudbury impact structure, it has been proposed that the pseudotachylytes and breccia are most abundant in concentric rings around the central Sudbury Basin and Sudbury Igneous Complex (SIC) (e.g. Thompson and Spray, 1996). The SIC represents the impact melt sheet. Figure 8.26 shows a map by Rousell et al. (2003) including data from the literature, showing Sudbury Breccia occurrences, and overlain inferred pseudotachylyte-rich zones by Thompson and Spray (1996). Rousell et al. (2003) note the difficulty in compiling the data from the literature because of the variations in exposure and the "uneven recording of Sudbury Breccia occurrences by various field geologist". The authors also record the challenge of quantifying the extent of the Sudbury Breccia from the local geological map on a scale of 1 : 50 000, where a substantially sized breccia body of 50 by 50 metres must be represented as a point.

The maps of both impact structures show to a larger or lesser extent the occurrence of metre sized pseudotachylytes or pseudotachylyte abundance in two zones. The inner circular zone can be attributed to a central uplift, and the outer zone is roughly between 50 and 100 km from the geometrical centre of the structure. In the Vredefort case, the outer zone falls together with a zone of deformation which records both outward and inward motion. In both localities, pseudotachylyte development is partly lithologically controlled (Fletcher and Reimold, 1989; Spray et al., 2004). The preferential occurrence of deformation zones and pseudotachylytes in specific lithologies has also been documented for fault zones (e.g. Garde et al., 2015; Mitchell et al., 2011).

In summary, seismic shaking is a viable process to form quasi-conglomerates or massive pseudotachylyte occurrences. The structural observations published

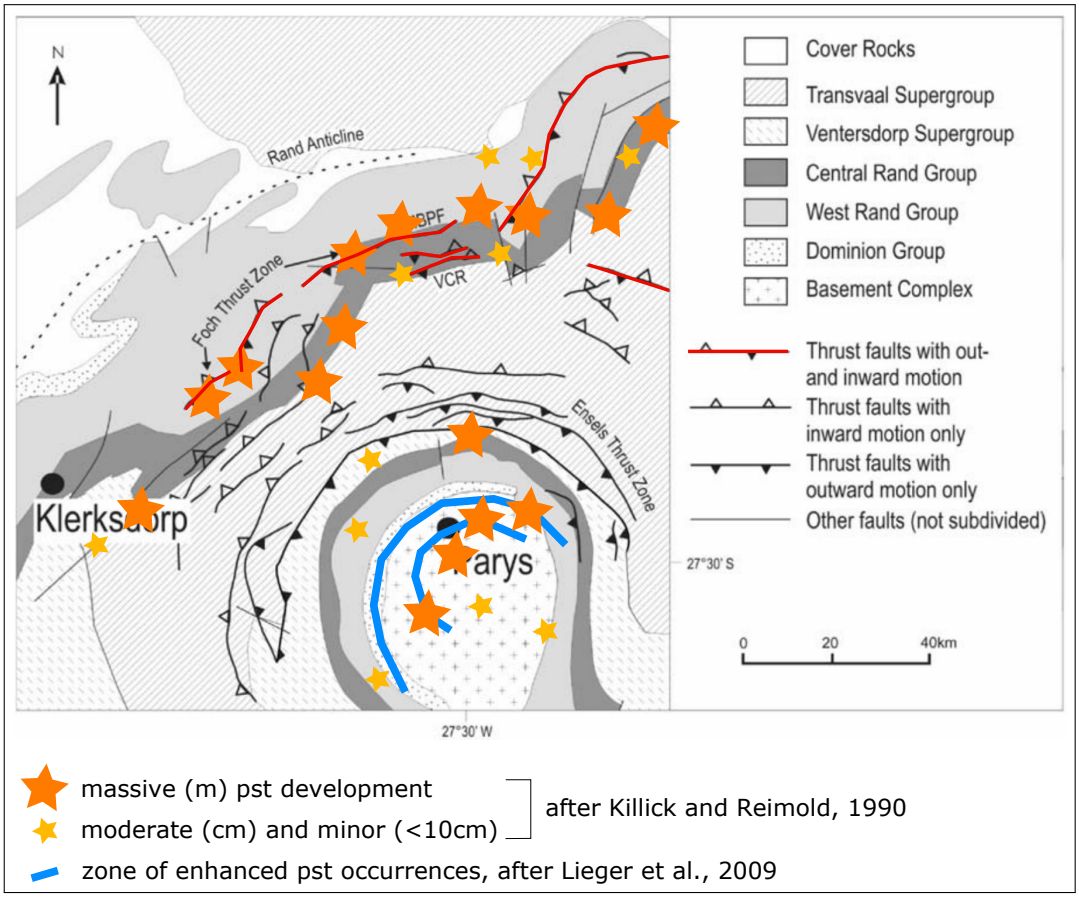

Figure 8.25 – Figure 3 in Grieve et al. (2008) of the Vredefort impact structure as base figure, with pseudotachylyte occurrence data added from Killick and Reimold (1990) (stars) and Lieger et al. (2009) (blue lines). The circular structure in the bottom right of the map is the Vredefort Dome (the central uplift), whereas the Rand Anticline is located towards the rim of the impact structure. Most of the thrust faults which record both outward and inward motion (highlighted in red) are roughly aligned in a SW-NE trending belt which extends over 100 km and is characterised by an abundance of pseudotachylyte occurrence. Note that the Transvaal Supergroup consists predominantly of sedimentary rock (Kröner and Hofmann, 2019), which may play a role for the distribution of pseudotachylyte occurrences.

in the literature in the context of seismic shaking match the observations from this study. It has been shown that where seismic shaking has been proposed as a formation mechanism of fault rocks, the deformation results in pulverised rocks, cataclasites and subordinated pseudotachylytes. The occurrences of impact related pseudotachylyte in Vredefort and Sudbury are more similar to the quasi-conglomerates on Barra than fault related pseudotachylytes. Acoustic fluidisation and seismic shaking have been proposed to be responsible for the formation of Sudbury breccias (Rousell et al., 2003) and the Vredefort pseudotachylytes (Garde and Klausen, 2016).

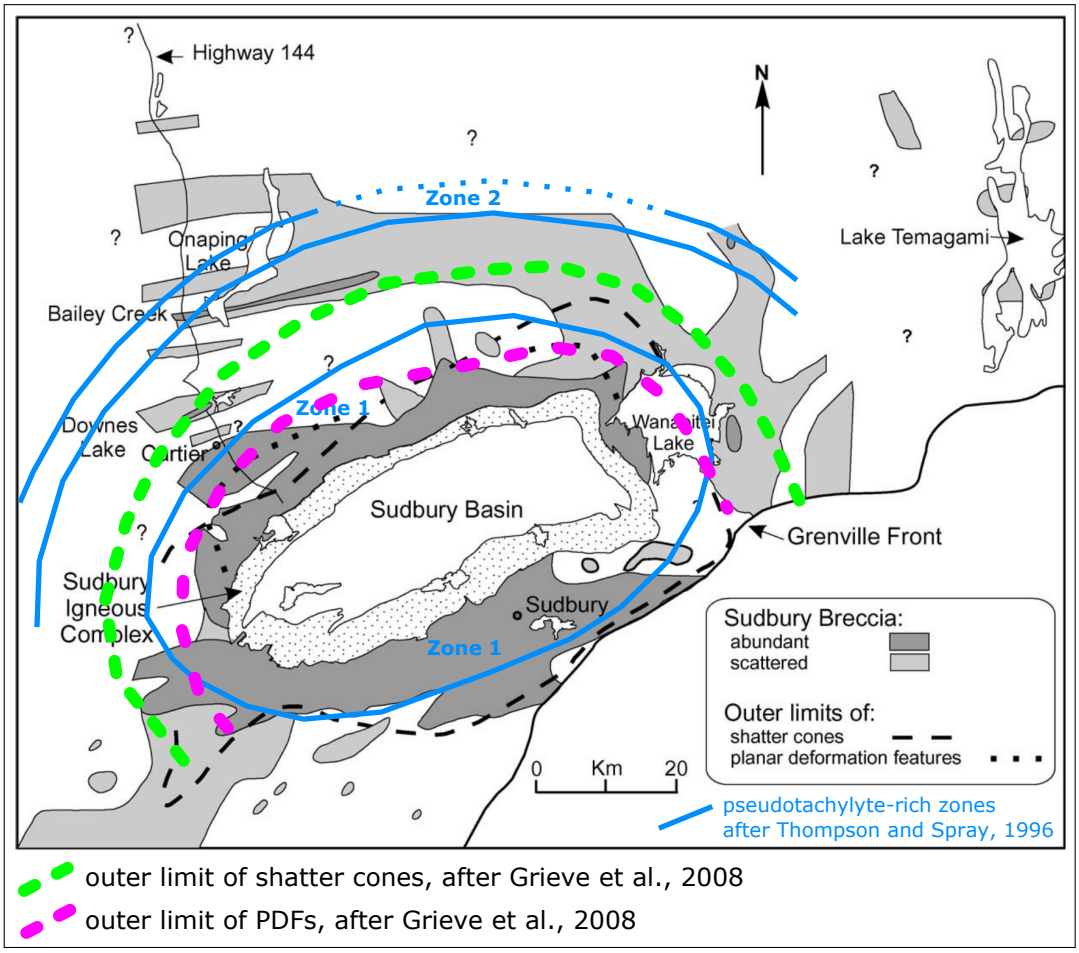

Figure 8.26 – Figure 6 in Rousell et al. (2003) of the Sudbury impact structure as base figure, showing the regional distribution of Sudbury Breccia. White areas with question marks indicated lack of data. Note the Sudbury Breccia encompasses both lithic breccias and pseudotachylyte. Overlain in blue are pseudotachylyte-rich zones as published in Thompson and Spray (1996). Zone 1 extends around the Sudbury Igneous Complex to the blue ellipse, Zone 2 is concentric to Zone 1 (and dashed where inferred due to their map's extent). The dashed pink and green lines are data from Grieve et al. (2008).

8.4.5 Barra Pseudotachylytes in the Wider Geographical Context

The quasi-conglomerates on Àird Ghrèin are in close vicinity to what is generally referred to as the (main) trace of the OHFZ on Barra. Figure 8.27 shows the pseudotachylyte occurrences on Barra and the trace of the OHFZ (Figure repeated from Chapter 4 for ease). Note that most publications omit the western 'branch' of the OHFZ on their maps (in recent publications only found in MacDonald and Goodenough, 2013). Some authors state that the pseudotachylytes on Àird Ghrèin are to be treated separately from the OHFZ (Francis and Sibson, 1973; Sibson, 1977b), whereas other authors explicitly (O'Callaghan and Osinski,

2019) or implicitly (Wenk, 1978; Sherlock et al., 2009) integrate them into their interpretation of the OHFZ. In the Outer Hebrides, quasi-conglomerates are not exclusively found on Àird Ghrèin on Barra. They have also been reported from South Uist and North Uist (Jehu and Craig, 1924; Francis and Sibson, 1973; Campbell, 2016) and smaller occurrences (a few decimetres) were seen e.g. on South Lewis (Seafort Head, NB 308 220). Campbell (2016) compiled data from the literature and her own observations from the field on pseudotachylyte occurrence for the entire island chain which is shown in Figure 8.28. Pseudotachylytes occur along the entire island chain of the Outer Hebrides.

What is mapped as the trace of the OHFZ is not defined by pseudotachylyte occurrence (compare Figure 8.27 and Figure 8.29). Kinny et al. (2005) note that the rocks of the footwall of the OHFZ show affinity with the gneisses in Eastern Greenland (Friend and Kinny, 2001) whereas the limited data of the hanging wall gneisses points to a relationship with the Lewisian of the mainland. This suggests that the OHFZ potentially formed during a time when Eastern Greenland and the NW of Scotland were in close proximity. Figure 8.30 shows a reconstruction for the late Proterozoic displaying the location of NW Scotland and Greenland and their position with regards to the Grenville belt. Greenland and NW Scotland were in a similar position with respect to each other again at the Iapetus suture during the Caledonian orogeny (Figure 8.31). Imber et al. (2002) argue that the Grenvillian events (commencing approx. 1250 Ma and active until 980 Ma) played a significant role for some of the geology of Northern Scotland, even though the evidence is sparse (Cliff and Rex, 1989). According to Cliff and Rex (1989), the South Harris Shear Zone was active around 1 Ga.

The deformation history of the OHFZ has been divided into two geographical sections (Northern and Southern Segment) and a variety of deformation episodes. A general summary of the deformation history was shown in Chapter 3. For its entire length, the OHFZ consists roughly of 1. Thrusting, 2. Pseudotachylyte formation, and 3. Extension and late Normal faulting. The ductile thrusting (mylonites) in the Northern Segment of the OHFZ (i.e. Harris and Lewis) is interpreted to have taken place either during the Laxfordian or Grenvillian (Imber et al., 2002). According to some authors, this deformation phase is absent on Barra (Butler et al., 1995; Imber et al., 2001, 2002; White and Glasser, 1987), whereas other authors have found evidence of the top-to-NW ductile thrusting (Macinnes et al., 2000; Osinski et al., 2001). The pseudotachylyte formation is part of the brittle deformation episode which is evident on the entire length of the OHFZ. The brittle episode has been divided into a first phase of either brittle thrusting followed by strike slip (Butler et al., 1995; Imber et al., 2001; **?**), or a mixed mode brittle event which records both compressional and extensional deformation (White and Glasser, 1987; Osinski et al., 2001), and a second phase of extension (including phyllonitisation), the latter predating the brittle normal

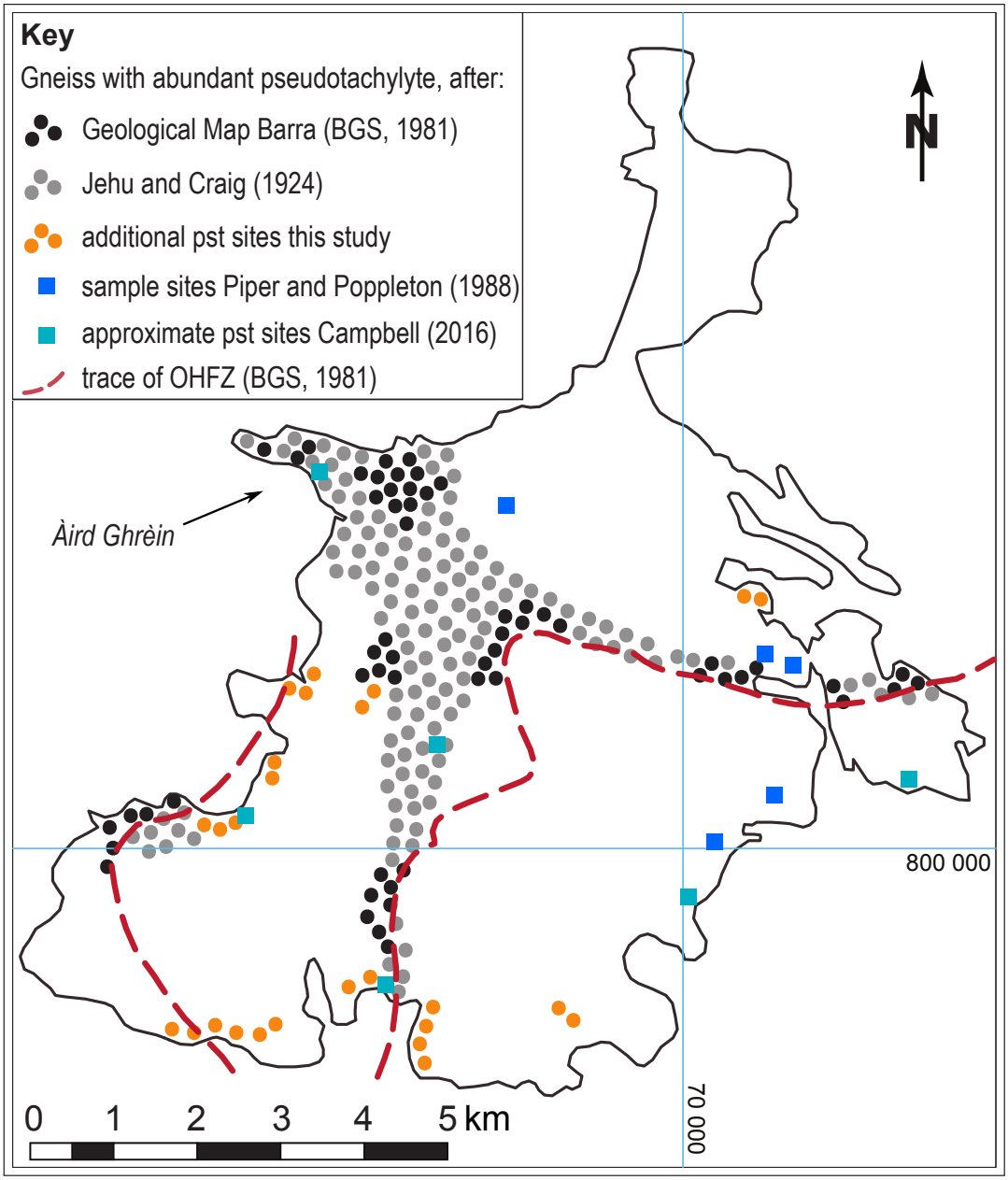

Figure 8.27 – Map of Barra with abundant pseudotachylyte occurrences in circles and pseudotachylyte (pst) sites after Piper and Poppleton (1988) and Campbell (2016) in squares. The trace of the OHFZ is from the Geological Map Barra (BGS, 1981). Note that most publications omit on their maps the western 'branch' of the OHFZ (in recent publications only presented in MacDonald and Goodenough, 2013) and show a map based on Francis and Sibson (1973) showing only the Eastern trace. What is commonly referred to as the 'foot wall' of the OHFZ therefore refers to W and N of the Eastern trace. Same figure shown in Chapter 4 and repeated here for convenience.

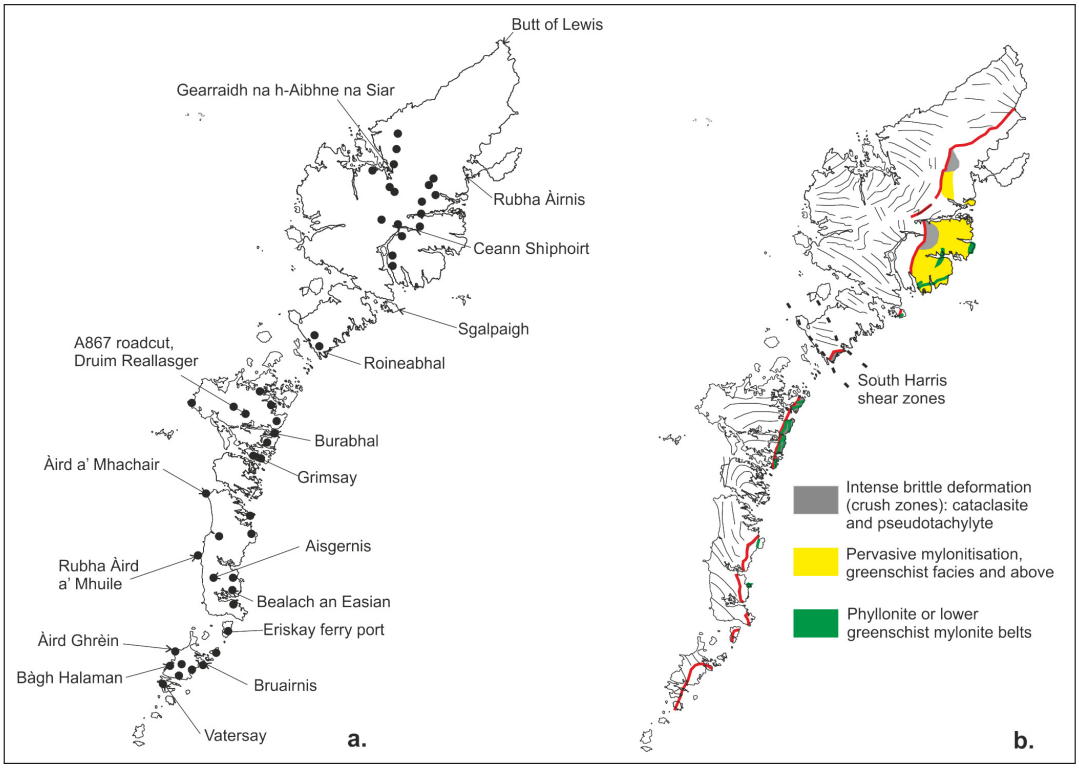

Figure 8.28 – Figure 2.3a in Campbell (2016) – Pseudotachylyte outcrops: a compilation of her own data and locations from the literature.

faulting of the Mesozoic. This brittle episode is commonly attributed to the Caledonian (e.g. Fossen, 2010), thanks to the geometrical parallelism to the Moine thrust which was initiated around 430 Ma ago (Holdsworth et al., 2007), and the interpretation of $^{40}Ar/^{39}Ar$ dating results by Kelley et al. (1994) (see discussion in Section 8.2.1 for the viability of this single date). The Caledonian deformation on the mainland is characterised by a top-to NW thrusting of imbricated nappes, some of which have Lewisian Gneiss slices incorporated (e.g. Butler and Coward, 1984). Both 'thin-skinned' (with a generally undisturbed basement foreland Coward, 1990), and 'thick-skinned' tectonic models have been proposed (Smythe, 1987), the latter involving the Lewisian basement to a deeper extent, and the OHFZ has been suggested as a Western Caledonian imbricate (Butler and Coward, 1984). Seismic profiles and sampling (Stein and Blundell, 1990) suggest that the oldest sediments in the Minch Basin – bound in the West by the OHFZ – are the Stoer group and / or Torrionian group, which implies that at least the initial extensional movements on the OHFZ would need to be of Grenvillian age or older (Smythe et al., 1982). The earliest extensional movements on the OHFZ are recorded as part of the brittle deformation episode which entails the pseudotachylyte formation, and unequivocally extensional deformation is attributed to

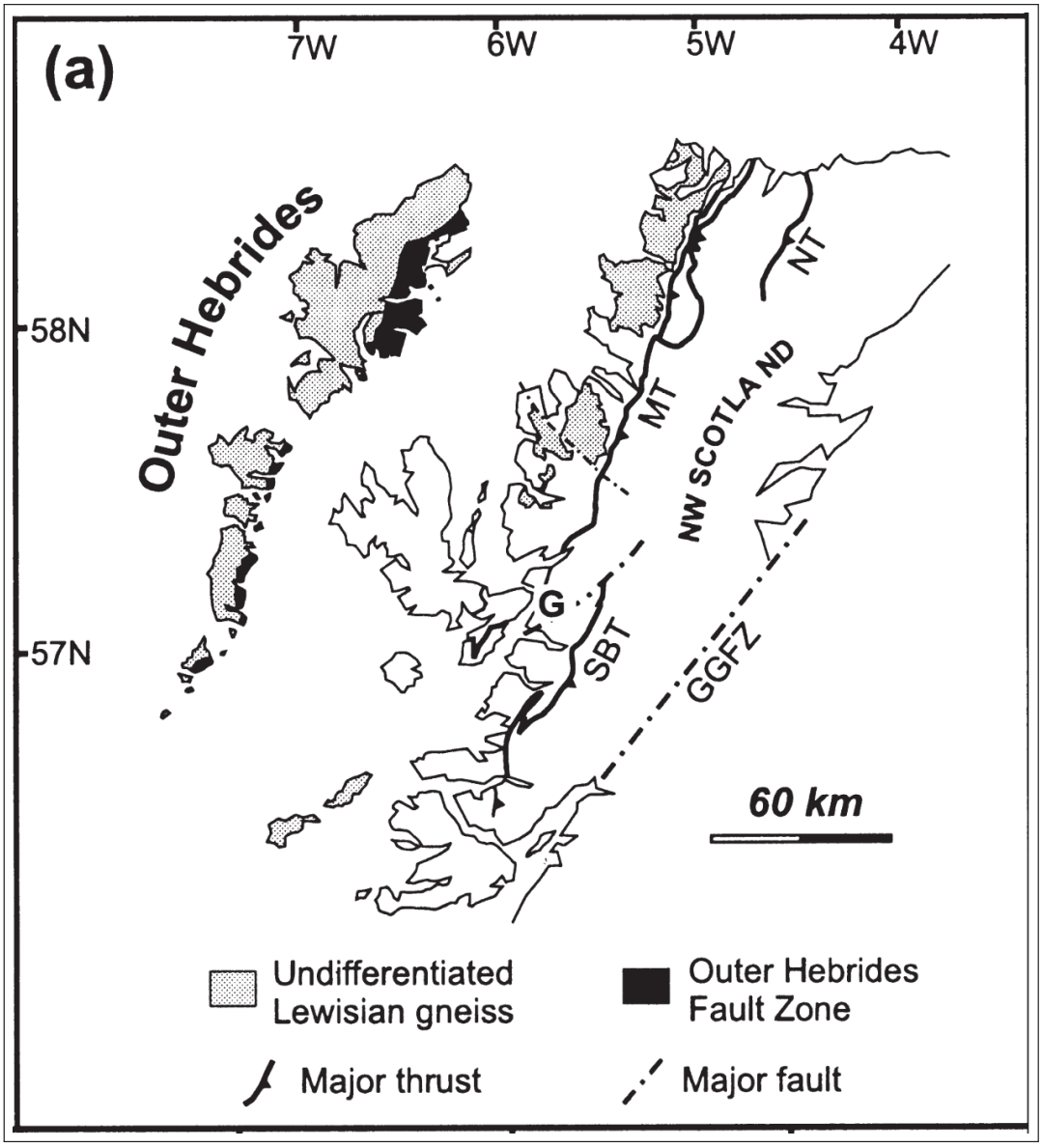

Figure 8.29 – Figure 1a in Imber et al. (2002) – Overview of NW Scotland showing the outcrops of Lewisian Gneiss in grey and the Outer Hebrides Fault Zone (OHFZ) in black.

the phyllonitisation (see above). It should be noted that offshore data records extensional offset only along the OHFZ (Smythe, 1987). Roberts and Holdsworth (1999) argue that the Minch Fault is responsible for the relative uplift of the Outer Hebrides in the Mesozoic and suggest that offshore 'reactivation' might not be more than spatial proximity of structures. Figure 8.32 shows a schematic cross section from the Outer Hebrides to the Great Glen Fault (GGF) during Jurassic times. The current sea level is thought to be 1-2 km below the indicated

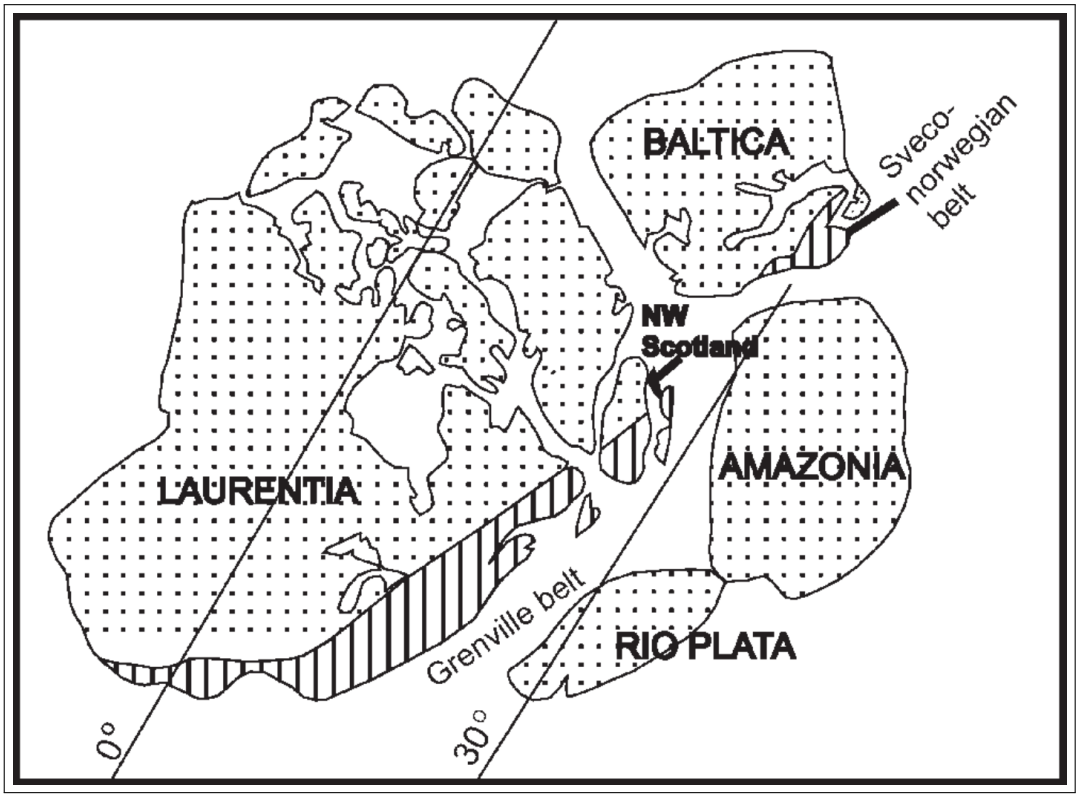

Figure 8.30 – Figure 1 in Sherlock et al. (2008) – Paleogeographic reconstruction for the Late Proterozoic showing the NW of Scotland and its position in the Grenville belt.

sea level.

MacDonald and Goodenough (2013), based on fieldwork on the gneisses on SE of Barra (in the 'hanging wall'), find that what Francis and Sibson (1973) interpreted as a synform is in fact a steep shear zone with a NW-SE trace which was active during the Inverian and Laxfordian. MacDonald and Goodenough (2013) suggest that this South Barra Shear Zone could be a terrane boundary and shows similarities to the Laxford Shear Zone in NW Scotland (located approximately 200 km NW of Barra). The Laxfordian events ended around 1.6 Ga and predate movements on the OHFZ (Imber et al., 2002). According to Piper (1992) and Butler et al. (1995), a sinistral strike slip event along the Minch Fault and parts of the OHFZ displaced the Outer Hebrides with respect to the mainland by approximately 100 km (Figure 8.33).

For the Outer Hebrides, a variety of depths of pseudotachylyte formation have been proposed. Sibson (1975) estimated by an empirical stress to friction relationship the formation of pseudotachylyte to have occurred at 4-5 km depth, however

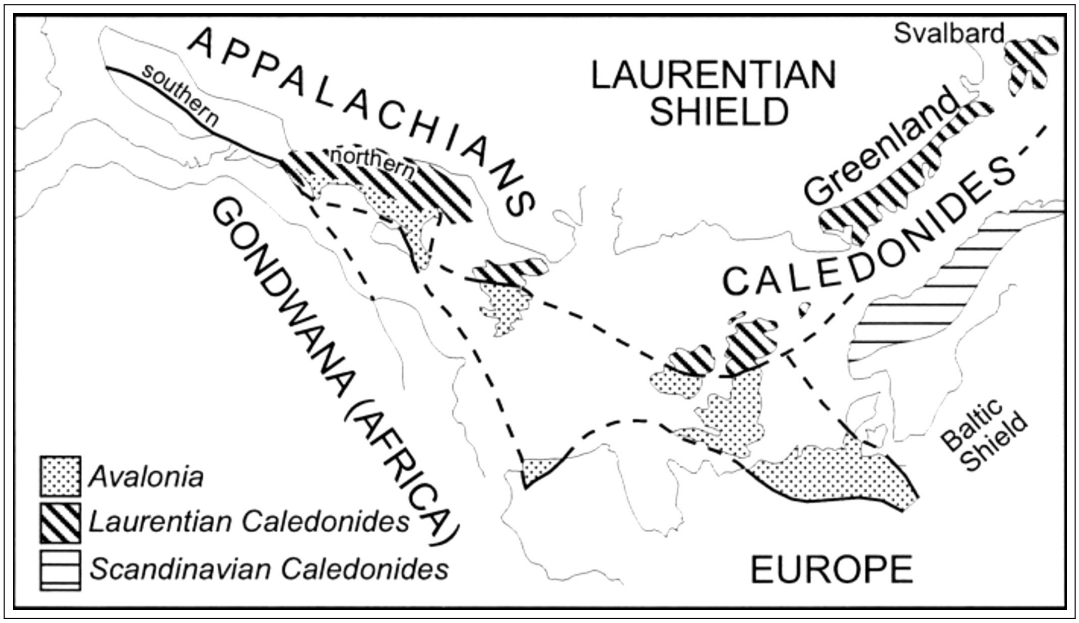

Figure 8.31 – Figure 1 in McKerrow et al. (2000) – Paleogeographic reconstruction for the Caledonian orogeny showing the NW of Scotland and its partake in the Caledonian belt together with Greenland.

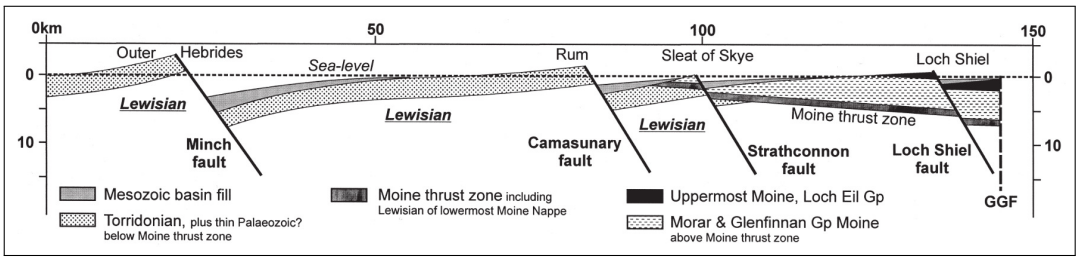

Figure 8.32 – Figure 2 in Roberts and Holdsworth (1999) – Jurassic time schematic cross section (current sea level is thought to be 1-2 km below indicated sea level) showing their interpretations of onshore observations and offshore data. According to Roberts and Holdsworth (1999) the Minch fault might be in close proximity to the OHFZ, however the authors question the reactivation of older structures.

revising his results later to 4-10 km and 17-25 km in their figure and 5-10 km and 20 ± 5 in the text (p. 161) without stating why (Sibson and Toy, 2006). White (1996) argue for higher lithostatic pressures which would suggest 18 km depth. Campbell (2016) proposes depths in the region of 12-15 km, but definitely more than 10 km. These results are based on geobarometry on amphibole-plagioclase compositions, with one sample giving a depth of 30 km. Campbell (2016) notes that the method is based on equilibrium crystallisation whereas primary crystallisation of pseudotachylytes represents a disequilibrium process. Roberts and

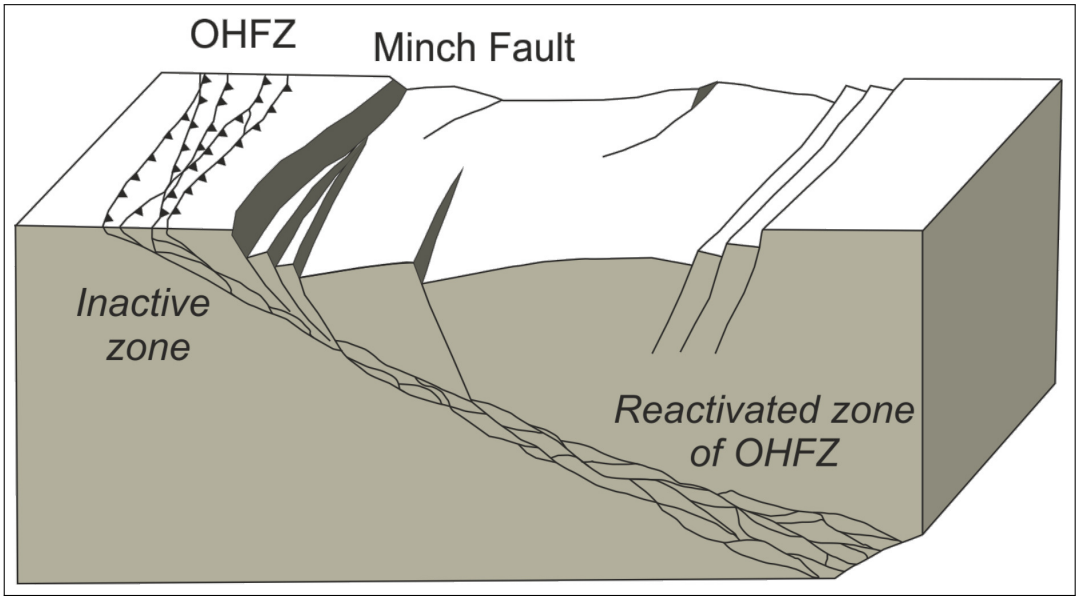

Figure 8.33 – Figure 2.5b in Campbell (2016), after Stein and Blundell (1990) – It has been suggested that the Minch Fault reactivated (mainly deeper situated) parts of the OHFZ as oblique sinistral normal faults (cf Roberts and Holdsworth (1999) and Figure 8.32). Based on seismic data interpretation.

Holdsworth (1999) suggest major uplift has taken place along the Mesozoic Minch fault.

In summary, the earliest extensional movements along the OHFZ complex which are recorded offshore in the Minch Basin are of mid to late Grenvillian age. The pseudotachylytes therefore must be older, and thus pre-Caledonian. The significance of the deformation along the exposed nearly 200 km long and 30 km wide OHFZ is evident and recorded in numerous publications, and at the same time its interpretation in a larger tectonic context remains largely enigmatic or speculative at best (e.g. Butler et al., 1995; Sherlock et al., 2009; MacDonald and Goodenough, 2013; Campbell, 2016; Campbell et al., 2020a).

The aforementioned sequence of movements on the OHFZ is: thrusting (though questioned by some, e.g. White and Glasser, 1987), brittle deformation recording a variety of modes – some authors claim a sequence of thrusting followed by extension – (this episode contains the pseudotachylytes), extensional low angle movements (phyllonitisation) and extensional normal faulting. As illustrated in Figure 8.34, crater formation imposes a dynamic stress field, which can be dissected into an initial (at the rim) outward / upward movement (thrusting), followed by an inward / downward motion ('extension'). The brittle episode of the OHFZ and its various expressions of modes of deformation and pseudotachylyte

formation, in absence of any significant tectonic event recorded in its vicinity, can readily be explained by an exogenic event, that is an impact of a large bolide. Apart from the questionable age dating interpretations (*cf* their validity in the context of larger scale structural evidence discussed in the above paragraphs), none of the results found in the literature fundamentally contradict the possibility that, at least some of the brittle aspects of the OHFZ, and thus the formation of the quasi-conglomerates, could be part of a large scale impact structure.

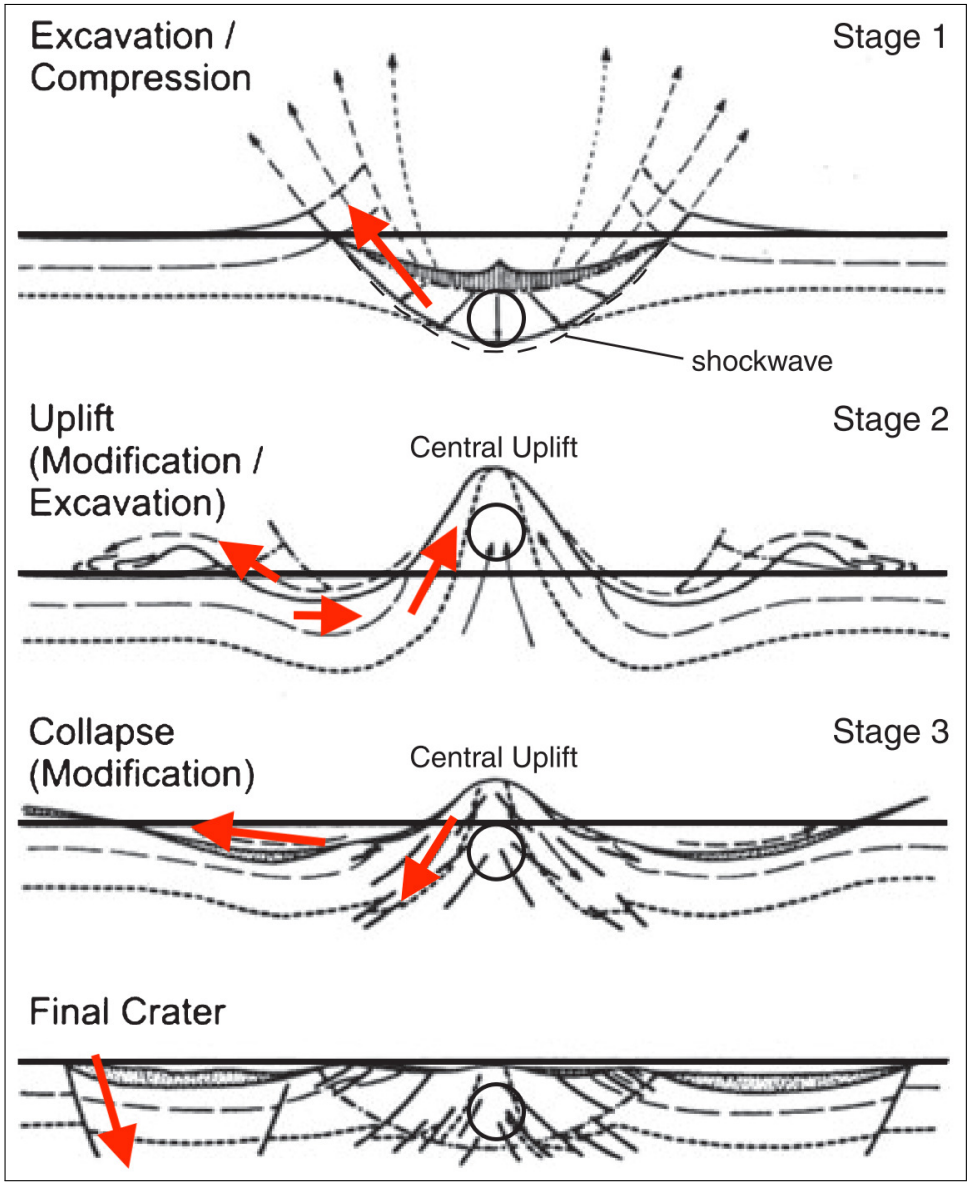

Figure 8.34 – Figure 7 in Mohr-Westheide and Reimold (2011), annotated with red arrows – Schematic illustration of the formation of a complex crater. The red arrows highlight flow direction on the left hand side of the sequence, i.e. where the geometries are represented that show similarities to a North facing W-E section of the OHFZ. Compare to Figure 8.32 and Figure 8.33.

8.4.6 Evidence for Impact

There is the possibility for the Barra quasi-conglomerates to be impact related. The following paragraphs aim to discuss this hypothetical case, summarising where in an impact structure the quasi-conglomerates would be situated and how the apparent lack of definite impact criteria such as shock metamorphic evidence can be supportive of this hypothesis. The current situation with regards to impact structures in Scotland is presented and the findings of this study set in its geographical and geochronological context.

To date (October 2020) in the UK there are no impact structures recognised by respected specialists (e.g. Reimold et al., 2016; Earth Impact Database). According to estimates combined from different approaches, French (1998) suggest that the frequency of impacts which create a crater of approximately 200 km diameter (such as the Sudbury, Vredefort or Chicxulub) for the whole Earth is 0.007 per Ma, which results in about 20 for 3 Ga which is approximately the age of the oldest rocks on Earth. For a crater diameter of 100 km this number goes up to 120 (these numbers are for illustration only). Most of those impact structures will have vanished from the Earth's surface due to erosion and plate tectonic processes. However, there is the likelihood that not all impact structures which (partially) survived have been discovered up to date. Hergarten and Kenkmann (2015) estimate that about 350 impact structures are yet to be discovered, however, they suggest that our record of impact structures with a diameter of over 6 km is complete.

The Stac Fada member, a sedimentary formation in the NW of Scotland formerly interpreted to be of volcanoclastic origin has in the past years been shown to contain multiple evidence of being impact related (Amor et al., 2008; Parnell et al., 2011; Simms, 2015; Amor et al., 2019). Amor et al. (2008) published evidence for an iridium anomaly, an extra-terrestrial chromium isotope signature and planar deformation features in quartz. Figure 8.35 shows the sites of Stac Fada member outcrops and the two proposed centres of its associated impact structure. One site is located near Lairg (Simms, 2015) and its locality founded on a gravity low in that area and interpretation of ejecta flow direction. The other site lies in the Minch Basin, and its location has been worked out based on the flow directions of the ejecta using several independent methods (Amor et al., 2019). On the map, the Outer Hebridean island chain has been moved roughly NNE for 100 km along a schematic Minch Fault (red dashed line), a paleogeographic reconstruction from the post-Laxfordian sinistral strike slip movement (Piper, 1992). The age of the Stac Fada member is 1177 ± 5 Ma (Parnell et al., 2011), confirming earlier dating with lower precision (Turnbull et al., 1996). The age of the impact would correlate well with the age constraints on the pseudotachylytes on the Outer Hebrides as outlined above (between post-Laxfordian and pre- to

early Grenvillian). Simms (2015) base their crater size estimate of approximately 50 km on the size of the gravity anomaly. (Amor et al., 2019) estimate the size of the final impact crater to be between 13 and 20 km, based on calculations involving the type of ejecta, its underlying layers, and its distance from the impact site. The suggested size of the impact in the Minch Basin is approximately 10 times smaller than other impact structures where quasi-conglomerates have been found. The blue circle in Figure 8.35 has a diameter of 100 km (about half the size of Vredefort and Sudbury) and contains all the islands on which quasi-conglomerates of over 1 m^2 have been documented (that is Barra, South Uist and North Uist). The circle overlaps with the impact site proposed by Amor et al. (2019), it is however 5 times larger and the proposed flow directions of the ejecta would not necessarily correlate.

The only definite impact diagnostic features which are not extra-terrestrial geochemical signatures or actual fragments of the projectile, are shock metamorphic features (e.g. Grieve, 1998). Circular structures and gravity or magnetic anomalies are not considered diagnostic (e.g. French and Koeberl, 2010). A more detailed account of this topic is given in Chapter 2. Extra-terrestrial material is expected in impact melts and ejecta, that is material which had been in contact with the projectile (French, 1998). The shock pressures experienced and recorded in impact structures depend on several factors such as the target lithologies or the angle at which the projectile hits the surface. Figure 8.36 shows the effect of the impact angle on the theoretical shock distribution illustrating the significant reduction of the shocked volume (A) and the peak shock pressure (B) at lower impact angles. It should also be pointed out that the depth to which the shock pressures extend strongly depends on the impact angle.

At relatively elevated shock pressures, diaplectic glass formation (Chapter 2) or high pressure polymorphs may be expected. Planar deformation features (PDFs) in quartz are found to form at 5-10 GPa or higher and are the most common impact diagnostic feature (Grieve, 1998). Shatter cones are the only mesoscopic impact features and form at shock pressures as low as 2-6 GPa (Grieve, 1998). They are best developed in fine grained and homogeneous lithologies such a carbonates and quartzites and are rare and poorly defined in coarser grained rocks such as granites (Dietz and Holden, 1972). Shatter cones are most often exposed in the eroded central uplift of complex impact structures (Grieve, 1998). Figure 8.37 shows a map of Vredefort with the outer limits of published occurrences of shatter cones (green) and PDFs (pink) indicated. As stated by Grieve (1998), the shatter cones are limited to the central uplift of the impact structure, the circular structure in the bottom right of the image.

Despite their overlap in terms of area of occurrence within the central uplift, high pressure minerals have never, and rock fragments with PDFs only

rarely, been documented for off-fault pseudotachylytes such as quasi-conglomerates (French and Koeberl, 2010). The *outer zone* of pseudotachylyte occurrence (i.e. outwith the central uplift, labelled *zone 2* in Figure 8.26) is – at the current erosion level – located several tens of kilometres away from the shock pressures which facilitate the formation of shatter cones and PDFs. This suggests that a large fraction of quasi-conglomerates is formed outside the shock pressure regime. The quasi-conglomerates on Barra have been shown to be more likely located in the outer zone of pseudotachylyte occurrence, and not in the central uplift, due to the shear movements recorded in the area (Section 8.4.5, e.g. Figure 8.34). It is thus very unlikely that, if these rocks formed due to an impact event, shock metamorphic evidence such as PDFs or shatter cones would be found in the vicinity of the quasi-conglomerates on Àird Ghrèin, and potentially on the entire island of Barra whose diameter is less than 10 km.

French and Koeberl (2010), in their comprehensive publication 'The convincing identification of terrestrial meteorite impact structures: What works, what doesn't, and why', state that pseudotachylytes, because they lack shock features and may be identical to the products of tectonic faults, cannot be used as a unique indicator of meteorite impact. However, they note that unusually large pseudotachylyte bodies may point to an impact origin because "[t]he size of the larger impact-related pseudotachylytes is in marked contrast to the centimetre-wide pseudotachylytes typical of crustal fault zones of non-impact origin" (Spray, 1998). In fact, the outer zone of pseudotachylyte occurrence, both in the Vredefort and the Sudbury impact structures (Figures 8.37 and 8.26) are outside the outer limits and thus devoid of shock metamorphic features, and are nonetheless believed to be associated with the respective impacts because of their 'massive occurrence' and geochronological data (Reimold and Gibson, 2005; Grieve et al., 2008). French and Koeberl (2010) conclude that the occurrence of large pseudotachylyte bodies should encourage the search for more definite impact diagnostic features. However, as Garde et al. (2013) note, the current criteria for recognition of terrestrial impact structures may not be appropriate for 'giant' and deeply eroded or only partially exposed impact structures. Given the small number of 'giant' impact structures on Earth, it might be unwise to be satisfied that we understand the involved processes and resulting products enough to omit the necessity to occasionally revise definite criteria.

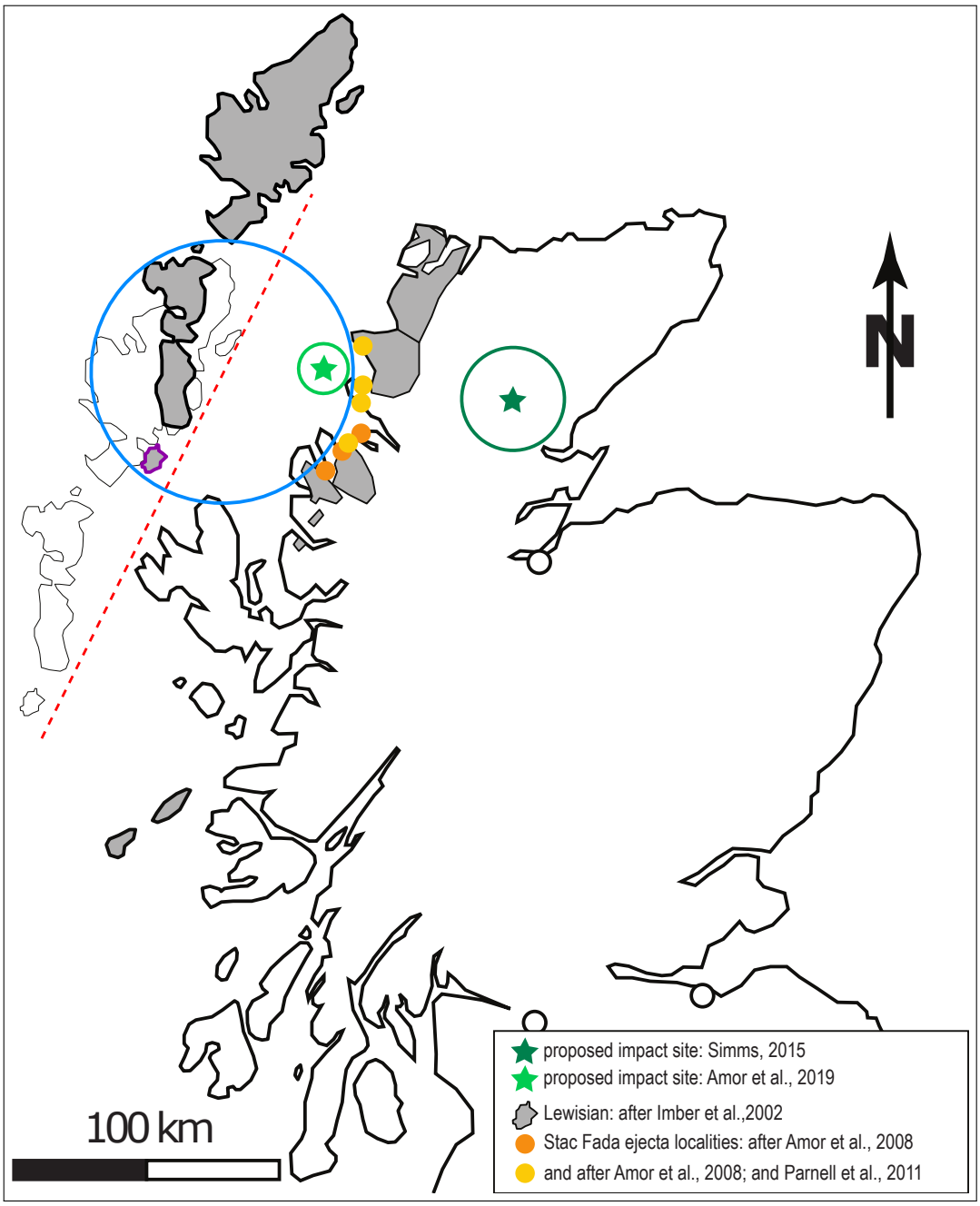

Figure 8.35 – Map of Scotland with the Outer Hebridean island chain moved 100 km NW along the red dashed line (schematically representing the Minch Fault) to a position pre-strike slip movement. The Isle of Barra is lined in purple. Sites of ejecta localities are shown in coloured circles and the stars represent the impact site proposed by Amor et al. (2019) (light green) and Simms (2015) (darker green), with their respective proposed sizes indicated by green circles. The blue circle has a diameter of 100 km and contains Barra, South Uist and North Uist and with that all islands of the Outer Hebrides where quasi-conglomerates of over 1 m^2 have been found.

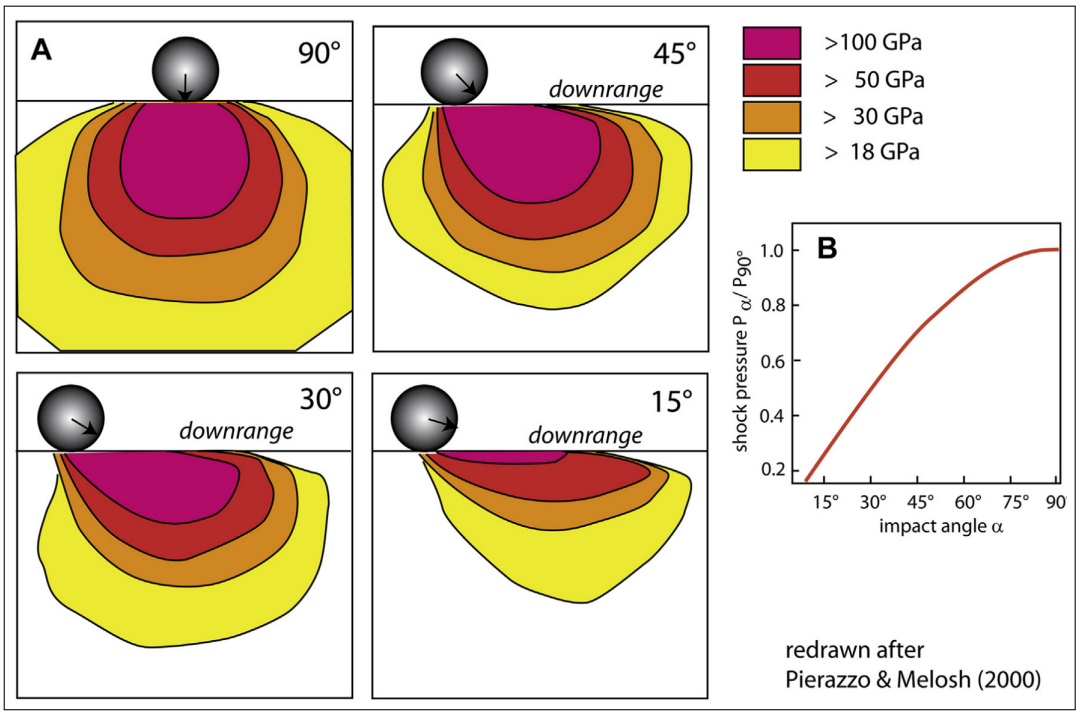

Figure 8.36 – Figure 3 in Kenkmann et al. (2014) – "A) Numerical simulations of a 10 km dunite asteroid striking a granitic target at 20 km / s at different angles. Regions of high shock pressures are located downrange relative to the point of impact. A general reduction of the volume of shocked material occurs at lower impact angles. B) Peak shock pressures calculated from the simulations in A) decrease with decreasing impact angle, following a simple sinusoidal dependence. (Modified from Pierazzo and Melosh, 2000)."

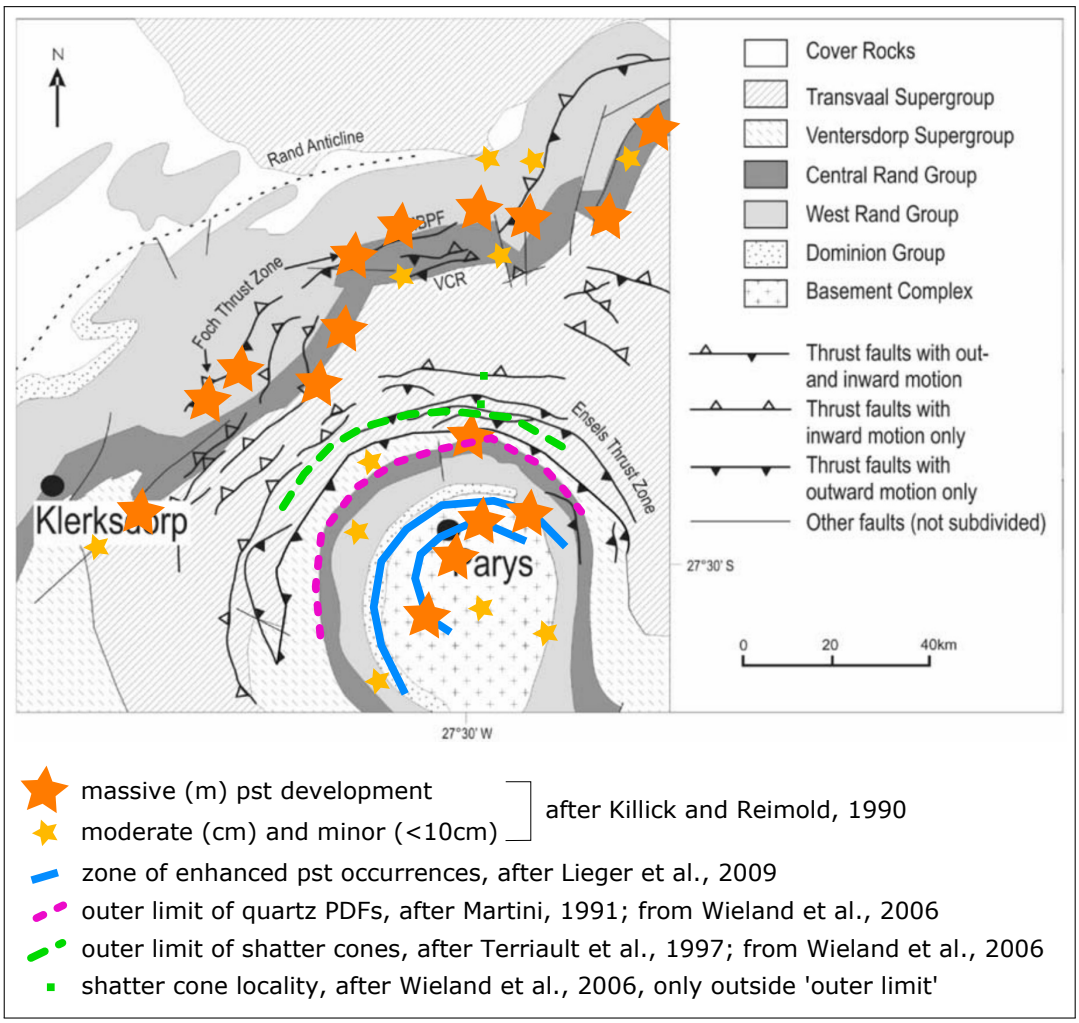

Figure 8.37 – Base map from Grieve et al. (2008) with data added from the literature listed in the key. The approximate outer limit of the occurrence of shock metamorphic features, represented here with relatively low shock pressure requiring planar deformation features (PDFs) and shatter cones, is around the central uplift of the Vredefort structure. From this data compilation it appears that in Vredefort, the *outer zone* of pseudotachylyte occurrence is located several tens of kilometres away from the shock pressures which facilitate the formation of shock metamorphic features.

Chapter 9

Conclusions and Future Work

All outcrops visited on the headland of Àird Ghrèin on Barra have incurred deformation related to the formation of pseudotachylyte. The quasi-conglomerates seem to occur in three quasi continuous zones which the mapping strategy used here was not able to capture. A future study could use aerial photographs as base maps to cover the variety of scales required for this task and better capture features on non-horizontal outcrops. The quasi-conglomerate zones are mostly parallel to the foliation, whereas the pseudotachylyte veins occur both concordant and discordant to the foliation. Two thirds of the outcrops on the headland were found to show quasi-conglomerate development. Between 1 and 14% of the mapped area consist of pseudotachylyte sensu stricto. The 'Minor Intrusives' constitute a major lithology on the headland.

With the new mapping strategy, the different modes of occurrence of pseudotachylyte (veins, networks and quasi-conglomerates) could be recorded and defined, which allows for comparison with other sites of "large" pseudotachylyte occurrence. Previous studies have either not left details of the data collection methodology, or have left rather vague information, making it very difficult to systematically compare between studies. Comparison of data, collected with the same method, to other sites such as the Vredefort and Sudbury impact structures could help with the establishment of quasi-conglomerates as a criterion for impact.

The pseudotachylyte matrix forms by two localised and separate processes: mafic minerals melt (though seemingly not by temperature induced contact melting) and felsic minerals deform cataclastically forming a granular material (fluid?). The mafic fluid gives the pseudotachylyte the characteristic dark colour. Incomplete mixing of the felsic granular fluid and the mafic fluid leads to mingling structures, which have also been referred to as schlieren and flow structures. It

is possible that no pseudotachylyte would form in the absence of mafic minerals. During continued deformation, the initial processes of mafic melting and felsic cataclasis continue to be initiated which leads to apparent cross cutting relationships on the micro scale and mingling of newer and older fluid, the results of which have in the literature previously been interpreted as two separate events. A combined microstructural and geochemical study could help better understand these processes and their interplay. TEM analyses of unaltered samples could help to better understand the (de)formation of the two fluids and understand how the felsic micro clasts are absorbed into the matrix.

In the Sm / Nd and Rb / Sr isotope space the pseudotachylytes and the gneissic host rock constitute one system. This means no melt fractionation took place and the pseudotachylytes formed in a dry crust and closed system. The later Minor Intrusives have not remobilised the pseudotachylyte structures.

The age of formation of the quasi-conglomerates is unknown, however a post-Laxfordian to early Grenvillian (pre-Torridonian) age is most feasible. The impact documented by Amor et al. (2008, 2019) falls in this age bracket with 1177 ± 5 Ma (Parnell et al., 2011). In this time window and geographical area this event is the only significant geological event known. The variety of stress fields recorded in the pseudotachylytes along the Outer Hebrides Fault Zone (OHFZ) (Campbell et al., 2020a) can be readily explained by an impact scenario. A combined analysis of microstructures and dating techniques such as the $^{40}Ar/^{39}Ar$ and a mixing model could be of great value to help unravel the history of the quasi-conglomerates. A study going along-strike the OHFZ with an impact in mind, or drilling into the basement in the Minch to look for shocked minerals could supply further evidence for an impact.

Seismic shaking is proposed as the process of formation for the quasi-conglomerates. This process can – in contrast to frictional melting – explain observations such as the lack of final shear displacement and the characteristic high volumes of pseudotachylyte matrix that seemingly formed in situ. Microstructural observations (Chapter 6) show that the pseudotachylyte matrix replaced rock rather than intruded. Cross cutting relationships are markedly absent in the quasi-conglomerate, and the features on the outcrop scale have formed during one single event. The lack of evidence of shear displacement and the abundance of dilational deformation points to a deformation source type dominated by volume change, such as an implosion, explosion or impact, rather than a shear dominated earthquake. An analysis of field structures in the shear displacement versus volume change space (similar to a Hudson source type plot, following forensic seismics) could potentially help unpick the impact and tectonic geological settings in the future.

On the balance of evidence for very large volumes of pseudotachylytes requiring significant energy input, the evidence that the quasi-conglomerates on Barra formed in a single event which is likely to have taken longer than the duration of a large earthquake, the lack of evidence for association with faulting, and the fact that they formed in a closed, dry system with the gneiss, it seems most likely that the Barra quasi-conglomerate pseudotachylytes were formed in an impact event. There is no unequivocal evidence in the sense of impact diagnostic features such as shocked minerals or meteoritic elements. However, in large impact structures, these impact diagnostic features are only expected in the central part whereas quasi-conglomerates occur also in deeper and more distal areas.

The evidence presented in this thesis builds upon work from the Vredefort and Sudbury impact structures to suggest that the quasi-conglomerates which record a volume change deformation rather than a shear deformation can be used as an indicator for impact structures.

Bibliography

Allen, J. L. (2005). A multi-kilometer pseudotachylyte system as an exhumed record of earthquake rupture geometry at hypocentral depths (Colorado, USA). *Tectonophysics*, 402(1-4):37–54.

Allmendinger, R. W., Cardozo, N. C., and Fisher, D. (2013). *Structural Geology Algorithms: Vectors & Tensors*. Cambridge University Press, Cambridge, England.

Alvarez, L. W., Alvarez, W., Asaro, F., Michel, H. V., Alvarez, L. W., Alvarez, W., Asaro, F., and Michel, H. V. (1980). Extraterrestrial Cause for the Cretaceous-Tertiary Extinction. *Science*, 208(4448):1095–1108.

Amor, K., Hesselbo, S. P., Porcelli, D., Price, A., Saunders, N., Sykes, M., Stevanović, J., and Macniocaill, C. (2019). The Mesoproterozoic Stac Fada proximal ejecta blanket, NW Scotland: Constraints on crater location from field observations, anisotropy of magnetic susceptibility, petrography and geochemistry. *Journal of the Geological Society*, 176:830–846.

Amor, K., Hesselbo, S. P., Porcelli, D., Thackrey, S., and Parnell, J. (2008). A precambrian proximal ejecta blanket from Scotland. *Geology*, 36(4):303–306.

Andrews, B., Roberts, J., Shipton, Z., Bigi, S., Chiara Tartarello, M., and Johnson, G. (2019). How do we see fractures? Quantifying subjective bias in fracture data collection. *Solid Earth*, 10(2):487–516.

Arndt, N. T. and Goldstein, S. L. (1987). Use and abuse of crust-formation ages. *Geology*, 15(10):893–895.

Barrett, S. (2013). Image SXM Version 195. *http://www.ImageSXM.org.uk*.

Beeler, N. (2006). Inferring earthquake source properties from laboratory observations and the scope of lab contributions to source physics. In *Earthquakes: Radiated Energy and the Physics of ...*, pages 99–119. American Geophysical Union.

Ben-Zion, Y. (2001). *Dynamic ruptures in recent models of earthquake faults*, volume 49.

Bestmann, M., Pennacchioni, G., Frank, G., Göken, M., and de Wall, H. (2011). Pseudotachylyte in muscovite-bearing quartzite: Coseismic friction-induced melting and plastic deformation of quartz. *Journal of Structural Geology*, 33(2):169–186.

BGS (1981). Solid Geology Uist and Barra.

Bizzarri, A. (2014). The Destiny of a Clast within a Molten Pseudotachylyte Vein. *Bulletin of the Seismological Society of America*, 104(5):2399–2411.

Bourne, H. (1993). Transitions between crack patterns in quenched glass plates. *Nature*, 362:329–331.

Brewer, J. A. and Smythe, D. K. (1984). MOIST and the continuity of crustal reflector geometry along the Caledonian–Appalachian orogen. *Journal of the Geological Society*, 141(1):105–120.

British Geological Survey. Earthquake magnitude calculations. *https://www.bgs.ac.uk/discoveringGeology/hazards/earthquakes/magnitudeScaleCalculations.html*, accessed: 2020-06-04.

Brune, J. N., Brown, S., and Johnson, P. A. (1993). Rupture mechanism and interface separation in foam rubber models of earthquakes: a possible solution to the heat flow paradox and the paradox of large overthrusts. *Tectonophysics*, 218(1):59–67.

Buehler, M. (2010). Tu(r)ning weakness to strength. *Nano Today*, 5:379–383.

Bunch, T. E. and Cohen, A. J. (1964). Shock deformation of quartz from two meteorite craters. *Geological Society of America Bulletin*, 75(December):1263–1266.

Burt, R. M. and Brown, P. E. (1997). The Ben Nevis intrusive ring tuff, Scotland: Re-interpretation of the 'flinty crush rock' as part of an ignimbrite conduit in the roots of an ancient caldera. *Scottish Journal of Geology*, 33(2):149–155.

Butler, C. A. (1995). *Basement Fault Reactivation: The Kinematic Evolution of the Outer Hebrides Fault Zone, Scotland*. Doctoral thesis, Durham.

Butler, C. A., Holdsworth, R. E., and Strachan, R. A. (1995). Evidence for Caledonian sinistral strike-slip motion and associated fault zone weakening, Outer Hebrides Fault Zone, NW Scotland. *Journal of the Geological Society*, 152(5):743–746.

Butler, R. W. H. and Coward, M. P. (1984). Geological constraints, structural evolution, and deep geology of the northwest scottish caledonides. *Tectonics*, 3(3):347–365.

Camacho, A., Vernon, R. H., and Fitz Gerald, J. D. (1995). Large volumes of anhydrous pseudotachylyte in the Woodroffe Thrust, eastern Musgrave Ranges, Australia. *Journal of Structural Geology*, 17(3):371–383.

Campbell, L., Lloyd, G., Phillips, R., Walcott, R., and Holdsworth, R. (2020a). Stress fields of ancient seismicity recorded in the dynamic geometry of pseudotachylyte in the Outer Hebrides Fault Zone, UK. *Journal of the Geological Society*, pages jgs2020–101.

Campbell, L. R. (2016). *Constraining the parameters of deformation recorded in fault-generated pseudotachylytes*. Doctoral thesis, Univeristy of Leeds.

Campbell, L. R., Menegon, L., Fagereng, and Pennacchioni, G. (2020b). Earthquake nucleation in the lower crust by local stress amplification. *Nature Communications*, 11(1):1–9.

Cardozo, N. C. and Allmendinger, R. W. (2013). Sperical projections with OSXStereonet. *Computers & Geosciences*, 51:193–205.

Carporzen, L., Gilder, S. A., and Hart, R. J. (2005). Palaeomagnetism of the Vredefort meteorite crater and implications for craters on Mars. *Nature*, 435(7039):198–201.

Chamberlin, T. C. (1965). The method of multiple working hypotheses. *Science*, 148(3671):754–759.

Cliff, R. A. and Rex, D. C. (1989). Short Paper: Evidence for a 'Grenville' event in the Lewisian of the northern Outer Hebrides. *Journal of the Geological Society*, 146(6):921–924.

Collins, G. S., Melosh, H. J., and Marcus, R. A. (2005). Earth Impact Effects Program: A Web-based computer program for calculating the regional environmental consequences of a meteoroid impact on Earth. *Meteoritics & Planetary Science*, 40(6):817–840.

Cowan, D. (1999). Do faults preserve a record of seismic slip? A field geologist's opinion. *Journal of Structural Geology*, 21:995–1001.

Coward, M. P. (1990). The Precambrian, Caledonian and Variscan framework to NW Europe. *Geological Society Special Publication*, 55(55):1–34.

Curewitz, D. and Karson, J. A. (1999). Ultracataclasis, sintering, and frictional melting in pseudotachylytes from East Greenland. *Journal of Structural Geology*, 21(12):1693–1713.

Daly, R. A. (1947). The Vredefort Ring-Structure of South Africa. *The Journal of Geology*, 55(3, Part 1):125–145.

Di Toro, G., Mittempergher, S., Ferri, F., Mitchell, T. M., and Pennacchioni, G. (2012). The contribution of structural geology, experimental rock deformation and numerical modelling to an improved understanding of the seismic cycle. *Journal of Structural Geology*, 38:3–10.

Di Toro, G. and Pennacchioni, G. (2005). Fault plane processes and mesoscopic structure of a strong-type seismogenic fault in tonalites (Adamello batholith, Southern Alps). *Tectonophysics*, 402(1-4 SPEC. ISS):55–80.

Di Toro, G., Pennacchioni, G., and Nielsen, S. (2009). Pseudotachylytes and earthquake source mechanics. In Fukuyama, E., editor, *Fault-Zone Properties and Earthquake Rupture Dynamics*, volume 94, chapter 5, pages 87–133. Academic Press Inc.

Di Toro, G., Pennacchioni, G., and Teza, G. (2005). Can pseudotachylytes be used to infer earthquake source parameters? An example of limitations in the study of exhumed faults. *Tectonophysics*, 402(1-4):3–20.

Di Vincenzo, G., Rocchi, S., Rossetti, F., and Storti, F. (2004). 40Ar-39Ar dating of pseudotachylytes: The effect of clast-hosted extraneous argon in Cenozoic fault-generated friction melts from the West Antarctic Rift System. *Earth and Planetary Science Letters*, 223(3-4):349–364.

Dietz, R. S. (1961). Vredefort Ring Structure: Meteorite Impact Scar? *The Journal of Geology*, 69(5):499–516.

Dietz, R. S. and Holden, J. C. (1972). Continents Adrift: New Orthodoxy or Persuasive Joker? In *Nato Symposium on Continental Drift*, pages 1105–1121. National Oceanic and Atmospheric Administration.

Dixon, J. E. and Dixon, T. H. (1989). Vesicles, amygdales and similar structures in fault-generated pseudotachylites - comment. *Lithos*, 23(3):225–227.

Dor, O., Ben-Zion, Y., Rockwell, T. K., and Brune, J. (2006). Pulverized rocks in the Mojave section of the San Andreas Fault Zone. *Earth and Planetary Science Letters*, 245(3-4):642–654.

Dressler, B. O. and Reimold, W. U. (2004). Order or chaos? Origin and mode of emplacement of breccias in floors of large impact structures. *Earth-Science Reviews*, 67:1–54.

Dürig, T. and Zimanowski, B. (2012). "Breaking news" on the formation of volcanic ash: Fracture dynamics in silicate glass. *Earth and Planetary Science Letters*, 336:1–8.

Earth Impact Database. Spray, John G. *http://www.passc.net/EarthImpact Database*, accessed: 2020-06-23.

Ellam, R. (1998a). Rb–Sr$_{}$V4.02.xls.

Ellam, R. (1998b). Sm–Nd$_{}$V4.01.xls.

Ernstson, K., Rampino, M. R., and Hiltl, M. (2001). Cratered cobbles in Triassic Bundsandstein conglomerates in Northeastern Spain: An indicator of shock deformation in thevicinity of large impacts. *Geology*, 29(November):11–14.

Fedorowich, J., Rousell, D., and Peredery, W. (1999). Sudbury Breccia distribution and orientation in an embayment environment. In Dressler, B. and Sharpton, V., editors, *Large Meteorite Impacts and Planetary Evolution II*, pages 305–315. Geological Society of America Special Paper 339, Boulder, Colorado.

Fettes, D. J., Mendum, J. R., Smith, D. I., and Watson, J. V. (1992). *Geology of the Outer Hebrides*. Memoir of the British Geological Survey, Sheets (solid edition) Lewis and Harris, Uist and Barra (Scotland), London.

Fletcher, P. and Reimold, W. U. (1989). Some notes and speculations on the pseudotachylites in the Witwatersrand Basin and Vredefort Dome, South Africa. *South African Journal of Geology*, 92(3):223–234.

Fondriest, M., Smith, S. A., Di Toro, G., Zampieri, D., and Mittempergher, S. (2012). Fault zone structure and seismic slip localization in dolostones, an example from the Southern Alps, Italy. *Journal of Structural Geology*, 45:52–67.

Fossen, H. (2010). Extensional tectonics in the North Atlantic Caledonides: a regional view. In Law, R. D., Butler, R. W. H., Holdsworth, R. E., Krabbendam, M., and Strachan, R. A., editors, *Continental Tectonics and Mountain Building: The Legacy of Peach and Horne*, pages 767–793. Geological Society, London, Special Publications.

Francis, P. W. and Sibson, R. H. (1973). The Outer Hebrides Thrust. In Park, R. G. and Tarney, J., editors, *The Early Precambrian of Scotland and Related Rocks of Greenland*, pages 95–104. Department of Geology, University of Keele.

Frank, F. C. and Lawn, B. R. (1967). On the theory of Hertzian fracture. *Proceedings of the Royal Society A: Mathematical, Physical and Engineering Sciences*, 229:291–306.

French, B. M. (1998). *Traces of Catatrophe - A Handbook of Shock-Metamorphic Effects in Terrestrial Meteorite Impact Structures*. Lunar and Planetary Institute, Houston, 1st edition.

French, B. M. and Koeberl, C. (2010). The convincing identification of terrestrial meteorite impact structures: What works, what doesn't, and why. *Earth-Science Reviews*, 98(1-2):123–170.

Friend, C. R. and Kinny, P. D. (2001). A reappraisal of the Lewisian Gneiss Complex: Geochronological evidence for its tectonic assembly from disparate terranes in the Proterozoic. *Contributions to Mineralogy and Petrology*, 142(2):198–218.

Garde, A., Boriani, A., and Sørensen, E. (2015). Crustal modelling of the Ivrea–Verbano zone in northern Italy re-examined: coseismic cataclasis v. extensional shear zones and sideways rotation. *Tectonophysics*, 662:291–311.

Garde, A. A. and Klausen, M. B. (2016). A centennial reappraisal of the Vredefort pseudotachylytes: shaken, not stirred by meteorite impact. *Journal of the Geological Society*, June(10):jgs2015–147.

Garde, A. A. and Klausen, M. B. (2018). Comments on "The impact pseudotachylitic breccia controversy: Insights from first isotope analysis of Vredefort impact-generated melt rocks" by Reimold et al. 2017 (GCA 214, 266–282). *Geochimica et Cosmochimica Acta*, 233:187–190.

Garde, A. A., McDonald, I., Dyck, B., and Keulen, N. (2013). Reply on "Searching for giant, ancient impact structures on Earth: The Mesoarchaean Maniitsoq structure, West Greenland". *Earth and Planetary Science Letters*, 337-338:197–210.

Gillespie, M., Barnes, R., and Milodowski, A. (2011). British Geological Survey scheme for classifying discontinuities and filings. Technical report.

Glass, B. P. and Simonson, B. M. (2013). *Distal Impact Ejecta Layers - A Record of Large Impacts in Sedimentary Deposits*. Springer Berlin Heidelberg, Berlin, Heidelberg, 1st edition.

Goodenough, K. M., Park, R. G., Krabbendam, M., Myers, J. S., Wheeler, J., Loughlin, S. C., Crowley, Q. G., Friend, C. R. L., Beach, A., Kinny, P. D., and Graham, R. H. (2010). The Laxford Shear Zone: an end-Archaean terrane boundary? In Law, R. D., Butler, R. W. H., Holdsworth, R. E., Krabbendam, M., and Strachan, R. A., editors, *Continental Tectonics and Mountain Building: The Legacy of Peach and Horne*, chapter 335, pages 103–120. Geological Society, London, Special Publications.

Google Maps. Greian Head, Barra (online). accessed: 2018-08-08.

Gratz, A., Tyburczy, J. A., Christie, J., Ahrens, T. J., Pongratz, P., Nasa, L., and Planetary Institute Tx, United States,, H. (1988). Shock of deformed quartz. *Physics and Chemistry of Minerals*, 16:221–233.

Grieve, R. A., Reimold, W. U., Morgan, J., Riller, U., and Pilkington, M. (2008). Observations and interpretations at Vredefort, Sudbury, and Chicxulub: Towards an empirical model of terrestrial impact basin formation. *Meteoritics and Planetary Science*, 43(5):855–882.

Grieve, R. A. F. (1998). Extraterrestrial impacts on earth: the evidence and the consequences. In Grady, M. M., Hutchinson, R., McCall, G. J. H., and Rothery, D. A., editors, *Meteorites: Flux with Time and Impact Effects*, volume 140, pages 105–131. Geological Society, London, Special Publications.

Grieve, R. A. F. and Therriault, A. M. (2013). Impactites: their characteristics and spatial distribution. In Osinski, G. R. and Pierazzo, E., editors, *Impact cratering: processes and products*, volume 3, chapter 7, pages 139–147. Blackwell Publishing Ltd.

Gross, D. and Seelig, T. (2011). *Fracture Mechanics with an Introduction to Micromechanics*. Springer Berlin Heidelberg, 2nd edition.

Heaton, T. H. (1990). Evidence for and implications of self-healing pulses of slip in earthquake rupture. *Physics of the Earth and Planetary Interiors*, 64:1–20.

Hergarten, S. and Kenkmann, T. (2015). The number of impact craters on Earth: Any room for further discoveries? *Earth and Planetary Science Letters*, 425:187–192.

Hirose, T. and Shimamoto, T. (2003). Fractal dimension of molten surfaces as a possible parameter to infer the slip-weakening distance of faults from natural pseudotachylytes. *Journal of Structural Geology*, 25(10):1569–1574.

Hisada, E. (2004). Clast-size analysis of impact-generated pseudotachylite from Vredefort Dome, South Africa. *Journal of Structural Geology*, 26(8):1419–1424.

Hodgson, R. A. (1961). Classification of structures on joint surfaces. *American Journal of Science*, 259:493–502.

Holdsworth, R. E., Alsop, G. I., and Strachan, R. A. (2007). Tectonic stratigraphy and structural continuity of the northernmost Moine Thrust Zone and Moine Nappe, Scottish Caledonides. *Geological Society Special Publication*, 272(May):121–142.

Holt, W. E., Kreemer, C., Haines, a. J., Estey, L., Meertens, C., Blewitt, G., and Lavallée, D. (2005). Project helps constrain continental dynamics and seismic hazards. *Eos, Transactions American Geophysical Union*, 86(41):383.

Hudson, J. A., Pearce, R. G., and Rogers, R. M. (1989). Soure Type Plot for Inversion of the Moment Tensor. *Journal of Geophysical Research*, 94(B1):765–774.

Imber, J., Holdsworth, R., Butler, C., and Strachan, R. (2001). A reappraisal of the Sibson-Scholz fault zone model: The nature of the frictional to viscous ("brittle-ductile") transition along a long-lived, crustal-scale fault, Outer Hebrides, Scotland. *Tectonics*, 44(5):601–624.

Imber, J., Strachan, R. A., Holdsworth, R. E., and Butler, C. A. (2002). The initiation and early tectonic significance of the Outer Hebrides Fault Zone, Scotland. *Geological Magazine*, 139(6):609–619.

Ivanov, B. a. (2005). Numerical modeling of the largest terrestrial meteorite craters. *Solar System Research*, 39(5):381–409.

Jehu, T. J. and Craig, R. M. (1924). XXII.—Geology of the Outer Hebrides. Part I.—The Barra Isles. *Transactions of the Royal Society of Edinburgh*, 53(02):419–441.

Kanamori, H. and Brodsky, E. E. (2004). The physics of earthquakes. *Reports on Progress in Physics*, 67(8):1429–1496.

Kanamori, H. and Rivera, L. (2006). Energy partitioning during an earthquake. *Geophysical Monograph Series*.

Karson, J., Brooks, C., Storey, M., and Pringle, M. (1998). Tertiary faulting and pseudotachylytes in the East Greenland volcanic rifted margin: Seismogenic faulting during magmatic construction. *Geology*, 26:39–42.

Kelley, S. P., Reddy, S. M., and Maddock, R. (1994). Laser-probe 40Ar/39Ar investigation of a pseudotachylyte and its host rock from the Outer Isles thrust, Scotland. *Geology*, 22(May):443–446.

Kenkmann, T., Poelchau, M. H., and Wulf, G. (2014). Structural geology of impact craters. *Journal of Structural Geology*, 62:156–182.

Killick, A. M. and Reimold, W. U. (1990). Review of the pseudotachylites in and around the Vredefort "Dome", South Africa. *South African Journal of Geology*, 93(2):350–365.

Kinnaird, T., Prave, A., Kirkland, C., Horstwood, M., Parrish, R. R., and Batchelor, R. (2007). The late Mesoproterozoic–early Neoproterozoic tectonostratigraphic evolution of NW Scotland: the Torridonian revisited. *Journal of the Geological Society of London*, 164:541–551.

Kinny, P., Friend, C., and Love, G. (2005). Proposal for a terrane-based nomenclature for the Lewisian Gneiss Complex of NW Scotland. *Journal of the Geological Society*, 162(1):175–186.

Kirkpatrick, J. D., Dobson, K. J., Mark, D. F., Shipton, Z. K., Brodsky, E. E., and Stuart, F. M. (2012). The depth of pseudotachylyte formation from detailed thermochronology and constraints on coseismic stress drop variability. *Journal of Geophysical Research*, 117(B6):B06406.

Kirkpatrick, J. D. and Rowe, C. D. (2013). Disappearing ink: How pseudotachylytes are lost from the rock record. *Journal of Structural Geology*, 52(1):183–198.

Kirkpatrick, J. D. and Shipton, Z. K. (2009). Geologic evidence for multiple slip weakening mechanisms during seismic slip in crystalline rock. *Journal of Geophysical Research*, 114(B12).

Kirkpatrick, J. D., Shipton, Z. K., and Persano, C. (2009). Pseudotachylytes: Rarely Generated, Rarely Preserved, or Rarely Reported? *Bulletin of the Seismological Society of America*, 99(1):382–388.

Kirstein, L. a., Davies, G. R., and Heeremans, M. (2006). The petrogenesis of Carboniferous–Permian dyke and sill intrusions across northern Europe. *Contributions to Mineralogy and Petrology*, 152(6):721–742.

Kocer, C. and Collins, R. E. (1998). Angle of Hertzian Cone Cracks. *Journal of American Ceramic Society*, 81(7):1736–1742.

Kokelaar, P. (2007). Friction melting, catastrophic dilation and breccia formation along caldera superfaults. *Journal of the Geological Society*, 164(4):751–754.

Konstantinou, K. I. (2014). Moment magnitude–rupture area scaling and stress-drop variations for Earthquakes in the Mediterranean region. *Bulletin of the Seismological Society of America*, 104(5):2378–2386.

Krabbendam, M., Prave, T., and Cheer, D. (2008). A fluvial origin for the Neoproterozoic Morar Group, NW Scotland; implications for Torridon Morar Group correlation and the Grenville Orogen foreland basin. *Journal of the Geological Society*, 165(1):379–394.

Krehl, P. O. K. (2011). Shock wave physics and detonation physics - A stimulus for the emergence of numerous new branches in science and engineering. *European Physical Journal H*, 36:85–152.

Kröner, A. and Hofmann, A., editors (2019). *The Archaean Geology of the Kaapvaal Craton, Southern Africa*. Springer Nature Switzerland, Cham.

Lafrance, B. and Kamber, B. S. (2010). Geochemical and microstructural evidence for in situ formation of pseudotachylitic Sudbury breccia by shock-induced compression and cataclasis. *Precambrian Research*, 180(3-4):237–250.

Lailey, M., Stein, a. M., and Reston, T. J. (1989). The Outer Hebrides fault: a major Proterozoic structure in NW Britain. *Journal of the Geological Society*, 146(2):253–259.

Langenhorst, F. (2002). Shock metamorphism of some minerals: Basic introduction and microstructural observations. *Bulletin of the Czech Geological Survey*, 77(4):265–282.

Lawn, B. and Wilshaw, R. (1975). Indentation fracture: principles and applications. *Journal of Materials Science*, 10(6):1049–1081.

Lawn, B. R. and Swain, M. V. (1975). Microfracture beneath point indentations in brittle solids. *Journal of Materials Science*, 10(1):113–122.

Lawn, B. R., Wilshaw, T. R., and Hartley, N. E. W. (1974). A computer simulation study of Hertzian cone crack growth. *International Journal of Fracture*, 10:1–16.

Lieger, D., Riller, U., and Gibson, R. L. (2009). Generation of fragment-rich pseudotachylite bodies during central uplift formation in the Vredefort impact structure, South Africa. *Earth and Planetary Science Letters*, 279(1-2):53–64.

Lieger, D., Riller, U., and Gibson, R. L. (2011). Petrographic and geochemical evidence for an allochthonous, possibly impact melt, origin of pseudotachylite from the Vredefort Dome, South Africa. *Geochimica et Cosmochimica Acta*, 75(16):4490–4514.

Lin, A. (1999). Roundness of clasts in pseudotachylytes and cataclastic rocks as an indicator of frictional melting. *Journal of Structural Geology*, 21:473–478.

Lin, A. (2008). Seismic slip in the lower crust Inferred from granulite-related pseudotachylyte in the woodroffe thrust, Central Australia. *Pure and Applied Geophysics*, 165:215–233.

Lin, A., Maruyama, T., Aaron, S., Michibayashi, K., Camacho, A., and Kano, K. I. (2005). Propagation of seismic slip from brittle to ductile crust: Evidence from pseudotachylyte of the Woodroffe thrust, central Australia. *Tectonophysics*, 402:21–35.

Lofgren, G. and Hargraves, R. B. (1980). Experimental studies on the dynamic crystallization of silicate melts. *Physics of magmatic processes*, 487:551.

Lowrie, W. (2006). *Fundamentals of Geophysics*. Cambridge University Press.

Macaudière, J. and Brown, W. L. (1982). Transcrystalline shear fracturing and pseudotachylite generation in a meta-anorthosite (Harris, Scotland). *Journal of Structural Geology*, 4(4):395–406.

MacDonald, J. M. and Goodenough, K. M. (2013). The South Barra shear zone: A composite Inverian–Laxfordian shear zone and possible Terrane boundary in the Lewisian gneiss complex of the Isle of Barra, NW Scotland. *Scottish Journal of Geology*, 49(2):93–104.

Macinnes, E. A., Alsop, G. I., and Oliver, G. J. H. (2000). Contrasting modes of reactivation in the Outer Hebrides Fault Zone, northern Barra, Scotland. *Journal of the Geological Society*, 157(5):1009–1017.

Maddock, R. (1983). Melt origin of fault-generated pseudotachylytes demonstrated by textures. *Geology*, 11:105–108.

Maddock, R. (1986). Partial melting of lithic porphyroclasts in fault-generated pseudotachylites. *Neues Jahrbuch fuer Mineralogie. Abhandlungen*, 155(1):1–14.

Maddock, R., Grocott, J., and Van Nes, M. (1987). Vesicles, amygdales and similar structures in fault-generated pseudotachylytes. *Lithos*, 20(5):419–432.

Maddock, R. H. (1992). Effects of lithology, cataclasis and melting on the composition of fault-generated pseudotachylytes in Lewisian gneiss, Scotland. *Tectonophysics*, 204(3-4):261–278.

Magloughlin, J. F. (2003). An evaluation of Rb-Sr dating of pseudotachylyte: Structural-chemical models and the role of fluids. *Geochemical Journal*, 37(1):21–33.

Magloughlin, J. F. and Spray, J. G. (1992). Frictional melting processes and products in geological materials: introduction and discussion. *Tectonophysics*, 204(3-4):197–204.

Martini, J. (1991). The nature, distribution and genesis of the coesite and stishovite associated with the pseudotachylite of the Vredefort Dome, South Africa. *Earth and Planetary Science Letters*, 103(1-4):285–300.

Masch, L., Wenk, H. R., and Preuss, E. (1985). Electron microscopy study of hyalomylonites—evidence for frictional melting in landslides. *Tectonophysics*, 115(1):131–160.

McKenzie, D. and Brune, J. N. (1972). Melting on Fault Planes During Large Earthquakes. *Geophysical Journal of the Royal Astronomical Society*, 29:65–78.

McKerrow, W. S., Mac Niocaill, C., and Dewey, J. F. (2000). The Caledonian Orogeny redefined. *Journal of the Geological Society*, 157(6):1149–1154.

Melosh, H. (1996). Dynamical weakening of faults by acoustic fluidization. *Nature*, 379:601–606.

Melosh, H. J. (2005). The Mechanics of Pseudotachylite Formation in Impact Events. In Koeberl, C. and Henkel, H., editors, *Impact Tectonics*, chapter 2, pages 55–80. Springer Berlin Heidelberg.

Melosh, H. J. and Ivanov, B. A. (1999). Impact Crater Collapse. *Annual Review of Earth and Planetary Sciences*, 27(1):385–415.

Melosh, J. H. (1979). Acoustic Fluidization: A New Geologic Process? *Journal of Geophysical Research*, 84(B13):7513–7520.

Melosh, J. H. (1989). *Impact Cratering: A Geologic Process*. Oxford University Press, New York.

Meyer, R., Nicoll, G., Hertogen, J., Troll, V., Ellam, R., and Emeleus, C. (2009). Trace element and isotope constraints on crustal anatexis by upwelling mantle melts in the North Atlantic Igneous Province: an example form the Isle of Rum, NW Scotland. *Geological Magazine*, 146(3):382–399.

Mitchell, T., Ben-Zion, Y., and Shimamoto, T. (2011). Pulverized fault rocks and damage asymmetry along the Arima-Takatsuki Tectonic Line, Japan. *Earth and Planetary Science Letters*, 308(3-4):284–297.

Mitchell, T. M., Toy, V., Di Toro, G., Renner, J., and Sibson, R. H. (2016). Fault welding by pseudotachylyte formation. *Geology*, 44(12):1059–1062.

Moecher, D. P. and Sharp, Z. D. (2004). Stable isotope and chemical systematics of pseudotachylyte and wall rock, Homestake shear zone, Colorado, USA: Meteoric fluid or rock-buffered conditions during coseismic fusion? *Journal of Geophysical Research: Solid Earth*, 109(12):1–11.

Mohr-Westheide, T. and Reimold, W. U. (2011). Formation of pseudotachylitic breccias in the central uplifts of very large impact structures: Scaling the melt formation. *Meteoritics & Planetary Science*, 46(4):543–555.

Mohr-Westheide, T., Reimold, W. U., Riller, U., and Gibson, R. L. (2009). Pseudotachylitic breccia and microfracture networks in archean gneiss of the central uplift of the Vredefort Impact Structure, South Africa. *South African Journal of Geology*, 112:1–22.

Muir, R. J. (2017). Moving faults and building fracture models in a digital world—an example from Glen Coe, Scotland. *Geology Today*, 33(2):54–59.

Müller, W., Kelley, S. P., and Villa, I. M. (2002). Dating fault-generated pseudotachylytes: comparison of 40Ar/39Ar stepwise-heating, laser ablation and Rb-Sr microsampling analyses. *Contributions to Mineralogy and Petrology*, 144:57–77.

Nakamura, N., Hirose, T., and Borradaile, G. J. (2002). Laboratory verification of submicron magnetite production in pseudotachylytes: Relevance for paleointensity studies. *Earth and Planetary Science Letters*, 201(1):13–18.

Nakamura, N. and Iyeda, Y. (2005). Magnetic properties and paleointensity of pseudotachylytes from the Sudbury structure, Canada: Petrologic control. *Tectonophysics*, 402(1-4 SPEC. ISS):141–152.

Niemeijer, A., Di Toro, G., Griffith, W. A., Bistacchi, A., a.F. Smith, S., and Nielsen, S. (2012). Inferring earthquake physics and chemistry using an integrated field and laboratory approach. *Journal of Structural Geology*, 39:2–36.

Niemeijer, A., Di Toro, G., Nielsen, S., and Di Felice, F. (2011). Frictional melting of gabbro under extreme experimental conditions of normal stress, acceleration, and sliding velocity. *Journal of Geophysical Research: Solid Earth*, 116(7):1–18.

Niemeijer, A., Spiers, C., and Peach, C. (2008). Frictional behaviour of simulated quartz fault gouges under hydrothermal conditions: Results from ultra-high strain rotary shear experiments. *Tectonophysics*, 460(1-4):288–303.

O'Brien, T. M. and van der Pluijm, B. A. (2012). Timing of Iapetus Ocean rifting from ar geochronology of pseudotachylytes in the St. Lawrence rift system of southern Quebec. *Geology*, 40(5):443–446.

O'Callaghan, J. W. and Osinski, G. R. (2019). Geochemical and petrographic variations in pseudotachylyte along the outer hebrides fault zone, Scotland. *Journal of the Geological Society*, 177(1):50–65.

O'Hara, K. D. (2001). A pseudotachylyte geothermometer. *Journal of Structural Geology*, 23:1345–1357.

Okrusch, M. and Matthes, S. (2005). *Mineralogie*. Springer Berlin Heidelberg, 7th edition.

Olson, E. L. and Allen, R. M. (2005). The deterministic nature of earthquake rupture. *Nature*, 438(7065):212–215.

Ordnance Survey (2014). Grein Head, Barra (1:25 000). *Retrieved from http://edina.ac.iuk/digimap/*.

Osinski, G. R., Alsop, G. I., and Oliver, G. J. H. (2001). Extensional tectonics of the Outer Hebrides Fault Zone, South Uist, northwest Scotland. *Geological Magazine*, 138(3):325–344.

Osinski, G. R., Spray, J. G., and Lee, P. (2005). Impactites of the Haughton impact structure, Devon Island, Canadian High Arctic. *Meteoritics and Planetary Science*, 40(12):1789–1812.

Osinski, G. R., Tornabene, L. L., and Grieve, R. A. F. (2011). Impact ejecta emplacement on terrestrial planets. *Earth and Planetary Science Letters*, 310(3-4):167–181.

Oxford University Press (2020). Oxford Dictionary of English. *www.mobisystems.com*, accessed:11-08-2020.

Park, R. G., Crane, a., and Niamatullah, M. (1987). Early Proterozoic structure and kinematic evolution of the southern mainland Lewisian. *Geological Society, London, Special Publications*, 27(1):139–151.

Parnell, J., Mark, D., Fallick, A., Boyce, A., and Thackrey, S. (2011). The age of the Mesoproterozoic Stoer Group sedimentary and impact deposits, NW Scotland. *Journal of the Geological Society of London*, 168:349–358.

Pec, M., Stünitz, H., Heilbronner, R., Drury, M., and de Capitani, C. (2012). Origin of pseudotachylites in slow creep experiments. *Earth and Planetary Science Letters*, 355-356:299–310.

Piper, J. D. (1992). Post-Laxfordian magnetic imprint in the Lewisian metamorphic complex and strike-slip motion in the Minches, NW Scotland. *Journal of the Geologic Society, London*, 149(1):127–137.

Piper, J. D. A. and Poppleton, T. J. (1988). Palaeomagnetic dating of pseudotachylyte formation in the Lewisian complex. *Scottish Journal of Geology*, 24(3):263–272.

Pittarello, L., Di Toro, G., Bizzarri, A., Pennacchioni, G., Hadizadeh, J., and Cocco, M. (2008). Energy partitioning during seismic slip in pseudotachylyte-bearing faults (Gole Larghe Fault, Adamello, Italy). *Earth and Planetary Science Letters*, 269(1-2):131–139.

Pons, A. J. and Karma, A. (2010). Helical crack-front instability in mixed-mode fracture. *Nature*, 464(7285):85–89.

Potts, P. J. (1987). *A Handbook of Silicate Rock Analysis*. Springer US, Boston, MA.

Ravi-Chandar, K. and Knauss, W. G. (1984). An experimental investigation into dynamic fracture: II. Microstructural aspects. *International Journal of Fracture*, 26:65–80.

Ray, S. (2004). Melt–clast interaction and power-law size distribution of clasts in pseudotachylytes. *Journal of structural geology*, 26:1831–1843.

Ray, S. K. (1999). Transformation of cataclastically deformed rocks to pseudotachylyte by pervasion of frictional melt: inferences from clast-size analysis. *Tectonophysics*, 301:283–304.

Reddy, S. M., Johnson, T. E., Fischer, S., Rickard, W. D., and Taylor, R. J. (2015). Precambrian reidite discovered in shocked zircon from the Stac Fada impactite, Scotland. *Geology*, 43(10):899–902.

Reimold, W. (1995). Pseudotachylite in impact structures - generation by friction melting and shock brecciation?: A review and discussion. *Earth-Science Reviews*, 39:247–265.

Reimold, W. U. (1998). Exogenic and endogenic breccias: a discussion of major problematics. *Earth Science Reviews*, 43:25–47.

Reimold, W. U. (2012). Comment on "Pseudotachylite in the South Boundary Fault At the Cooke Shaft, Witwatersrand Basin, South Africa By P.W. Mambane Et Al., South African Journal of Geology 114.2, 109-120. *South African Journal of Geology*, 115:251–255.

Reimold, W. U., Andreoli, M., and Hart, R. (1985). Pseudotachylite from the Vredefort Dome. *Lunar and Planetray Science Conference*, 16:691–692.

Reimold, W. U. and Collistion, W. P. (1994). Pseudotachylytes of the Vredefort Dome and the surrounding Witwatersrand Basin, South Africa. *Geological Society of America Special Papers*, 293(2):177–196.

Reimold, W. U. and Gibson, R. L. (1996). Geology and evolution of the Vredefort impact structure, South Africa. *Journal of African Earth Sciences*, 23:125–162.

Reimold, W. U. and Gibson, R. L. (2005). "Pseudotachylites" in Large Impact Structures. In Koeberl, C. and Henkel, H., editors, *Impact Tectonics*, chapter 1, pages 1–49. Springer Berlin Heidelberg.

Reimold, W. U. and Gibson, R. L. (2006). The melt rocks of the Vredefort impact structure – Vredefort Granophyre and pseudotachylitic breccias: Implications for impact cratering and the evolution of the Witwatersrand Basin. *Chemie der Erde - Geochemistry*, 66(1):1–35.

Reimold, W. U., Hauser, N., Hansen, B., Thirlwall, M., and Hoffmann, M. (2018). Reply to "Comments on "The impact pseudotachylitic breccia controversy: Insights from first isotope analysis of Vredefort impact-generated melt rocks" by Reimold et al. 2017 (GCA 214, 266–282)" by A.A. Garde and M.B. Klausen (GCA 233, 187–190). *Geochimica et Cosmochimica Acta*, 240:331–332.

Reimold, W. U., Hauser, N., Hansen, B. T., Thirlwall, M., and Hoffmann, M. (2017). The impact pseudotachylitic breccia controversy: Insights from first isotope analysis of Vredefort impact-generated melt rocks. *Geochimica et Cosmochimica Acta*, 214:266–281.

Reimold, W. U., Hoffmann, M., Hauser, N., Schmitt, R. T., Zaag, P. T., and Mohr-Westerheide, T. (2016). A geochemical contribution to the discussion about the genesis of impact-related pseudotachylitic breccias: Studies of PTB in the Otavi and Kudu Quarries of the Vredefort Dome support the "In Situ Formation" hypothesis. *South African Journal of Geology*, 119(3):453–472.

Reimold, W. U., Jessberger, E. K., and Stephan, T. (1990). $^{40}Ar/^{39}Ar$ dating of pseudotachylite from the Vredefort dome, South Africa: a progress report. *Tectonophysics*, 171(1-4):139–152.

Reimold, W. U. and Koeberl, C. (2014). Impact structures in Africa: A review. *Journal of African Earth Sciences*, 93:57–175.

Reimold, W. U., Koeberl, C., and Bishop, J. (1994). Roter Kamm impact crater, Namibia: Geochemistry of basement rocks and breccias. *Geochimica et Cosmochimica Acta*, 58(12):2689–2710.

Reimold, W. U., Koeberl, C., Fletcher, P., Killick, A. M., and Wilson, J. D. (1999). Pseudotachylitic breccias from fault zones in the Witwatersrand Basin, South Africa; evidence of autometasomatism and post-brecciation alteration processes. *Witwatersrand and Vredefort; metamorphism and mineralization.*, 66; 1-3:25–53.

Ren, B., Li, S., Qian, J., and Zeng, X. (2011). Meshfree simulations of spall fracture. *Computer Methods in Applied Mechanics and Engineering*, 200(5-8):797–811.

Riller, U., Lieger, D., Gibson, R. L., Grieve, R. A. F., and Stöffler, D. (2010). Origin of large-volume pseudotachylite in terrestrial impact structures. *Geology*, 38(7):619–622.

Roberts, A. M. and Holdsworth, R. E. (1999). Linking onshore and offshore structures: Mesozoic extension in the Scottish Highlands. *Journal of the Geologic Society, London*, 156:1061–1064.

Roten, D., Olsen, K. B., Day, S. M., Cui, Y., and Fäh, D. (2014). Expected seismic shaking in Los Angeles reduced by San Andreas fault zone plasticity. *Geophysical Research Letters*, 41(8):2769–2777.

Rousell, D., Fedorowich, J., and Dressler, B. (2003). Sudbury Breccia (Canada): a product of the 1850 Ma Sudbury Event and host to footwall Cu–Ni–PGE deposits. *Earth-Science Reviews*, 60:147–174.

Rowe, C. D., Kirkpatrick, J. D., and Brodsky, E. E. (2012). Fault rock injections record paleo-earthquakes. *Earth and Planetary Science Letters*, 335-336:154–166.

Rowe, C. D., Moore, J. C., Meneghini, F., and McKeirnan, A. W. (2005). Large-scale pseudotachylytes and fluidized cataclasites from an ancient subduction thrust fault. *Geology*, 33(12):937–940.

Sagy, A., Reches, Z., and Roman, I. (2001). Dynamic fracturing: Field and experimental observations. *Journal of Structural Geology*, 23:1223–1239.

Saunders, A., Fitton, J., Kerr, A., Norry, M., and Kent, R. (1997). The North Atlantic Igneous Province. In *Geophysical Monograph Series: Large Igneous Provinces: Continental, Oceanic, and Planetary Flood Volcanism*, pages 45–93. American Geophysical Union.

Schmid, S. M. and Handy, M. (1991). Towards a Genetic Classiftcation of Fault Rocks : Geological Usage and Tectonophysical lmplications. *Press, London*, (May 2014):339–361.

Schneider, C. A., Rasband, W. S., and Eliceiri, K. W. (2012). NIH Image to ImageJ: 25 years of image analysis. *Nature Methods*, 9(7):671–675.

Schulte, P., Alegret, L., Arenillas, I., Arz, J. A., Barton, P. J., Bown, P. R., Bralower, T. J., Christeson, G. L., Claeys, P., Cockell, C. S., Collins, G. S., Deutsch, A., Goldin, T. J., Goto, K., Grajales-Nishimura, J. M., Grieve, R. A. F., Gulick, S. P. S., Johnson, K. R., Kiessling, W., Koeberl, C., Kring, D. A., MacLeod, K. G., Matsui, T., Melosh, J., Montanari, A., Morgan, J. V., Neal, C. R., Nichols, D. J., Norris, R. D., Pierazzo, E., Ravizza, G., Rebolledo-Vieyra, M., Reimold, W. U., Robin, E., Salge, T., Speijer, R. P., Sweet, A. R., Urrutia-Fucugauchi, J., Vajda, V., Whalen, M. T., and Willumsen, P. S. (2010). The Chicxulub Asteroid Impact and Mass Extinction at the Cretaceous-Paleogene Boundary. *Science*, 327(5970):1214–1218.

Serpelloni, E., Anzidei, M., Baldi, P., Casula, G., and Galvani, A. (2005). Crustal velocity and strain-rate fields in Italy and surrounding regions: New results from the analysis of permanent and non-permanent GPS networks. *Geophysical Journal International*, 161(3):861–880.

Shand, S. J. (1916). The Pseudotachylyte of Parijs (Orange Free State), and its Relation to 'Trap-Shotten Gneiss' and 'Flinty Crush-Rock'. *Quarterly Journal of the Geological Society*, 72(1-4):198–221.

Sherlock, S., Jones, K. A., and Park, R. G. (2008). Grenville-age pseudotachylite in the Lewisian: laserprobe $^{40}Ar/^{39}Ar$ ages from the Gairloch region of Scotland (UK). *Journal of the Geological ...*, 165:73–83.

Sherlock, S., Strachan, R. A., and Jones, K. A. (2009). Spatial resolution $^{40}Ar/^{39}Ar$ dating of pseudotachylites: geochronological evidence for multiple phases of faulting within basement gneisses of the Outer Hebrides (UK). *Journal of the Geological Society*, 166:1049–1059.

Shimamoto, T. and Nagahama, H. (1992). An argument against the crush origin of pseudotachylytes based on the analysis of clast-size distribution. *Journal of Structural Geology*, 14(8-9):999–1006.

Shipton, Z. K. and Cowie, P. a. (2003). A conceptual model for the origin of fault damage zone structures in high-porosity sandstone. *Journal of Structural Geology*, 25(3):333–344.

Shipton, Z. K., Roberts, J. J., Comrie, E. L., Kremer, Y., Lunn, R. J., and Caine, J. S. (2019). Fault fictions: systematic biases in the conceptualization of fault-zone architecture. *Geological Society, London, Special Publications*, pages SP496–2018–161.

Sibson, R. (1975). Generation of Pseudotachylyte by Ancient Seismic Faulting. *Geophysical Journal International*, 43:775–794.

Sibson, R. (1977a). Fault rocks and fault mechanisms. *Journal of the Geological Society*, 133:191–213.

Sibson, R. and Toy, V. (2006). The habitat of fault-generated pseudotachylyte: Presence vs. absence of friction-melt. In *Geophysical Monograph Series: Earthquakes: Radiated Energy and the Physics of Faulting*, number 17, pages 153–166. American Geophysical Union.

Sibson, R. H. (1977b). *The outer Hebrides Thrust: its structure, mechanism and deformation environment*. Unpublished phd thesis, Imperial College London.

Sibson, R. H. (2003). Thickness of the seismic slip zone. *Bulletin of the Seismological Society of America*, 93(3):1169–1178.

Simms, M. J. (2015). The Stac Fada impact ejecta deposit and the Lairg Gravity Low: Evidence for a buried Precambrian impact crater in Scotland? *Proceedings of the Geologists' Association*, 126(6):742–761.

Sleep, N. H. (2014). Ambient tectonic stress as fragile geological feature. *Geochemistry, Geophysics, Geosystems*, 15(9):3628–3644.

Sleep, N. H. and Erickson, B. A. (2014). Nonlinear attenuation of S-waves and Love waves within ambient rock. *Geochemistry, Geophysics, Geosystems*, 15:1419–1440.

Smythe, D., Dobinson, A., McQuillin, R., Brewer, J. A., Matthews, D. H., Blundell, D. J., and Kelk, B. (1982). Deep structure of the Scottish Caledonides revealed by the MOIST reflection profile. *Nature*, 299:338–340.

Smythe, D. K. (1987). Deep seismic reflection profiling of the Lewisian foreland. *Geological Society, London, Special Publications*, 27(1):193–203.

Spray, J. (1992). A physical basis for the frictional melting of some rock-forming minerals. *Tectonophysics*, 204:205–221.

Spray, J. (1995). Pseudotachylyte controversy: Fact or friction? *Geology*, 23:1119–1122.

Spray, J. (1997). Superfaults. *Geology*, 25:579–582.

Spray, J. (2016). Experimental Vibration Melting Without Offset: Post-Shock Materials Behaviour. In *79th Annual Meeting of the Meteoritical Society*, page 6118, Berlin.

Spray, J. G. (1987). Artificial generation of pseudotachylyte using friction welding apparatus: simulation of melting on a fault plane. *Journal of Structural Geology*, 9(1):49–60.

Spray, J. G. (1998). Localized shock- and friction-induced melting in response to hypervelocity impact. In Grady, M. M., Hutchinson, R., McCall, G. J. H., and Rothery, D. A., editors, *Meteorites: Flux with Time and Impact Effects*, volume 140, pages 195–204. Geological Society, London, Special Publications.

Spray, J. G. (2010). Frictional Melting Processes in Planetary Materials: From Hypervelocity Impact to Earthquakes. *Annual Review of Earth and Planetary Sciences*, 38(1):221–254.

Spray, J. G., Butler, H. R., and Thompson, L. M. (2004). Tectonic influences on the morphometry of the Sudbury impact structure: Implications for terrestrial cratering and modeling. *Meteoritics & Planetary Science*, 39(2):287–301.

Spray, J. G. and Thompson, L. M. (1995). Friction melt distribution in a multi-ring impact basin. *Nature*.

Steel, R. J. and Wilson, A. C. (1975). Sedimentation and tectonism (?Perom-Triassic) on the margin of the North Minch Basin, Lewis. *Journal of the Geological Society of London*, 131:183–202.

Stein, A. and Blundell, D. (1990). Geological inheritance and crystal dynamics of the northwest Scottish continental shelf. *Tectonophysics*, 173(1-4):455–467.

Stein, A. M. (1992). Basins on the Atlantic Seaboard: Petroleum Geology, Sedimentology and Basin Evolution. In Parnell, J., editor, *Basins on the Atlantic Seaboard: Petroleum Geology, Sedimentology and Basin Evolution*, volume 62, pages 17–20. Geological Society, London, Special Publications.

Stewart, S. A. and Allen, P. J. (2002). A 20-km-diameter multi-ringed impact structure in the North Sea. *Nature*, 418(August):520–523.

Stöffler, D. and Grieve, R. a. F. (2007). Impactites. *Metamorphic rocks: A classification and glossary of terms, Recommendations of the International Union of Geological Sciences Subcommission on the Systematics of Metamorphic Rocks*, pages 82–92.

Stöffler, D. and Langenhorst, F. (1994). Shock metamorphism of quartz in nature and experiment: 1. Basic observation and theory. *Meteoritics*, 29:155–181.

Storetvedt, K. and Steel, R. (1977). Palaeomagnetic evidence for the age of the stornoway formation. *Scottish Journal of Geology*, 13(3):263–268.

Swanson, M. T. (1989). Sidewall ripouts in strike-slip faults. *Journal of Structural Geology*, 11(8):933–948.

Swanson, M. T. (1992). Fault structure, wear mechanisms and rupture processes in pseudotachylyte generation. *Tectonophysics*, 204(3-4):223–242.

Techmer, K. S., Ahrendt, H., and Weber, K. (1992). The development of pseudotachylyte in the Ivrea-Verbano Zone of the Italian Alps. *Tectonophysics*, 204(3-4):307–322.

Thompson, L. and Spray, J. (1996). Pseudotachylyte petrogenesis: constraints from the Sudbury impact structure. *Contributions to Mineralogy and Petrology*, 125:359–374.

Thompson, L. M., Spray, J. G., and Kelley, S. P. (1998). Laser probe argon-40/argon-39 dating of pseudotachylyte from the Sudbury structure: Evidence for postimpact thermal overprinting in the North Range. *Meteoritics and Planetary Science*, 33(6):1259–1269.

Tsutsumi, A. (1999). Size distribution of clasts in experimentally produced pseudotachylytes. *Journal of Structural Geology*, 21:305–312.

Turnbull, M. J. M., Whitehouse, M. J., and Moorbath, S. (1996). New isotopic age determinations for the Torridonian, NW Scotland. *Journal of the Geological Society*, 153(6):955–964.

Walter, K. L. L. N. L. (2009). Sleuthering Seismic Signals. *Science and Technology Review*, (March):4–12.

Warr, L. N., van der Pluijm, B. A., and Tourscher, S. (2007). The age and depth of exhaumed friction melts along the Alpine fault, New Zealand. *Geology*, 35(7):603–606.

Wechsler, N., Allen, E. E., Rockwell, T. K., Girty, G., Chester, J. S., and Ben-Zion, Y. (2011). Characterization of pulverized granitoids in a shallow core along the San Andreas Fault, Littlerock, CA. *Geophysical Journal International*, 186(2):401–417.

Wenk, H.-R. (1978). Are pseudotachylites the product of fracture or fusion? *Geology*, 6:507–511.

Wenk, H. R., Johnson, L. R., and Ratschbacher, L. (2000). Pseudotachylites in the Eastern Peninsular Ranges of California. *Tectonophysics*, 321(2):253–277.

Westbrook, G. K. (1972). Structure and metamorphism of the Lewisian of east Tiree, Inner Hebrides. *Scottish Journal of Geology*, 8(1):13–30.

Wheeler, J., Park, R. G., Rollinson, H. R., and Beach, A. (2010). The Lewisian Complex: insights into deep crustal evolution. In Law, R. D., Butler, R. W. H., Holdsworth, R. E., Krabbendam, M., and Strachan, R. A., editors, *Continental Tectonics and Mountain Building: The Legacy of Peach and Horne*, volume 335, chapter 335, pages 51–79. Geological Society, London, Special Publications.

White, J. C. (1996). Transient discontinuities revisited: pseudotachylyte, plastic instability and the influence of low pore fluid pressure on deformation processes in the mid-crust. *Journal of Structural Geology*, 18(12):1471–1486.

White, S. H. and Glasser, J. (1987). The Outer Hebrides Fault Zone: evidence for normal movements. In Park, R. G. and Tarney, J., editors, *Evolution of the Lewisian and Comparable Precambrian High Grade Terrains*, number 27, pages 175–183. Geological Society Special Publications, London.

Whitehouse, M. (1989). Sm-Nd evidence for diachronous crustal accretion in the Lewisian complex of northwest Scotland. *Tectonophysics*, 161(3-4):245–256.

Winter, J. D. (2010). *Principles of Igneous and Metamorphic Petrology*. Prentice Hall, Upper Saddle River, 2nd edition.

Woodcock, N. and Mort, K. (2008). Classification of fault breccias and related fault rocks. *Geological Magazine*, 145(3):435–440.

Young, G. M. (2002). Stratigraphy and geochemistry of volcanic mass flows in the Stac Fada Member of the Stoer Group, Torridonian, NW Scotland. *Earth and Environmental Science Transactions of the Royal Society of Edinburgh*, 93(2002):1–16.

Appendix A

Appendix

This Appendix comprises all the meso scale data, only some of which was shown in Chapter 5. Table A.1 gives an overview of all meso maps, their grid references, reference scales and relationships. Figures A.1 to A.8 provide overviews over the outcrops at way points 19, part of 38 and part of 39, followed by Figures A.9 to A.29 with all the meso maps.

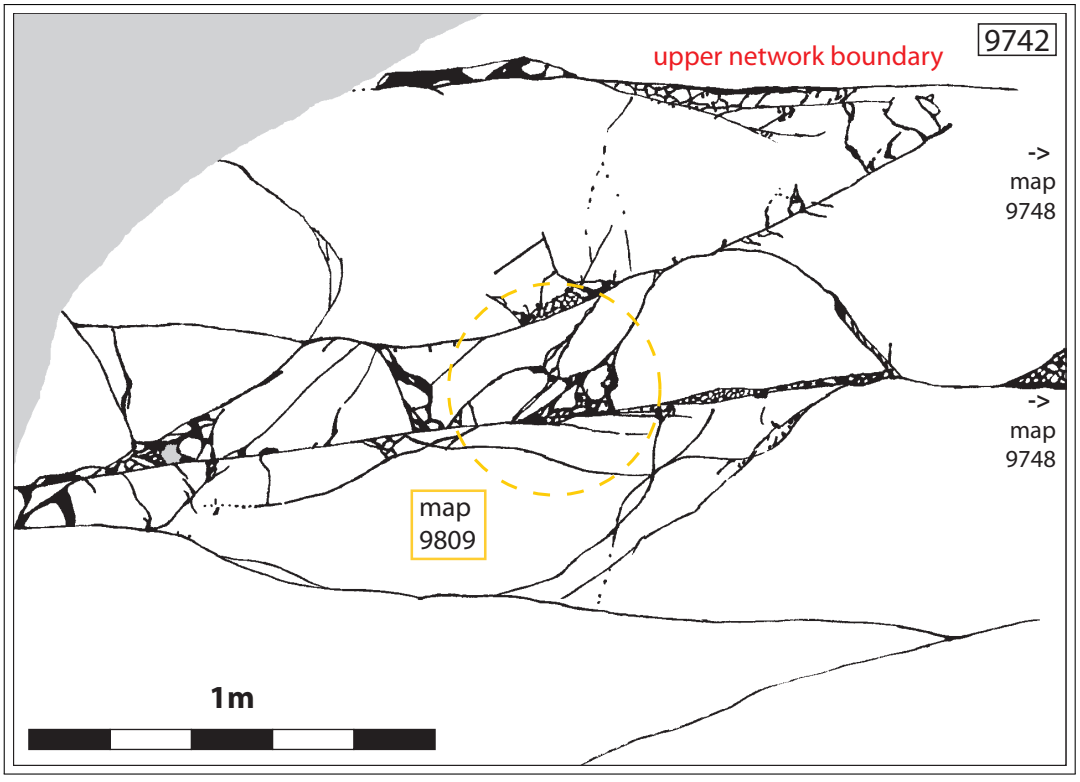

Figure A.1 – Overview over the left hand side of way point 19.

Way Points	*Coord.* E	N	*Where*	*Maps*	*Reference Scale* [cm]	*Relationships*
19	65950	04333	Golf nr. 6	9742	100	overview, including 9809
				9809	30	part of 9742
				9748	100	overview, including 9749 and 9806
				9749	30	part of 9748, including 9806
				9806	10	part of 9749 part of 9748
25	65712	04685	wall	9627	30	none
38	65585	04241	Seal Bay South	0729	30	front
				0547	30	top front
				0568	30	overview, top back
				0571	30	part of 0568, including 0572
				0572	10	part of 0571, part of 0568
				0567	30	none
39	65576	04279	Seal Bay North	0037	30	next to 0043, 0047
				0043	30	next to 0037, 0045, 0047
				0045	30	next to 0043, 0047
				0047	30	next to 0037, 0043, 0045
				0007	10	part of 0047
				0008	10	part of 0047
				0009	10	part of 0047
				0010	10	part of 0047
				0094	10	none

Table A.1 – Overview over all way points with meso scale maps, their grid references and meso map relationships.

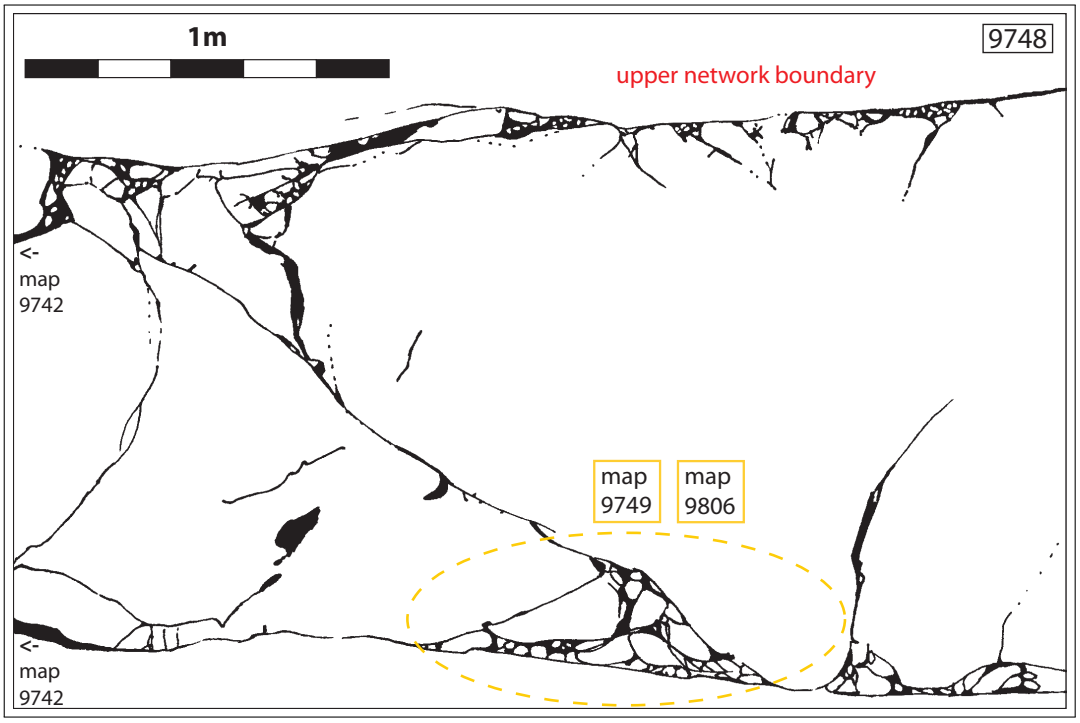

Figure A.2 – Overview over the right hand side of way point 19.

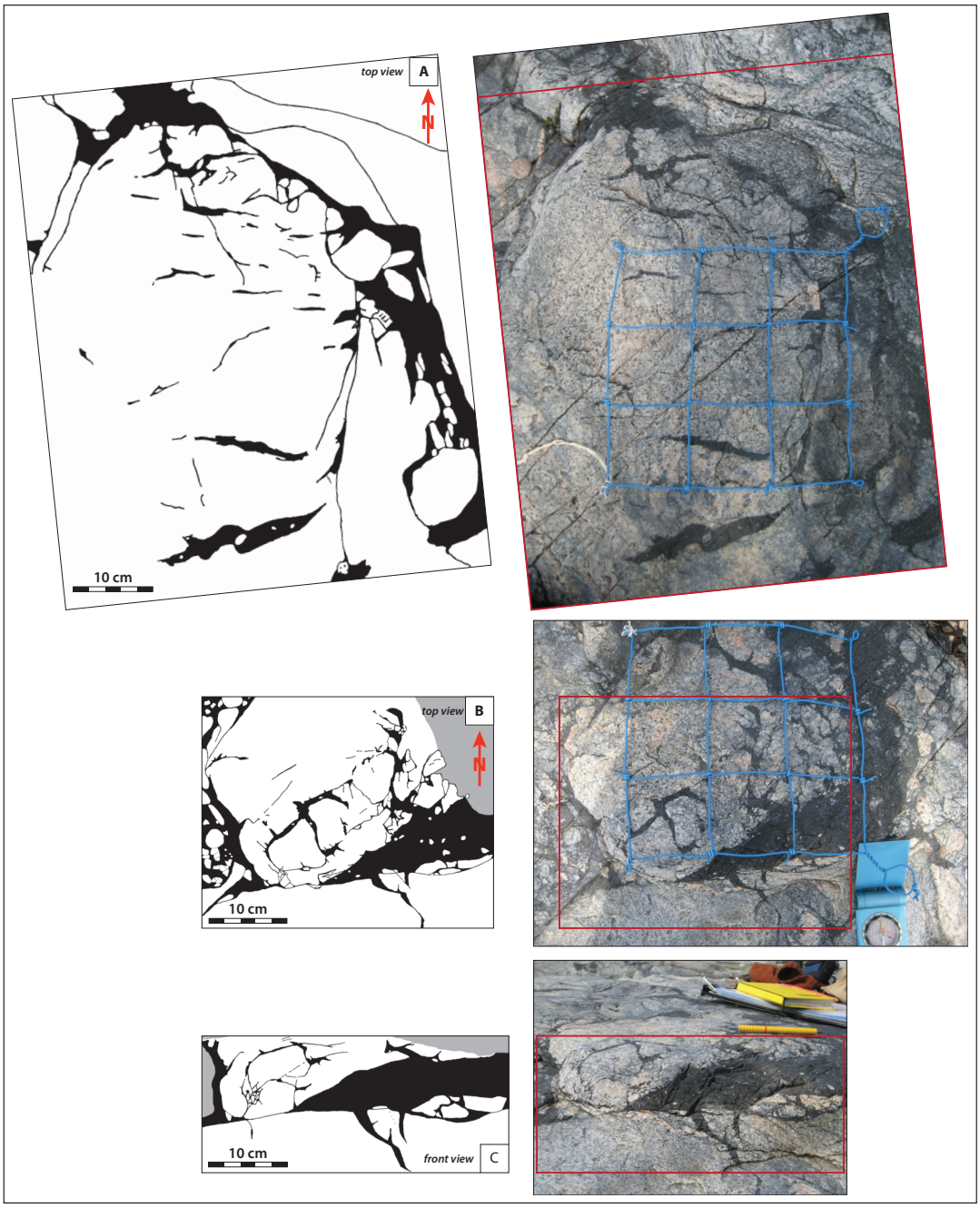

Figure A.3 – Overview over part of the outcrop at way point 38 (Seal Bay South)

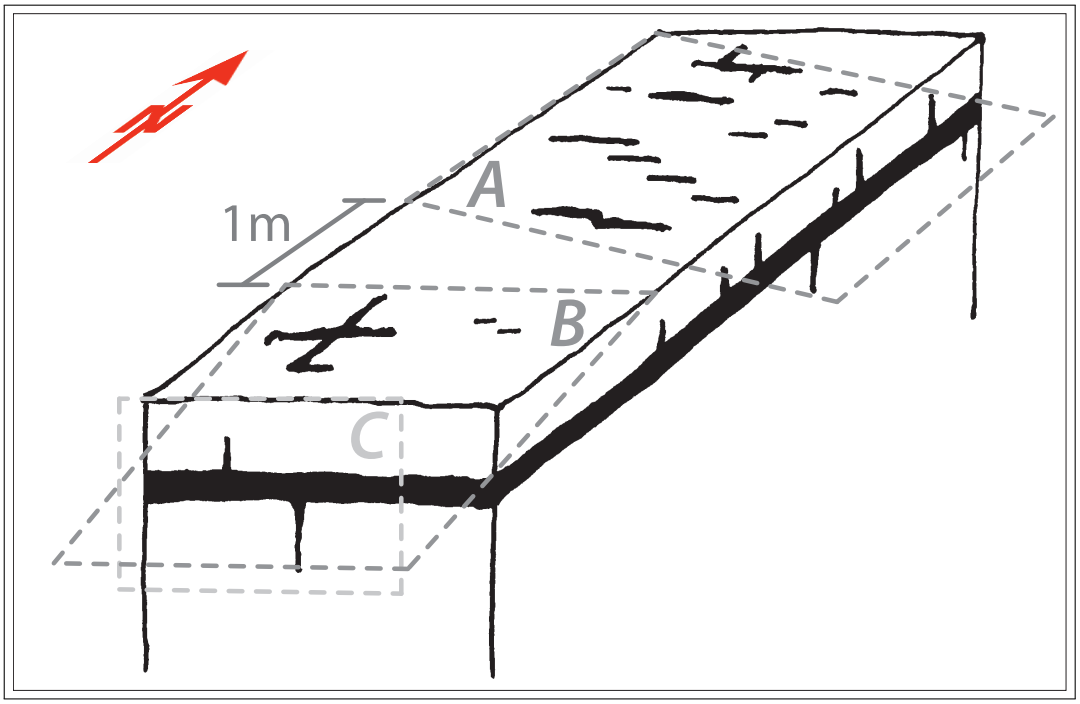

Figure A.4 – Block diagram showing the relationships of the maps shown in A.3, way point 38.

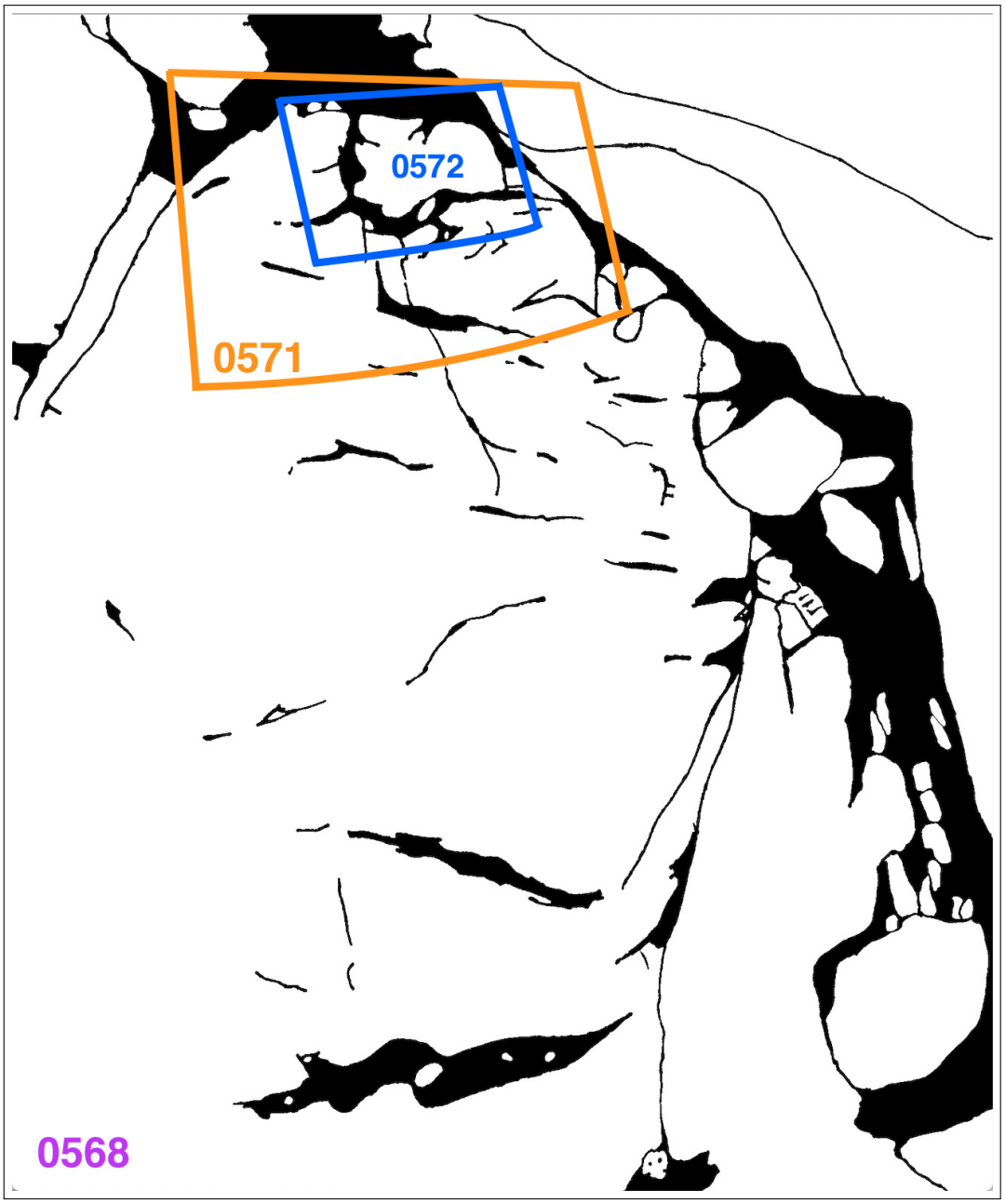

Figure A.5 – Overview over three nested maps, map A in Figures A.3 and A.4, way point 38.

Figure A.6 – Photo of part of the outcrop at way point 39 (Seal Bay North), same photo as shown in Figure A.7. Pen in the low centre for scale.

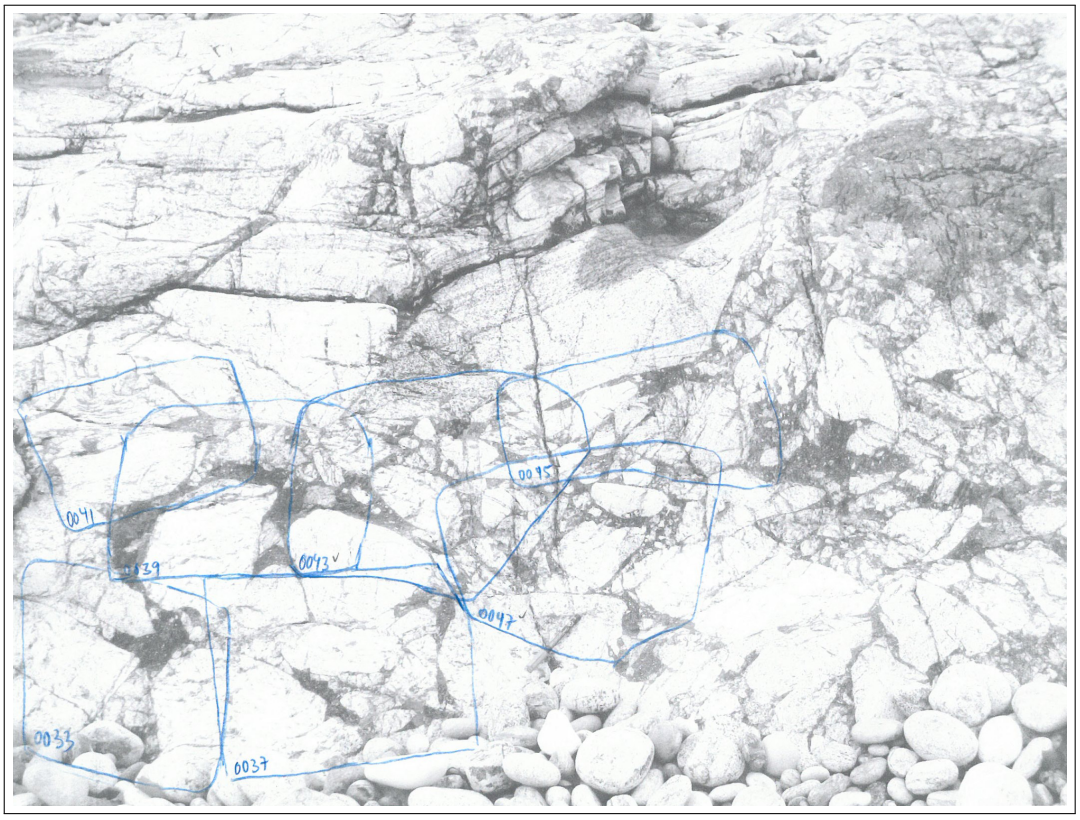

Figure A.7 – Overview of way point 39 (Seal Bay North), showing the location of the 30cm reference scale maps.

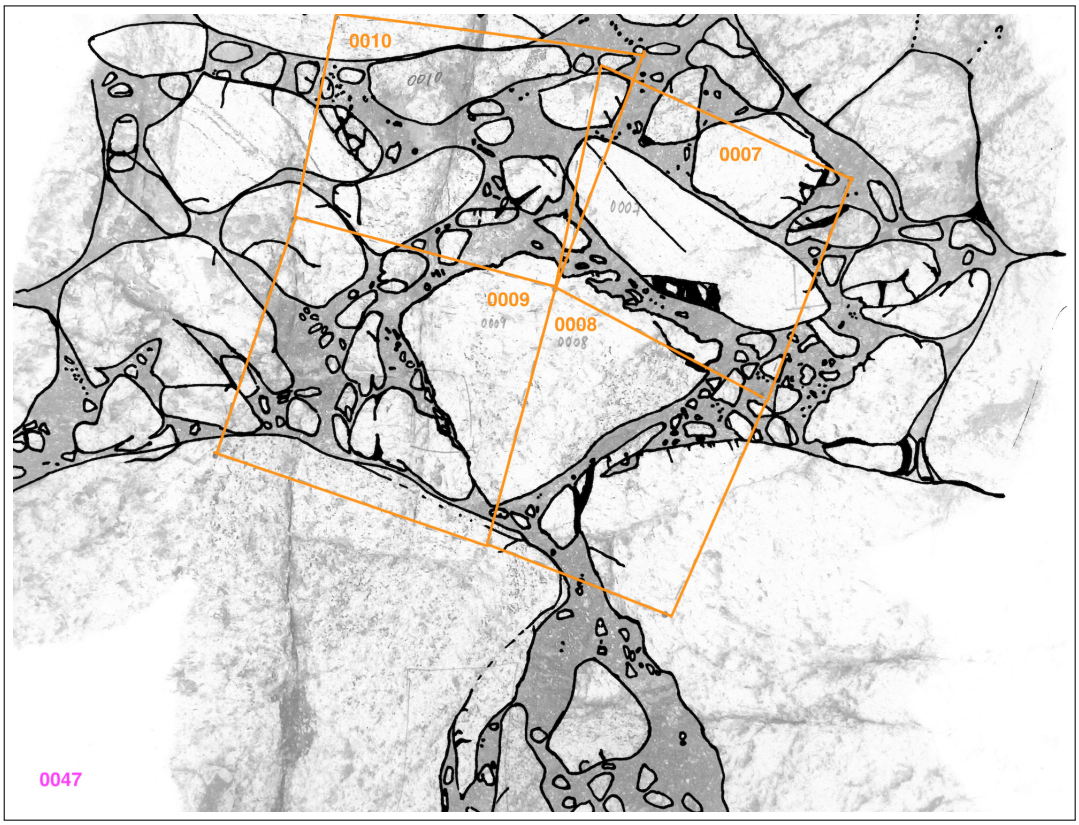

Figure A.8 – Meso scale map 0047 with location of detailed (10cm reference scale) maps.

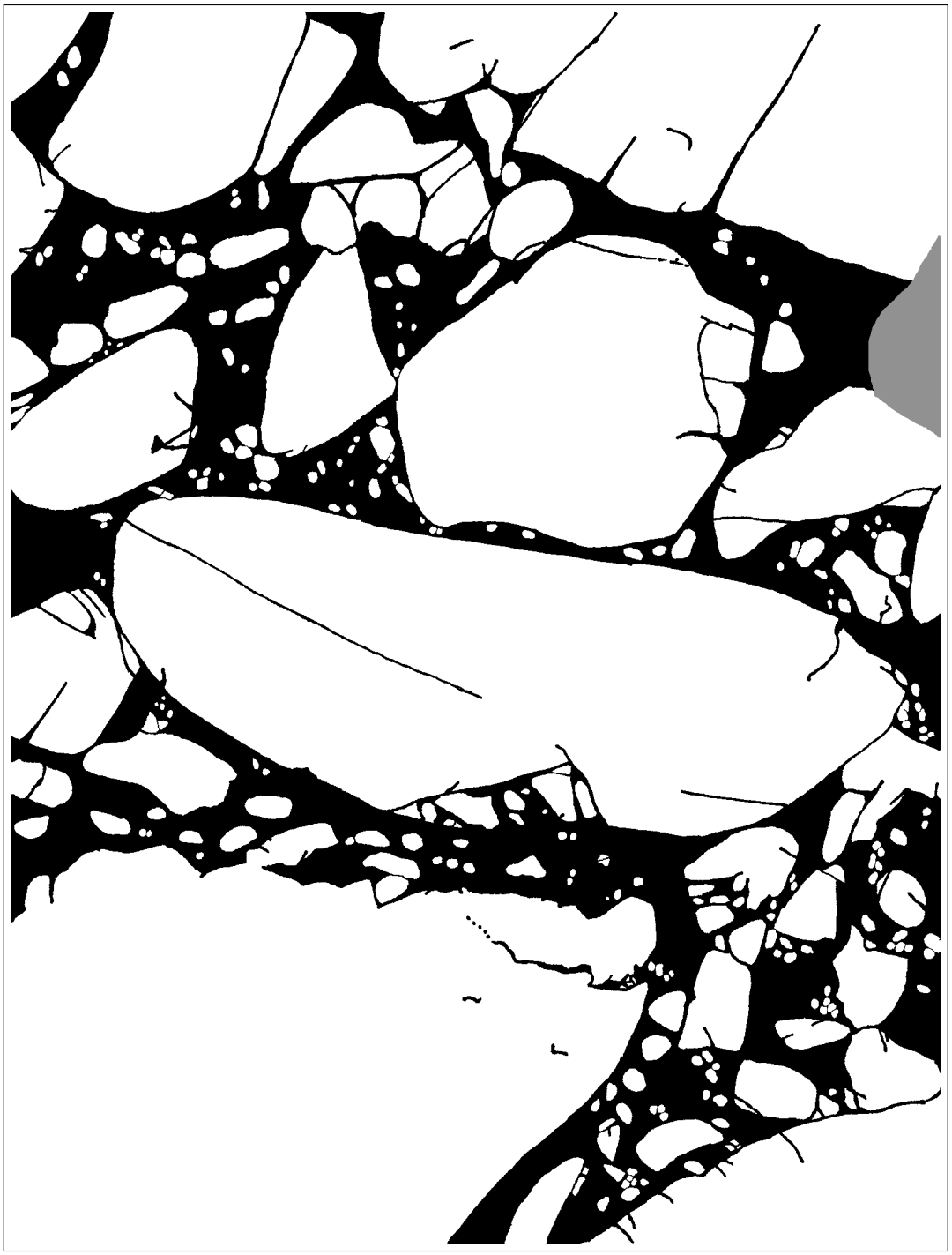

Figure A.9 – Map 0007, reference scale 10cm, Seal Bay North (WP 39).

Figure A.10 – Map 0008, reference scale 10cm, Seal Bay North (WP 39).

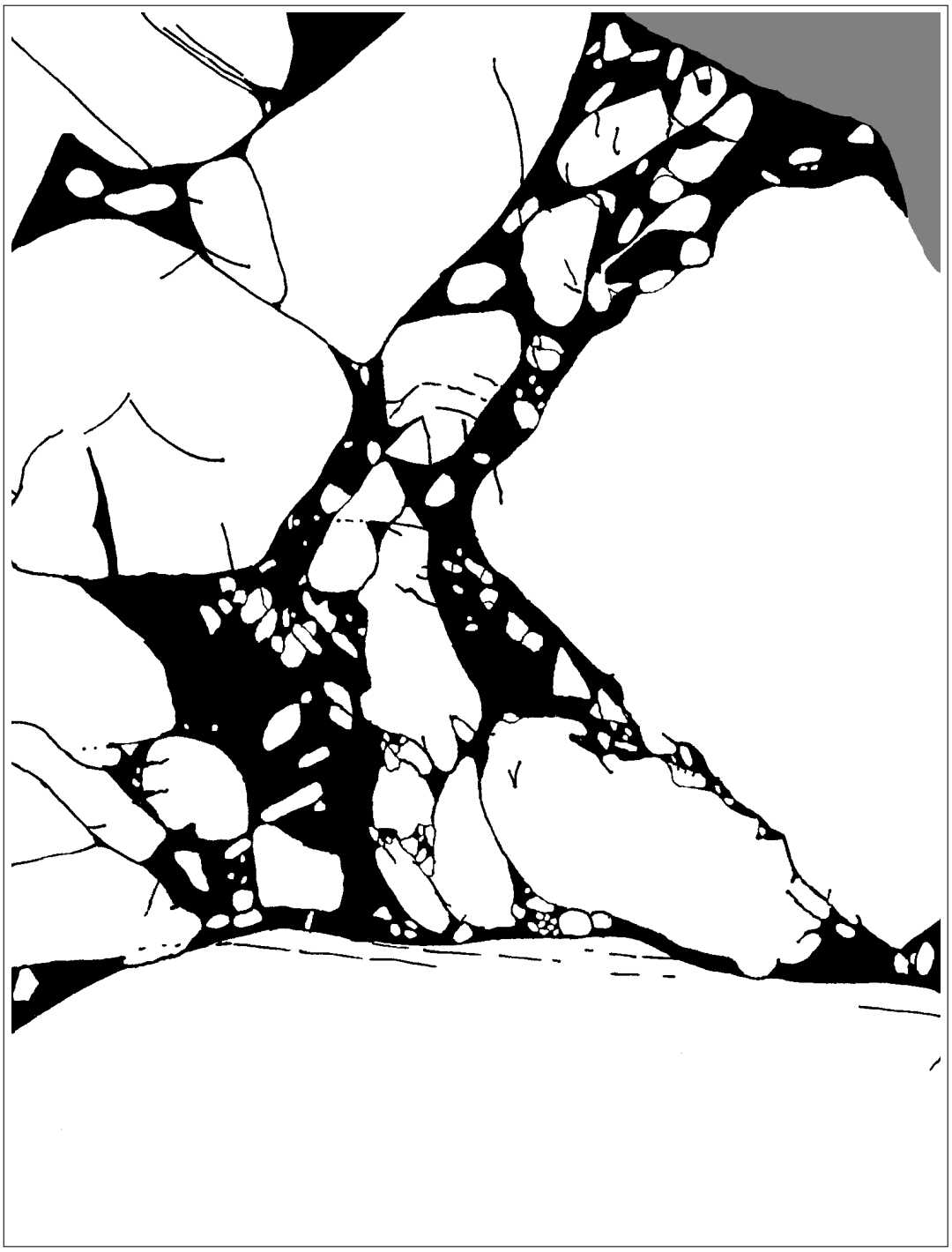

Figure A.11 – Map 0009, reference scale 10cm, Seal Bay North (WP 39).

Figure A.12 – Map 0010, reference scale 10cm, Seal Bay North (WP 39).

Figure A.13 – Map 0037, reference scale 30cm, Seal Bay North (WP 39).

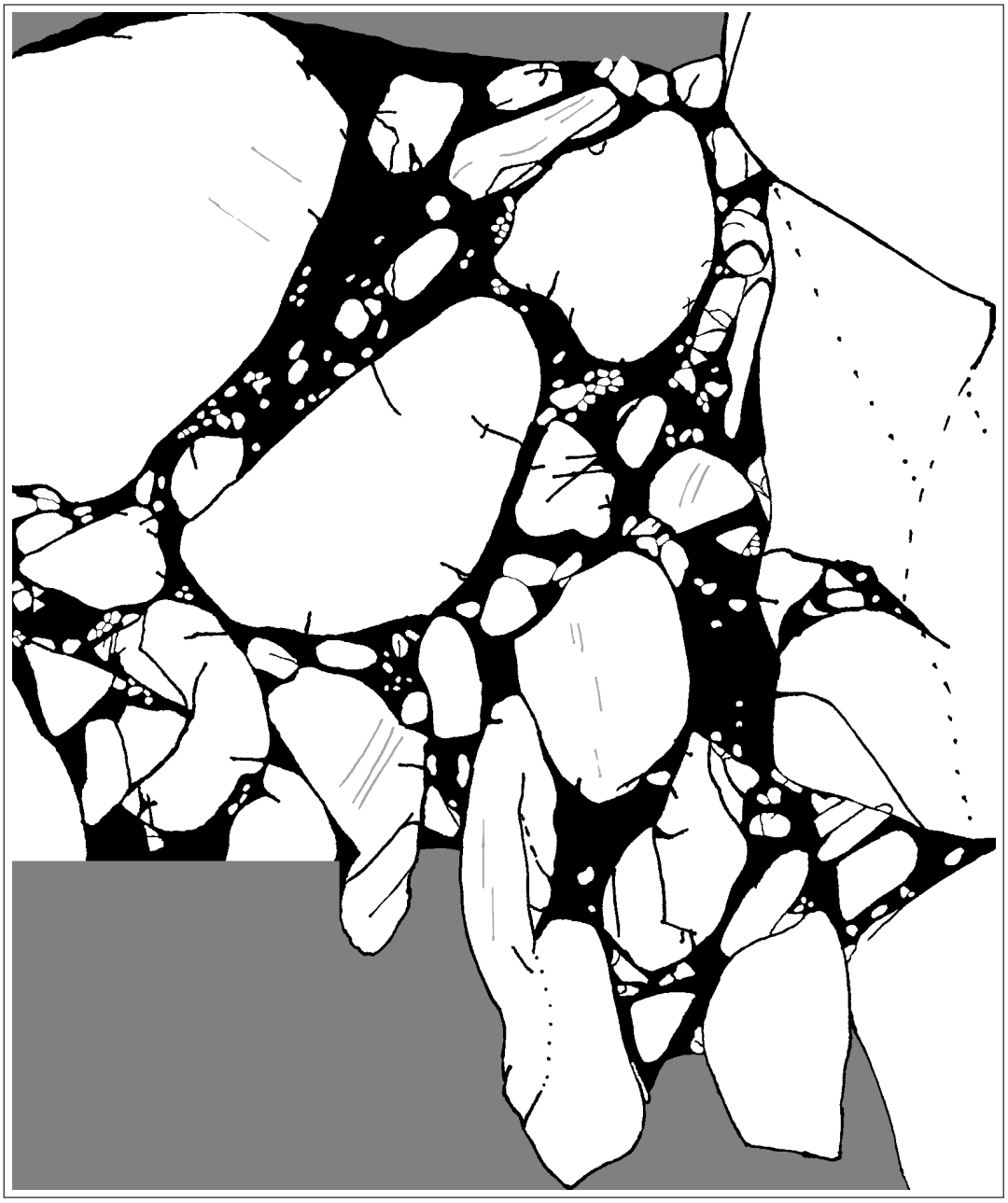

Figure A.14 – Map 0043, reference scale 30cm, Seal Bay North (WP 39).

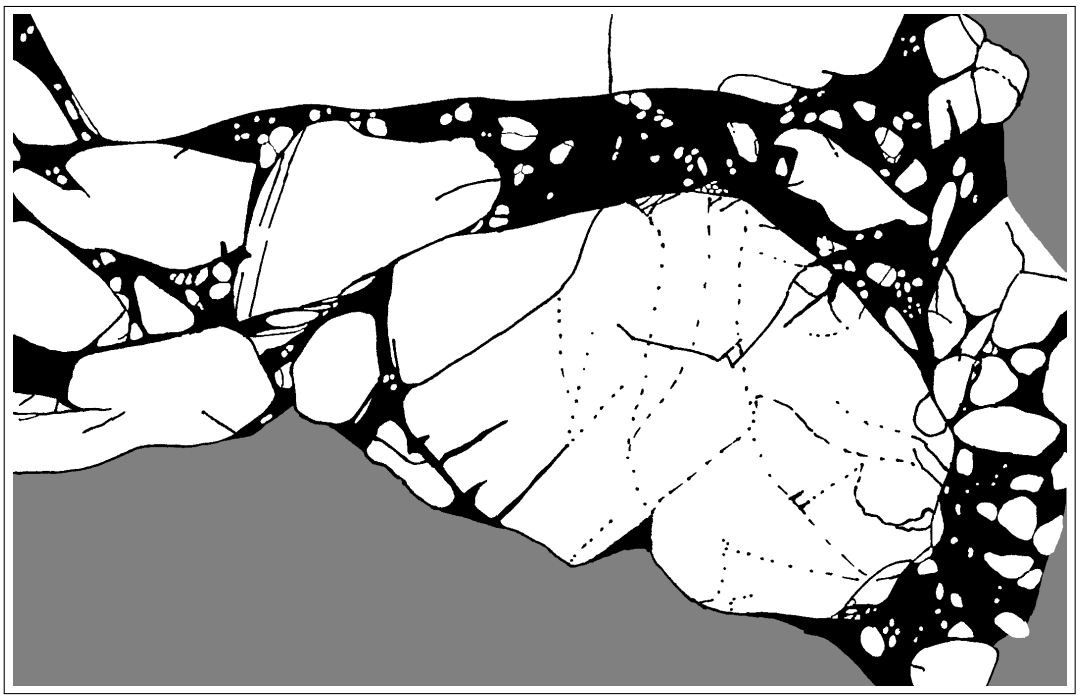

Figure A.15 – Map 0045, reference scale 30cm, Seal Bay North (WP 39).

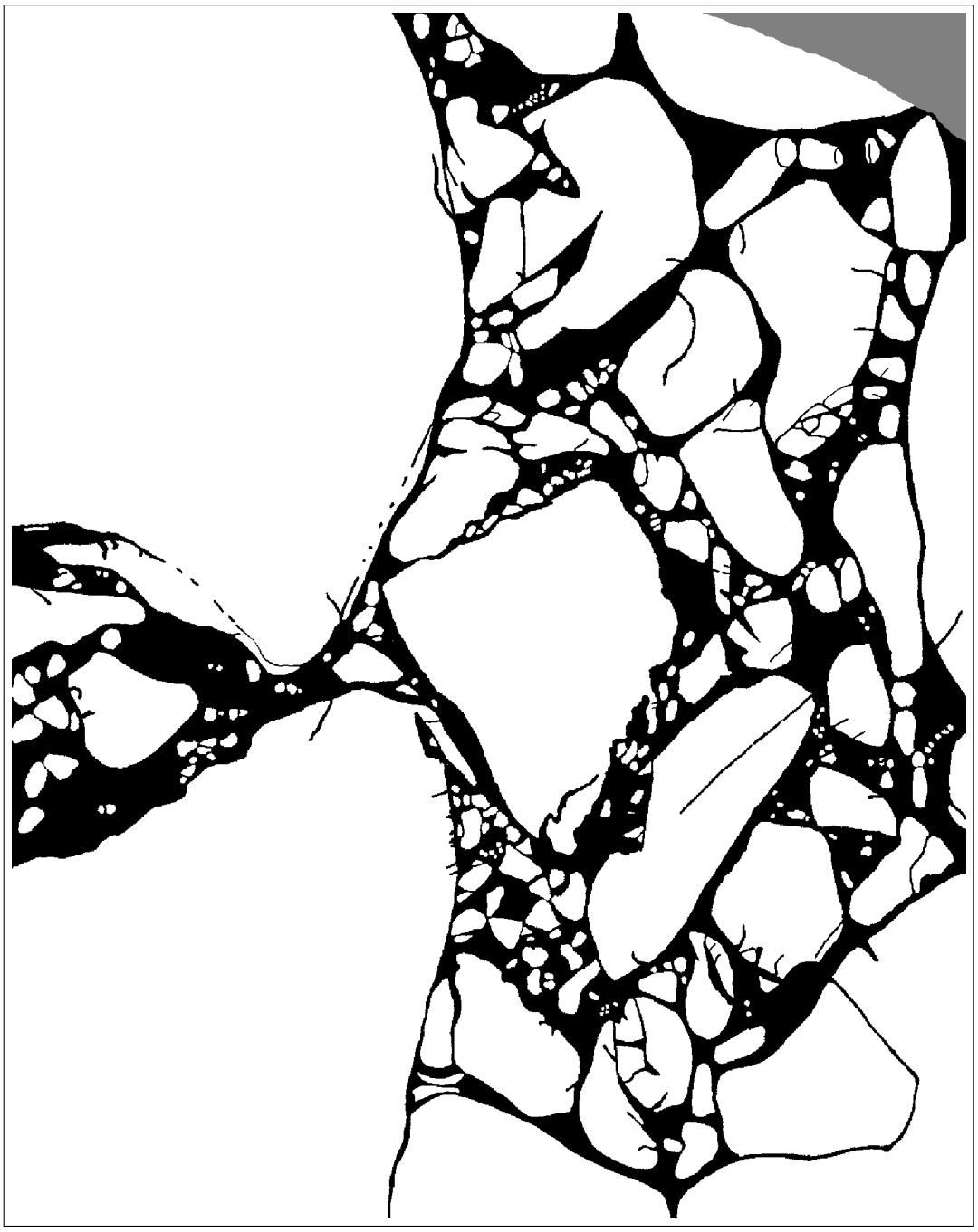

Figure A.16 – Map 0047, reference scale 30cm, Seal Bay North (WP 39).

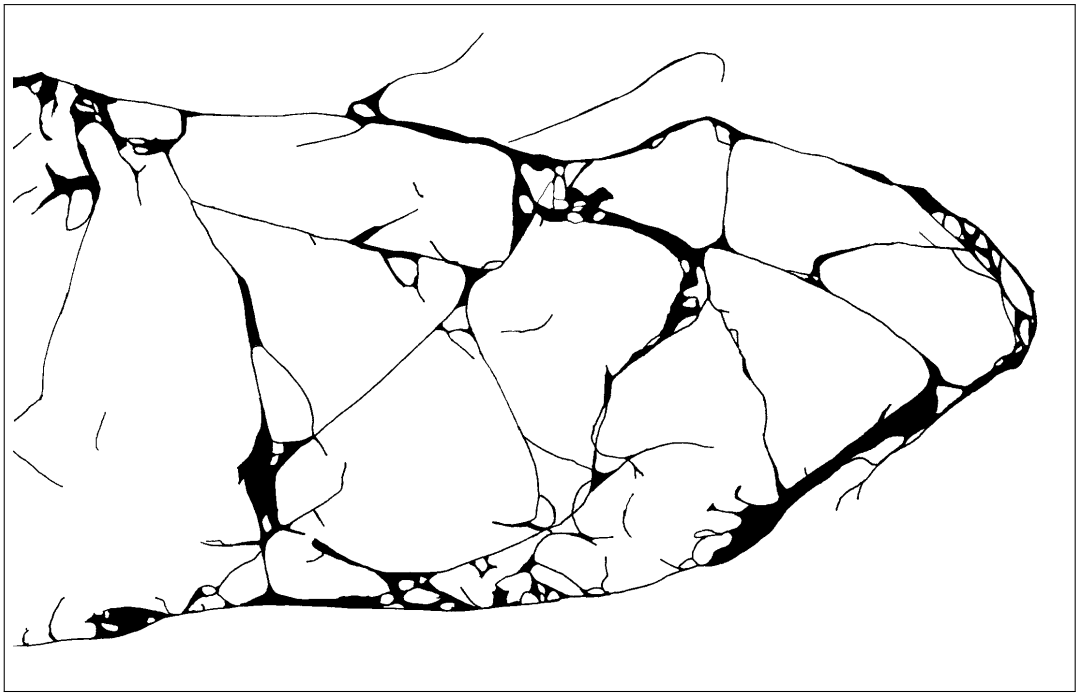

Figure A.17 – Map 0094, reference scale 30cm, Seal Bay North (WP 39).

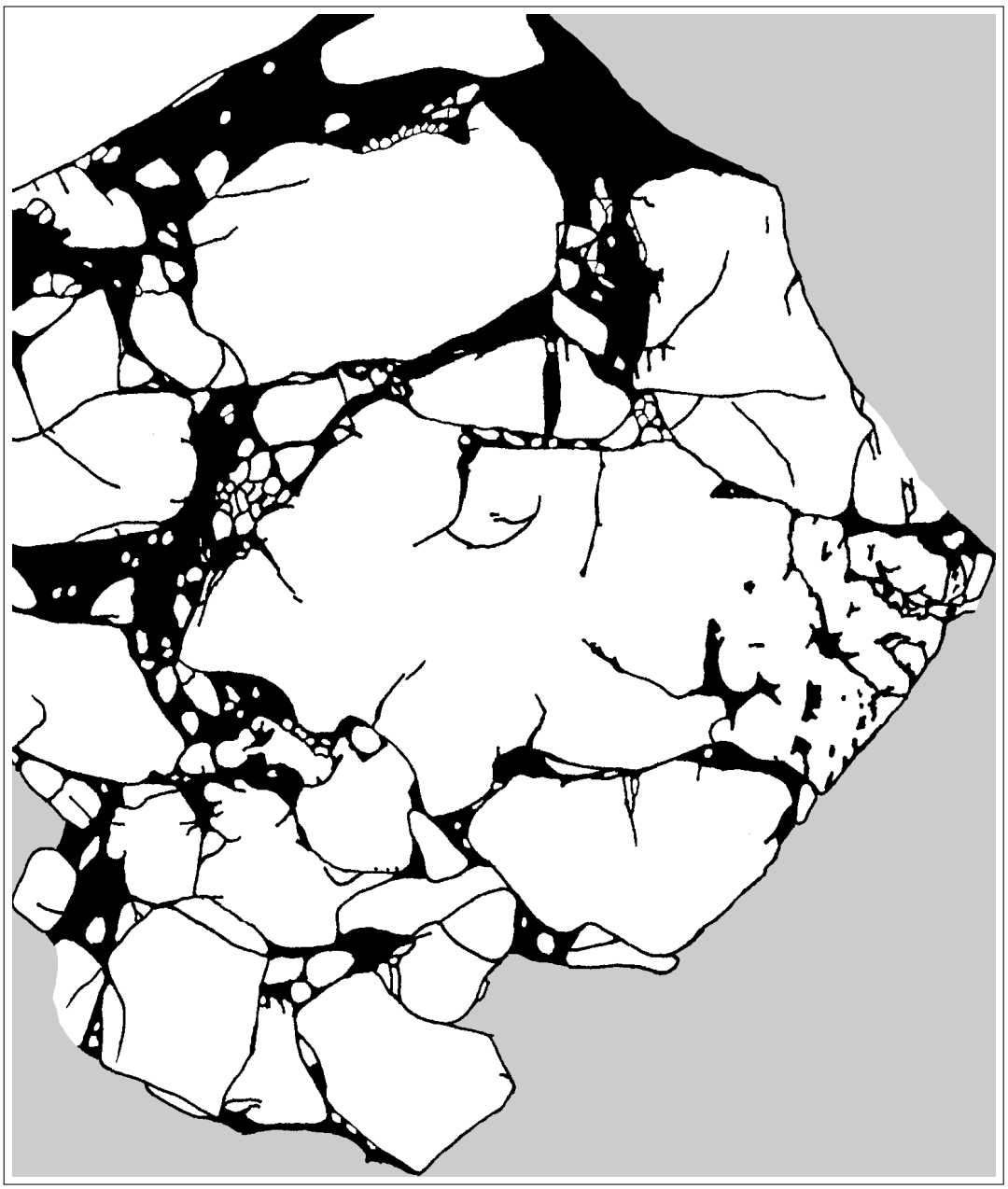

Figure A.18 – Map 0567, reference scale 30cm, wall (WP 25).

Figure A.19 – Map 0729, 'front', reference scale 30cm, Seal Bay South (WP 38).

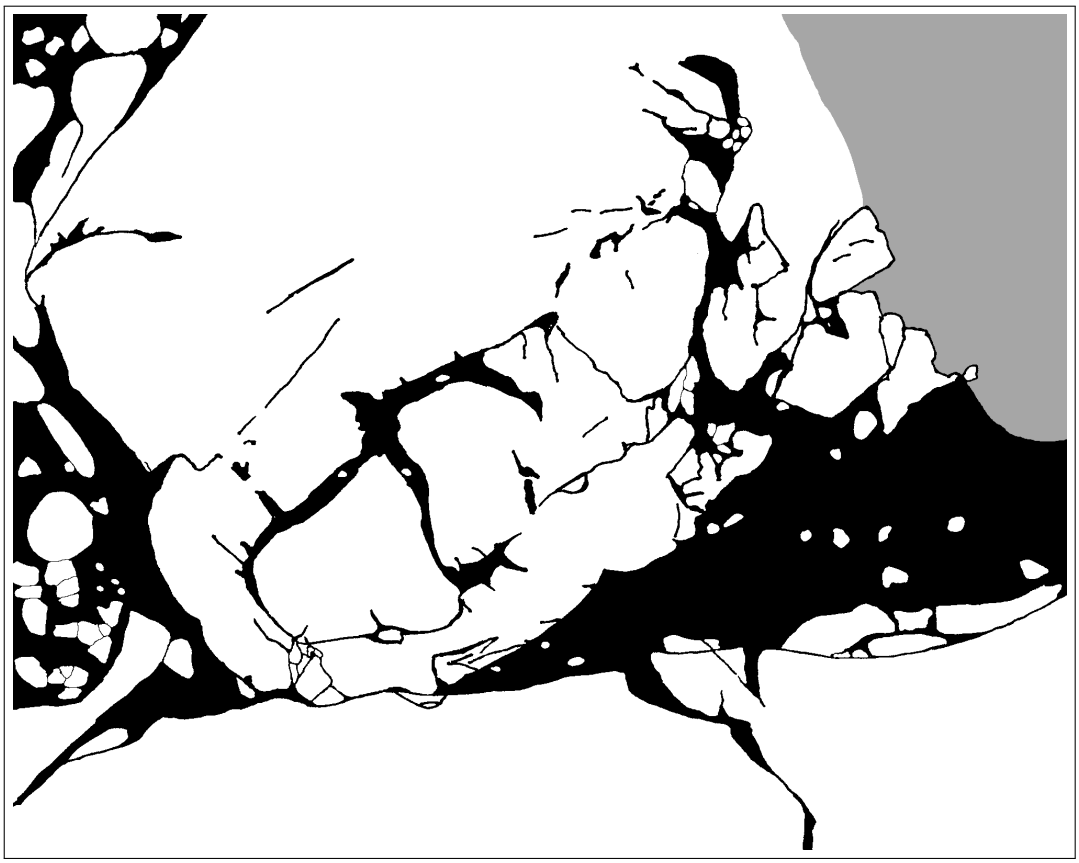

Figure A.20 – Map 0547, 'top front', reference scale 30cm, Seal Bay South (WP 38).

Figure A.21 – Map 0568, 'back', reference scale 30cm, Seal Bay South (WP 38).

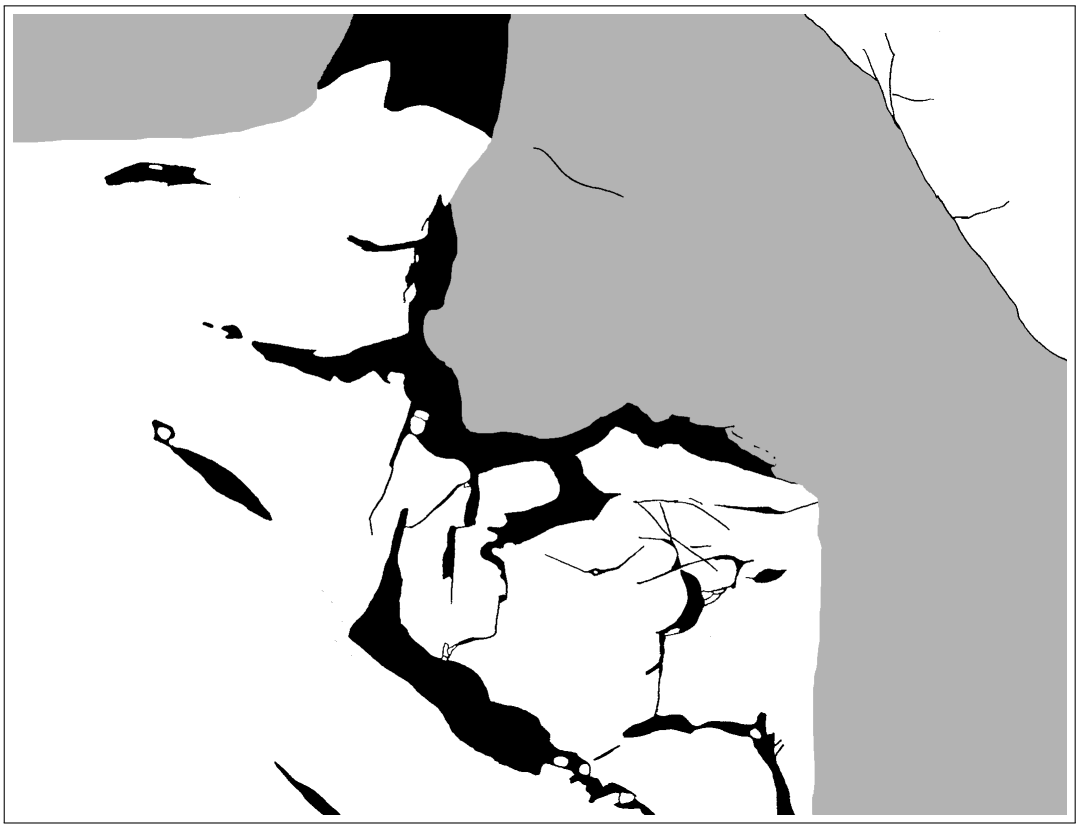

Figure A.22 – Map 0571, part of 0568, including 0572, reference scale 30cm, Seal Bay South (WP 38).

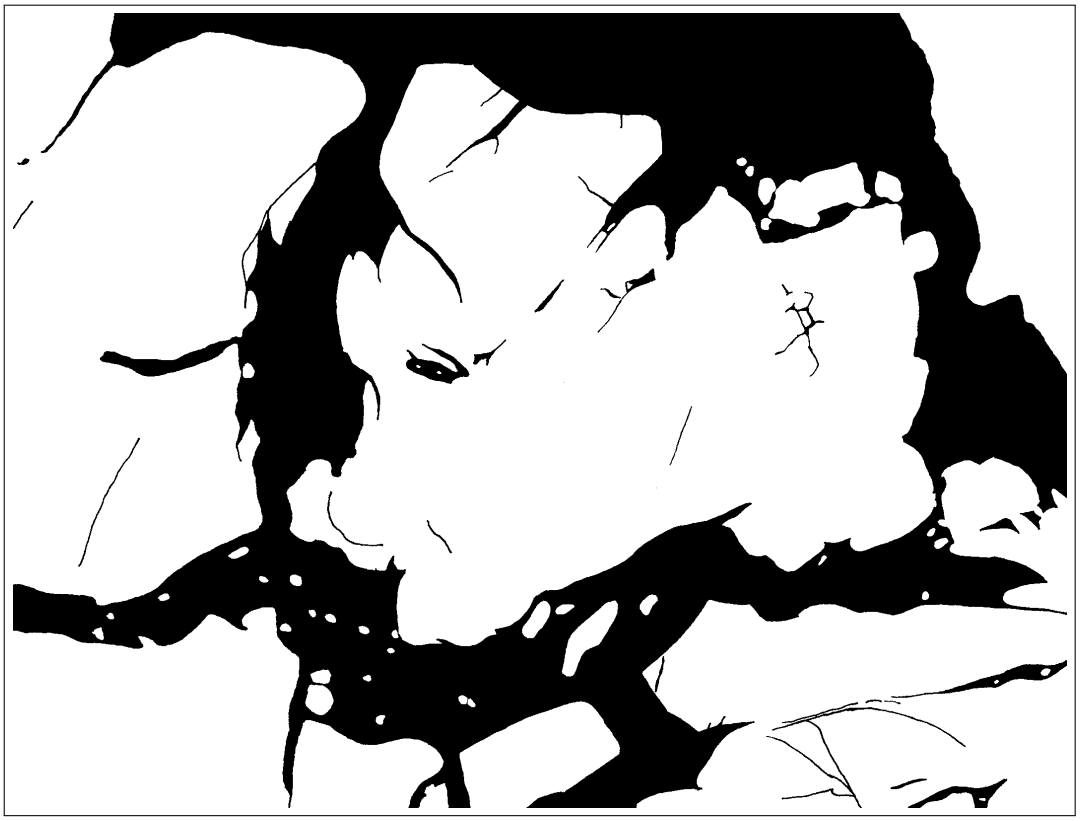

Figure A.23 – Map 0572, part of 0568, including 0571, reference scale 10cm, Seal Bay South (WP 38).

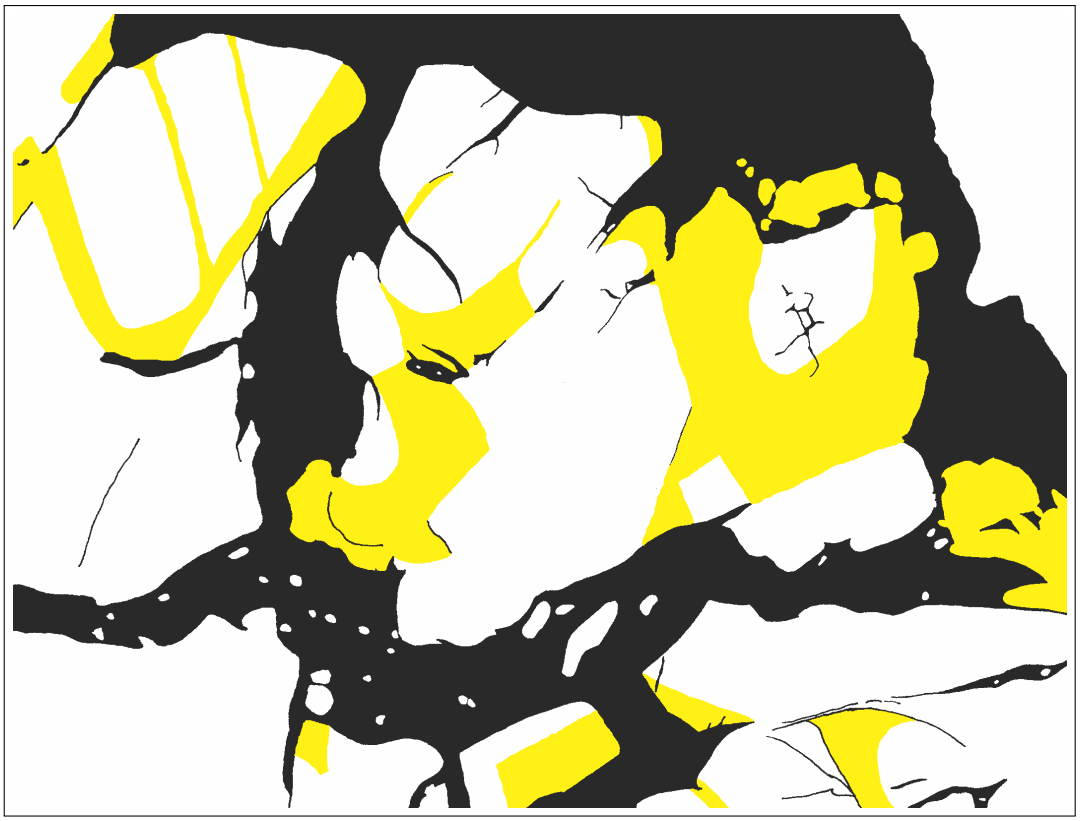

Figure A.24 – Map 0572, part of 0568, including 0571, reference scale 10cm, Seal Bay South (WP 38). In yellow are the areas which appear to be transparent in the outcrop, suggesting there is dark pseudotachylyte below.

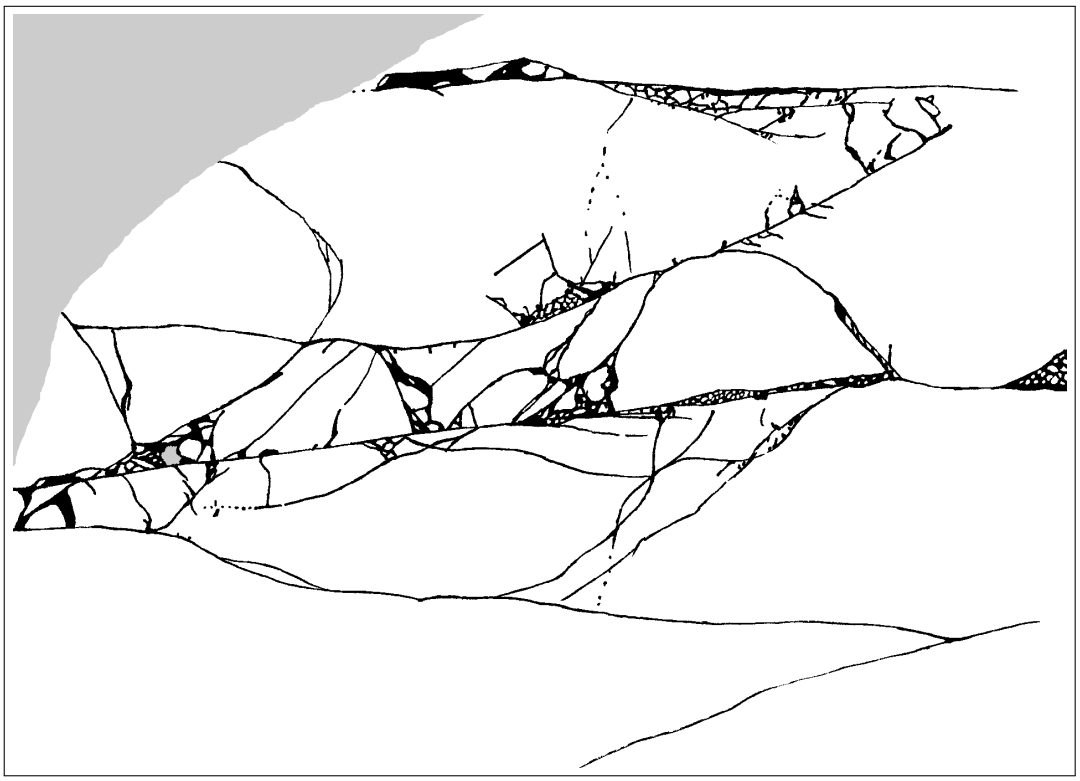

Figure A.25 – Map 9742, including 9809, reference scale 100cm, Golf Course nr. 6 (WP 19).

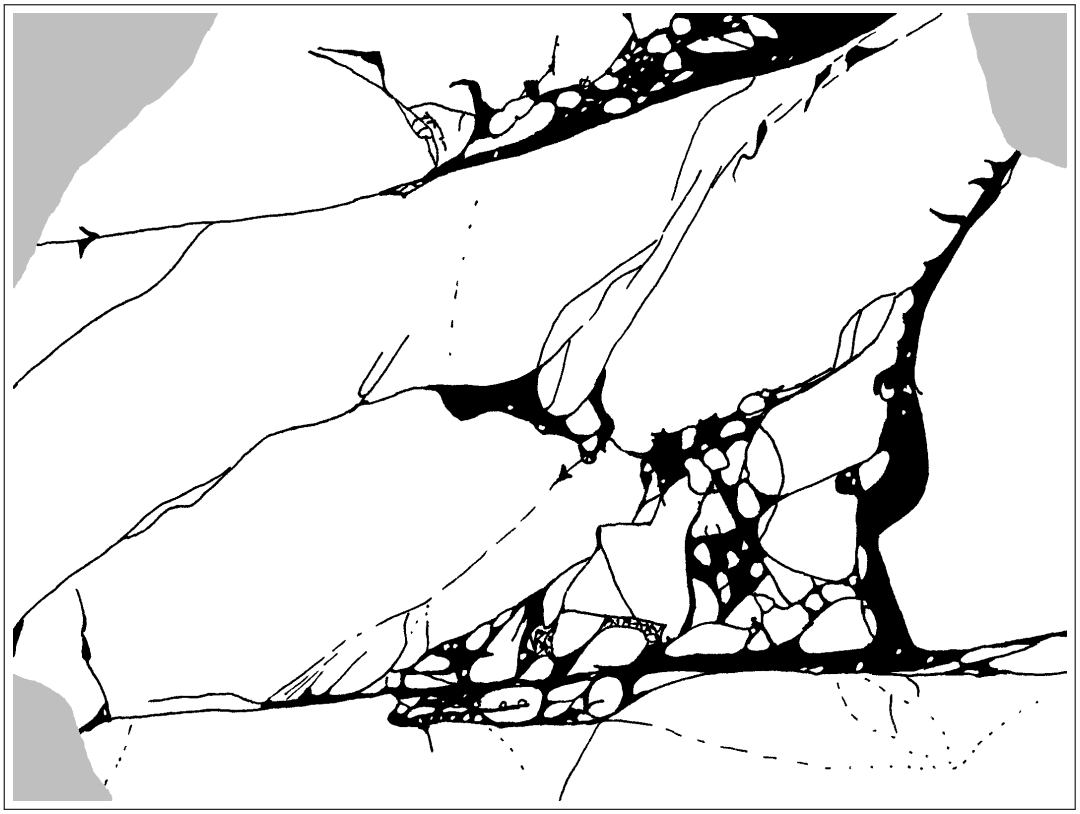

Figure A.26 – Map 9809, part of 9742, reference scale 30cm, Golf Course nr. 6 (WP 19).

Figure A.27 – Map 9748, including 9749 and 9806, reference scale 100cm, Golf Course nr. 6 (WP 19).

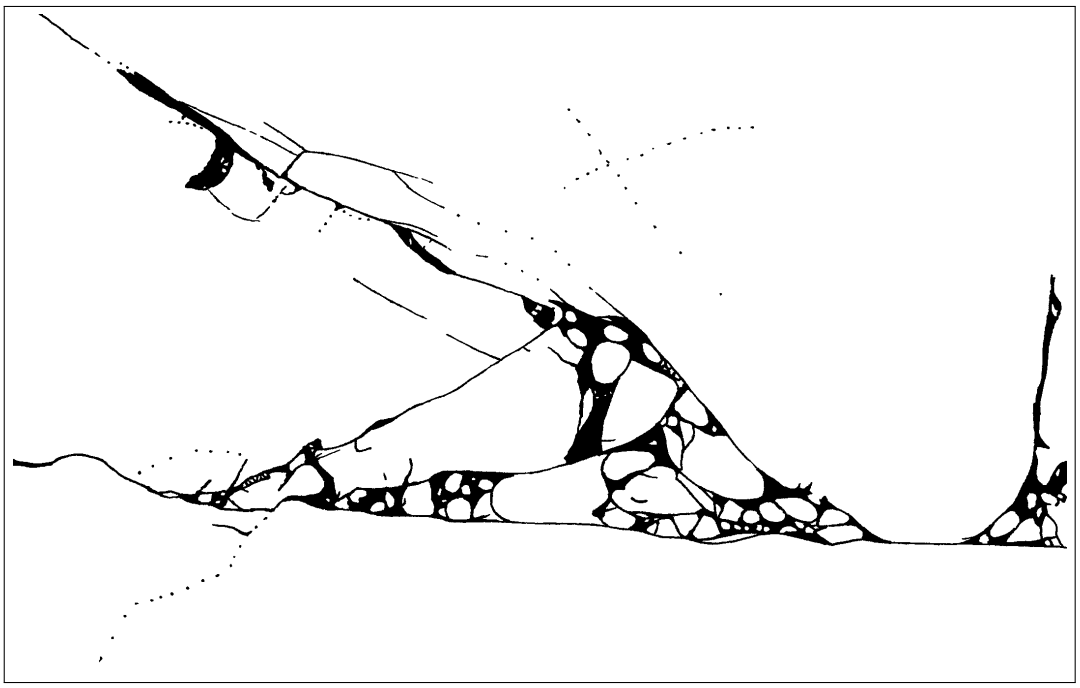

Figure A.28 – Map 9749, part of 9742, including 9806, reference scale 30cm, Golf Course nr. 6 (WP 19).

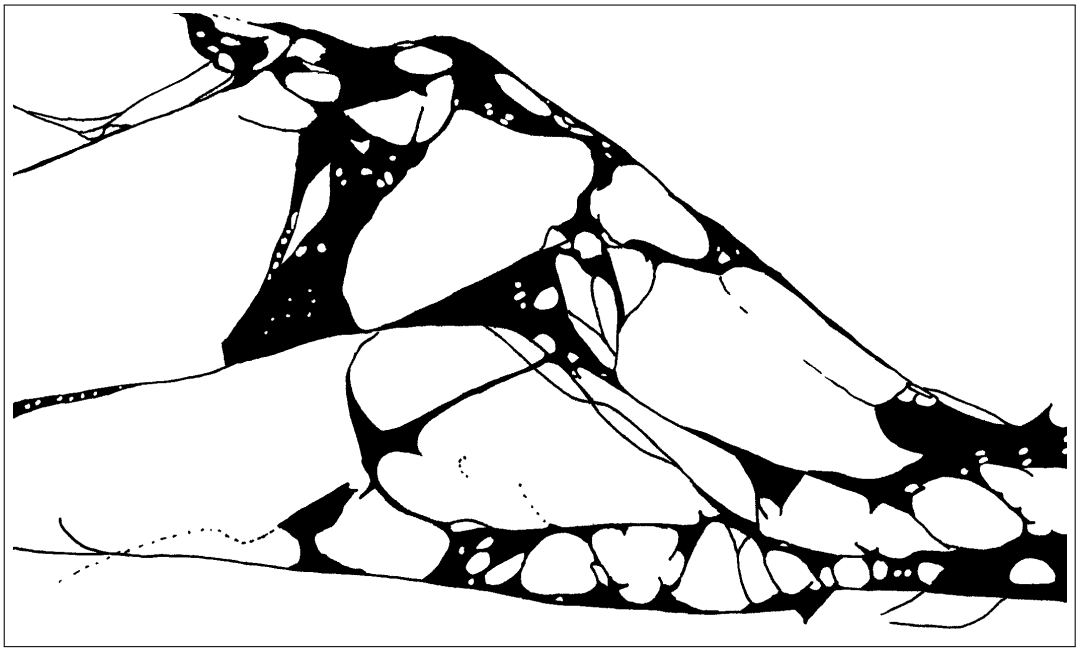

Figure A.29 – Map 9806, part of 9749 and 9748, reference scale 10cm, Golf Course nr. 6 (WP 19).